The University Of Sheffield.

Access to Electronic Thesis

Author:	Zana Uthman
Thesis title:	Configuration Forces in Structural and Continuum Optimisation
Qualification:	PhD
Date awarded:	9 June 2009

CONFIGURATIONAL FORCES IN STRUCTURAL AND CONTINUUM OPTIMISATION

Name: ZANA UTHMAN
Degree: Doctor of Philosophy in Civil and Structural Engineering
Department: Department of Civil and Structural Engineering at the University of Sheffield
Date of submission: 2008-10-05

TABLE OF CONTENTS

ACKNOWLEGMENT

It is a pleasure to acknowledge the generous help of Prof. Harm Askes for his support and valuable advice during my research career. A great help during my MSc and PhD degree research projects. He provided the space and flexibility to cover wide range of areas in research. I am grateful for his assistance, offering valuable comments and suggestions through the years. Also my appreciation to SIMULIA Benelux for the flexibility and support provided during the final stage of this research.

I would like to thank my family for their support throughout my career. Many thanks, to my father MSc Abdul Rahman where he gave great motivation and advice, to my mother Almas for her kind and warm words and to my girl friend Suhua for her continuous support and encouragement.

Zana Uthman,
2008-10-05
Sheffield

Summary

This thesis deals with optimisation using the principles of continuum mechanics. Both shape and mesh optimisation will be covered. A unified approach will be introduced to obtain shape and mesh optimisation for hyperelastic, hyperelastodynamic and hyperelastoplastic settings. The approach makes use of the generated material force method in mesh optimisation and the so-called imposed material force method in shape optimisation. To this end, the appropriate spatial and material continuum mechanic Equations will be developed in hyperelastic, hyperelastodynamic and hyperelastoplastic settings. A summary of the four main parts is as follows.

The first part begins with structural optimisation in hyperelastic setting. After introducing the necessary Equations, the effectiveness of the material force method to obtain global optimised solutions for truss structures will be demonstrated. The implementation produces the global optimised undeformed configuration and the global optimised deformed configuration. The shape and mesh optimisation will be tested for two and three dimensional truss structures under small and large deformations. In addition, these formulations will be extended to obtain constrained optimised solutions. The penalty method is used to realise optimised truss structures within certain design criteria.

The second part develops a new Arbitrary Lagrangian Eulerian (ALE) hyperelastic setting in rate form. It will deal with two systems of partial differential Equations, namely the spatial and the material momentum Equation. Both are discretised with the finite element method. The spatial Equation will then be linearised by taking the material time derivative while the material Equation will be linearised by taking the spatial time derivative. The solution defines the optimal spatial and material configuration in the context of energy minimisation in hyperelastic setting. The implemented examples will illustrate shape optimisation under the effect of mesh refinement

The third part provides the formulation and implementation details of ALE hyperelastodynamic problem classes. This ALE formulation is based on the dual balance of momentum in terms of both spatial and material forces. The balance of spatial momentum results in the usual Equation of motion, whereas the balance of the material momentum indicates deficiencies in the nodal positions, hence providing an objective criterion to optimise the finite element mesh. The main difference with traditional ALE approaches is that the combination of the Lagrangian and Eulerian description is no longer arbitrary. In other words the mesh motion is no longer user defined but completely embedded within the formulation.

This presents a discretisation and linearisation for a recently developed variational arbitrary Lagrangian Eulerian framework in hyperelastodynamics setting. The spatial and material variational Equations will be discretised to obtain the weak form of the momentum and continuity Equations. The

discretised ALE Hamiltonian Equations of the spatial motion problem introduces the balance of the discretised spatial momentum and the discretised spatial continuity Equation while the corresponding material motion problem defines the balance of the discretised material (or configurational) momentum and the discretised material continuity Equation. We will deal with two systems of partial differential Equations: the scalar continuity Equation and the vector balance of momentum Equation. The momentum and continuity Equations will then be linearised. The time integration of both the spatial and the material Equations is performed with Newmark scheme. A monolithic solution strategy solving both the spatial and the material momentum Equations has been carried out while updating of the spatial and the material densities were attained through solving the spatial and material continuity Equations (mass conservation). The concept of generated material force has been implemented to optimise the mesh and consequently the wave propagation. The solution defines the optimal spatial and material configuration in the context of energy minimisation.

The fourth part provides the framework and implementational details of ALE hyperelastoplasticity problem classes. This ALE formulation is based on the dual balance of momentum in terms of spatial forces (the well-known Newtonian forces) as well as material forces (also known as configurational forces). The balance of spatial momentum results in the usual Equation of motion, whereas the balance of the material momentum indicates deficiencies in the nodal positions, hence providing an objective criterion to optimise the shape or the finite element mesh.

The earlier developed ALE hyperelastic setting will provide the platform to extend the formulation to include plasticity. The new ALE hyperelastoplasticity setting will be developed at finite strain. In ALE hyperelastoplastic formulation additional Equations are required to update the stresses. The principle of maximum plastic dissipation as well as the consistency conditions in spatial and material setting will introduce the spatial and material plastic parameters and rate form of the stress-strain relations. The solution defines the optimal spatial and material configuration in the context of energy minimisation in hyperelastoplasticity setting. The concepts of imposed and generated material force are implemented to provide improvements over Lagrangian solutions.

The scope

This thesis develops new mathematical tools to optimise the mesh and shape of structures. Optimal structures adapt the construction to its goal and loading conditions, mesh optimisations improve the quality and the accuracy of the finite element solution while shape optimisation provide the necessary tool to obtain the best design shape of the structure in terms of weight, energy etc. Mathematically, the problem is formulated as a variational equality or inequality problem. Variational equality problems are known in systems such as hyperelastic, hyperviscoelastic and hyperelastodynamic systems while variational inequality problems are known in systems such as hyperelastoplastic or hyperelastic viscoplastic systems. The numerical solution of these problems continues to be a difficult task.

The classical mesh optimisation methods generally lack a theoretical background and are limited to two or three dimensions, further more new Equations are required to describe the mesh motion. These Equations are usually complicated. An extra problem that faces these methods is the requirement of a reliable error estimation that directs the mesh motion. Another problem is the computational costs of these methods that are quite high.

The aim in this work is to overcome these difficulties through the development of new mathematical formulations that answer all these problems. The new formulations are firmly rooted; this means that the mesh and the shape optimisation problem are fully developed from the inequality variational principle. Thus no additional Equations are required to describe the mesh motion, estimating discretization errors and to optimise the shape. These additional arbitrary Equations are embedded in the new formulation, furthermore they are general. The new developed formulation has been implemented for three dimensional cases but can be easily reduced to two or one dimensional case. Another advantage of the method, it combines the treatment of shape and mesh optimisation in a single formulation. This means that different formulations are not required to be developed for shape and mesh.

The ALE hyperelastic setting developed in total form will be reintroduced in rate form. This will provide the basis for introducing the hyperelastodynamic and hyperelastoplastic settings.

In hyperelastodynamic systems the aim is to develop a system of coupled nonlinear Equations based on the configurational forces to provide the necessary tool to capture the wave propagation accurately. The new method improves the quality of the mesh under severe distortion and as a result the accuracy of the results. The advantage over previous remeshing methods developed for hyperelastodynamic systems is that no additional remeshing Equations are required or error estimators or indicators for mesh refinement. These are as in static and plasticity settings fully embedded in the formulations.

Although the newly developed mesh optimisation for hyperelastoplastic systems does have similar solution steps as the traditional methods, the computational cost is lower due to the fact that no error estimators are required and the remeshing is totally embedded in the solution. Thus no expensive remeshing Equations especially in the case of three dimensional cases are needed.

The configurational force method that was developed to optimise truss structures for hyperelastic coupled solution is intended to search for the optimum location of the internal nodes. In this thesis the method will be generalised, to include the external nodes and to include certain constrained. In practice, the location of joints where the loads are applied may need optimisation. Unfortunately the configurational force up to today does not provide any method to achieve it.

The current thesis introduces a new method, the so called imposed material force that is a generalisation of the generated material force method that has been developed in the last years for hyperelastic systems. The method provides the tool to optimise the traction boundary nodes.

Outline of the thesis

The first chapter of the thesis provides a review of the state of the art, in truss optimisation using size, shape and topology optimizations. After a comparison between the methods with their advantage and disadvantage, the material force method will be reviewed as a special case of shape optimisation. A brief review of the new method for truss optimisation will be given and highlighted with a simple example.

An extensive review of the arbitrary Lagrangian Eulerian method follows with the emphasis on the spatial and material motion and its relation to the Lagrangian and Eulerian formulation. Furthermore the A.L.E method and its role in improving the mesh quality for statics, dynamics, plasticity etc will be outlined. The physical and inverse motion will then be introduced as a particular case of the spatial and material motion as illustrated in many recent works of Paul Steinmann. A comprehensive review of Paul Steinmann's works for different settings using the material force method will be illustrated. The basic formulation that these settings are based on and the mapping between the spatial and material configuration are reviewed.

The final part of the first chapter is concerned with the variational principles. Since these principles will have a major role in subsequent developments of our formulations, a review of equality and inequality formulations will be presented. In the equality variational principle the focus will be on the D' Alembert and the Hamiltonian principles. These principles form the ground for the development of new formulations in the following chapters for hyperelastic and hyperelastodynamics settings. Special attention will be paid to the framework of Paul Steinmann on the Hamiltonian principle in combination with the use of the material force method (A.L.E Hyperelastodynamics). The concept and the formulation are outlined which will give the basis for subsequent developments of a detailed formulation. The inequality variational principle will have an important role in this thesis for deriving A.L.E Hyperelastoplastic setting. As a result the principle of maximum plastic dissipation will be viewed as particular case. As an important tool to form equality from an inequality constraint the penalty method will be discussed with a simple example.

In the second chapter the focus will be on truss optimisation through comparison between coupled and decoupled spatial and material solutions and the advantage of a coupled solution will be outlined. Furthermore the imposed material force will be introduced as a general case of the generated material force in truss optimisation. The method of imposed material force will be applied first on a simple truss structure where an analytical solution is known.

The method of imposed material force will be extensively investigated on different examples and a clear comparison will be made with the generated material force in these applications. The optimised spatial and material configurations will be viewed through the iterations and increments. Also the rate of convergence will be discussed. The next part of the section will be concerned with providing constrained optimised solutions. The penalty method will be the tool to obtain optimised truss structures under inequality constraints. The method will be applied on different engineering design problems to obtain an optimised configuration. The focus will be on optimising the structure within a certain space or within a certain amount of allowable deflection of a certain joints. The method material force shows that these design requirements are fulfilled under the required constrains.

The last part of chapter two will be concerned with extending the structural optimisation from two dimensional cases to three dimensions. The imposed and generated material force will be tested for three dimensional examples.

In chapter three the A.L.E hyperelastic formulation will be reintroduced. The formulation will be parameterised in term of the velocity instead of the displacement. In the early work by Paul Steinmann, Harm Askes and Ellen Kuhl the formulation was introduced; the spatial and material momentum Equations were developed and linearised. Both spatial and material momentum Equations are linearised with respect to the spatial and material coordinates. In the current work the parameterisation will be introduced in terms of the velocity where both the spatial and the material momentum Equations are linearised by taking their spatial and material time derivative. The resulting linearised spatial and material Equations can be solved in coupled or uncoupled manner. The final part of chapter three presents two examples to illustrate the effectiveness of the formulation. The solution is carried out in an uncoupled manner using the iterative Newton Raphson scheme. The imposed material force method has been used and the results are compared with a Lagrangian solution.

The formulation will be extended to ALE hyperelastodynamic setting in chapter four. The ALE hyperelastodynamic formulation will be developed in terms of the physical and inverse motion using the Hamiltonian principle. The resulting Equations are the momentum and continuity Equations. As in chapter three these Equations will be developed in the spatial as well as the material domain. Next, a time discretisation will be carried out on the spatial and the material momentum Equations, followed by linearisation with respect to the spatial coordinates at fixed material coordinates and linearisation with respect to the material coordinates at fixed spatial coordinates. In similar manner we carry out temporal discretisation according to the Newmark algorithm on the spatial and material continuity Equations and linearising them with respect to the spatial and material densities respectively. A solution scheme will be introduced where the Newton-Raphson method is embedded in the implicit Newmark time integration scheme for the spatial and material momentum Equations enforced by the continuity Equations. In other words the spatial and material momentum Equations will be solved first in a coupled manner to provide the new spatial and material coordinates. The spatial and

material continuity Equations will be enforced next where the spatial and material densities are updated. Thus the developed hyperelastodynamic setting of spatial and material Equations are not fully coupled since the spatial and material continuity Equations are enforced in a different sub step. The chapter concludes with two examples where the focus will be on impact forces and wave propagation towards the boundary. Another important aspect is the mesh concentration around the propagated wave.

The final chapter presents a new ALE hyperelastoplastic formulation. The chapter begins with presenting the basic formulation followed by developing the spatial and material momentum Equations. The formulation makes use of the physical and inverse motion. The material rate of the stress and strain tensors developed in the spatial domain needs to be convected. The necessary Equations will be developed for convection of these spatial tensors from material rate form to spatial rate form. Next the constitutive spatial and material rate Equations will be developed. The material domain will be developed within the elastic range to represent the remeshing processes while the spatial domain will give the material behaviour within the elastoplastic range. The resulting ALE hyperelastoplastic formulation combines the traditional and the new concept of ALE. The traditional part in solving the spatial setting first to obtain the material behaviour is followed by solving the material setting to improve the quality of the mesh and a final stage to convect the state variables. The novel part consists in using the concept of physical and inverse motion, in which no arbitrary remeshing Equations need to be developed, as these Equations are derived from the energy function. The last part of chapter five illustrates the effectiveness of the formulation with two examples. The first example compares the Lagrangian solution with the newly developed ALE hyperelastoplastic setting using the imposed and generated material force methods. The second example illustrates the effectiveness of the imposed material force as improving the mesh quality and smoothen the stresses. The final part of the thesis gives the conclusions and remarks on the work with recommendations and future work.

1 STATE OF THE ART

Intensive research work has been conducted in the last three decades on structural optimisation using the finite element method. Due to the computational cost of nonlinear analysis, most studies have been performed on optimisation in a linear finite element setting, while much less work has been done on the optimisation in nonlinear finite element setting. The main reason behind that is that the result obtained by the optimising linear settings was considered reliable; the computational cost is much higher due to the complexity of the non-linear setting. Therefore most research in structural optimisation problems focused on linear settings and the discussion below will review some important work in that field.

1.1 Truss optimisation

In the field of optimisation of truss structures, three major areas have been researched intensively. These are known as size optimisation (cross sectional areas), shape optimisation (joint position) and topology optimisation (removal and introductions of bars). Also using these design variables size optimisation, shape optimisation and topology optimisation have been carried out simultaneously.

1.1.1 Size optimisation of trusses

Size or cross-sectional truss optimisation assumes a fixed topology and geometry (the number of bars and joints, their connectivity, and locations) and find the shape of the bars that will best, either in terms of mass or stiffness, support a given load. Different numerical methods have been applied due to their advantages over analytical methods. This is due to the availability of powerful computers and their capability of solving highly non-linear problems. The earliest work in optimising truss structures using numerical methods was initiated by P. Fleron [1] (1964). The work was to optimise the structure through minimising the weight of trusses. Other works, P. Pedersen [2, 3] (1969, 1973) show the possibility of using the cross-sectional area of the bars and the coordinates as the design variables.

Other works focussed on minimising the total weight of the bars, e.g. W. Prager [4] (1974) for linearly statically determinate structures. W. Prager showed through an example the nonuniqueness of the optimal layout for stress constraint trusses. Other more recent interest areas were to minimise the weight under certain constraints. This has major advantages for practical applications. For example the work by P. A. Makris et al. [5] (2001) where the constraints did not only involve the displacement but also the stress.

Other design variables such as eigenfrequencies and control buckling on the element level were included in addition to the displacement and stress for 3D truss structures (see N.L. Pedersen and A.K. Nielsen [6] (2003)). The work combined size optimisation with shape optimisation under these constraints subject to multiple load cases.

1.1.2 Topology optimisation of trusses

The other area that has been intensely worked on is topology optimisation. The objective of truss topology optimisation is to find, for a given weight, the stiffest truss, defined as a subset of an initially chosen set of bars called the ground structure. The field is rapidly expanding which can result in much greater savings than cross-section optimisation.

The field of topology optimisation of discrete structures was introduced by Dorn et al. [7] (1964) who applied a linear programming method to optimize truss topology. In most of these studies, the cross-sectional area of each bar may take a zero value, in which case the bar is eliminated from the structure. Unfortunately the method encounters some difficulties where some of these bars cannot be eliminated from the structure, whence the structural problem should have a combinatorial nature. This have been shown by W. Dobbs and Felton [8] (1969) and G. Sved and Z. Ginos [9] (1968).

Another drawback of these studies is the possibility of the optimal topology to correspond to a singular point of the design admissible domain. This fact is a consequence of the discontinuity of some constraints when the cross-sectional area is zero. The singularity of the optimal topology in trusses was firstly shown thorouly by G. Sved and Z. Ginos [9] (1968) and afterwards by U. Ringertz [10] (1985). This problem has also been examined by U. Kirsch [11] (1990). It was shown that the problem of singular point in topological optimisation is not well understood and singular solutions are obtained mainly due to the nature of stress constraints. Other researchers who worked on singular structural topologies are G. I. N. Rozvany and T. Birker [12] (1994) who outlined the reasons for a global optimum to be obtained with iterative computational algorithms. The study was carried out to find exact optimal layouts for a single load and for two load conditions with stress constraints.

Other difficulties that topology optimisation of structures encounter is buckling constraints. This has been shown by M. Zhou [13] (1996) and G. I. N. Rozvany [14] (1996). In more recent work by G.I.N. Rozvany [15] (2001) new methods for treating design dependent constraint and singular topologies have been presented. Additional insights and a comprehensive review of these computational difficulties have also been given. It was shown that singularities can be removed by employing smooth envelope function method in which an exponential function representing the stresses has been used.

The drawback of this method was that it did not help in finding the global optimum. This comes through the widening of its spook that contains the optimal solution due to these envelope functions.

Research on topological optimisation of truss structures was carried out not only in the elastic range but also in the material and geometrical non-linear range. The first thorough research has been carried out by Prager [4] (1974) where he investigates a linear-elastic and perfectly plastic topology optimisation of truss structure. More recent work on work-hardening elastoplastic materials has been carried out by S. V. Selyugin [16] (1992). The work focussed on shape optimisation of bar structures for statically determinate and indeterminate structures. On the basis of the deformation theory of plasticity two optimisation criteria for minimizing energy have been used and compared, namely the minimum of the total complementary energy and the minimum of the total elasto-plastic strain potential energy. It has been shown that both criteria lead to equally stressed structures. Regarding geometrically non-linear topology optimisation we can refer to the work by T. Buhl. et. al. [17] (2000). The works deal with topology optimisation of structures under large deformation. A Lagrangian formulation has been used to model the geometrical non-linear behaviour. The finite element method with Newton-Raphson iterative schemes has been used to solve the resulting equilibrium Equations. The objective was to minimise the complementary elastic work for multiple load conditions. The results show that differences in stiffness of structures optimised using linear and non-linear modelling are generally small. More recent work by S.V. Selyugin 2004 [18] was focussed on multi-material (linear and non-linear) elastic truss structures where the objective was to obtain optimal topology and minimisation of mass. The result for multi-material trusses gives different optimal topology than the one with single material. Also the result shows that the optimal topology for linear elastic structures is not lighter than the non-linear one.

1.1.3 Shape optimisation of trusses

In the case of shape optimisation, the objective is to minimise the energy under certain displacement constraints of the connecting joints while keeping the number of elements and the connectivity fixed. This is very similar to certain mesh adaptive procedures, e.g. r-adaptive or arbitrary Lagrangian Eulerian formulations. The computational cost is usually lower than topology optimisation but some major drawbacks of the method are the optimisation procedure tends sometimes to fall into local minima. This means that the solution will be close to the initial design and no major changes are allowed.

In 1978 K. Dems and Z. Mroz carried out shape optimisation on elastic structures of a non-linear material by means of the finite element method. The objective was to determine shape parameters according to a derived

optimality criterion for the case of mean compliance design of elastic structures [19]. In 1995 S.V. Selyugin carried out research on problems for physically non-linear hyperelastic trusses statically loaded by a single system of loads. Use of a hyperelastic material implies that corresponding potentials of stresses and strains exist. The work focussed on determinate as well as indeterminate trusses in finding the optimal physical non-linear truss layouts [20]. More recent work combines shape and cross-section optimisation of truss structures by L. Gil and A. Andreu [21] (2001). The work focused on plane truss structures under stress and geometrical constraints. A penalty function has been used for the constraints. The optimisation procedure was carried out in finding the best geometrical layout (bars and nodes) and then finding the best cross sectional area for these bars. A conjugate-gradient strategy has been used to obtain the optimised nodal coordinates while the cross sectional areas were obtained by the fully stress design strategy. The conclusions were lighter truss structures with better carrying capacity. The drawbacks were that the solution gives a local optimum and the constraints were slightly violated. Other work on truss shape optimisation is due to D. Wang, et. al. with the objective of minimizing the weight under displacement constraint [22] (2002). As it is known shape optimisation provides an effective and highly efficient approach for minimising the weight of the structure. The optimum configuration was obtained by gradually relocating the most efficient nodes with minimum weight increase. The calculations were carried out for truss structures under multiple load cases subjected to multiple displacement constraints. The results show that shape optimisation cannot reduce the displacement to arbitrary small values.

More recent work on shape optimisation was carried out by Y.C. Toklu [23] (2004) where the objective was to minimise the total potential energy of the truss structure. As it is known, taking the minimum of the potential energy Equation provides the equilibrium Equation. This may provide a local minimum. In order to obtain a global minimum or a further reduction of the potential energy extra search methods should be added. These methods can be arbitrary or firmly rooted in continuum mechanics. The arbitrary search methods make use of a developed adaptive local search procedures where better and better shapes are sought with smaller potential energy after each iteration until a relative minimum is reached. Y.C. Toklu has illustrated this for problems with material and geometrical non-linearties on plan trusses. This resulted in more reductions in the potential energy.

1.2 Material force method

Although arbitrary adaptive methods were successful in finding a relative optimum solution, these methods could not find the optimum global solution due to their arbitrariness. A method that is firmly rooted is using the so-called material forces in structural optimisation.

The material force or more generally configurational force is the derivative of the strain energy with respect to the *undeformed* coordinates. The relocation of the nodes in such a way to allow for these forces to be vanished will result in minimising the total potential energy. As a result an optimum initial shape for the truss structure will be obtained. M. Braun [24] (2005) demonstrated the concept of material force in shape optimisation of truss structures. Other works on material force in structural optimisation in hyperelastic setting is carried out by H. Askes et al. [25] (2005). The work is based on finding the optimum location of the nodes through equilibrating the spatial and material forces. The spatial forces (also known as physical forces or Newtonian forces) are spatial variations of the potential energy at fixed material positions while the material forces (also known as configurational forces or Eshelbian forces) are material variations at fixed spatial positions. The solutions of the resulting spatial and material Equations were carried out in coupled manner. All previous works on material solutions were carried out in a staggered manner, which means solving the spatial Equation in the first substep followed by solving the material Equation in the second substep. The advantages of the coupled spatial and material solution over the decoupled one are not only a reduction of the computational costs but a remarkable accuracy in obtaining a global solution. This will be illustrated later with an example.

Another type of generating the material force, which will be the focus of this report, is through numerical discretisation. M. Braun [26] (1997) has first introduced this concept where the finite element discretization result in non-smooth stress fields that turn in configurational force residuals. More recent work by R. Mueller and G. A. Maugin [27] (2002) uses the same principle of the material force as a softening indicator for the finite element mesh.

The current work will exploit further the use of material force in structural optimisation through introducing the term imposed material force. All previous works make use of generated material force in optimisation [24, 25, 26, and 27]. Z. Uthman and H. Askes [28] (2006) have first introduced the term imposed material force in structural optimisation. In this report the result obtained from the so-called imposed material force will be compared to existing analytical solutions for validations.

1.2.1 Illustrative example

The following will give the analytical solution of a simple truss structure consisting of two bars. The bars have the same stiffness EA, fixed at one end and subjected to an applied load P at the other connected end (see Figure 1).

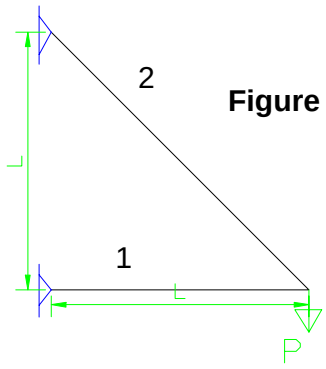

Figure 1 Truss structure

The load in the horizontal and the diagonal bars can be given respectively as:

$$N_1 = -\frac{P\cos\alpha}{\sin\alpha} \quad \text{and} \quad N_2 = \frac{P}{\sin\alpha} \qquad 1$$

where α is the angle between the two bars. The energy for the bars can be obtained from:

$$U = \frac{1}{2}\sigma_1\varepsilon_1 Vol_1 + \frac{1}{2}\sigma_2\varepsilon_2 Vol_2 \qquad 2$$

where σ_1 and σ_2 are the stresses, ε_1 and ε_2 are the strains and Vol_1 and Vol_2 are the volumes in the horizontal and diagonal bars respectively. This Equation can be written as:

$$U = \frac{1}{2E}\left(\frac{N_1}{A}\right)^2 LA + \frac{1}{2E}\left(\frac{N_2}{A}\right)^2 AL/\cos\alpha \qquad 3$$

Substituting the values for N_1 and N_2 as given above will result in:

$$U = \frac{P^2 L}{2EA}\left(\frac{\cos^3\alpha + 1}{\cos\alpha\sin^2\alpha}\right) \qquad 4$$

In order to obtain an optimal shape of the structure, the complementary energy should be minimised. This can be achieved through taking the derivative of the complementary energy with respect to α:

$$\frac{\partial U}{\partial\alpha} = \frac{P^2 L}{2EA}\left(\frac{-2\cos^3\alpha\sin^3\alpha - 2\cos^5\alpha\sin\alpha + \sin^3\alpha - 2\sin\alpha\cos^2\alpha}{\cos^2\alpha\sin^4\alpha}\right) = 0 \qquad 5$$

Solving this Equation will result in:

$$(\cos\alpha - 0.5)(\cos\alpha + 1)^2 = 0 \qquad \textbf{6}$$

The optimal shape of the truss structure will have $\alpha = 60^0$ from the first root of the above Equation. Another way of solving this problem is by numerical method. Let the displacement for the connecting node in the vertical direction be denoted as v while the displacement in the horizontal direction is u. The total potential energy of the truss structure can be obtained as:

$$\begin{aligned} U_{pot} &= \frac{1}{2}\sigma_1\varepsilon_1 Vol_1 + \frac{1}{2}\sigma_2\varepsilon_2 Vol_2 - Pv \\ &= \frac{1}{2}E\varepsilon_1^2 AL + \frac{1}{2}E\varepsilon_2^2 A\frac{L}{\cos\alpha} - Pv \\ &= \frac{E}{2L^2}u^2 AL + \frac{E}{2L^2}\left(u\cos^2\alpha + v\sin\alpha\cos\alpha\right)^2 A\frac{L}{\cos\alpha} - Pv \end{aligned} \qquad \textbf{7}$$

Taking the first and the second derivative of the total potential energy with respect to the displacements u, v and the angle α will produce the following system of Equations (see [29]):

$$\begin{pmatrix} \frac{\partial^2 U_{pot}}{\partial u^2} & \frac{\partial^2 U_{pot}}{\partial u\partial v} & \frac{\partial^2 U_{pot}}{\partial u\partial\alpha} \\ \frac{\partial^2 U_{pot}}{\partial v\partial u} & \frac{\partial^2 U_{pot}}{\partial v^2} & \frac{\partial^2 U_{pot}}{\partial v\partial\alpha} \\ \frac{\partial^2 U_{pot}}{\partial\alpha\partial u} & \frac{\partial^2 U_{pot}}{\partial\alpha\partial v} & \frac{\partial^2 U_{pot}}{\partial\alpha^2} \end{pmatrix} \begin{pmatrix} \Delta u \\ \Delta v \\ \Delta\alpha \end{pmatrix} = \begin{pmatrix} \frac{\partial U_{pot}}{\partial u} \\ \frac{\partial U_{pot}}{\partial v} \\ \frac{\partial U_{pot}}{\partial\alpha} \end{pmatrix} \qquad \textbf{8}$$

The first and second Equations represent the spatial contribution while the third gives the material contribution. A coupled solution is a one time step solution where the spatial and material Equations are solved together. This coupled system of Equations can be solved with the Newton-Raphson scheme. A decoupled solution consists of two substeps where the spatial Equations are solved first followed by solving the material Equations. The result for $E = 10000$, $L = 100$ and an initial angle $\alpha = 45^0$ gives an optimal shape of the truss structure of $\alpha = 60^0$, $u = -\sqrt{3}/3$ and $v = 3$.

In this report a computational solution will be presented using the imposed material force in a hyperelastic setting. The results will be compared with the above analytical solution. The new method has the advantages over size, topology and previous shape optimisation methods for being able to reach a global solution, being firmly rooted in continuum mechanics and providing a solution within one step instead of two substeps. The method has been demonstrated for a plane truss structures using the generated material force [25, 29]. The method will be extended to three-dimensional space and inequality constraints will be applied.

An example of two substeps problem and inequality constraint on large displacement with the objective of energy minimisation is by M. Ohsaki. [30] (2003). It has been shown that an optimal solution satisfying the inequality constraint cannot be found if the specified displacement is too large. The advantages of this new material force optimisation method in providing a coupled solution will help in constraining the solution in one step. Thus the inequality constraint will be applied simultaneously on the spatial and the material Equations. This will give a better constraint solution than previous constraining methods due to the accuracy provided by the coupled solution.

1.2.2 Combined truss optimisation methods

A lot of work has been done on simultaneous shape, cross section and topology of truss structures. On simultaneous shape and cross section optimisation, we already mentioned the work by L. Gil and A. Andreu [21] (2001) and more recently by A. Kaveh. and V. Kalatjari. [31] (2004). The latter authors used new generic algorithms to avoid local optima. The objective was to minimise the weight of the truss structure. This was carried out in two stages. The first stage was to keep the shape of the truss structure fixed while optimising the cross section of the bars using the force method rather than the displacement method. The second stage was to find the optimum shape of the truss structure by Generic Algorithm keeping the cross section fixed. This procedure was repeated in search for improved optimum. The disadvantages were that a large number of iterations are required and due to the arbitrariness of these methods the solutions failed to converge to a global optimum. Other works by O. Hasancebi and F. Erbatur [32] (2002) take into account size, shape and topology as the design variables using simulated annealing algorithm. The work has been carried out to optimise complex space truss structures with emphasis on topology optimisation. The simulated annealing algorithm like other search algorithms such as generic algorithm avoids a gradient-based search to reduce the possibility of ending with a local optimum solution. Other work that combines the cross section, topology, and shape optimisation carried out is due to P. Martinez, et al. [33] (2006). The optimisation process is carried out using the growth method, which consists of five steps. The first step is to specify the location of the loads, boundary conditions, material properties and the space that occupies; the second step is to carry out topology and size optimisation; the third is for shape optimisation; fourth for optimality verification and the final step is for topology growth. These steps will be repeated till the number of iterations reaches a specified maximum limit. The calculations were carried out on a cantilever beam. The result shows good agreement with the analytical result.

Although these methods were successful in improving the optimum solution, they failed in finding a global solution due to their arbitrariness, their computational cost is usually high, a multistep solution is often required and

they lack a firm theoretical background that the material force method possesses.

The use of the material force in optimisation is not new and is not limited to the shape optimisation of truss structures. The idea of material force comes from the creation of non-smooth stress field due to material inhomogeneities. The earliest work on material inhomogeneities dates back to the work done by Eshelby [34] (1951). The work presents the theory of forces acting on imperfections such as dislocations in a stressed crystal lattice. A particular case, which has been the focus, is the force on a singularity in elastic setting. This force was calculated from the difference between the elastic field quantities surrounding the singularity in an infinite medium and those actually present. In [35] (1975) J. D. Eshelby has derived a general formulation for an energy momentum tensor in nonlinear elastic setting. Integrating the normals of this new energy momentum tensor over a closed surface will result in the force on defects and inhomogeneities. In this work J. D. Eshelby made attempts to relate the energy momentum tensor in Eulerian coordinates to the force on defects (material force). The spatial and material settings of continuum mechanics are related to the Lagrangian and Eulerian description and consequently to arbitrary Lagrangian Eulerian A.L.E formulations.

1.3 Arbitrary Lagrangian Eulerian Formulation.

In general there are two main approaches to describe the continuum behaviour; namely, the Lagrangian and the Eulerian descriptions. The Lagrangian description is employed extensively in solid mechanics where the calculations follow the motion of the material and the finite element mesh coincides with the same set of material points throughout the computations. As a result, when the material deforms the mesh deforms with it. In this case there is no material motion relative to the convected mesh. This will give an exact displacement of each material particle, which is an important property in tracking motions in solid mechanics. Another important property of the Lagrangian formulation is mass conservation. This is satisfied since each element of the mesh always contains the same amount of mass.

Since the motion of the material points coincides with the mesh motion, this will provide another advantage for the Lagrangian description: that of the simplicity of the governing Equations and the accuracy of defining its material properties, boundary conditions and stress-strain states. The disadvantage of the Lagrangian description is that the mesh can become distorted under large deformation resulting in a reduction in accuracy and smaller time steps are required. Another disadvantage of the Lagrangian formulation is the difficulty in providing solutions for fluid mechanics problems. Unlike solid particles, the fluid particles are not cohesive and as a result they do not stay close to each other. It will be difficult even for a very fine mesh to map the motion of the

particles as they flow in different directions independently and away from each other. This will result in excessive mesh distortion and severe overlapping problems.

The Eulerian description is preferable in fluid mechanics due to the reasons mentioned above. In the Eulerian formulation the mesh will be kept fixed in space while the material particles flow though it. Although this property will prevent any overlapping and distortion of the mesh, it raises numerical difficulties due to the convective effects between the flow of material and the fixed mesh. Additional measures are required to be taken for the material interfaces and boundaries that may move through the mesh. Also mass conservation must explicitly be taken into account through measuring the flux in and out of each part of the mesh.

In engineering many problems cannot be handled either with Lagrangian nor with the Eulerian description such as contact, penetration, impact and fluid-structure interaction problems. The ALE (stands for Arbitrary Lagrangian Eulerian) description was developed to overcome these difficulties encountered by the Lagrangian description and the Eulerian description. In solid mechanics, the ALE description usually consists of two substeps; the first substep is purely Lagrangian where the mesh motion is neglected and the Equations of mechanics are solved, the second substep is purely Eulerian where the mesh motion is determined and the state variables are transferred from the old mesh positions to the new mesh positions (convection). It is an important method to deal with problems undergoing large deformations. It allows the mesh to track the material to some extent or acceptable limit usually given as an admissible aspect ratio of the elements. This Lagrangian stage will continue while the mesh deforms up to that acceptable point and behind that point another stage will start adjusting the mesh. This adjustment is carried out through remeshing the deformed parts of the mesh while measuring the flux of the material for the adjusted parts of the mesh. Although the arbitrary Lagrangian Eulerian formulation has advantages, unresolved issues are to which extent the mesh is allowed to deform before remeshing starts, how often this remeshing should be carried out, and how much flux to allow. Moreover the method requires more complex formulation for the remeshing stage and it is computationally more expensive than the Lagrangian and Eulerian methods.

The early work in the field of ALE using the finite element method for compressible, inviscid flows was by T. Belytschko et al. [36] (1978) and J. Donea et al. [37] (1979) on fluid-structure interaction problems. These works present the independent motion of the mesh from the material motion. The boundary nodes remain on the boundary and the interior elements describing the flow remain undistorted. T. J. R. Hughes et al. [38] (1979) established the theoretical framework for mixed Lagrangian-Eulerian finite element description. The work focused on fluid-structure interaction for incompressible,

viscous flows. Donea et al. [39] (1982) have carried out work on two dimensional non-linear fluid structure interaction problems subject to transient dynamic loading. The A.L.E. finite element formulation representing the fluid structure coupling was presented. The material behaviour of the structure is given by strain rate dependent elastic-plastic constitutive model and the use of automatic motion of the hydrodynamic mesh. The flow of a compressible inviscid fluid is represented with an A.L.E. formulation where the fluid mesh was chosen completely independent from the movement of the fluid itself. In this work special attention is paid to the treatment of interfaces involving sharp corners. Similar work has been conducted by T.J.R. Hughes et al. [40] (1981) and T.J.R. Hughes et al. [41] (1983) on developing A.L.E finite element formulation for fluid-structure interaction. These works are an extension of previous work [38] on incompressible viscous flows.

In the last decades fluid-structure interaction has been an important field of research for arbitrary Lagrangian Eulerian methods. The A.L.E. method was more efficient in combination with either the Eulerian or Lagrangian method. For example, the interaction between the fluid and structure were modelled with A.L.E method, the fluid away from the structure by the Eulerian method and structure away from the fluid by the Lagrangian method. In this framework the mesh representing the Eulerian part does not need to deform and the fluid will pass through it while the A.L.E method representing the fluid part near the structure will overcome the difficulties of the Eulerian representation.

The A.L.E method had not only many advantages for fluid structure interaction problems but also in simulating purely solid mechanics problems. In (1986) W.K. Liu et al. [42] introduced an A.L.E framework for path-dependent materials. The geometrical and material non-linearity was included. An explicit finite element procedure was used to provide the solution for the non-linear A.L.E setting. In other words an explicit time integration algorithm was provided for the continuity, the momentum and the energy Equations. Also special attention was paid on providing a solution for the stress update procedure. Since mesh points do not coincide with material points in A.L.E setting, in path dependent materials such as elastic-plastic materials the stresses must be convected. These stresses can be convected with the relative velocity between the material and the mesh. Other internal variables should be convected in a similar manner. A one-dimensional example was presented for an elastoplastic wave propagation problem. Moreover, upwind techniques were used to obtain the nodal values of the stresses and the state variables from their values in the quadrature points. The upwind technique is a particular case of the artificial viscosity technique (streamline upwind) for the one-dimensional case.

A total form of arbitrary Lagrangian Eulerian finite element method for large deformation was introduced by T. Yamada and F. Kikuchi [43] (1993). The formulations were introduced for incompressible hyperelastic materials such

as rubber like materials. The formulation was restricted to the plane strain case and an problem-specific mesh motion was included. A comparison has been made between the Lagrangian method and the developed A.L.E method for different examples; the results show an improved mesh quality under large deformation for the A.L.E method compared to the Lagrangian method. Also in the Lagrangian calculation the initial mesh has to be chosen very carefully to obtain results under large deformation while much less care is needed for the initial choice of the mesh in the case of A.L.E method. The work shows difficulties in the choice of an appropriate node relocation strategy in the general case.

This has been followed by A. Huerta and F. Casade [44] (1994) in non-linear path dependent materials for fast transient solid dynamics setting. The computational cost of the presented A.L.E approach was competitive to the Lagrangian approach. This has been realised through use of an explicit stress update scheme for the A.L.E approach. As has been mentioned earlier, in many cases the A.L.E approach is the only way to provide solutions to many solid mechanics problems like impact, coining or forming analysis, but the computational cost is often much higher than the Lagrangian method. The use of an explicit integration scheme instead of implicit integration scheme for the stress update procedure reduces the computational cost dramatically. This has not been done without a price, as it is well known that explicit integration schemes provide less accurate solution then an implicit integration schemes. The accuracy of the explicit calculations can be improved by taking smaller steps. The work demonstrates the applicability and advantages of the new A.L.E approach over those obtained under similar conditions using the Lagrangian formulation. This has been shown for a one-dimensional bar under impact, a bar under tension and for simulating forming process. In these cases the Lagrangian formulation suffers from excessive element distortion while the A.L.E allows a regular element size distribution.

More recent work from A. Rodriguez-Ferran et al. [45] (2002) focussed on A.L.E formulation for hyperelastoplasticity. The work is an extension of previous works on hypoelastic-plastic models. In hypoelastic materials the stress rate should be objective and related to an objective rate of deformation. This is a requirement in order to satisfy the principle of material frame indifference. The advantage of using hyperelastic models is that the stored energy (potential) is function of principal invariants of the Cauchy-Green deformation tensor. As a result the material laws (constitutive relations) derived from the potential function will already satisfy the objectivity requirement (frame indifference).

The hyperelastoplastic formulation was introduced in updated form rather than the total form. This means that the last converged deformed configuration is used as a reference. The paper presents a stress based A.L.E hyperelastoplastic algorithm and compares it to the Lagrangian algorithm. The proposed A.L.E algorithm consists of three steps: a purely Lagrangian step is

taken first where the motion of the material particles were accounted for. This will be followed by a remeshing step where the nodes are relocated to improve the quality of the spatial mesh. A final step is to convect the internal variables from the old mesh to the new mesh. This multistep procedure for the A.L.E governing Equations is usually called fractional step method. In this fractional step method an initial purely Lagrangian step is implemented while neglecting the convective terms and a correcting step of convection follows the remeshing step. Different numerical examples were carried on necking, coining and compaction tests. The conclusions from these examples were that the developed A.L.E method can keep mesh distortion under control compared to the Lagrangian method. This gave the A.L.E description a better quality of numerical solution compared to the Lagrangian description.

F. Armero and E. Love [46] (2003) presented an alternative hyperelastoplasticity framework in static and dynamic settings. The A.L.E formulation is presented in total form and can be considered as an extension of [43]. The difference from the updated formulation mentioned above is that the spatial and the material motion will be measured with respect to the same original reference mesh. In contrast to the previous method, this will require not only a control on the spatial displacement but also on the material displacement. These controls were carried out to avoid mesh distortion in the material and spatial domain. An advantage in total hyperelastic formulation is that no convection is required compared to the updated form. In total hyperelastoplastic formulation the internal plastic variables need to be convected irrespective of whether a total or an updated formulation is chosen. Another advantage of the total ALE hyperelastic or hyperelastoplastic is the possibility of a coupled solution where the spatial and material Equations can be solved simultaneously. In the work presented by F. Armero and E. Love the total A.L.E solution was implemented in a staggered form. This means that the Lagrangian and Eulerian solutions were considered in different phases. The staggered solution of the proposed A.L.E hyperelastoplastic total form consists of a smoothing phase, an advection phase and a Lagrangian phase. In the smoothing phase the distortion of the spatial mesh is avoided through the redefinition of new smoothed spatial displacement. The A.L.E kinematics is given here again in Figure 2 for convenience [46]:

$$\tilde{\varphi} = \tilde{\Phi}^{-1} \quad \text{and} \quad \overline{\Phi} = \overline{\varphi}^{-1}$$

The symbols φ, $\tilde{\Phi}$ and $\overline{\varphi}$ represents the physical, material and spatial motions respectively. The physical motion of a solid is decomposed as follows:

$$\varphi = \overline{\varphi} \circ \tilde{\Phi}^{-1} \qquad \textbf{9}$$

The spatial position x can be given in term of the material position X as:

$$x = \varphi(X) \qquad \textbf{10}$$

The deformation gradient as shown in Figure 2 can be given as:

$$F = \overline{F}\tilde{f}^{-1} \qquad \textbf{11}$$

where F represent the total deformation gradient, $\overline{F}$ represent the deformation of the spatial mesh with respect to the reference points and $\tilde{f}$ represent the deformation of the material particles with respect to the reference points.

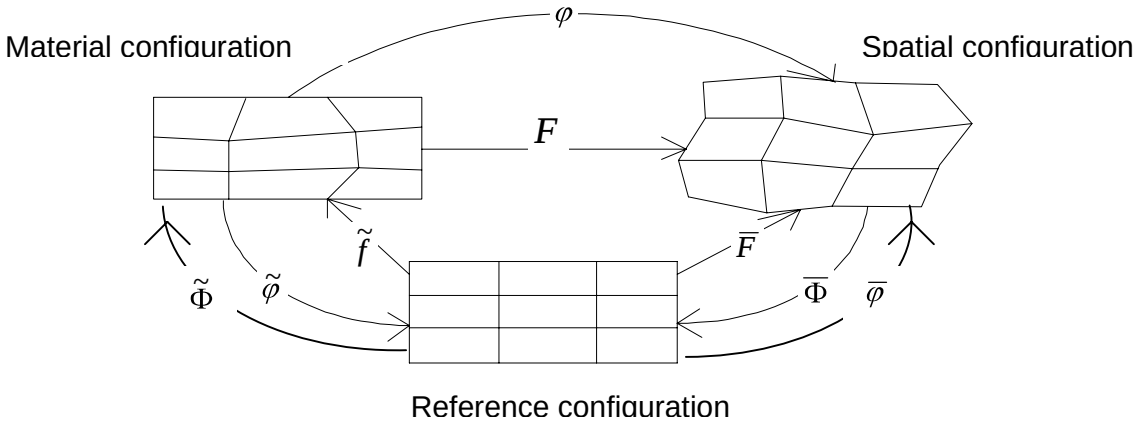

Figure 2 Referential, material and spatial configurations.

In the smoothing phase the total deformation (physical deformation) will be kept fixed while smoothening the spatial and material mapping. In other words and in terms of the symbols given in Figure 2 this smoothing phase can be written as:

$$\varphi = \overline{\varphi} \circ \tilde{\Phi}^{-1} = \varphi'' \circ \Phi'' \qquad \textbf{12}$$

where φ'' and Φ'' are the spatial and material smoothed mapping respectively. This spatial and material mesh smoothing process can be defined in terms of the partial derivative of the potential energy with respect to the corresponding deformation gradient, that measures the distortion of the spatial or material mesh with respect to the reference mesh while keeping the deformation of the material or spatial mesh with respect to the reference mesh fixed respectively. This smoothing procedure will provide a new material mapping, which will produce the advection phase for the internal plastic and dynamic variables. These variables have to be advected to account for the effects of the material time derivative due to the new material mapping. In other words, since the material mapping was fixed during the Lagrangian phase, the advection of these variables can only take place after the new material mapping has been obtained in the smoothing phase. The Lagrangian phase will follow the advection stage where the governing Equations will be solved for a new spatial mapping while keeping the material mapping fixed. Hence, this phase

will be a purely Lagrangian phase where the calculations ends with an updated deformation state. F. Armero and E. Love introduced this formulation in quasi-static as well as a dynamic setting. In the dynamic setting the standard Newmark scheme was used to solve the balance Equation. A mixed variational finite element formulation has been used which allows for separating the volumetric strain and the pressure.

Their paper presents examples on a plane strain tension test and on the necking of a circular bar in quasi-static setting. The calculations were carried out for different smoothing ratios and compared to the Lagrangian solution. The result shows an improvement in the mesh quality as the smoothing ratio increases. As a result this will improve the obtained solution compared to the Lagrangian solution where no smoothing has been used. This improvement is due to the fact that the smoothing process allows distributing the distortion between the spatial and material meshes. Another example presents the A.L.E formulation in dynamic setting involving a circular bar under impact. The results show good agreement with the experimental results.

Although previous methods were able to improve the quality of the finite element mesh in different settings as well as the accuracy of the solution, these methods were arbitrary and limited. The arbitrariness of the mesh movement is due to the fact that the mesh motion is user defined and the solution is limited to two dimension in most cases due to the complication of developing the necessary Equation for the mesh motion in the three dimensional case. As we mentioned earlier different solutions were obtained for different levels of mesh smoothening. The amount of smoothening usually depends on different factors which are difficult to predict. It depends on the setting of the problem at hand, the sort of discontinuity, load and boundary conditions, etc.

The methods for eliminating discretisation errors were not limited to relocation of nodes (R adaptivity) where the same number of degrees of freedom and element connectivity is maintained. Other mesh adaptive techniques such as H adaptivity and P adaptivity have more capability than R adaptivity in obtaining a smoothed solution. H adaptivity was easier to implement compared to R adaptivity, the connectivity of the elements as well as the total number of the degree of freedom may change while the polynomial degree of the shape functions remains the same. P adaptivity has the fastest rate to smoothen the solution by changing the polynomial degree for the shape functions, which result in changing the total number of degree of freedom. P adaptivity is difficult to implement and is computationally the most expensive one, which were the reasons of being not popular. H adaptivity is more effective then R adaptivity and less expensive than P adaptivity for problems concerned with two dimensions. A comprehensive treatment, comparison and implementation of these strategies for different settings can be found in the work by H. Askes [47] (2000). The work introduced a new non-linear formulation for relocation of the nodes for two-dimensional problems. Z. Uthman [48] (2002) performed another study of R adaptivity, which was an

extension of the work carried out by H. Askes. The work was carried out on convex as well as non-convex systems in two dimensions. The works present the capability of R adaptivity based on different error measures in eliminating pure discretization errors. Although it shows the shortcoming of this strategy in dealing with singularities in linear elastic setting, it shows the effectiveness of the H adaptive strategy in containing these discontinuities. The work presents a new algorithm for H adaptivity based on different error assessment. An example [48] of R adaptive and H adaptive strategies is shown in Figure 3. The results are shown through different iterations. The numbers show the critical singular locations where the meshes intensify around in H adaptivity or relocated towards these locations in R adaptivity.

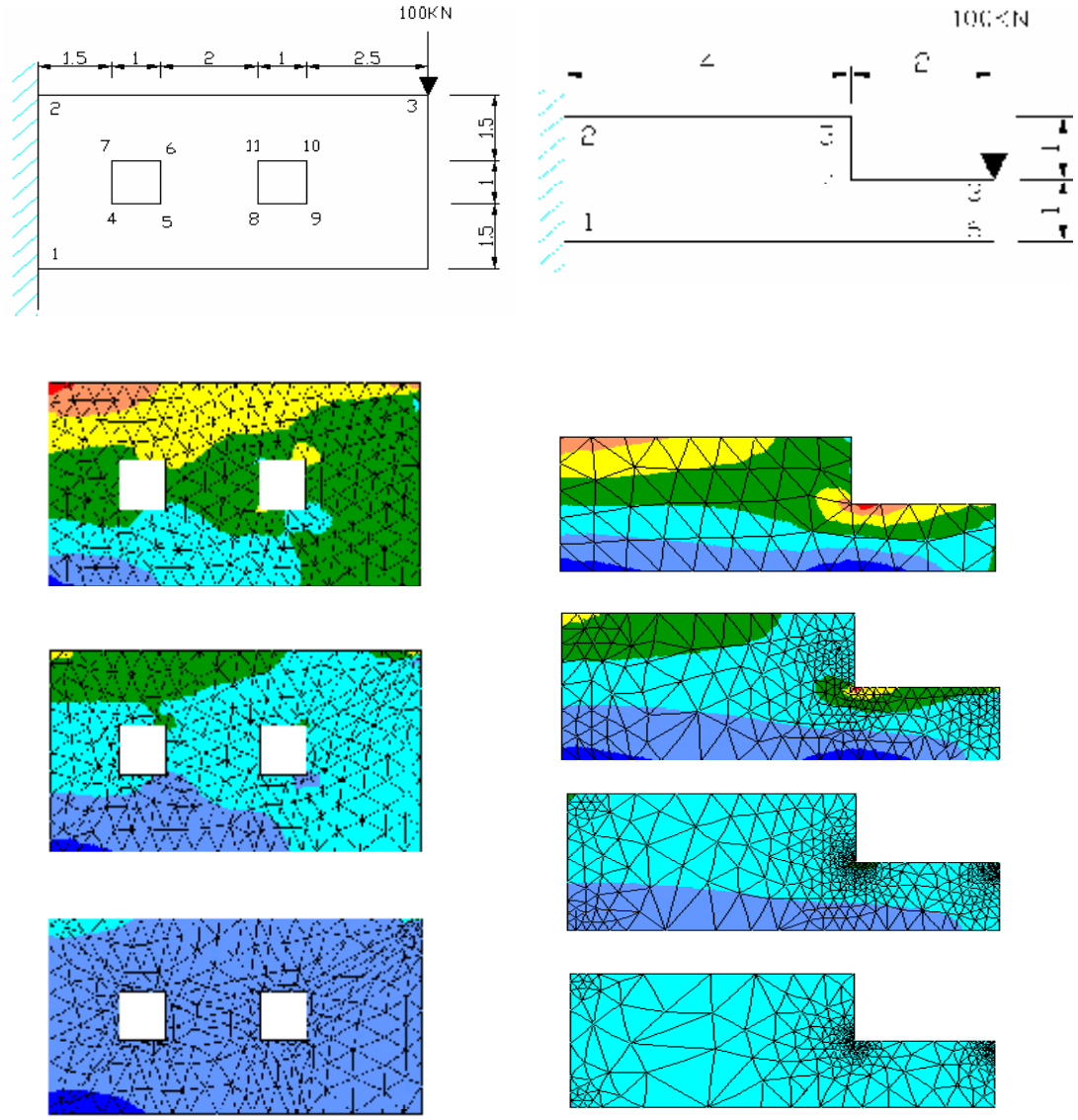

Figure 3 R-adaptivity iterations left and H-adaptivity iterations right

As can be seen the elements are added and removed based on error estimation to reach a smoothed solution with an optimum mesh. More recent work on R [27] and H [49] adaptivity make use of material forces. The works were carried out by R. Mueller, D. Gross and G. A. Maugin where the magnitude of the material force that results from finite element discretisation has been used as an indicator for mesh refinement. As was mentioned earlier the early work focused on the r-adaptive strategy in hyperelastic setting. The later work makes use of an H adaptive strategy in hyperelastic setting. The new procedure was tested on different examples where high gradients (singularities) can be observed. The conclusion was that only a relative reduction of the error in the material force balance can be achieved. The work also extends the formulation from static to a dynamic setting.

1.4 Physical versus inverse motion

The material force application is not limited to mesh optimisation. The material force can be a result of discontinuities resulting from discretisation by the finite element mesh, as it was explained above, but it can also be related to the J integral for fracture in elastic setting. G. A. Maugin [50] (1993) has established this relation and developed a new variational principle in the material domain. Material inhomogeneities due to brittle hyperelastostatic fracture mechanics have been described in detail in terms of the material force (1995) [51]. More recently, the work by P. Steinmann [52] (2000) introduces a reformulation of the material force application for hyperelastic fracture mechanics. The main aspect of that work was the introduction of the balance Equation in the material domain based on the inverse motion. The motion and the inverse motion are shown in Figure 4.

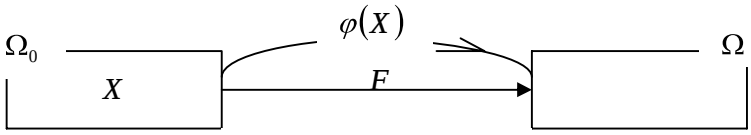

The physical motion

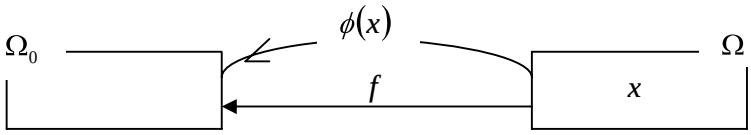

The inverse motion

Figure 4 The physical and inverse motion.

The physical and inverse motion can be given respectively as:

$$x = \varphi(X) \qquad \textbf{and} \qquad X = \phi(x) \qquad \textbf{13}$$

where x, X are the placements of the material particles in the spatial and material configurations respectively, Ω, Ω_0 are the spatial and material configurations, $\varphi(X)$ is the non-linear spatial deformation map in terms of the placement X of the material particles in the material configuration, $\phi(x)$ is the non-linear material deformation map in term of the placement x of the same material particles in the spatial configuration. The deformation gradients can be defined as:

$$F = \frac{\partial x}{\partial X} \qquad \text{and} \qquad f = \frac{\partial X}{\partial x} \qquad \textbf{14}$$

where F is the spatial or physical deformation gradient and f is the material or inverse deformation gradient, i.e.

$$f = F^{-1} \quad \text{and} \quad F \cdot f = I \tag{15}$$

This direct and inverse motion provide a strong duality for the hyperelastic stress measures and the quasi-static balance Equations in the physical and material configurations. The framework is straightforward. The J integral results from elementary equilibrium consideration in the material configuration. As a result no assumption is required to present the energy change. Further, these derived quasi-static balances of physical and pseudomomentum Equations are related to appropriate variational setting, which give the method a solid theoretical background. Another important aspect of the direct and inverse motion is that the volume forces and surface tractions are already known not only for the physical domain but also for the material domain. In other words, in all previous works the material forces were obtained after solving the physical motion; this is not the case any more since both motions can be initially obtained.

This inverse motion did not only provide a new platform for hyperelastic fracture mechanics but also for hyperelastodynamics, thermo-hyperelastodynamics, hyperelastostatic crystal defects by P. Steinmann [53, 54, 55] (2002) and on thermo-hyperelastodynamics for open systems by E. Kuhl and P. Steinmann [56] (2003]. Since the focus of this work will be on hyperelastodynamics closed setting and the kinematics introduced by the inverse motion, a short review of the work by P. Steinmann is appropriate.

1.5 Paul Steinmann's work

The work begins by presenting the geometric non-linear kinematics of the spatial and material motion problem. The spatial motion represents the Lagrangian viewpoint where the material placement is fixed, and the material motion represents the Eulerian viewpoint where the spatial placement is fixed. In the spatial configuration the standard kinematics of the Lagrangian formulation is recovered. The linear tangent map associated with the spatial motion deformation map is given as (Figure 4):

$$F = \nabla_X \varphi(X,t) = \nabla_X x \tag{16}$$

and its Jacobian as:

$$J = \det F \tag{17}$$

The right and left spatial motion Cauchy-Green strain tensors are given respectively as

$$C = F^t \cdot F \quad \text{and} \quad b = F \cdot F^t \tag{18}$$

The right and left material motion Cauchy-Green strain tensors are given respectively as

$$c = f^t \cdot f \quad \textbf{and} \quad B = f \cdot f^t \tag{19}$$

The kinematics for the spatial and material strain is shown in Figure 5. Furthermore, the spatial velocity is given as the material time derivative D_t of the spatial deformation map at a fixed material placement X as:

$$v = D_t \varphi(X,t) = D_t x \qquad \textbf{20}$$

The material velocity on the other hand is given as the spatial time derivative d_t of the material deformation map at a fixed spatial placement x as:

$$V = d_t \phi(x,t) = d_t X \qquad \textbf{21}$$

The work presents also the relation between the spatial and material motion as follows. The relations between a spatial and material time derivative of scalar or tensorial quantities $\{\bullet\}$ are given as:

$$D_t\{\bullet\} = d_t\{\bullet\} + \nabla_x\{\bullet\}\cdot v \quad \text{and} \quad d_t\{\bullet\} = D_t\{\bullet\} + \nabla_X\{\bullet\}\cdot V \qquad \textbf{22}$$

In both Equations, the second term on the right side represents the convective contribution. Making use of the above relations (13, 14, 20, 21 and 22) and knowing that:

$$D_t \phi(x,t) = 0 \quad \text{and} \quad d_t \varphi(X,t) = 0 \qquad \textbf{23}$$

the relation between the spatial and material velocities can be derived as:

$$V = -f \cdot v \quad \text{and} \quad v = -F \cdot V \qquad \textbf{24}$$

After presenting the kinematics and the relation between the spatial and material motion, the balance of mass, balance of momentum and the balance of mechanical energy in the spatial and material configurations are presented. P. Steinmann gives the relation for the continuity Equation in the material domain in its local form as:

$$D_t \rho_0 = 0 \qquad \textbf{25}$$

ρ_0 is the material density, it is an obvious representation of the traditional viewpoint of mass conservation in a local material domain. Integration over the whole material domain will produce the global continuity Equation:

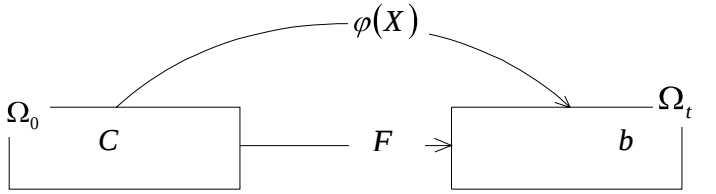

Strain tensor of the spatial motion

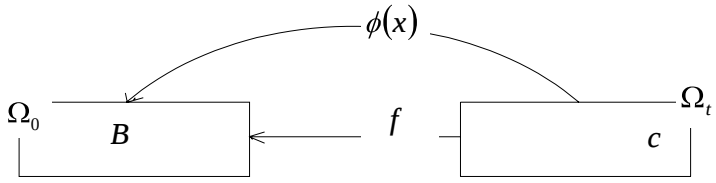

Strain tensor of the material motion

Figure 5 spatial and material strain tensors

$$D_t \int_{\Omega_0} \rho_0 d\overline{V} = 0 \qquad \textbf{26}$$

In the spatial domain the local balance Equation can be given as:

$$d_t \rho_t = -div(\rho_t v) \qquad \textbf{27}$$

where ρ_t is the spatial density. This Equation has been obtained by making use of the transport theorem and the local material continuity Equation (for details see [53]). Integration over the spatial domain and making use of Gauss theorem will produce the global spatial continuity Equation:

$$d_t \int_{\Omega_t} \rho_t d\overline{v} = \int_{\partial\Omega_0} \rho_0 \overline{V} dA_0 \qquad \textbf{28}$$

where dA_0 is a part of the whole material area $\partial\Omega_0$ over which the integration is taken. The next part of the paper presents the derivation of the spatial and material momentum Equation from the Dirichlet principle, as it is well known this variational principle holds for conservative mechanical systems of hyperelastostatic setting. According to the Dirichlet principle, the total potential energy in a hyperelastostatic setting can be given as the sum of the internal energy and the external energy. In the material and spatial configuration the energy densities can be given respectively as [53]:

$$U_0 = W_0(F;X) + V_0(\varphi;X) \quad \text{and} \quad U_t = W_t(f;\phi) + V_t(x;\phi) \qquad \textbf{29}$$

where U_0 and U_t are the material and spatial total potential energy respectively; W_0 and W_t are the material and spatial internal potential energy respectively; V_0 and V_t are the material and spatial external potential energy respectively. A minimum of the total potential energy in the material and spatial domain can be obtained by taking the derivative of the total densities with respect to the dependent variables [53]:

$$0 = DIV(D_F U_0) - \partial_x U_0 \quad \text{and} \quad 0 = div(d_f U_t) - \partial_X U_t \qquad \textbf{30}$$

Here, DIV and div represent the divergence with respect to the material and spatial coordinates; D_F and d_f are the derivative with respect to the spatial and material deformation gradient respectively.

These Equations can be written in different form as follows (see for details [53]):

$$0 = DIV\Pi + b_0 \quad \text{and} \quad 0 = div\pi + B_t \qquad \textbf{31}$$

The above Equations represent the statıc material and spatial local momentum Equation. The symbols Π and π represent the material and the spatial first Piola-Kirchhoff stress tensors respectively while b_0 and B_t are the material and the spatial volume forces densities per unit volume respectively.

The work also presents the Hamiltonian principle for hyperelastodynamic settings in terms of the direct and inverse motion. As it is well known, the

Lagrangian per unit volume is the difference between the kinetic energy per unit volume and the total potential energy per unit volume. The material and spatial Lagrange energies are given respectively as [53]:

$$L_0 = K_0(v;X) - U_0(\varphi,F;X) \quad \text{and} \quad L_t = K_t(V,f,\phi) - U_t(x;f,\phi) \qquad \textbf{32}$$

Here, K_0 and K_t are the material and spatial kinetic energies, which can be given as [53]:

$$K_0 = \frac{1}{2}\rho_0(X)v\cdot g\cdot v \quad \text{and} \quad K = \frac{1}{2}\rho_t(f,\phi)V\cdot C\cdot V \qquad \textbf{33}$$

where g and C are the spatial and material metric tensors, respectively. A stationary point can be found for the above Euler-Lagrange functional Equations as follows [53]:

$$D_t(\partial_v L_0) = \partial_x L_0 - DIV(D_F L_0) \quad \text{and} \quad d_t(\partial_V L) = \partial_X L - div(d_f L) \qquad \textbf{34}$$

These Equations can be worked out to obtain the material and spatial momentum balance Equations in hyperelastodynamics setting (see for details [53]):

$$D_t p_0 = DIV\Pi_D + b_0 \quad \text{and} \quad d_t P_t = div\pi_d + B_t \qquad \textbf{35}$$

where p_0 and P_t are the material and spatial momentum densities respectively, Π_D and π_d are the material and spatial dynamic momentum fluxes respectively. These momentum fluxes were derived in the spatial and material configuration. The corresponding constitutive laws were given in the static and dynamic settings respectively. Also the static and dynamic momentum fluxes in the spatial and material domain were transformed into their corresponding material and spatial representations respectively. The work gives also the derived balance Equations of mechanical energy in the material and the spatial settings. In all these derivations the standard Lagrangian formulation was recovered from the spatial motion problem. Furthermore the strong duality between the spatial and material Equations was illustrated. This can clearly be seen from that all Equations appear twice; upper and lowercase symbols are chosen to highlight their duality.

The direct and inverse motion problems were extended to include biomechanical applications. The derivation of the appropriate framework was carried out by E. Kuhl and P. Steinmann [56] (2003) for the thermodynamics of open systems. The term “open system” as it is well known for allowing to loss or gain in the mass and it makes use of the first and second laws of thermodynamics. The paper illustrates again the duality between the spatial and material balance Equations in thermodynamics setting. Furthermore the relations between the spatial and material fluxes and sources were elaborated.

More recent work couples the spatial and the material Equations in hyperelastic setting are the ones by E. Kuhl et al (2004) [57] and H. Askes et

al (2004) [58]. The Dirichlet variational principle has been used for the development of the spatial and material Equations. The work is based on the direct and inverse motion illustrated previously [52-56]. The total variation of the potential energy is given as the sum of its variation with respect to the spatial coordinates at fixed material positions and it is variation with respect to the material coordinates at fixed spatial positions. This new variation replaces the traditional variation of the total potential energy with respect to a fixed reference configuration and produces a new Eulerian-Lagrangian formulation. As a result of this overall energy minimisation, an optimum location of the nodes can be obtained. In order to clarify this new methodology and due to its importance in our new subsequent development, a short review of the kinematics as illustrated in [57&58] is necessary.

In Figure 2 the mapping $\tilde{\phi}$ between the physical particles in their fixed positions ξ in the referential domain to their material positions X in the material domain is given as:

$$X = \tilde{\phi}(\xi, t) \qquad \textbf{36}$$

and its inverse map is given as:

$$\xi = \tilde{\varphi}(X, t) \qquad \textbf{37}$$

Its referential gradient $\tilde{f}$ with the related Jacobian $\tilde{j}$ are given respectively as:

$$\tilde{f} = \nabla_{\xi} \tilde{\phi}(\xi, t) \qquad \text{and} \qquad \tilde{j} = \det \tilde{f} \qquad \textbf{38}$$

Its inverse referential gradient $\tilde{F}$ with the related Jacobian $\tilde{J}$ are given respectively as:

$$\tilde{F} = \nabla_{X} \tilde{\varphi}(X, t) = \tilde{f}^{-1} \qquad \text{and} \qquad \tilde{J} = \det \tilde{F} = \tilde{j}^{-1} \qquad \textbf{39}$$

In a similar manner the mapping between the referential domain and the spatial domain is given as:

$$x = \bar{\varphi}(\xi, t) \qquad \textbf{40}$$

and its inverse map is given as:

$$\xi = \bar{\phi}(x, t) \qquad \textbf{41}$$

Its referential gradient $\bar{F}$ with the related Jacobian $\bar{J}$ are given respectively as:

$$\bar{F} = \nabla_{\xi} \bar{\varphi}(\xi, t) \qquad \text{and} \qquad \bar{J} = \det \bar{F} \qquad \textbf{42}$$

its inversion referential gradient $\bar{f}$ with the related Jacobian $\bar{j}$ are given respectively as:

$$\bar{f} = \nabla_{x} \bar{\phi}(x, t) = \bar{F}^{-1} \qquad \text{and} \qquad \bar{j} = \det \bar{f} = \bar{J}^{-1} \qquad \textbf{43}$$

The work illustrates the new kinematics in terms of the direct (spatial) motion as a composition of the referential map $\bar{\varphi}(\xi, t)$ and the inverse referential map $\tilde{\varphi}(X, t)$ as follows (see Figure 4):

$$x = \bar{\varphi}(\xi) \qquad \text{and} \qquad \xi = \tilde{\varphi}(X) \qquad \textbf{44}$$

This can be written as:

$$x = \overline{\varphi}\left(\widetilde{\varphi}\left(X\right)\right) \qquad \textbf{45}$$

By which it follows that:

$$\varphi = \overline{\varphi} \circ \widetilde{\varphi} \qquad \textbf{46}$$

The direct motion deformation gradient is given as multiplicative decomposition of the referential gradient $\overline{F}$ and the inverse referential gradient $\widetilde{F}$:

$$F = \nabla_X \varphi(X,t) = \overline{F} \cdot \widetilde{F} \qquad \textbf{47}$$

The Jacobian of the direct deformation gradient can be obtained as:

$$J = \det F = \overline{J}\widetilde{J} \qquad \textbf{48}$$

The new kinematics in term of the inverse motion as a composition of the referential map $\widetilde{\phi}(\xi,t)$ and the inverse referential map $\overline{\phi}(x,t)$ read (see Figure 4):

$$X = \widetilde{\phi}(\xi) \qquad \text{and} \qquad \xi = \overline{\phi}(x) \qquad \textbf{49}$$

This can be written as:

$$X = \widetilde{\phi}\left(\overline{\phi}\left(x\right)\right) \qquad \textbf{50}$$

By which it follows that:

$$\varphi = \widetilde{\phi} \circ \overline{\phi} \qquad \textbf{51}$$

The inverse motion deformation gradient is given as the multiplicative decomposition of the referential gradient $\widetilde{f}$ and the inverse referential gradient $\bar{f}$:

$$f = \nabla_x \phi(x,t) = \widetilde{f} \cdot \bar{f} \qquad \textbf{52}$$

The Jacobian of the inverse deformation gradient can be obtained as:

$$j = \det f = \widetilde{j}\bar{j} \qquad \textbf{53}$$

After introducing the new A.L.E kinematics, the work proceeds by introducing the A.L.E Dirichlet principle for the hyperelastostatic case based on this new kinematics. Thereby the internal and external potential energy per unit volume in the reference domain can be given in terms of its spatial and material representations as follows:

$$\begin{aligned} W_\Diamond\left(\overline{F}, \widetilde{f}; \xi\right) &= \widetilde{j} W_0(F; X) = \overline{J} W(f, \phi) \\ V_\Diamond\left(\overline{\varphi}, \widetilde{\phi}; \xi\right) &= \widetilde{j} V_0(\varphi; X) = \overline{J} V(\phi; x) \end{aligned} \qquad \textbf{54}$$

where $W_\Diamond$ and $V_\Diamond$ are the internal and external potential energy per unit volume respectively in the reference domain. In a similar manner the total potential energy density $U_\Diamond$ per unit volume in the reference domain can be expressed in terms of its material and spatial representations as follows:

$$U_{\Diamond}\left(\overline{F},\widetilde{f},\overline{\varphi},\widetilde{\phi};\xi\right)=\widetilde{j}U_0\left(F,\varphi;X\right)=\overline{J}U\left(f,\phi;x\right) \quad \textbf{55}$$

The potential energy density per unit volume in the reference domain can also be given as the sum of the internal and external energy density in the reference domain. The total energy ℓ of the conservative mechanical system can be obtained by integrating the potential energy density over the reference domain as:

$$\ell\left(\overline{\varphi},\widetilde{\phi}\right)=\int_{\Omega_{\Diamond}}U_{\Diamond}d\overline{V}_{\Diamond} \quad \textbf{56}$$

where $d\overline{V}_{\Diamond}$ is the volume differential element. As illustrated earlier a vanishing total variation of the total energy $\delta\ell$ gives the optimum location of the nodes:

$$\delta\ell=\delta_x\ell+\delta_X\ell=0 \quad \textbf{57}$$

Thereby $\delta_x\ell$ represents the variation of the total energy with respect to the spatial coordinated at fixed material position, while $\delta_X\ell$ represents the variation of the total energy with respect to the material coordinates at fixed spatial positions. The spatial variation part $\delta_x\ell$ will provide the classical spatial momentum Equation while the material variation part $\delta_X\ell$ will provide the material momentum Equation. The paper derives the momentum fluxes and sources in the spatial and material domain. These correspond to the particular case of a classical compressible Neo-Hooke material.

In order to solve these highly non-linear spatial and material momentum Equations, these Equations are discretised and solved iteratively within the framework of the Newton Raphson scheme. To this end these Equations were linearised, a total linearisation of the total variational Equation is taken with respect to the spatial coordinates at fixed material position plus it is linearisation with respect to the material coordinates at fixed spatial positions as:

$$\Delta\delta\ell=\Delta_x\delta_x\ell+\Delta_X\delta_x\ell+\Delta_x\delta_X\ell+\Delta_X\delta_X\ell \quad \textbf{58}$$

where the symbols δ and Δ give the variation and the linearisation. The above Equation provides coupled spatial and material Equations. This coupling has major advantages over previous traditional A.L.E methods that make use of staggered (decoupled) solution schemes. The work [58] illustrates these advantages through examples applied on the derived spatial and material Equation. The first example focuses on the one dimensional case of a bar clamped at both ends and subjected to uniform body loads. The bar was discretised with two finite elements giving the freedom only for the middle node to move while the other two boundary nodes were fixed. The result shows the effectiveness of the monolithic solution in minimising the potential energy while the optimum location of the node was found. This has been clearly illustrated for different initial positions of the middle node where the same results are obtained in each of these cases within a few iterations. On the other hand the staggered solution shows improvement proportional to an increasing number of increments.

A one increment solution provides the Lagrangian solution because the calculations will involve the spatial Equation only. The staggered solution shows improvement while increasing the number of increments and approaches the monolithic solution above 100 increments. Other examples focus on the multidimensional case of a homogeneous block under tension and bending, in both these examples the decrease in the potential energy was obtained within a few iterations. The work illustrates clearly the movement of the interior nodes in opposite direction to the generated material forces and its resulting reduction of the total energy. The boundary nodes were kept fixed in the material domain avoiding high level of inhomogeneities compared to the interior nodes.

More recent work by E. Kuhl and P. Steinmann [59] (2005) extends the work to hyperelastodynamics. The work introduces a variational arbitrary Lagrangian Eulerian formulation framework based on the Hamiltonian principle. As in the hyperelastic case [57, 58], the total variation is taken as the sum of the variation of the Lagrangian with respect to the spatial coordinates at fixed material position plus the variation of the Lagrangian with respect to the material coordinates at fixed spatial positions. The difference between the Hamiltonian principle for hyperelastodynamics and the D' Alembert principle for hyperelastostatics is the energy density which is given in the former case as the difference between the kinetic energy density and the potential energy density as [59]:

$$L_\Diamond = K_\Diamond - U_\Diamond = K_\Diamond - W_\Diamond - V_\Diamond \qquad \textbf{59}$$

Thereby $L_\Diamond$ and $U_\Diamond$ are the Lagrange and kinetic energy densities per unit volume in the reference domain. The total Lagrangian of the hyperelastodynamics conservative mechanical system is given through integrating the Lagrange density over the reference volume and the time as (59):

$$\ell\left(\overline{\varphi}, \tilde{\phi}\right) = \int_T \int_{\Omega_\Diamond} L_\Diamond dV_\Diamond dt$$

As in the case of hyperelasticity, the paper presents the total variation as the variation of the total Lagrangian (given by the above Equation) with respect to the spatial coordinates at fixed material positions plus its variation with respect to the material coordinates at fixed spatial positions. These variations present the spatial and material balance Equations. Furthermore, the work derives the appropriate spatial and material momentum densities, the dynamic momentum fluxes and the momentum sources.

In this contribution, the same concept of the total variation of the Lagrangian outlined in [59] will be the starting point. The work outlined in this report will differ in terms of the parameterisation of the Lagrangian in the spatial and material domain. The parameterisation of the Lagrangian is given in [59] as:

$$L = L(\varphi, v, F; X) \qquad \text{and} \qquad L_0 = L_0(\phi, V, f; x) \qquad \textbf{60}$$

The above shows that the spatial Lagrangian density is parameterised in terms of the spatial motion mapping, spatial velocity and the spatial deformation gradient while the material Lagrangian density is parameterised in terms of the material motion mapping, material velocity and the material

deformation gradient. The work here will give the spatial Lagrangian density in terms of the spatial velocity only while the material Lagrangian density is expressed in terms of the material velocity. As it will be shown, this will provide a more simplified and straightforward formulation. Furthermore, in contrast to of the work on hyperelastostatic formulation that was based on total formulations [57 & 58], the followed approach here will provide rate formulation. This means that the spatial and material balance Equations will be linearised in time instead of the coordinates.

1.6 Variational methods

In general, the strong form of partial deferential Equation is used for describing the governing Equations in solid mechanics. Although the method is exact, it is limited to solutions for simple mechanical loads and simple geometries. The solution in more complex problems is to obtain the weak form of the partial deferential Equation through weighted residual or as variation of underlying energy (in case these exist). In more complex problems the continuous variational methods are ineffective in solving geometrically complex problems, discontinuities in material properties, in load and in material properties. The finite element method is the solution in these cases where the philosophy of the variational methods can be used to derive solvable Equations. The domain will be divided into sub domains, these sub domains are simple in shape, which allows for functional approximation over. This subdivision can be achieved through a finite number of elements where the stress and displacement distributions can be represented by polynomials.

It was viewed earlier; the static equilibrium Equation in finite element solid mechanics is a result from the D' Alembert variational principle. In the static case the system is characterised by one energy function called the potential energy. The Hamiltonian's principle is an extension of the D' Alembert principle or the principles of virtual displacement to dynamics system of deformable solids. In this case the dynamic system can be characterised by two energy functions, a kinetic energy and a potential energy. The total potential energy can be given as the sum of strain energy and potential energy of external forces. In the static case (bodies involving no motion) the inertial force term is negligible and the forces are applied sufficiently slowly such that the motion is independent of time.

The variational formulation has been applied in a weak form to a wide range of problems. The early work of variational methods is described by Hellinger (1914) where the complementary energy principle for large deformation elasticity was proposed.

In [60] (1961) L. E. Elsgolc reviewed the calculus of variational methods. In general, the direct method has the advantage over analytical variational method in approximating multidimensional solutions. In the limit of some functional optimisation problems using the direct method, the solution will approach the variational problem. L. E. Elsgolc illustrates the difficulties of

solving variational problems and the needs to develop numerical techniques to overcome these difficulties.

The Hamilton principle was first presented as the “Law of Varying Action” by Hamilton [68] (1834). This Hamilton law can be reduced to the Hamilton principle through the conditions of stationary in accordance with the theory of classical mechanics.

Hestenes [67] (1956) introduced Hamilton’s principle as variational principle with the following statement; “One of the important principles in mechanics, commonly known as Hamilton’s principle, is a variational principle”. He continues to give the following statement on particle movement according to his definition of the Hamilton’s principle; “In a conservative field of force, a particle moves so as to minimize (over short intervals of time) the action integral”. This states that the extremals of the action integral give the trajectories of this variational based Hamilton’s principle.

A similar work by [61] (1957) K. Washizu presents the variational principle of elastodynamics from the Hamiltonian principle. It asserts that the variation of a specified functional over a set of admissible states vanishes at a certain state if and only if that state meets the field Equations and boundary conditions and to assume a given displacement distribution at the initial as well as at a later instant.

In the sixties the variational problems were extended to the nonlinear geometrical case. The variational problem was given as that of integrating the motion Equations of the geometrically nonlinear theory of elasticity with given boundary conditions. This was illustrated by L. Ya. Ainola [69] (1961) and Y. Y. Yu. [70] (1964).

A.I. Lurie [82] (2002) gives the following statement on the static and dynamic setting. The static setting of a homogenous chain with fixed ends can be represented with the differential Equations of the chain line obtained from analysis of forces acting on an infinitesimal element of the chain while in his definition of the dynamic setting “another definition is based on the idea that the centre of gravity of the sought-for curve must reach it is lowest position at equilibrium. This implies a variational formulation of the problem in question”.

K. Washizu [62] (1968) presented the variational principle for elastic and rigid-perfectly plastic solids. The possibility of establishing variational energy-principles in terms of stresses and strain rates for van Mises solids was recognised by Drucker [63] (1958). The paper proves the existence of two variational formulas which are somehow analogous to the stationarity theorems for potential and complementary energy of classical elasticity.

In [64] (1980) S. J. Lee and R. T. Shield developed a variational principle of the complementary energy for finitely deformed elastic bodies. The principle can be used in conjunction with the potential energy principle to provide bounds on the potential energy.

1.7 Hamilton principle

A short review of the Hamiltonian principle as illustrated by A.I. Lurie is important for subsequent development of A.L.E hyperelastodynamics setting. This is the original basic Hamiltonian principle given in the spatial domain as illustrated earlier. A closer review at the analytical derivation of this well known principle for varied path of coordinates describing the real motion of the material system gives the following variation of the kinetic potential (Lagrangian):

$$\delta L = \sum_{i=1}^{n}\left(\frac{\partial L}{\partial x_i}\delta x_i + \frac{\partial L}{\partial v_i}\delta v_i\right) \qquad \textbf{61}$$

Thereby the chain rule has been used with respect to the dependent variables (the spatial coordinates x_i and the spatial velocities v_i). Next, two arbitrary time instants t_0 and t_1 are selected where the motions are fixed:

$$\delta x_i(t_0) = 0 \quad \delta x_i(t_1) = 0 \qquad (i = 1,.....,n) \qquad \textbf{62}$$

The Hamilton's action over the time interval is given as:

$$\ell = \int_{t_0}^{t_1} L dt \qquad \textbf{63}$$

The increment or the variation in Hamilton's action can be written as:

$$\ell + \delta\ell = \int_{t_0}^{t_1}(L + \delta L)dt = \int_{t_0}^{t_1} L dt + \int_{t_0}^{t_1}\delta L dt \qquad \textbf{64}$$

With the help of the local variational Equation of the kinetic potential, the above Equation can be written as:

$$\delta\ell = \int_{t_0}^{t_1}\sum_{i=1}^{n}\left[\frac{\partial L}{\partial x}\delta x + \frac{\partial L}{\partial v}\delta\dot{x}\right]dt \qquad \textbf{65}$$

Integration by parts and talking into account the additional conditions given above will result into:

$$\int_{t_0}^{t_1}\frac{\partial L}{\partial v}\delta\dot{x}dt = \frac{\partial L}{\partial v}\delta x\Big|_{t_0}^{t_1} - \int_{t_0}^{t_1}\delta x\frac{d}{dt}\frac{\partial L}{\partial v}dt = -\int_{t_0}^{t_1}\delta x\frac{d}{dt}\frac{\partial L}{\partial v}dt \qquad \textbf{66}$$

Thus the variation in action is given as:

$$\delta\ell = \sum_{i=1}^{n}\int_{t_0}^{t_1}\left(\frac{\partial L}{\partial x} - \frac{d}{dt}\frac{\partial L}{\partial v}\right)\delta x dt \qquad \textbf{67}$$

A review of the Hamilton's variational principle in more details is given by A.I. Lurie [82].

1.8 Inequality variational principle

The variational principles were not restricted to equality formulations. As it is well known, plasticity can be written as an inequality variational principle. This can be formulated in either stress or strain space. C. Johnson [65&66] (1976) adopted this framework in a strain based formulation and proved the existence of an exact solution for this variational inequality Equation. A transformation of the inequality variational Equation into equality variational Equation was achieved by introducing a Lagrange multiplier.

Variational inequality theory was first introduced by Hartman and Stampacchia [71] (1966) as a tool for the study of partial differential Equations with mechanical applications. These variational inequalities were infinite-dimensional rather than finite dimensional. Dafermos [72] (1980) makes it possible to apply the variational inequality theory to the finite dimensional case. This methodology opens the door for applications in different problem fields such as engineering, economics, management science, operations research etc.

Variational inequality theory provides us with a tool for formulating a variety of equilibrium problems, qualitatively analysing the problems in terms of existence and uniqueness of solutions, stability and sensitivity analysis, and providing us with algorithms with accompanying convergence analysis for computational purposes. Indeed, many mechanical problems can be formulated as variational inequality problems such as incompressible hyperelastic response, nearly incompressible hyperelastic response, hyperelastoplastic response etc. In all these cases the inequality constraint problem can be reformulated as equality problem or in other words as an optimisation problem. A variational inequality problem can be reformulated as a convex optimisation problem in certain conditions. These are symmetry conditions and the semi definiteness condition for the Jacobian of the function characterising the problem. These conditions are satisfied in certain mechanical settings such as hyperelastostatic, hyperelastodynamics and hyperelastoplasticity. The variational inequality, therefore, is the more general problem in that it can also handle mechanical systems with an asymmetric stiffness matrix. In this report, the concern is with hyperelastic systems, that is, means only systems that satisfy the above conditions and consequently provide a convex optimisation problem. The proof of this convexity for the variational formulation of perfectly plastic and hardening plasticity is given in details by J. C. Simo and T. J. R. Hughes [75] (1997).

1.8.1 Principle of maximum plastic dissipation

An important inequality variational principle results from the principle of maximum plastic dissipation. This variational formulation of plasticity at finite strain provides a finite element approximation often credited to J. C. Simo [73&74] (1988). The work derived a new framework for finite strain elastoplasticity. This enables an extension of J_2 -flow theory to include

hyperelastic response along with a multiplicative decomposition of the deformation gradient.

The principle of maximum plastic dissipation, often credited to von Mises states that, "for given plastic strains ε^p among all possible stresses τ satisfying the yield criterion, the plastic dissipation D^p for perfect plasticity is given by" [75] :

$$D^p\left[\tau;\dot{\varepsilon}^p\right]:=\tau:\dot{\varepsilon}^p \qquad \textbf{68}$$

where $\dot{\varepsilon}^p$ is the rate of the plastic strain. The maximum plastic dissipation is attained for the actual stress σ as follows [75]:

$$D^p\left[\sigma;\dot{\varepsilon}^p\right]:=\underset{\mathrm{E}_\sigma}{MAX}\left\{D^p\left[\tau;\dot{\varepsilon}^p\right]\right\} \qquad \textbf{69}$$

where E_σ represent the closure of the elastic range in the stress space.

The next step is to transform the maximisation problem into a minimisation problem simply by changing the sign as [75]:

$$D^p\left[\sigma;\dot{\varepsilon}^p\right]:=\underset{\mathrm{E}_\sigma}{MIN}\left\{-D^p\left[\tau;\dot{\varepsilon}^p\right]\right\} \qquad \textbf{70}$$

The Lagrangian functional L^p can be obtained through transforming the constraint minimisation problem into an unconstrained problem. This can be done by introducing the Lagrange multiplier γ [75]:

$$L^p\left(\tau,\dot{\delta};\dot{\varepsilon}^p\right):=-\tau:\dot{\varepsilon}^p+\gamma\delta f\left(\tau\right) \qquad \textbf{71}$$

The solution of this problem is given by [75] as:

$$\frac{\partial L^p\left(\sigma,\gamma;\dot{\varepsilon}^p\right)}{\partial\tau}=-\dot{\varepsilon}^p+\gamma\nabla f\left(\sigma\right)=0 \qquad \textbf{72}$$

that satisfies the classical Kuhn-Tucker optimality conditions:

$$\gamma\geq 0,\ f\left(\sigma\right)\leq 0,\gamma f\left(\sigma\right)=0 \qquad \textbf{73}$$

Here f is the yield function and γ is the plastic multiplier. A stress based formulation for plastic hardening materials can also be considered [75] where additional terms defining the internal hardening variables will be included in the principle of maximum dissipation given above. A strain based formulation was also given by J. C. Simo [73&74]. The last formulation will be the basis for subsequent developments of the A.L.E hyperelastoplastic formulation in chapter 5. The above formulation with Lagrange multipliers can be recast as a formulation with penalty parameters. Thus the above transformation can also be viewed as a transformation from constrained optimisation problem to an unconstrained problem by appending a penalisation function of the constraints to the objective function.

1.8.2 Penalty method

The penalty method was introduced by Courant [80] (1943) in the context of the calculus of variations. The idea of the penalty method appeared also in the procedure of the direct differential gradient method [75] (1962). The argument penalty function is used to solve optimisation problems with constraints with faster convergence while adopting gradient techniques [76, 77, and 78] (1969-1972). Since then the penalty method found its applications in constrained variational problems, variational inequality, contact problems in continuum solid and fluid mechanics.

Since the penalty method will have an important role in our subsequent development in inequality constraint truss optimisation and forming the A.L.E hyperelastoplastic settings, a simple example illustrating the concept is important [81]. We consider:

$$\min_{x} \quad \frac{1}{2}(x+1)^2 \tag{74}$$

Subject to the following inequality constraint:

$$x \geq 0 \tag{75}$$

In order to solve this inequality constraint minimisation problem with the penalty method, the inequality constraint is enforced by adding the square of the constraints multiplied by the penalty parameter. The resulting Equation is [81]:

$$\frac{1}{2}(x+1)^2 + \frac{P}{2}\langle -x \rangle^2 \tag{76}$$

Here P is the penalty parameter. It is normally assigned large values to give a significant contribution to the extended unconstrained problem when the inequality constraint value is violated. The brackets in the above extended unconstrained problem are known as Macaulay brackets and are defined as follows:

$$\langle x \rangle = \begin{cases} 0 & x < 0 \\ x & x \geq 0 \end{cases} \tag{77}$$

According to the above definition the minus sign in the Macaulay bracket of the extended unconstrained problem ensures a zero contribution when the constraint is not violated. An illustration of Equation 76 is shown in Figure 6. It is clear that the penalty term becomes active when the condition (Equation 75) is violated. The minimum of the inequality constrained functional problem can be found by differentiating with respect to x:

$$(x+1) - P\langle -x \rangle = 0 \tag{78}$$

In this case it is obvious that the minimum can be found at $x = -0.5$ where the initial value of the penalty parameter is $P = 1$. Since this value violates the constrained condition, the value of the penalty parameter is increased by a factor of 10 until this violation is kept with an allowable tolerance. The Table below gives the corresponding value of x to the increasing penalty parameter.

P=1	P=10	P=100	P=1000	P=10000
$x = -0.5$	$x = -0.0909$	$x = -9.9E-03$	$x = -9.99E-04$	$x = -9.999E-05$

As we can see the results converge to satisfy the constraint requirements. One of the drawbacks of the penalty methods is the non-differentiability of the discontinuity introduced by Macaulay bracket. This will introduce convergence difficulties as outlined by many authors. Nevertheless, the simplicity of the method and lower computational cost provides an ideal method for a complicated A.L.E formulation and its expensive computational cost.

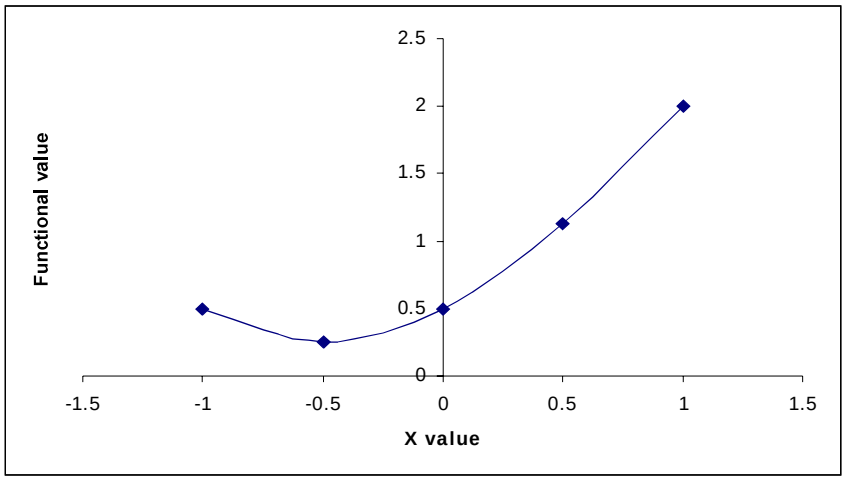

Figure 6 Illustration of penalty function

2 STRUCTURAL OPTIMISATION

2.1 Motivation

The material force method has recently been used in structural optimisation. A new formulation was developed to optimise two dimensional truss structures in static setting [25]. The aim is to generalise the theory in two-dimensional cases with introducing the concept of imposed material force in structural optimisation. As truss structures in engineering practice are normally three dimensional, the existing formulations are also extended from two-dimensional cases to three-dimensional cases.

2.2 Introduction

Recently, a material force based optimisation strategy was extended to the design of truss structures with nonlinear geometric response [25]. The approach searches for an optimal position of the nodes by minimising the total potential energy of the structure. This has been achieved by solving the spatial and material Equations simultaneously. While the first Equation corresponds to a variation of the total energy with respect to the spatial co-ordinates x at fixed material co-ordinates X , the latter gives the variation with respect to material co-ordinates X at fixed spatial co-ordinates x . This total variation is in terms of the A.L.E Dirichlet principle of hyperelastic conservative systems. This total variation is given as [25&29]:

$$\delta\ell = \delta_x \ell + \delta_X \ell = 0 \qquad \textbf{79}$$

The classical compressible Neo-Hooke material has been used, where the spatial energy density is given as:

$$W_t = \frac{1}{4} E\left(F^2 - 1 - 2\ln(F)\right) \qquad \textbf{80}$$

The material energy density is expressed in terms of the inverse deformation gradient f rather than the deformation gradient F , and reads:

$$W_0 = \frac{1}{J} W_t = \frac{1}{4} E\left(\frac{1}{f} - f - 2f\ln\frac{1}{f}\right) \qquad \textbf{81}$$

The first Piola Kirchhoff stress can be derived from Equation (80) as:

$$P = \frac{dW_0}{dF} = \frac{1}{2} E\left(F - \frac{1}{F}\right) \qquad \textbf{82}$$

The analogous material stress tensor can be derived from Equation (81) as:

$$\pi = \frac{dW}{df} = \frac{1}{4} E\left(-F^2 + 1 - 2\ln F\right) \qquad \textbf{83}$$

The total energy of the conservative mechanical system can be found as the integral of its internal energy density over the volume plus the external energy as [25 & 29]:

$$\ell\left(\overline{\varphi}, \tilde{\Phi}\right) = \int_{\Omega_\diamond} W dV_\diamond + V \qquad \textbf{84}$$

The variation of the total potential energy as given in Equation 79 will produce a stationary point:

$$\delta\ell\left(\overline{\varphi}, \tilde{\Phi}\right) = 0 \qquad \textbf{85}$$

The spatial variation of the total potential energy is given as [29]:

$$\delta_x \ell = \int_{\Omega} \nabla_x \delta\overline{\varphi} : P dV + \delta_x V \qquad \textbf{86}$$

This Equation represents the weak form of the spatial momentum Equation obtained form Equations 79, 82, and 84 (see [29] for details). Thereby the term $\nabla_x \delta\overline{\varphi}$ represents the derivative of the variation of the spatial joint position with respect to the spatial coordinates. The weak form of the material momentum Equation is given as [29]:

$$\delta_X \ell = \int_{\Omega_0} \nabla_X \delta\tilde{\Phi} : \pi dV_0 \qquad \textbf{87}$$

This Equation is derived from Equations 79, 83, and 84 (see [29] for details). Thereby $\nabla_X \delta\tilde{\Phi}$ represents the derivative of the variation of the material joint position with respect to the material coordinates. In terms of the linear shape functions $N^i_{\overline{\varphi}}$ and $N^j_{\tilde{\Phi}}$ the discretised spatial and material joint positions are given as [25]:

$$\delta\overline{\varphi}\big|_{\Omega_\diamond} = \sum_{i=1}^{n} N^i_{\overline{\varphi}} \delta\overline{\varphi}_i \qquad\qquad \delta\tilde{\Phi}\big|_{\Omega_\diamond} = \sum_{j=1}^{n} N^j_{\tilde{\Phi}} \delta\tilde{\Phi}_j \qquad \textbf{88}$$

These linear shape functions are given as $N_{\overline{\varphi},\tilde{\Phi}} = \left[1-\xi; +\xi\right]$ and their referential gradient as $\nabla_\xi N_{\overline{\varphi},\tilde{\Phi}} = \left[-1; +1\right]$. Substitution of Equation (88) into the spatial and material variational Equation (86, 87) will result into the following discretized spatial and material Equations respectively [25]:

$$R^I_{\overline{\varphi}}\left(\overline{\varphi}, \tilde{\Phi}\right) = \sum_{t=1}^{m} \nabla_\xi N^i_{\overline{\varphi}} PAn - F^{extI}_{\overline{\varphi}} = 0 \qquad \textbf{89}$$

$$R^J_{\tilde{\Phi}}\left(\overline{\varphi}, \tilde{\Phi}\right) = \sum_{t=1}^{m} \nabla_\xi N^j_{\tilde{\Phi}} PAn - F^{extJ}_{\tilde{\Phi}} = 0 \qquad \textbf{90}$$

Thereby an assembly over all m elements is taken. As in Equation (79) the

total variation will vanish, knowing that the spatial and material variational Equations are independent. This is equivalent to individually vanishing spatial and material residual Equations (89, 90). Thereby $R^{I}_{\overline{\varphi}}$ and $R^{J}_{\widetilde{\Phi}}$ are the spatial and material residuals respectively. These spatial and material residual Equations will be linearised to produce the following Equations [25]:

$$R^{I}_{\overline{\varphi}}{}^{K+1} = R^{I}_{\overline{\varphi}}{}^{K} + \sum_{K=1}^{m} K^{IK}_{\overline{\varphi}\overline{\varphi}} d\overline{\varphi}_K + \sum_{L=1}^{m} K^{IL}_{\overline{\varphi}\widetilde{\Phi}} d\widetilde{\Phi}_L = 0 \qquad \textbf{91}$$

$$R^{J}_{\widetilde{\Phi}}{}^{K+1} = R^{J}_{\widetilde{\Phi}}{}^{K} + \sum_{K=1}^{m} K^{JK}_{\widetilde{\Phi}\overline{\varphi}} d\overline{\varphi}_K + \sum_{L=1}^{m} K^{JL}_{\widetilde{\Phi}\widetilde{\Phi}} d\widetilde{\Phi}_L = 0 \qquad \textbf{92}$$

The linearisation of the spatial Equation (89) was performed by taking its derivative with respect to the spatial coordinates at fixed material position plus its derivative with respect to the material coordinates at fixed spatial positions. This will result in the linearised spatial Equation (89). In a similar way the linearisation of the material Equation (90) was obtained by taking its derivative with respect to the material coordinates at fixed spatial positions plus its derivative with respect to the spatial coordinates at fixed material positions. This will result in the linearised material Equation (90). The tangents terms in Equation (91, 92) are represented here for convenience [25]:

$$\begin{aligned}
K^{IK}_{\overline{\varphi}\overline{\varphi}} &= \frac{dR^{I}_{\overline{\varphi}}}{d\overline{\varphi}_K} = \sum_{t=1}^{m} \nabla_{\xi} N^{i}_{\overline{\varphi}} \frac{dP}{d\overline{F}} An \otimes n \nabla_{\xi} N^{K}_{\overline{\varphi}} + \nabla_{\xi} N^{i}_{\overline{\varphi}} PA \frac{1}{l} \left[\mathrm{I} - n \otimes n\right] \nabla_{\xi} N^{K}_{\overline{\varphi}} \\
K^{IL}_{\overline{\varphi}\widetilde{\Phi}} &= \frac{dR^{I}_{\overline{\varphi}}}{d\widetilde{\Phi}_L} = \sum_{t=1}^{m} \nabla_{\xi} N^{i}_{\overline{\varphi}} \frac{dP}{d\widetilde{f}} An \otimes N \nabla_{\xi} N^{l}_{\widetilde{\Phi}} \\
K^{JK}_{\widetilde{\Phi}\overline{\varphi}} &= \frac{dR^{J}_{\widetilde{\Phi}}}{d\overline{\varphi}_K} = \sum_{t=1}^{m} \nabla_{\xi} N^{j}_{\widetilde{\Phi}} \frac{d\pi}{d\overline{F}} AN \otimes n \nabla_{\xi} N^{K}_{\overline{\varphi}} \\
K^{JL}_{\widetilde{\Phi}\widetilde{\Phi}} &= \frac{dR^{J}_{\widetilde{\Phi}}}{d\widetilde{\Phi}_L} = \sum_{t=1}^{m} \nabla_{\xi} N^{j}_{\widetilde{\Phi}} \frac{d\pi}{d\widetilde{f}} AN \otimes N \nabla_{\xi} N^{l}_{\widetilde{\Phi}} + \nabla_{\xi} N^{j}_{\widetilde{\Phi}} \pi A \frac{1}{L} \left[\mathrm{I} - N \otimes N\right] \nabla_{\xi} N^{l}_{\widetilde{\Phi}}
\end{aligned} \qquad \textbf{93}$$

Thereby, l and L are the spatial and material member lengths given respectively as [25]:

$$l = \left\| \sum_{i=1}^{m} \overline{\varphi}_i \nabla_{\xi} N^{i}_{\overline{\varphi}} \right\| = \overline{F} \qquad L = \left\| \sum_{j=1}^{m} \widetilde{\Phi}_j \nabla_{\xi} N^{j}_{\widetilde{\Phi}} \right\| = \widetilde{f} \qquad \textbf{94}$$

The spatial and material normals are given respectively as [25]:

$$n = \frac{\sum_{i=1}^{m} \overline{\varphi}_i \nabla_{\xi} N^{i}_{\overline{\varphi}}}{\left\| \sum_{i=1}^{m} \overline{\varphi}_i \nabla_{\xi} N^{i}_{\overline{\varphi}} \right\|} \qquad N = \frac{\sum_{j=1}^{m} \widetilde{\Phi}_j \nabla_{\xi} N^{j}_{\widetilde{\Phi}}}{\left\| \sum_{j=1}^{m} \widetilde{\Phi}_j \nabla_{\xi} N^{j}_{\widetilde{\Phi}} \right\|} \qquad \textbf{95}$$

The linearisation of the first Piola Kirchhoff stress and the material stress tensor is given as [25]:

$$\frac{dP}{d\overline{\overline{F}}} = \frac{1}{2}E_0\left[\frac{1}{\widetilde{\widetilde{f}}} + \frac{\widetilde{\widetilde{f}}}{\overline{\overline{F}}^2}\right] \qquad \frac{d\pi}{d\widetilde{\widetilde{f}}} = \frac{1}{2}E_0\left[\frac{\overline{\overline{F}}^2}{\widetilde{\widetilde{f}}^3} + \frac{1}{\widetilde{\widetilde{f}}}\right]$$

$$\frac{dP}{d\widetilde{\widetilde{f}}} = -\frac{1}{2}E_0\left[\frac{1}{\overline{\overline{F}}} + \frac{\overline{\overline{F}}}{\widetilde{\widetilde{f}}^2}\right] = \frac{d\pi}{d\overline{\overline{F}}} \qquad \textbf{96}$$

The solution was performed by solving Equations (91, 92) in a coupled manner within a Newton Raphson solution scheme. In reference [25, 29] this has been illustrated with different examples. In all these examples the results give an optimum solution that is similar to existing analytical solutions. The previous works [25, 29] focus on generated material force in finding the optimised solution. In other words the second term in Equation (87) which represents the contribution of the external force in the material domain has been ignored in [29]. This external force contribution in the material domain is given in reference [25] without any further specification of the nature of this force or any implementation. This force was assigned a negative sign giving it a direction similar to the applied physical force [25] as we viewed earlier in Equation (90).

As mentioned earlier the aim is to generalise the material force method in structural optimisation to arbitrary support conditions or boundary conditions. In the next sections, this force will be introduced and specified. Its magnitude, direction and its relation to the physical force will be given in detail. Furthermore, different examples will be given for validation where an analytical solution exists. This force will be named the imposed material force due to its nature. Thus it is not a generated material force. Also a comparison will be made between a coupled and decoupled solution in terms of the imposed material force. The advantage in terms of the accuracy and computational cost will be demonstrated. In order to generalise further the method, an extension will be made from the two dimensional case to three dimensional. Finally, different examples will be given in three dimensions for generated as well as imposed material force.

2.3 Imposed material force

The generated material force has been first introduced by Eshelby [34] as the force resulting from the difference between the elastic field quantities surrounding the singularity in an infinite medium and those actually present. Since then the methods have found a large area of applications among which structural optimisation [25, 29] that is the focus of this section. Since this method comes short in dealing with structural optimisation in general case, it

is important to have an improved method that deals with these problems. This way we will introduce the term “imposed material force” in optimisation. The improved formulation of Equation (90) reads:

$$R^{J}_{\tilde{\Phi}}\left(\overline{\varphi},\tilde{\Phi}\right)=\sum_{t=1}^{n}\nabla_{\xi}N^{j}_{\tilde{\Phi}}PAn+F^{extJ}_{\overline{\varphi}}=0 \qquad \textbf{97}$$

The second term in the right hand side of this Equation is what we will call imposed material force. The property of this force is that it has the same magnitude as the physical force with opposite direction. Since the spatial and material settings were derived from the same potential energy function, an optimum solution can only be obtained when continuity between the spatial and material configuration exists. This means applying a physical force in the spatial domain will require applying a force equal in magnitude but opposite in direction in the material configuration. This force that will insure the continuity is what we will call imposed material force.

The major difference between imposed material force method and generated material force method is that in the generated material force method the aim is to optimise the mesh or interior nodes while in imposed material force the aim is to optimise the shape or outer geometry. In order to explain this further, a physical force applied on node that is free in the spatial domain while constrained in the material domain will generate material forces within the nodes that are free in the material domain. In this case the nodes where the physical forces were applied will not be optimised because their material degrees of freedom are restricted. This type of optimisation is denoted “generated material force” which has been illustrated for structural optimisation in [25, 29] and in mesh optimisation [57, 58]. In the case where an applied physical force on a spatially free node and a force equal in magnitude to the physical force but opposite in direction applied on the same node where the material degree of freedom is kept unconstrained will provide an optimum location not only for the internal materially free nodes but also for the boundary materially free nodes where the physical force is applied. This will produce an optimum shape because the traction boundary nodes will be included. This type of optimisation is what we will call “imposed material force”.

A simple example is presented here to understand the concept of imposed material force in structural optimisation. The structure consists of two bar elements fixed at both ends, each has the same length of 5, the same modulus of elasticity of 1000, the same area of 1, and subjected to external concentrated force of 500 at the middle node as shown in Figure 7. The deformed configuration for a Lagrangian solution is shown below (Figure 8). The Newton Raphson method was used to obtain the solution as illustrated in Table 1. It is clear that the Lagrangian solution gives a stationary point. This is clear from the reduction in the value of the total potential energy through the iterations.

Thereby the internal energy is calculated by the sum of the internal energy of

all its bars. The internal energy of each bar for compressible Neo-Hooke material is found by integrating Equation (80) over the volume of that bar. The external energy is simply the load multiplied by the displacement of the central node. The total potential energy is the total internal energy plus the total external energy as given in Table 1.

Iteration	Internal energy	External energy	Potential energy	ERROR
1	317.596	-625	-307.404	3.333E-02
2	298.418	-606.136	-307.718	1.0428E-04
3	298.358	-606.077	-307.718	1.0035E-09
4	298.358	-606.077	-307.718	1.11022E-19

Table 1 stationary point in Newton-Raphson scheme

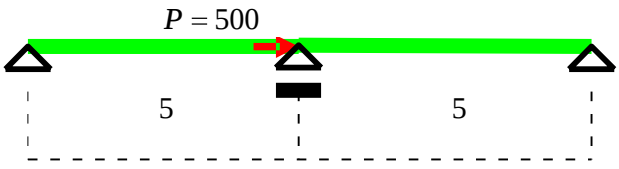

Figure 7 physical force in one dimensional truss structure

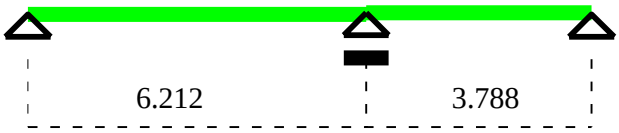

Figure 8 Lagrangian solution

In order to illustrate the advantage of the A.L.E method over the Lagrangian method and the concept of imposed material force, the same example will be solved with applied Newtonian force and applied Eshelbian force (Figure 9). The calculations were carried out by solving Equations (89 and 97) in a coupled manner with the Newton Raphson scheme. The solution produces the optimised undeformed (material) configuration and the optimised deformed (spatial) configuration (Figure 10). The results (Table 2) show clear reduction in the total potential energy. The first iteration in the A.L.E analysis gives similar results to the Lagrangian method. This is because the first iteration in the A.L.E method is pure Lagrangian. In the A.L.E method the applied material force will provide the magnitude and direction to search for a global optimum for the total potential energy of the system.

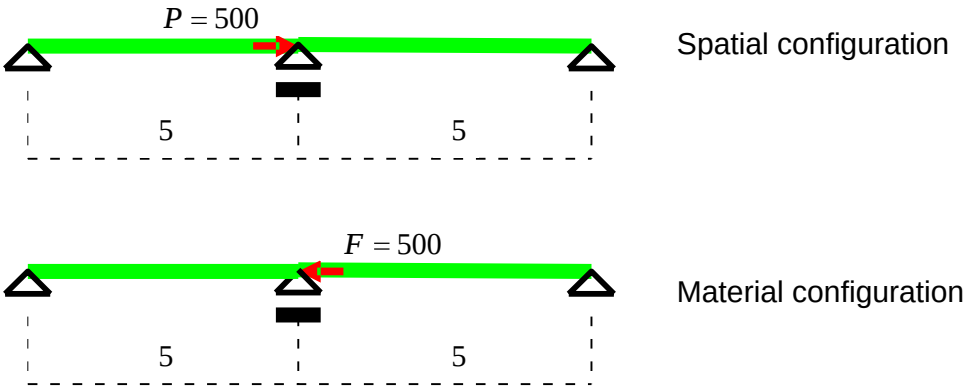

Figure 9 physical and material force in one dimensional truss structure

Iteration	Internal energy	External energy	Potential energy	ERROR
1	317.596	-625	-307.404	2.4782E-02
2	309.028	-618.847	-309.819	7.2176E-03
3	304.655	-614.498	-309.843	2.1268E-05
4	304.641	-614.485	-309.844	4.3125E-09
5	304.641	-614.485	-309.844	9.7846E-18

Table 2 optimised solution in Newton-Raphson scheme

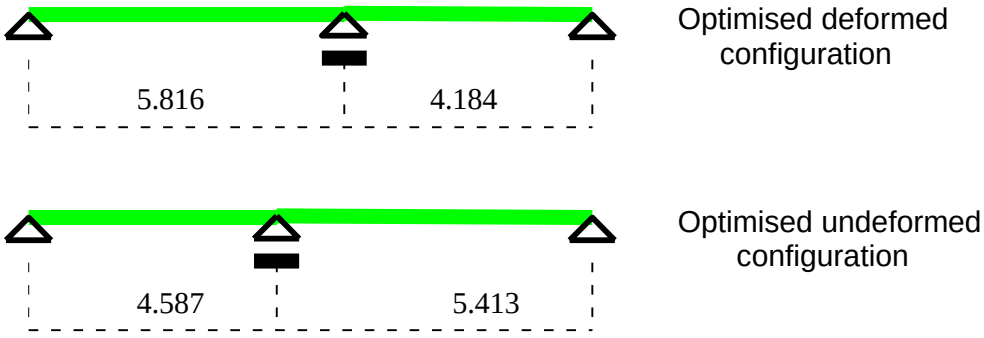

Figure 10 A.L.E Solution

A comparison between the results in Table 1 and 2 shows further improvement in the total potential energy in the A.L.E method compared to the Lagrangian method. The internal energy has been calculated in similar way as with the Lagrangian method as outlined before. The external energy in the A.L.E method has been found by multiplying the force with total displacement. Thereby the total displacement is the difference between the spatial and material coordinates. The total potential energy in the A.L.E method as in the Lagrangian method is the difference between the internal and external energy.

An important aspect of the coupled solution in term of applied material force compared to a decoupled solution will be explained here. A decoupled A.L.E solution as in traditional A.L.E methods means that the spatial setting will be solved first followed by solving the material setting. Thus a decoupled A.L.E consists of two sub steps compared to one step in coupled A.L.E solution. In order to illustrate the advantage of the A.L.E coupled solution over the decoupled A.L.E solution, the same example given in Figure 9 will be solved in

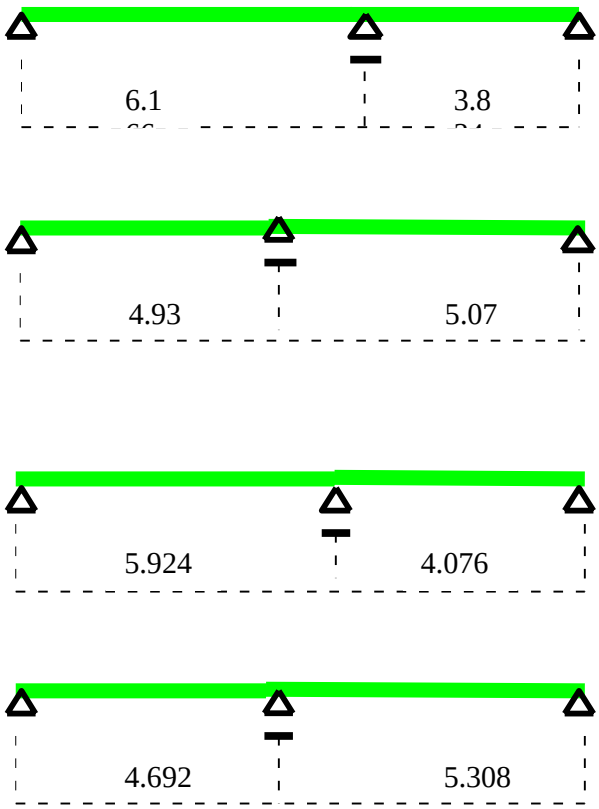

Optimised spatial configuration

10 increment solution

Optimised material configuration

Optimised spatial configuration

100 increment solution

Optimised material configuration

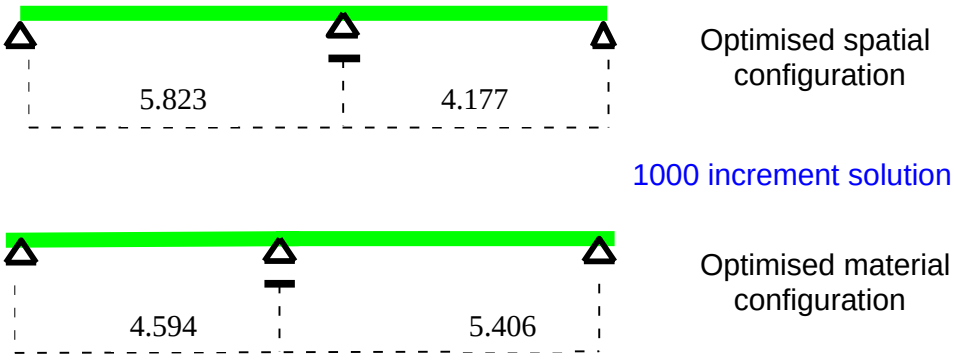

Figure 11 A.L.E decoupled solution

a decoupled manner. The solution for different number of increments is given in Figure 11. It is clear that the uncoupled solution approaches the coupled solution as the number of increments increases. The computational cost of decoupled solution is much higher and provides less accuracy than the coupled solution. This is clear from the A.L.E results where only one degree of freedom is involved.

Another illustration of the concept of imposed material force in two dimensional fields is for a truss structure consisting of two bars (see Figure 12). The bars have an area of $A = 1$ and modulus of elasticity of $E = 10000$. A spatial applied load of $F = 10$ is used together with a material imposed load equal in magnitude but opposite in direction. The aim is to find the optimum

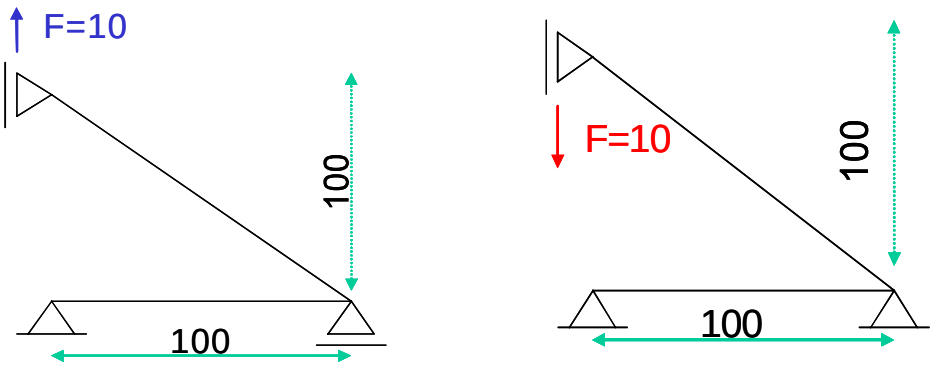

Figure 12 initial truss configurations

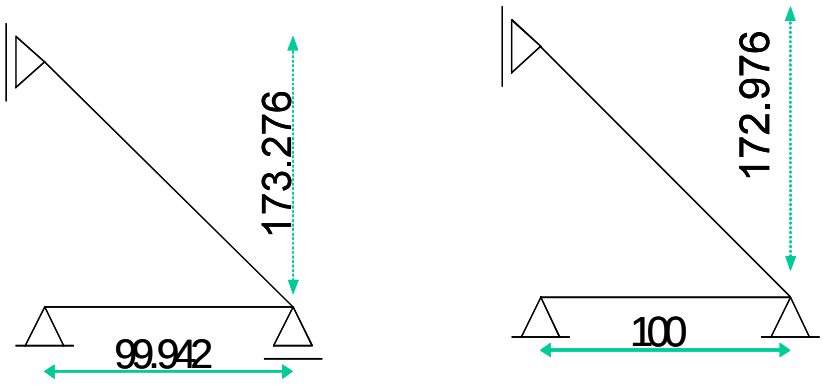

Spatial configuration Material configuration

Figure 13 optimised truss configurations

location of the node that was kept spatially as well as materially free. The A.L.E coupled solution was carried out with the Newton Raphson scheme resulting in optimised undeformed material configuration and in optimised deformed spatial configuration (Figure 13). This result is independent of the initial configuration. In order to show that, the A.L.E coupled solution was carried out for different initial configurations shown in Figures 14 and 15 below. The same results as these were obtained with the Newton Raphson scheme shown in Figure 13. The Newton Raphson scheme shows a quadratic rate of convergence for the three different initial configurations as shown in Figure 16. Note that for these moderate load values the optimised configurations resemble very close the results of the small strain theory that is an inclination angle of 60^0 .

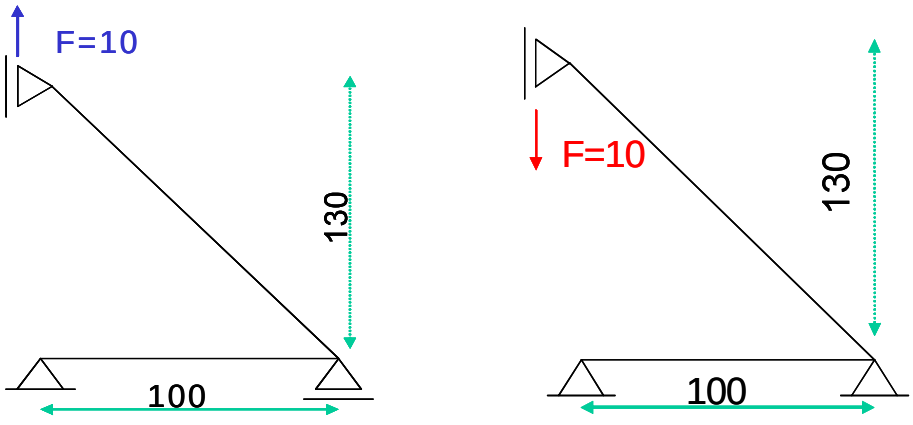

Figure 14 initial truss configurations

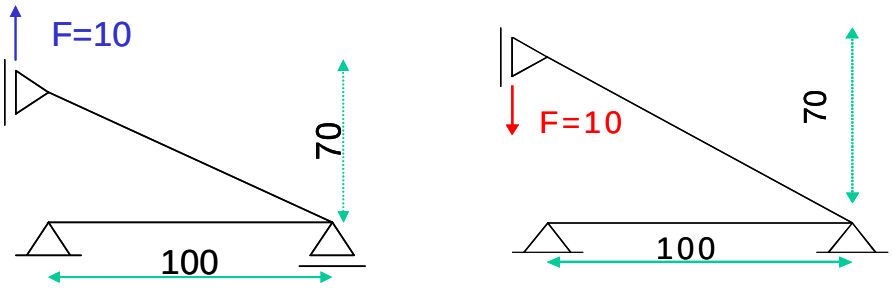

Figure 15 initial truss configurations

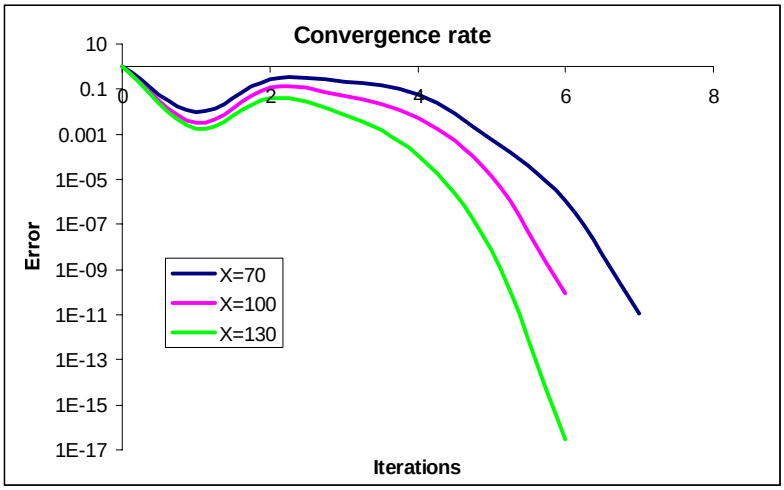

Figure 16 Newton-Raphson convergence rate

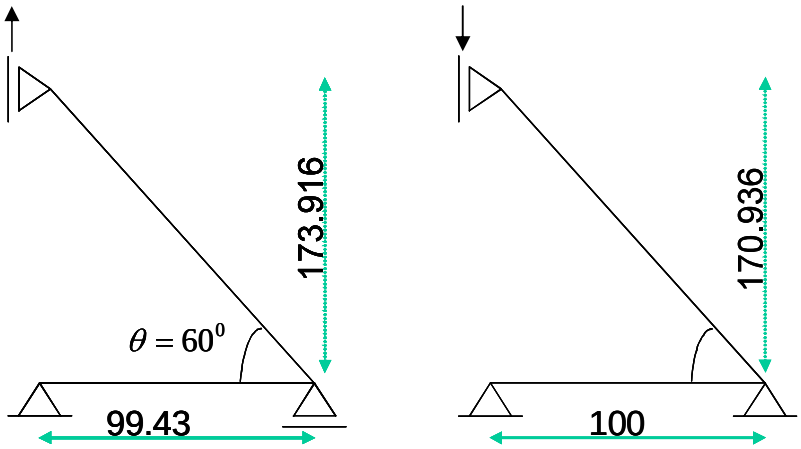

Figure 17 one incremental truss optimisation

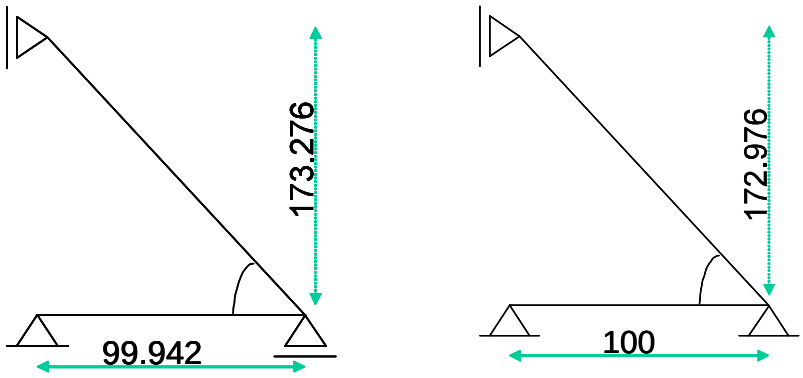

Spatial and material configurations after first increment

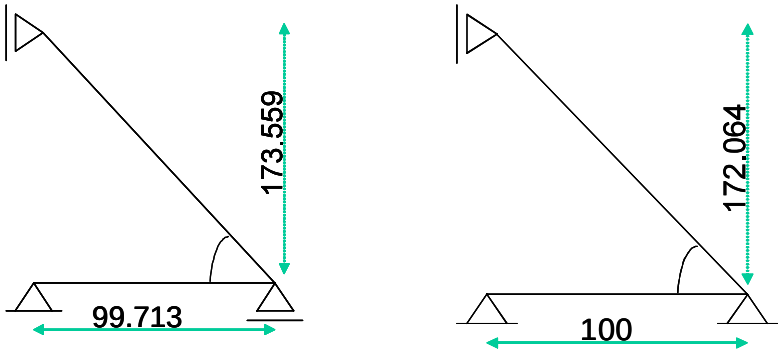

Spatial and material configurations after five increments

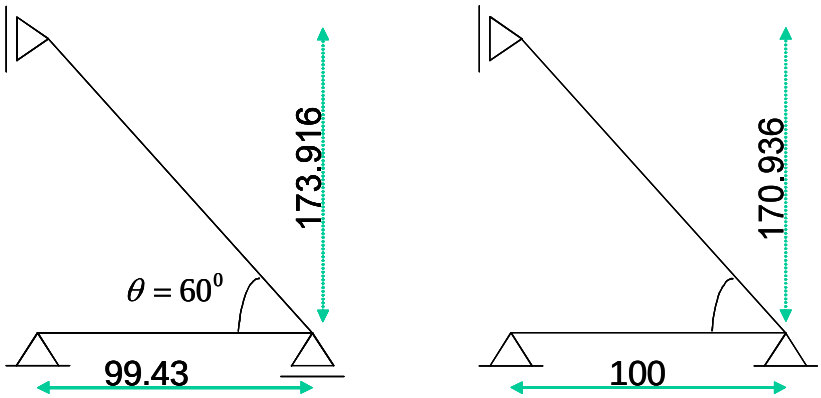

Spatial and material configurations after ten increments

Figure 18 ten incremental truss optimisation

In order to test the method under high level of nonlinearity, the A.L.E coupled solution were carried out for the same structure under spatial load of 100 (upwards) and material load of -100 (downwards). The results for one increment Newton Raphson is shown in Figure 17. A quadratic rate of convergence has been observed. The result gives a horizontal displacement of $u = -0.57$ and a total vertical displacement of $v = 3.02$. These results are similar to the ones obtained earlier in the literature review [29]. This shows the validity of the method in structural optimisation. The calculation can be also carried out in a number of increments to reduce the level of non linearity. The same example is solved using ten increments of 10 each in a coupled solution (see Figure 18); the same results were obtained as for the one increment solution shown in Figure 17. A quadratic rate of convergence was obtained in each of these increments. Hereby we should emphasise that the material force should be applied in the first iteration after the null iteration (see Figure 16). This should be the case in one incremental coupled solution knowing that the null iteration is purely Lagrangian. In an incremental coupled solution the subsequent increments that follow the first increment starts up the null iteration with a coupled spatial and material solution. Nevertheless; the applied material force should be applied in one iteration after applying the spatial force. It should also be applied incrementally as is the case with applying the spatial force.

The conclusion here is that the imposed material force is effective in optimising truss structures with arbitrary support conditions. In a coupled solution it requires only one increment to optimise a truss structure with high level of non linearity compared to a large number of increments in the decoupled solution. The imposed material force in a coupled solution gives accurate results compared to analytical solution while less accurate results were obtained in decoupled solution. The imposed material force method solves problems that the generated material method failed to solve, as for example the 60 degree optimised truss structure. Finally the optimised results for the same truss structure under applied spatial load of 1000 and applied material force of -1000 are shown below (Figure 19). The same result can be obtained for any number of increments.

2.4 Imposed versus generated material force

In order to illustrate the concept of imposed material force in more detail, a comparison with generated material force will be given in a number of examples. The aim is to show the application of each method and the conditions where each method can be implemented. We begin to review a two dimensional example solved with generated material force shown in Figure 20 [25 & 29]. In this case loads $p = -10$ are applied on the lower nodes which are spatially free while kept fixed in the material domain. In this case the

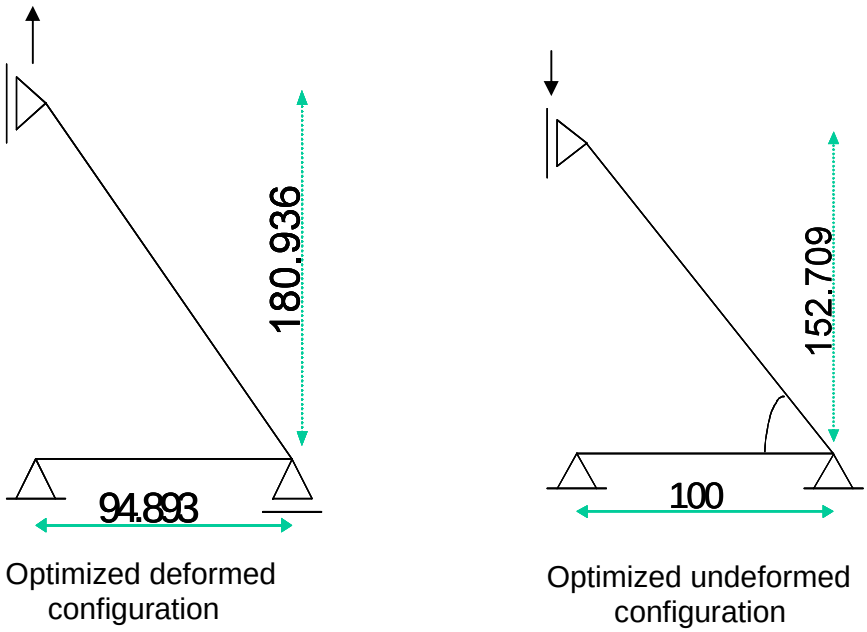

Figure 19 one incremental truss optimisation

requirement is to find the optimum location of the nodes that are spatially and materially free. Since the only forces present here are physical forces, the material force is generated through the discretisation. This method of optimisation driven by generated material force has been illustrated by different authors [24, 25, and 29]. The spatial and material problems were solved in coupled manner using Newton's Raphson scheme. The solution shows a quadratic rate of convergence (see Figure 21).

Now if the requirement is to optimise the same configuration but with the physical loads $p = -10$ applied on the nodes that are spatially and materially free (see Figure 22), then the solution cannot be obtained without imposing the material force $P = 10$. Previous approaches up to now failed to suggest a solution for this kind of problems. The method as has been illustrated earlier implies imposing a material force equal in magnitude but opposite in direction to the physical force as illustrated in Figure 22. The spatial and material Equations were solved in a coupled manner in one increment solution. The optimised spatial and material configurations are given in Figure 23 for subsequent iterations of the Newton's Raphson scheme. A quadratic rate of convergence is obtained as shown in Figure 24.

We can also apply the physical force in opposite direction $p = 10$ in the same configuration as shown in Figure 25. This will impose a material force in the opposite direction $P = -10$. The optimum solution gives spatial and material

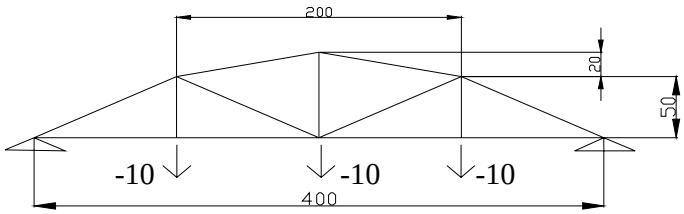

Spatial configuration

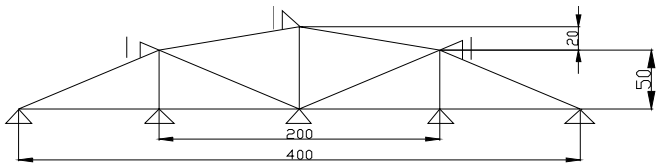

Material configuration

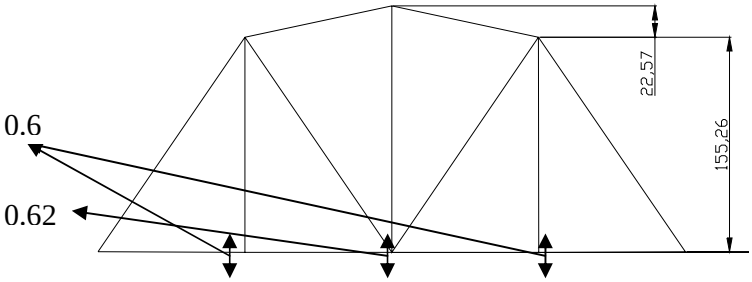

Optimized spatial configuration

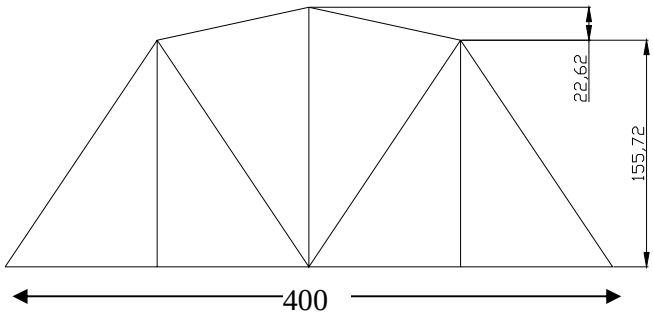

Optimized material configuration

Figure 20 two dimensional truss configuration

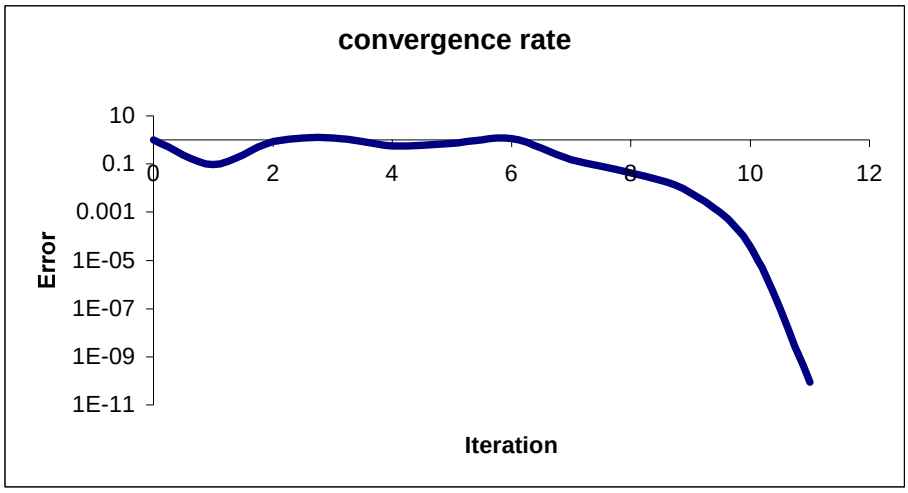

Figure 21 convergence rates in Newton-Raphson scheme

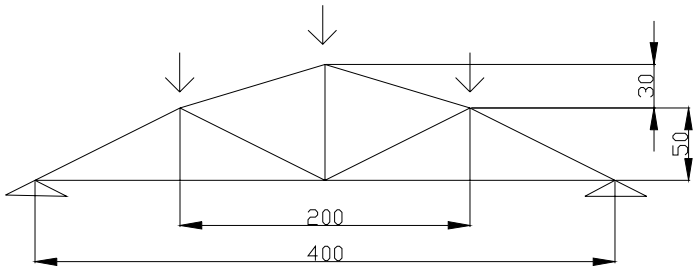

Spatial configuration

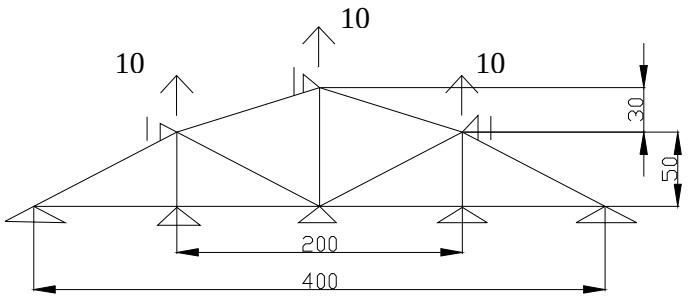

Material configuration

Figure 22 two dimensional truss configurations

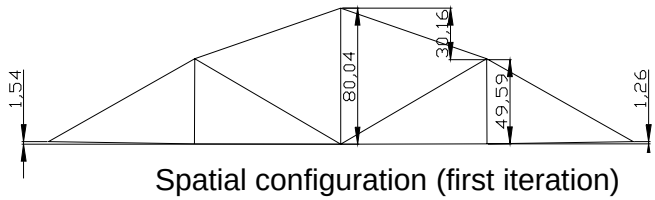

Spatial configuration (first iteration)

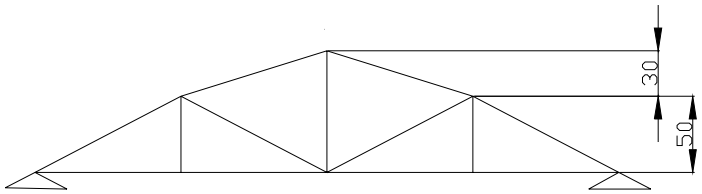

Material configuration (first iteration)

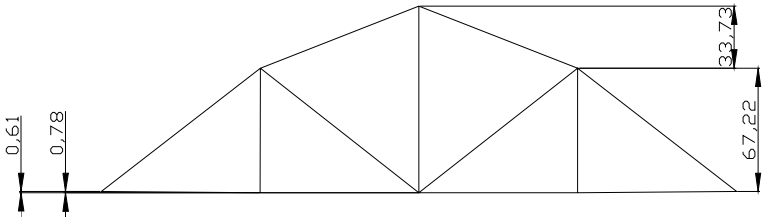

Spatial configuration (Second iteration)

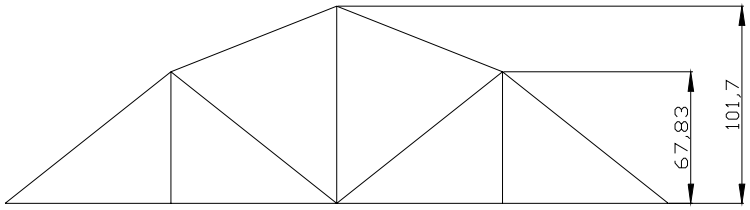

Material configuration (Second iteration)

Figure 23 optimised spatial and material configurations (continued)

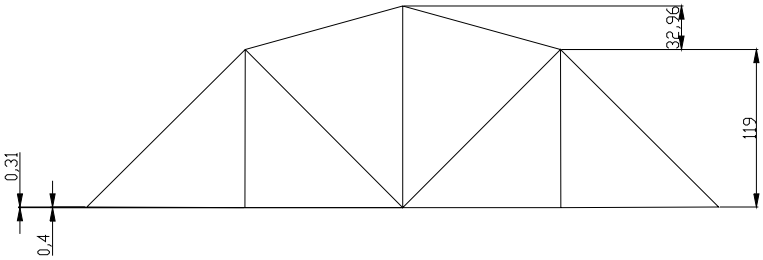

Spatial configuration (Third iteration)

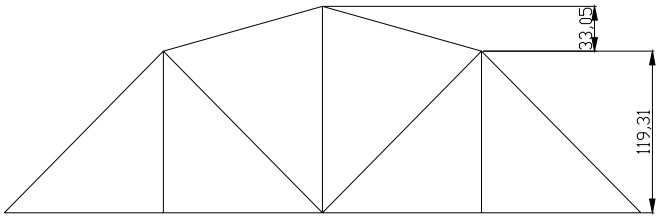

Material configuration (Third iteration)

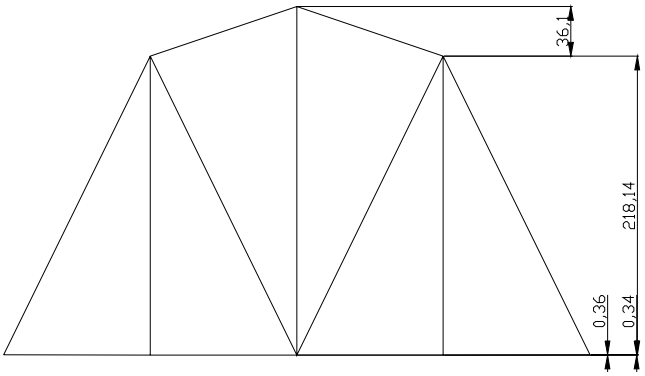

Spatial configuration (Fourth iteration)

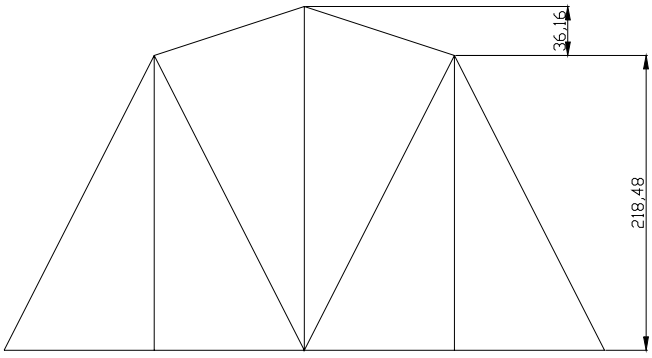

Material configuration (Fourth iteration)

Figure 23 optimised spatial and material configurations (continued)

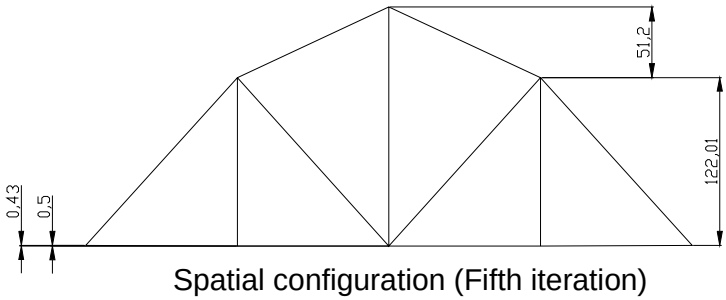

Spatial configuration (Fifth iteration)

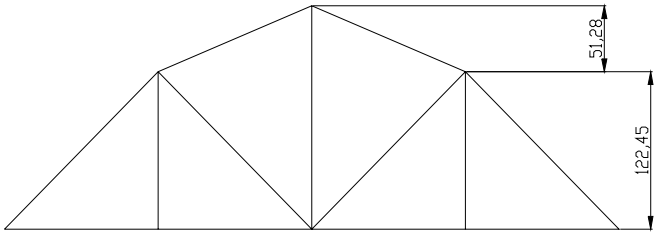

Material configuration (Fifth iteration)

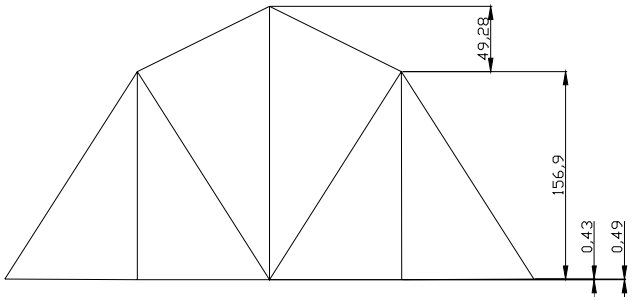

Spatial configuration (Sixth iteration)

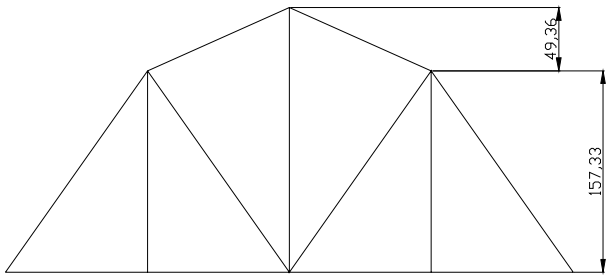

Material configuration (Sixth iteration)

Figure 23 optimised spatial and material configurations (continued)

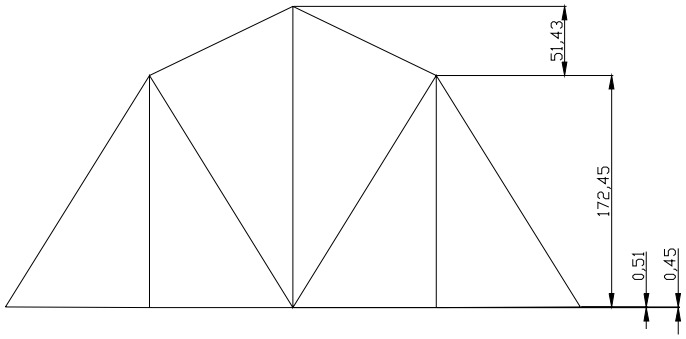

Spatial configuration (Seventh iteration)

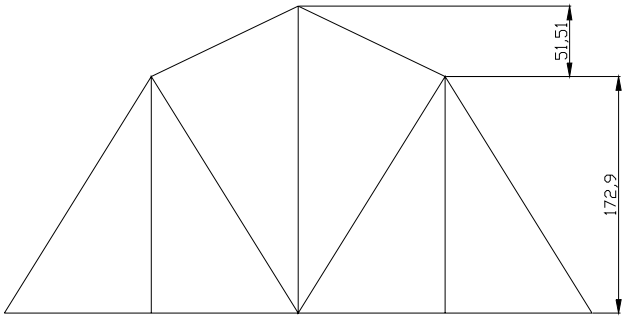

Material configuration (Seventh iteration)

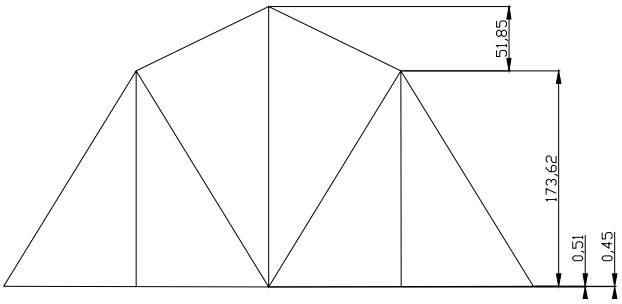

Spatial configuration (Eighth iteration)

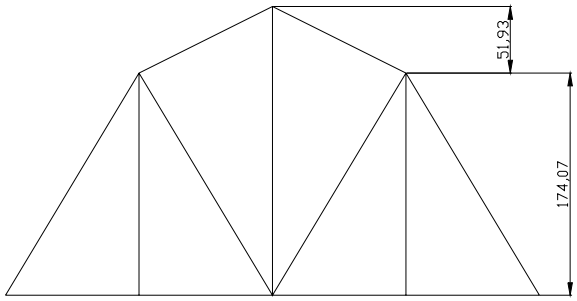

Material configuration (Eighth iteration)

Figure 23 optimised spatial and material configurations

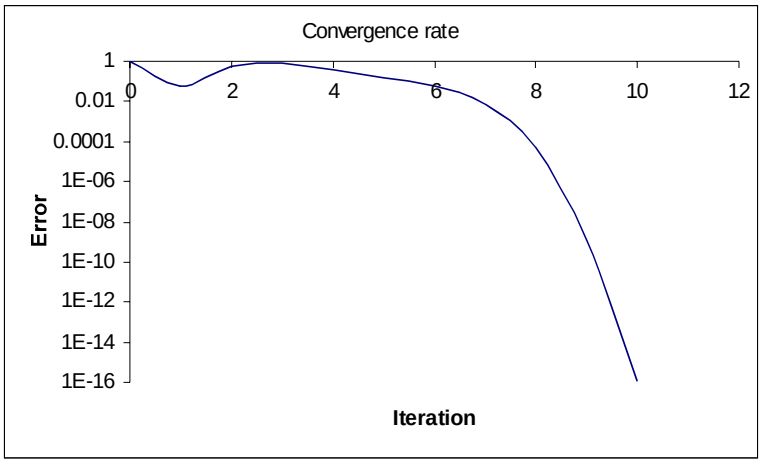

Figure 24 convergence rates in Newton-Raphson scheme

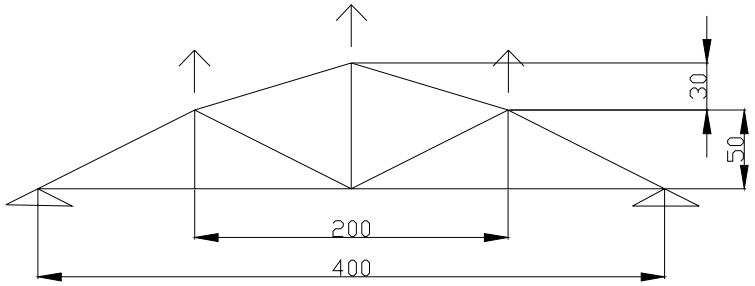

Spatial configuration

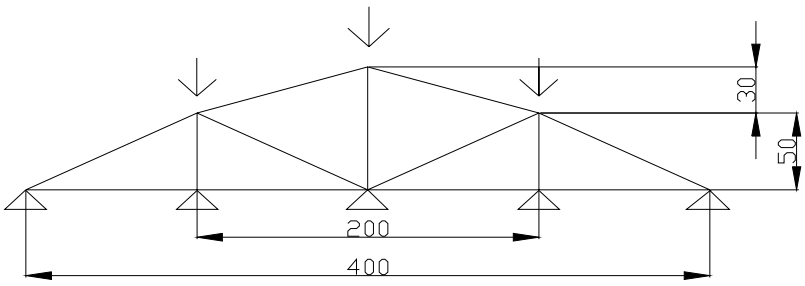

Material configuration

Figure 25 two dimensional truss configurations

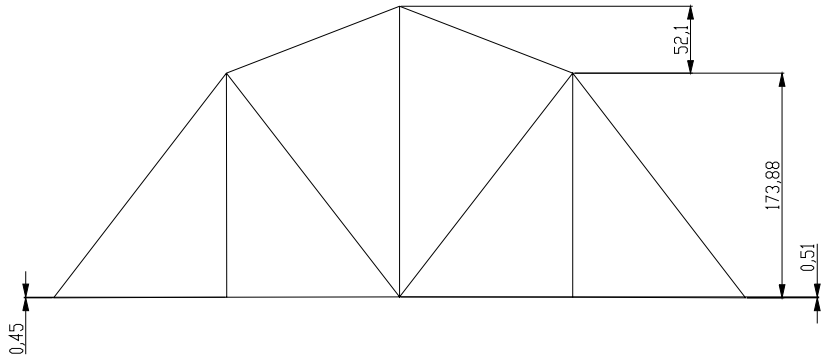

Optimised spatial configuration

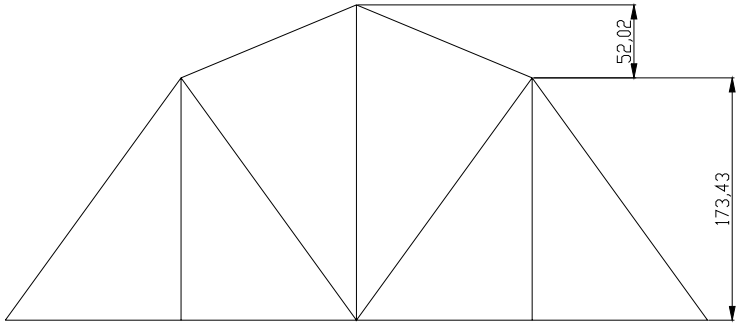

Optimised material configuration

Figure 26 Optimised truss configurations

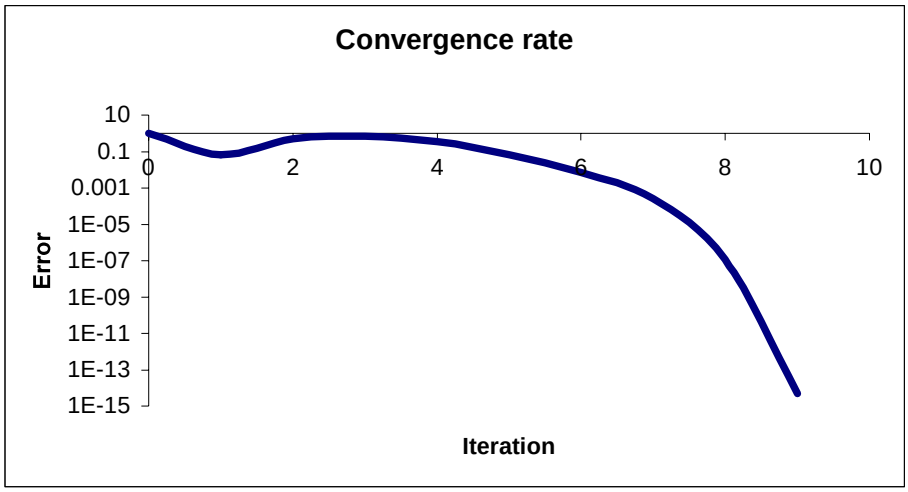

Figure 27 Convergence rate in Newton-Raphson scheme

configuration close to the one obtained previously (see Figure 23 and 26). The small differences are due to the properties of hyperelastic setting under tension load compared to compression load for the same configuration and load magnitude. The convergence rate is given in Figure 27. As shown, a quadratic rate of convergence has been observed again. Another example illustrating the difference of using imposed versus generated material force is given below. The first example of a simply supported two dimensional truss structure (Figure 28) demonstrates the use of generated material force in structural optimisation [25, 29]. The spatial configuration is loaded with concentrated loads of 25 each at the bottom nodes of the structure, while these nodes are kept constrained in the material configuration. The rods have a cross sectional area of 1 and modulus of elasticity of 10000. The aim is to find the optimum location of the top nodes in the vertical direction. These nodes are spatially and materially free in the vertical direction (Figure 28). The optimised spatial and material configurations are given in Figure 29 [25, 29]. The error versus the number of iterations is given in Figure 30. The solution converges quadratically within nine iterations. The solution illustrates the use of generated material force in structural optimisation where the loads are applied on a spatially free and materially fixed node. In case the requirements were different and the loads are applied at the nodes that need to be optimised.

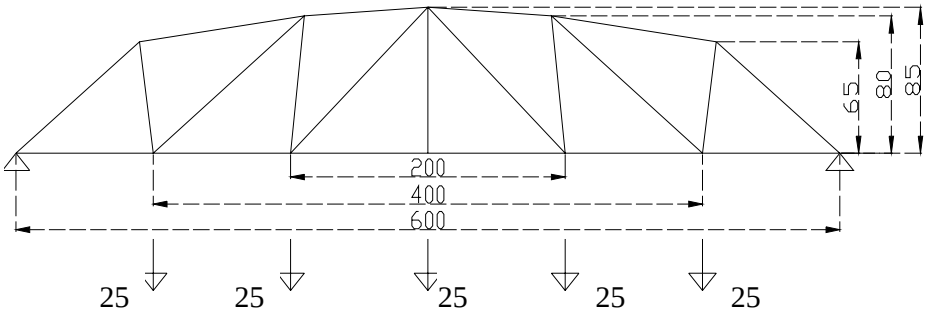

Spatial configuration

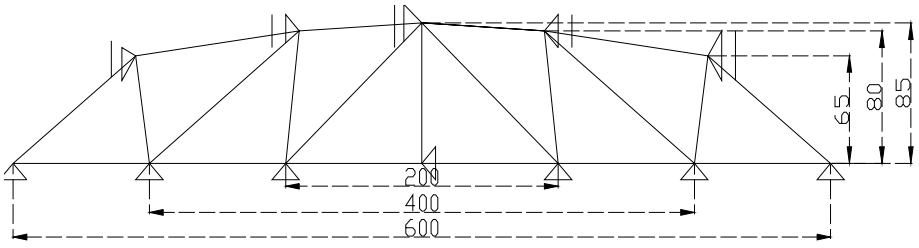

Material configuration

Figure 28 two dimensional truss configurations (generated material force)

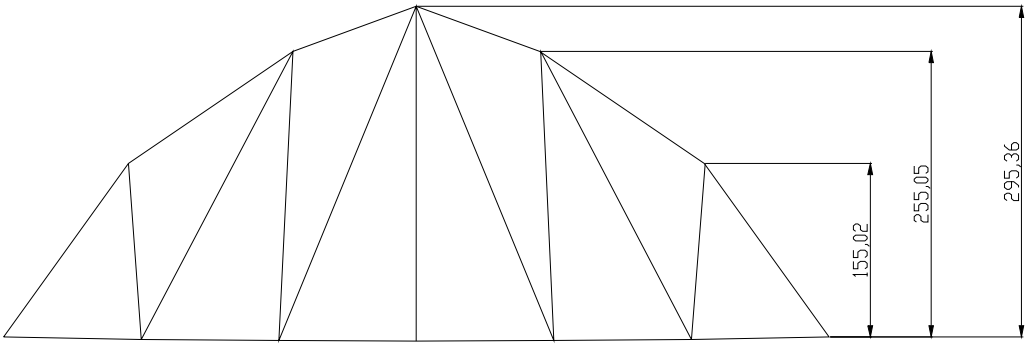

Optimised spatial configuration

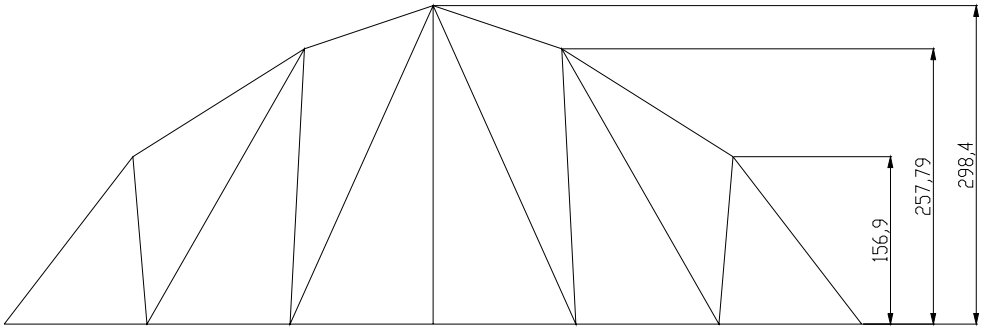

Optimised material configuration

Figure 29 Optimised truss configurations (generated material force)

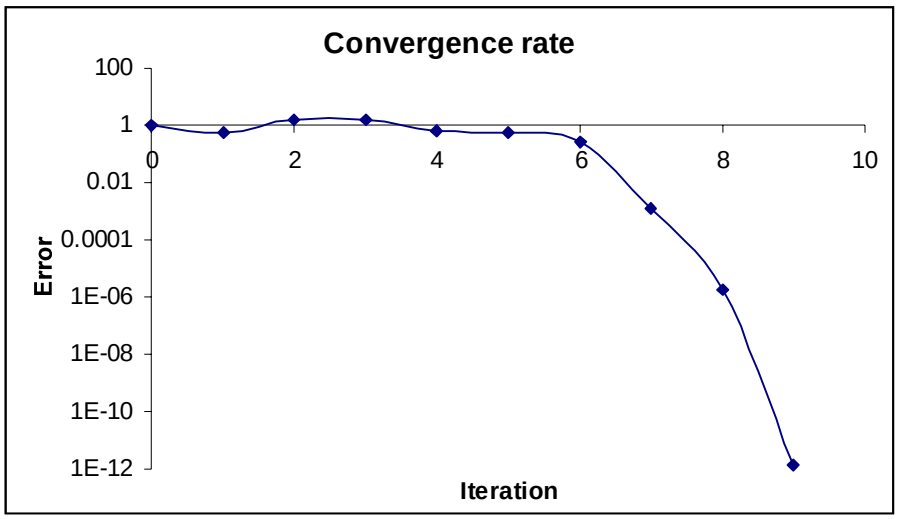

Figure 30 Convergence rate in Newton-Raphson scheme

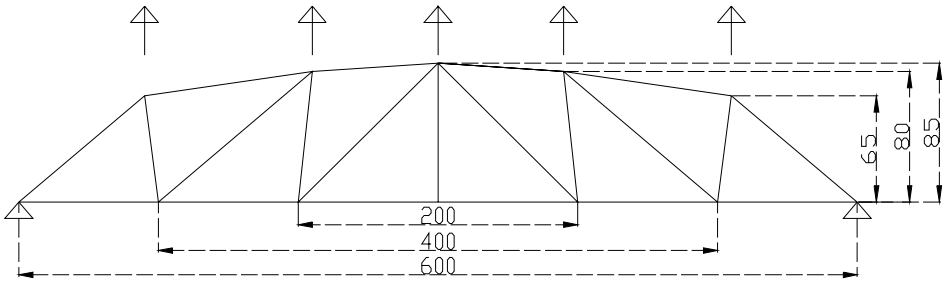

Spatial configuration

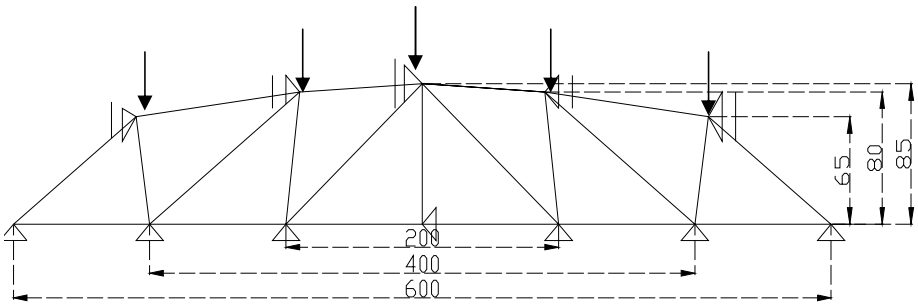

Material configuration

Figure 31 two dimensional truss configurations (imposed material force)

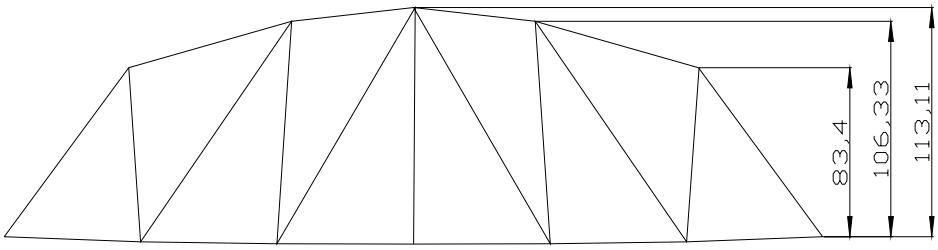

Spatial configuration (Second iteration)

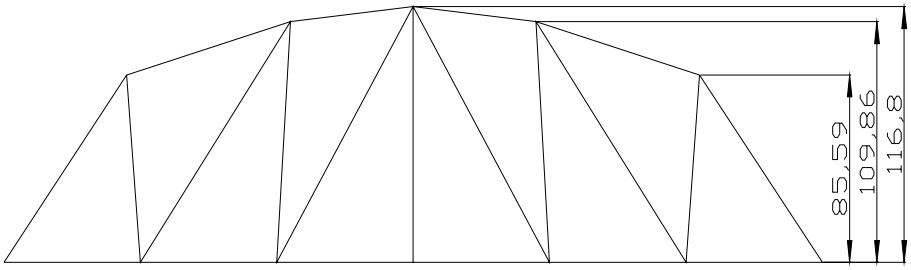

Material configuration (Second iteration)

Figure 32 Optimised truss configurations (imposed material force) (continued)

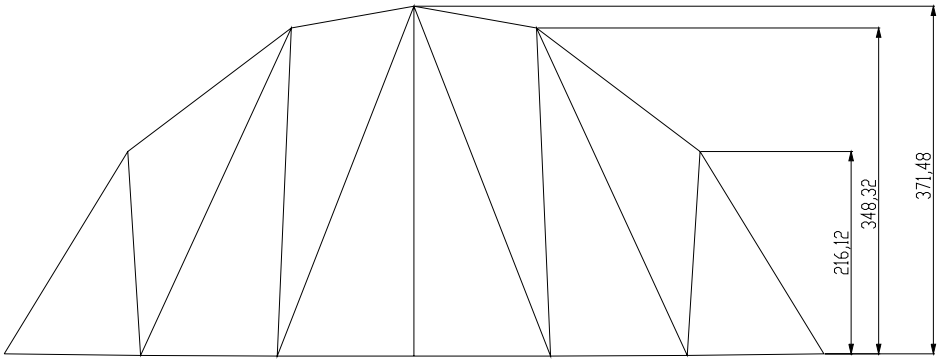

Spatial configuration (Fourth iteration)

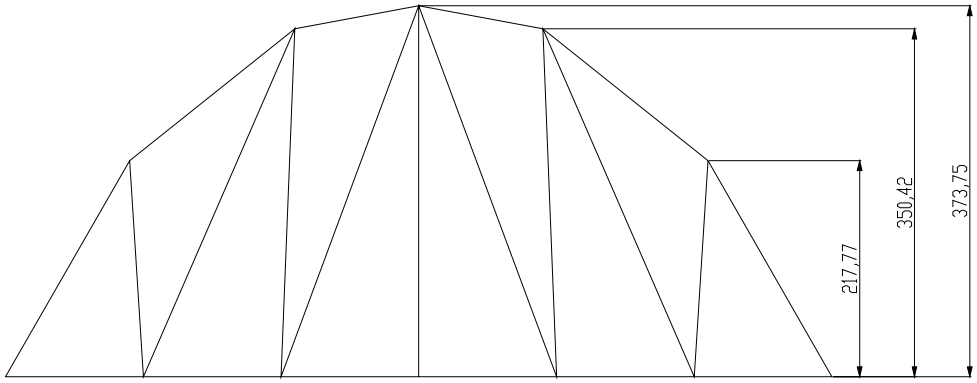

Material configuration (Fourth iteration)

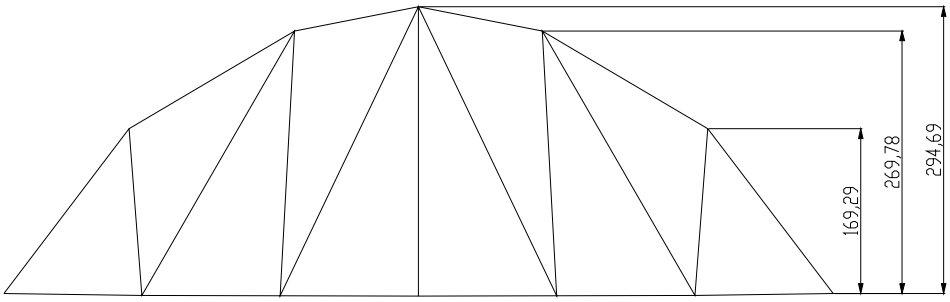

Spatial configuration (Sixth iteration)

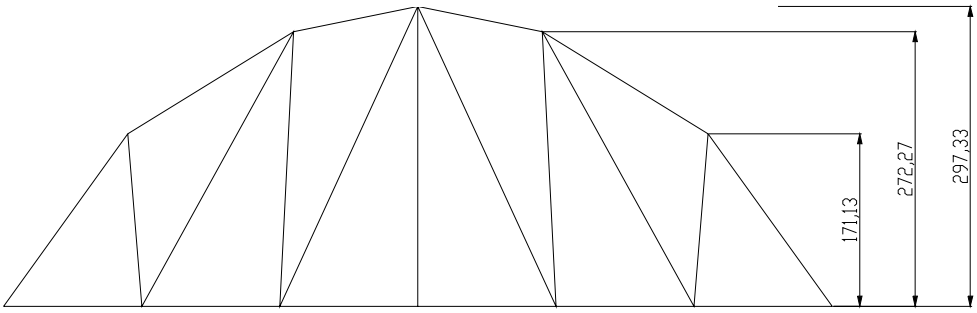

Material configuration (Sixth iteration)

Figure 32 Optimised truss configurations (imposed material force) (continued)

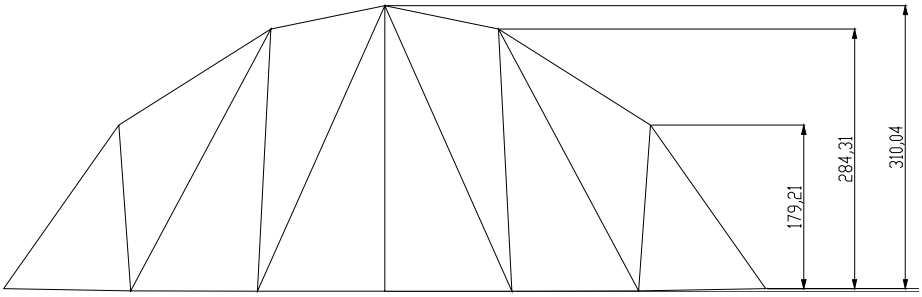

Spatial configuration (Eighth iteration)

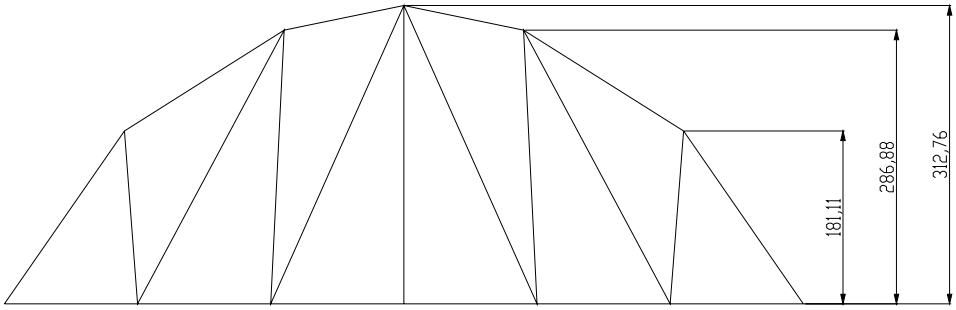

Material configuration (Eighth iteration)

Figure 32 Optimised truss configurations (imposed material force)

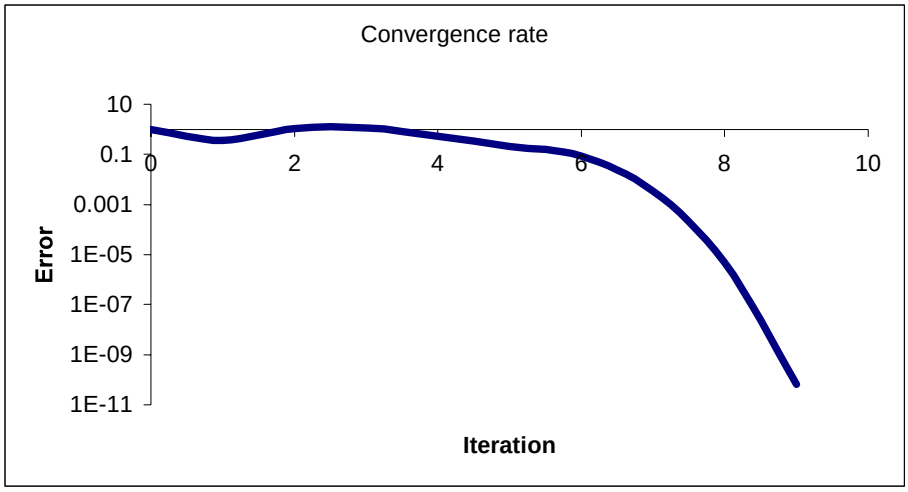

Figure 33 Convergence rate in Newton-Raphson scheme

This leads us to the second example (Figure 31) and the concept of imposed material force in structural optimisation. The same boundary conditions, cross sectional areas, dimensions and modulus of elasticity are used. The spatial loads as well as the imposed material forces were applied on the spatially and materially free top nodes. The imposed material forces have the same magnitude of 25 as the spatial forces but with opposite direction. The calculations were carried out with the Newton Raphson scheme. The optimised spatial and material configurations are given in Figure 32 through different iterations. The convergence rate shown in Figure 33 illustrates a quadratic rate of convergence.

2.5 Three dimensional truss optimisation using the material force

An extension of optimising truss structures from a two dimensional configuration to a three dimensional configuration will be given in this section. In two dimensional cases the spatial and material normals (Equation 95) is given respectively as:

$$n = \begin{bmatrix} \cos\theta & \sin\theta \end{bmatrix} \quad \text{and} \quad N = \begin{bmatrix} \cos\vartheta & \sin\vartheta \end{bmatrix} \qquad \textbf{98}$$

where θ and ϑ are the spatial and material angles to be determined from the geometry of the spatial and material configurations respectively, i.e., the spatial and material displacements. In a three dimensional spatial and material configuration these normals are given respectively as:

$$n = \begin{bmatrix} \cos\theta_x & \cos\theta_y & \cos\theta_z \end{bmatrix} \quad \text{and} \quad N = \begin{bmatrix} \cos\vartheta_X & \cos\vartheta_Y & \cos\vartheta_Z \end{bmatrix} \qquad \textbf{99}$$

where θ_x, θ_y and θ_z are the spatial angles between the global coordinates and the axial axis of the bar in the spatial configuration, ϑ_X, ϑ_Y and ϑ_Z are the material angles between the global coordinates and the axial axis of the bar in the material configuration.

2.5.1 Examples

In order to illustrate the method for a three dimensional case, two examples will be given. The first example gives a three bar structure fixed at the three corners in the spatial and material configuration (Figure 34). The dote lines forming the cube (100*100*100) show the planes. A load has been applied on the node that connects the three bars ($P = 10$). The bars have the same cross section area ($A = 1$) and modulus of elasticity ($E = 10000$). In order to find the optimum location for the connecting node across the horizontal plane, the spatial and material motion has been kept free. In the vertical direction only spatial motion is allowed. The problem illustrates the concept of generated

material force in three dimensional domains. The solution gives the optimum location of the connecting node in terms of minimising the potential energy (Figure 34). The solution shows a quadratic rate of convergence (Figure 35).

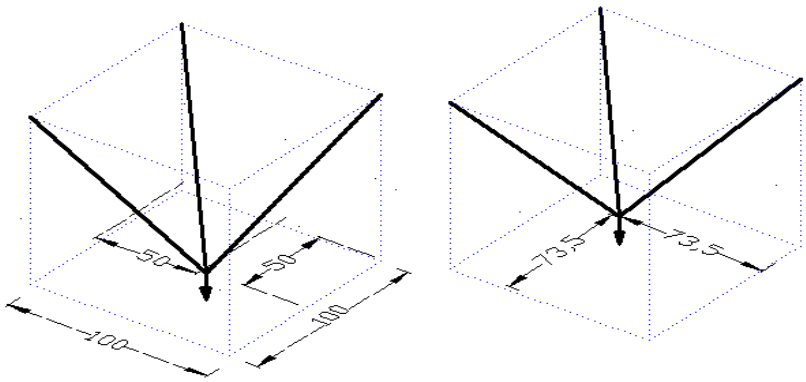

Initial configuration. Optimised configuration.

Figure 34 optimisation with generated material force in three dimensions

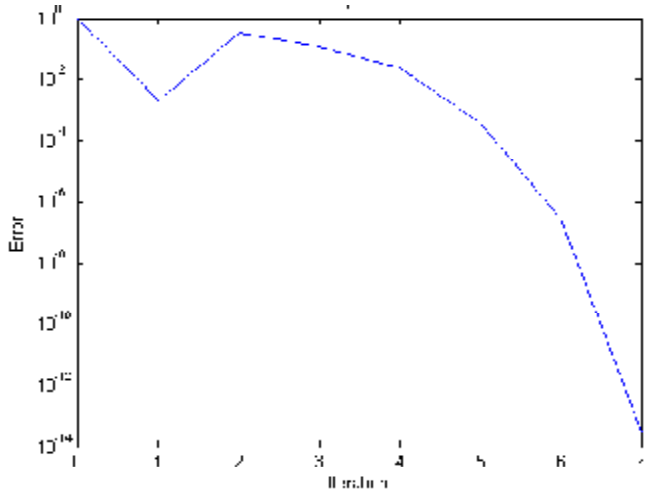

Figure 35 convergence rate (generated material force)

The second example to illustrate the concept of imposed material force in three dimensional truss optimisation is a truss structure consisting of five bar elements as shown in Figure 36 where the lower ends of the bars are spatially and materially fixed in three directions. The upper ends are kept spatially and materially free in the vertical direction where the loads are applied. As regards the degree of freedoms of the upper nodes, one is kept spatially and materially fixed while the other is spatially and materially free. The free

direction of the upper nodes in the horizontal plan is chosen to be perpendicular to each other to ensure the stability of the structure. The loads are applied downwards $(P=-100)$in the spatial configuration with imposing material loads upwards $(P=100)$ in the material configuration. The bars have the same area ($A=1$) and modulus of elasticity ($E=10000$). The Newton Raphson solution scheme has been carried out to solve the nonlinear spatial and material Equations simultaneously. The solution gives the optimised material (undeformed) configuration and the optimised spatial (deformed) configuration (Figure 36). The solution converges quadratically as shown in Figure 37. The same example was solved under a higher level of nonlinearity. The same geometry, boundary conditions and stiffness's have been used. The magnitudes of the spatial loads were increased to $(P=-1000)$ downwards while the magnitudes of the imposed material forces were also increased to $(P=1000)$ upwards. The optimised spatial (deformed) and material (undeformed) configurations are given in Figure 38.

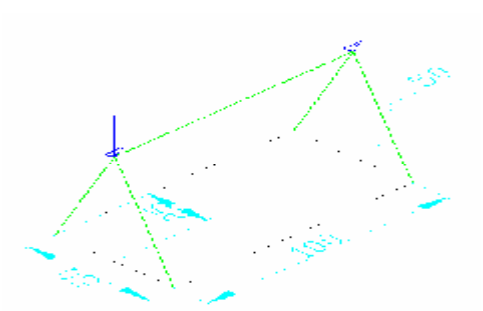

Initial spatial configuration

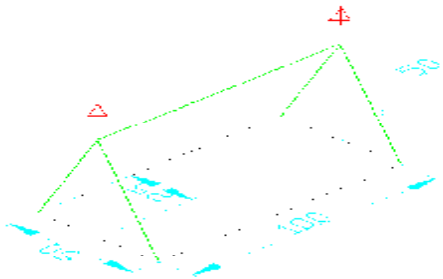

Initial material configuration

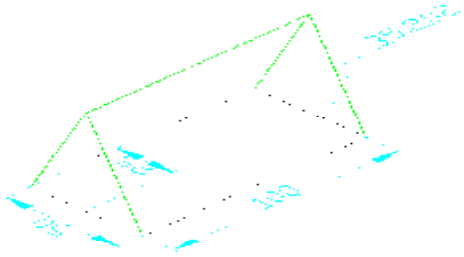

Optimised spatial configuration

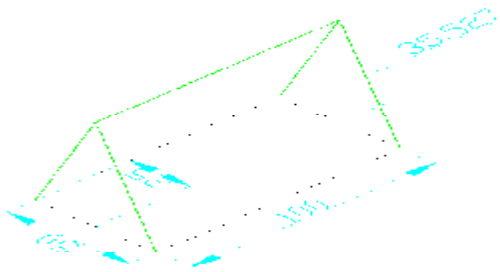

Optimised material configuration

Figure 36 optimisation with imposed material force in three dimensions

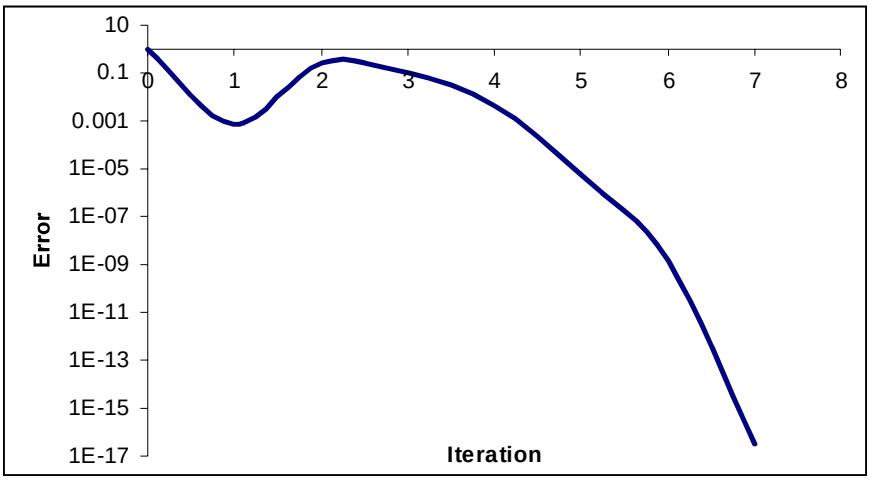

Figure 37 convergence rate (imposed material force)

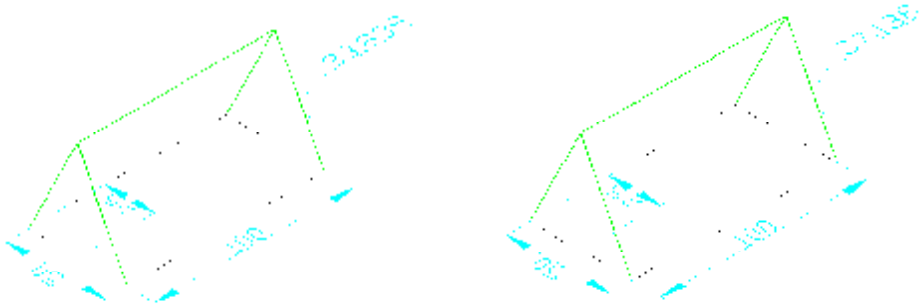

Optimised spatial configuration Optimised material configuration

Figure 38 optimisation with imposed material force in three dimensions

2.6 Constrained structural optimisation

2.6.1 Introduction

In previous sections, an illustration of the imposed and generated material force in 2D and 3D structural optimisation has been given. As we know the engineering design requirement differs in most cases from the optimised solution, it is therefore needed to develop a new formulation that not only optimises the structure but also fulfills these requirements at the same time. The requirement can be either a certain space or to limit the deflection of certain joints to a certain range. The aim is to develop the appropriate formulation and subsequently implement it.

The present section aims at adding inequality constraints by using the penalty method. The inequality constraints will be applied to the spatial and the material displacements. The essential idea is that if the penalty parameter is large enough, it will give a significant contribution to the extended unconstrained spatial and material problem when there constraint values are violated. Consequently, a vanishing variation of the potential energy with respect to the independent variables x, X at fixed X, x respectively cannot be attained without satisfying the spatial and material inequality constraints. Thus, the concept of a design space for the undeformed and deformed structure is introduced.

We will treat the effectiveness of the penalty method in constraining the solution of the spatial and material Equations. The solution will be carried out in a monolithic procedure. Two examples will be presented; the first will show the optimal solution for a spatial inequality constraint in a structure while keeping the material configuration unconstrained. This will provide the optimal configuration for a structure when the requirement is to a certain number of joints to have a maximum displacement within a certain range. The second example will give the optimal solution for the undeformed structure within certain space. This will be achieved through constraining the material configuration while keeping the spatial configuration unconstrained. In both procedures a comparison will be made with the unconstrained solution through their rate of convergence.

2.6.2 Inequality constraint

In order to constrain the optimisation problem using the penalty method, the square of the constraints multiplied by the penalty parameter will be added to the potential energy Equation. A large enough value of the penalty parameter will enforce the constraint accurately. The modified spatial and material potential energy Equations, respectively, are:

$$w_p = w + \frac{\beta}{2}\langle -g_I \rangle^2 \qquad \textbf{100}$$

$$W_P = W + \frac{\alpha}{2}\langle -G_I \rangle^2 \qquad \textbf{101}$$

w_p, W_P are the constraint spatial and material potential energy respectively
w, W are the unconstraint spatial and material potential energy respectively
β, α are the spatial and material penalty parameters respectively
g_I, G_I are the spatial and the material constraint respectively
$\langle\ \rangle$ is the Macaulay bracket

The minimum of the modified spatial and material potential energy are given as:

$$\frac{\partial w_p}{\partial \varphi} = \frac{\partial w}{\partial \varphi} + \beta\langle -g_I \rangle \frac{\partial g_I}{\partial \varphi} = 0 \qquad \textbf{102}$$

$$\frac{\partial W_P}{\partial \phi} = \frac{\partial W}{\partial \phi} + \alpha\langle -G_I \rangle \frac{\partial G_I}{\partial \phi} = 0 \qquad \textbf{103}$$

φ, ϕ are the spatial and the material coordinates respectively
Finally, linearisation of the coupled Equations with respect to the spatial and material coordinates will produce a monolithic set of Equations which can be solved with the Newton-Raphson iterative procedure. The linearisation of Equations 102 and 103 are:

$$\left(\frac{\partial_2 w}{\partial \varphi^2} + \beta\left\langle -\frac{\partial g_I}{\partial \varphi}\right\rangle \frac{\partial g_I}{\partial \varphi} + \beta\langle -g_I \rangle \frac{\partial_2 g_I}{\partial \varphi^2}\right)\Delta\varphi +$$
$$\left(\frac{\partial_2 w}{\partial \varphi \partial \phi} + \beta\left\langle -\frac{\partial g_I}{\partial \phi}\right\rangle \frac{\partial g_I}{\partial \varphi} + \beta\langle -g_I \rangle \frac{\partial_2 g_I}{\partial \varphi \partial \phi}\right)\Delta\phi = -\frac{\partial w}{\partial \varphi} - \beta\langle -g_I \rangle \frac{\partial g_I}{\partial \varphi} \qquad \textbf{104}$$

$$\left(\frac{\partial_2 W}{\partial \phi^2} + \alpha\left\langle -\frac{\partial G_I}{\partial \phi}\right\rangle \frac{\partial G_I}{\partial \phi} + \alpha\langle -G_I \rangle \frac{\partial_2 G_I}{\partial \phi^2}\right)\Delta\phi +$$
$$\left(\frac{\partial_2 W}{\partial \phi \partial \varphi} + \alpha\left\langle -\frac{\partial G_I}{\partial \varphi}\right\rangle \frac{\partial G_I}{\partial \phi} + \alpha\langle -G_I \rangle \frac{\partial_2 G_I}{\partial \phi \partial \varphi}\right)\Delta\varphi = -\frac{\partial W}{\partial \phi} - \alpha\langle -G_I \rangle \frac{\partial G_I}{\partial \phi} \qquad \textbf{105}$$

The first terms represent the tangents. In what follows we will show two examples illustrating the inequality constraints in truss optimisation and compare them with the unconstrained results.

2.7 Examples

The first example shown in Figure 39 is a simply supported truss subjected to three point loads each of 20. The first two Figures represent the spatial (Figure 39-A) and the material (Figure 39-B) configuration with their boundary conditions. This example was studied before by Askes et al. [25]. The optimised spatial solution of the unconstrained structure is given in Figure 39-C with the corresponding deflections in Figure 39-E. The inequality constraint can be used for different purposes, for example the design requirement for the deflections to be within a certain range. A spatial inequality constraint optimisation can be applied to the relevant nodes. In this particular case the material motion of these nodes are fixed while the spatial motion is kept within a certain range. The spatial motion for these nodes is constrained as -1.15< φ_i <0.001. Applying Equation (104), the unconstrained terms in Equation (105) will give the optimised solution for the structure within the specified range (Figures 39-D, F).

Here only the constrained spatial solution has been shown. A comparison between the rates of convergence shows a quadratic rate of convergence of the unconstraint solution while a linear rate of convergence is obtained for the inequality constraint (Figure 41).

The second example shows the spatial and material configuration of a simply supported truss structure (Figure 40). We apply loads each of 25 as shown and optimise the unconstrained structure. The optimised solutions for the spatial and material configurations are given in Figures 40-C&D respectively. Here we will view another type of inequality constraint optimisation, namely material inequality constraint. In order for example to limit the height of the structure within a certain range (0<h<200), we apply an inequality constraint to the material configuration (Equation 105) while keeping the spatial configuration unconstrained (the unconstrained part of Equation 104). Here we have applied only a material constraint (0< ϕ_i <200) and allow for a free deflection of spatial d.o.f. The optimised spatial and material configurations are given in Figures 40-E&F respectively. It can be verified that the solution satisfies the inequality constraint. Again we can obtain a quadratic convergence for the unconstrained configuration and a linear convergence for the constraint configuration (Figure 42).

The conclusion is both the spatial and material inequality constraint can be used. Although the convergence rates are linear, the two methods provide optimised configurations within the specified limits. We can also have results which give us a spatial motion as well as a material motion within a certain range by fully applying Equation 104 and 105. This will give more consistent tangent and as a result higher rate of convergence. Finally, we can also use a quadratic inequality constraint instead of the linear one that we used here which means constraining in x and y direction. In this case the second derivatives of the constraint terms in Equation 104 and 105 will be taken too.

-A- Initial spatial configuration.

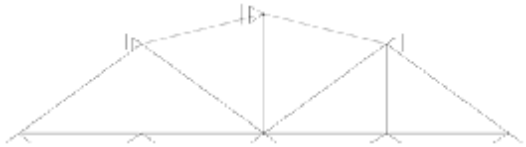

-B- Initial material configuration.

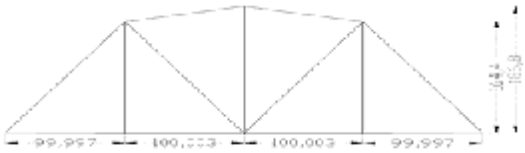

-C- Unconstrained optimised spatial configuration.

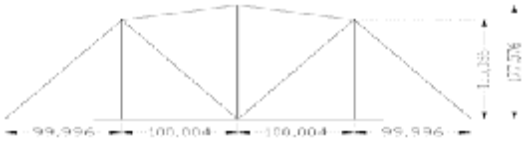

-D- Inequality constrained optimised spatial configuration.

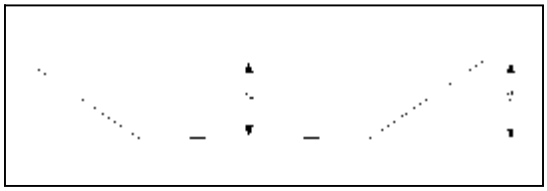

-E- The deflection of the lower nodes without constraint.

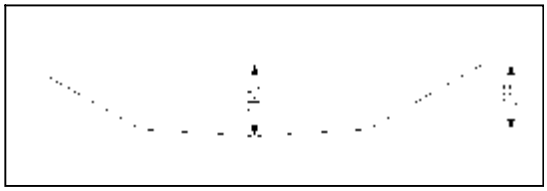

-F- The deflection of the lower nodes subjected to inequality constraint.

Figure 39 constrained versus unconstrained truss optimisation

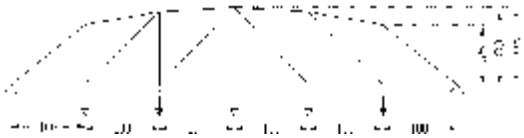

-A- Initial spatial configuration.

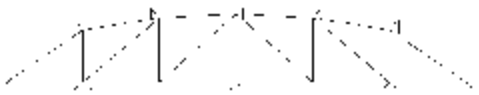

-B- Initial material configuration.

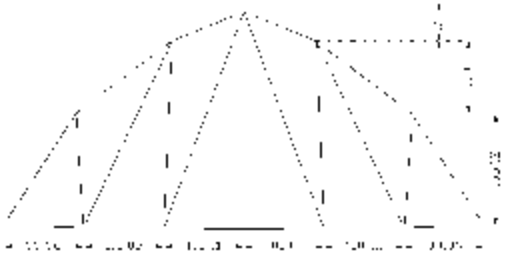

-C- Unconstrained optimised spatial configuration.

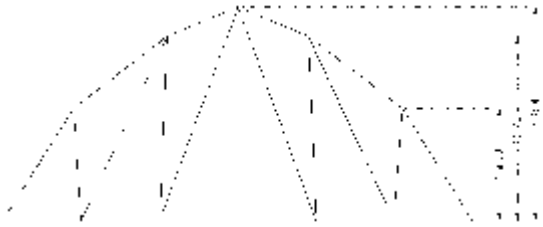

-D- Unconstrained optimised material configuration.

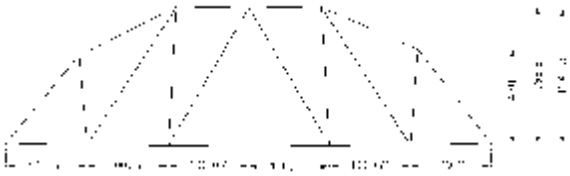

-E- Inequality optimised spatial configuration.

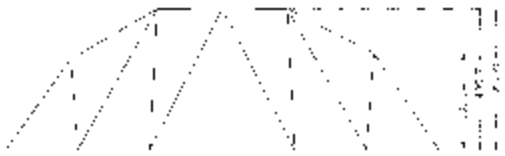

-F- Inequality optimised material configuration.

Figure 40 constrained versus unconstrained truss optimisation

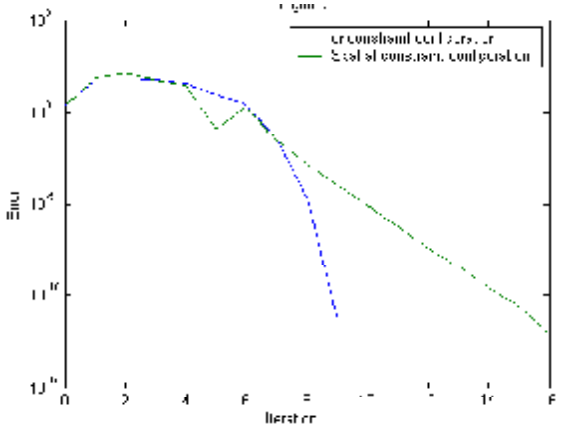

Figure 41 constrained versus unconstrained truss optimisation convergence rate.

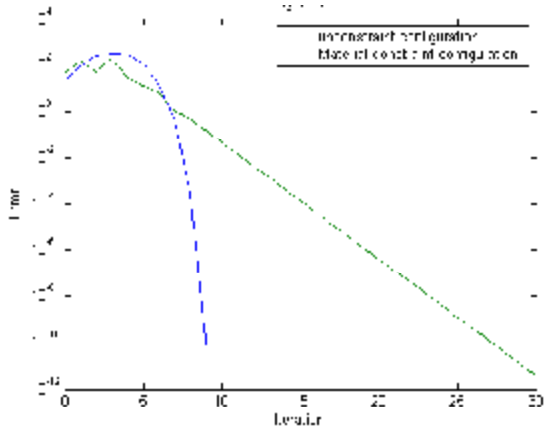

Figure 42 constrained versus unconstrained truss optimisation convergence rate.

3 A.L.E HYPERELASTIC FORMULATION OF CONTINUUM MECHANICS

3.1 Motivation

The material force method has recently also been used in mesh optimisation [57 & 58]. A new formulation was developed to optimise the finite element mesh in hyperelastic setting. The effectiveness and efficiency of the new method in solving the spatial and material Equations in coupled form was shown in terms of the computational cost and the method was shown to provide more accurate results compared to the decoupled solution [58]. The works which will be presented here provides a rate form of Equations rather than a total one presented earlier [57 & 58]. The aim is to provide the necessary platform for our subsequent development of A.L.E hyperelastodynamic and A.L.E hyperelastoplastic formulations. One advantage of this new rate A.L.E hyperelastic formulation over the traditional A.L.E hyperelastic rate formulation is the convection stage. In the new formulation the convection stage is totally embedded in the formulation. In other words, in contrast to earlier rate formulations, no separate convection stage is required in the new formulation. Another advantage over the traditional A.L.E formulation is that no heuristic Equations are required to be developed for the remeshing stage as those will be embedded in the formulation derived directly from the potential energy. As it is well known, the traditional A.L.E formulation requires Equations for estimating the error and Equations to be developed for remeshing based on these estimated errors. These remeshing Equations are rather complicated and the computational cost is high. Furthermore they have an arbitrary nature as they are not derived directly from the potential energy. All these drawbacks are avoided completely by the present A.L.E formulation based on spatial and material forces.

3.2 Introduction

Recently, a material force based optimisation strategy was developed for mesh optimisation in a geometrically nonlinear setting [57 & 58]. The approach searches for an optimal position of the nodes by minimising the total potential energy of the structure. This has been achieved by solving the spatial and material Equations simultaneously. While the first Equation corresponds to a variation of the total energy with respect to the spatial co-ordinates x at fixed material co-ordinates X , the latter gives the variation with respect to material co-ordinates X at fixed spatial co-ordinates x . This total variation is in terms of the A.L.E Dirichlet principle of hyperelastic conservative systems. This total variation is given as [57 & 58]:

$$\delta\ell = \delta_x \ell + \delta_X \ell = 0 \qquad \textbf{106}$$

The internal potential energy in the spatial and material domain can be presented respectively as follows [57 & 58]:

$$W_0 = \frac{1}{2}\lambda_0 \ln^2 J + \frac{1}{2}\mu_0 \left[F : F^t - n^{\dim} - 2\ln J\right] \qquad \textbf{107}$$

$$W_t = \frac{1}{2}\lambda_t \ln^2 \frac{1}{j} + \frac{1}{2}\mu_t \left[\left[f^{-1} : f^{-t}\right] - n^{\dim} - 2\ln\frac{1}{j}\right] \qquad \textbf{108}$$

$n^{\dim}$ is a scalar that gives the dimension of the problem; Since the terms in the right hand side of Equation (106) are independent, the resulting Equations can be solved independently. This will introduce the residual of the balance of momentum Equations in the spatial and material configuration as [57 & 58]:

$$R^I_{\overline{\varphi}}\left(\overline{\varphi}, \widetilde{\Phi}\right) = \sum_{e=1}^{n_{el}} \int_{\Omega_t} \nabla_x N^i_{\overline{\varphi}} \cdot \sigma d\Omega_t - \int_{\partial\Omega_t} N^i_{\overline{\varphi}} t_t dA_t - \int_{\Omega_t} N^i_{\overline{\varphi}} b_t d\Omega_t = 0 \qquad \textbf{109}$$

$$R^J_{\widetilde{\Phi}}\left(\overline{\varphi}, \widetilde{\Phi}\right) = \sum_{e=1}^{n_{el}} \int_{\Omega_0} \nabla_X N^j_{\widetilde{\Phi}} \cdot \sum d\Omega_0 - \int_{\partial\Omega_0} N^j_{\widetilde{\Phi}} T_0 dA_0 - \int_{\Omega_0} N^j_{\widetilde{\Phi}} b_0 d\Omega_0 = 0 \qquad \textbf{110}$$

Thereby $R^I_{\overline{\varphi}}$ and $R^J_{\widetilde{\Phi}}$ are the spatial and material residuals respectively. The spatial and material stress tensors in Equations (109 & 110) can be derived from there potential energy Equations (107 & 108) to give respectively [57 & 58]:

$$\sigma^t = \left[\lambda_t \ln J - \mu_t\right] I + \mu_t b \qquad \textbf{111}$$

$$\sum^t = \left[\frac{1}{2}\lambda_0 \ln J\left[\ln J - 2\right] + \frac{1}{2}\mu_0\left[I : C + 2 - n^{\dim} - 2\ln J\right]\right] I - \mu_t C \qquad \textbf{112}$$

Commonly, σ is known as the Cauchy stress whereas $\sum$ is the Eshelby stress; b and C are the left and right spatial motion Cauchy-Green strain tensors. In order to solve these highly non-linear spatial and material momentum Equations (109 and 110), these Equations are linearised and solved within the framework of Newton Raphson scheme. A total linearisation of the total variational Equation is taken with respect to the spatial coordinates at fixed material position plus its linearisation with respect to the material coordinates at fixed spatial positions as [57 & 58]:

$$\begin{aligned} R^{Ik+1}_{\overline{\varphi}} &= R^{Ik}_{\overline{\varphi}} + dR^I_{\overline{\varphi}} = 0 \\ R^{Jk+1}_{\widetilde{\Phi}} &= R^{Jk}_{\widetilde{\Phi}} + dR^J_{\widetilde{\Phi}} = 0 \end{aligned} \qquad \textbf{113}$$

with $dR^I_{\overline{\varphi}}$ and $dR^J_{\widetilde{\Phi}}$ denoting the iterative residual of iteration $k+1$, these are given as [57 & 58]:

$$dR^{I}_{\bar{\varphi}} = \sum_{K=1}^{n} K^{IK}_{\bar{\varphi}\bar{\varphi}} d\bar{\varphi}_K + \sum_{L=1}^{n} K^{IL}_{\bar{\varphi}\tilde{\Phi}} d\tilde{\Phi}_L$$

$$dR^{J}_{\tilde{\Phi}} = \sum_{K=1}^{n} K^{JK}_{\tilde{\Phi}\bar{\varphi}} d\bar{\varphi}_K + \sum_{L=1}^{n} K^{JL}_{\tilde{\Phi}\tilde{\Phi}} d\tilde{\Phi}_L \qquad \textbf{114}$$

where $K^{IK}_{\bar{\varphi}\bar{\varphi}}$ and $K^{JL}_{\tilde{\Phi}\tilde{\Phi}}$ are the diagonal tangents, $K^{IL}_{\bar{\varphi}\tilde{\Phi}}$ and $K^{JK}_{\tilde{\Phi}\bar{\varphi}}$ are the coupling tangents given as [57 & 58]:

$$\begin{aligned}
K^{IK}_{\bar{\varphi}\bar{\varphi}} &= \frac{\partial R^{I}_{\bar{\varphi}}}{\partial \bar{\varphi}_K} = \sum_{e=1}^{n_{el}} \int_{\Omega_0} \nabla_x N^{i}_{\bar{\varphi}} \cdot c \cdot \nabla_x N^{k}_{\bar{\varphi}} d\Omega_0 \\
K^{IL}_{\bar{\varphi}\tilde{\Phi}} &= \frac{\partial R^{I}_{\bar{\varphi}}}{\partial \tilde{\Phi}_L} = \sum_{e=1}^{n_{el}} \int_{\Omega_t} \nabla_x N^{i}_{\bar{\varphi}} \cdot d_f \sigma^t \cdot \nabla_x N^{l}_{\tilde{\Phi}} d\Omega_t - \int_{\Omega_t} N^{i}_{\bar{\varphi}} b_t \cdot \nabla_X N^{l}_{\tilde{\Phi}} d\Omega_t \\
K^{JK}_{\tilde{\Phi}\bar{\varphi}} &= \frac{\partial R^{J}_{\tilde{\Phi}}}{\partial \bar{\varphi}_K} = \sum_{e=1}^{n_{el}} \int_{\Omega_0} \nabla_X N^{j}_{\tilde{\Phi}} \cdot D_F \Sigma^t \cdot \nabla_X N^{K}_{\bar{\varphi}} d\Omega_0 - \int_{\Omega_0} \nabla_X N^{j}_{\tilde{\Phi}} \cdot b_0 N^{k}_{\bar{\varphi}} d\Omega_0 \qquad \textbf{115} \\
K^{JL}_{\tilde{\Phi}\tilde{\Phi}} &= \frac{\partial R^{J}_{\tilde{\Phi}}}{\partial \tilde{\Phi}_L} = \sum_{e=1}^{n_{el}} \int_{\Omega_t} \nabla_X N^{j}_{\tilde{\Phi}} \cdot C \cdot \nabla_X N^{l}_{\tilde{\Phi}} d\Omega_t
\end{aligned}$$

The fourth order tensors c, C_t, $d_f \sigma^t f^t$ and $D_F \Sigma^t F^t$ are given as [57, 58]:

$$c = \lambda_0 I \otimes I - \lambda_0 \ln J I \underline{\otimes} I + \mu_0 I \underline{\otimes} I + \mu_0 I \overline{\otimes} b \qquad \textbf{116}$$

$$\frac{d\sum}{dF} \cdot F = \left[\lambda_0 \left[\ln J - 1\right] - \mu_0\right] I \otimes I + \mu_0 \left[I \otimes b - F^T \underline{\otimes} F^T - F^T \overline{\otimes} F^T\right] \qquad \textbf{117}$$

$$\frac{d\sigma}{df} \cdot f = \left[\lambda_t \left[\ln J - 1\right] - \mu_t\right] I \otimes I + \mu_t \left[b \otimes I - F \underline{\otimes} F - F \overline{\otimes} F\right] \qquad \textbf{118}$$

$$\begin{aligned}
C_t = &\left[\frac{1}{2}\lambda_t \ln J \left[\ln J - 4\right] + \lambda_t + \frac{1}{2}\mu_t \left[I : C + 4 - n^{\dim} - 2\ln J\right]\right] I \otimes I \\
&+ \left[\frac{1}{2}\lambda_t \ln J \left[-\ln J + 2\right] + \frac{1}{2}\mu_t \left[-I : C - 2 + n^{\dim} + 2\ln J\right]\right] I \underline{\otimes} I - \\
&+ \mu_t \left[C \overline{\otimes} I + C \underline{\otimes} I + I \underline{\otimes} C - I \otimes C - C \otimes I\right]
\end{aligned} \qquad \textbf{119}$$

In the following sections, the coupled rate form will be developed in hyperelastic setting. This can be achieved be taking the spatial and material time derivative of Equation (106). In other words the linearisation will be with respect to time rather than with respect to the coordinates. This will provide a unified platform to extend the formulation to A.L.E hyperelastodynamics, A.L.E hyperelastoplastics etc. The resulting Equations derived for the rate

A.L.E hyperelastic setting will be similar to the one developed in [57 & 58]. The new rate formulation does not require a separate convection stage. This convection stage will be embedded in the derived formulation. This will provide a simplified rate formulation compared to the traditional A.L.E hyperelastic rate formulation where this convection stage has to be taken into account in a separate stage, thus implying additional computational costs. The remeshing stage in the new rate A.L.E hyperelastic formulation is no longer arbitrary as the case with the traditional A.L.E methods but totally embedded in the formulation. In other words it is derived directly from the potential energy. This will not only reduce the computational cost but simplifies the complications involved in deriving remeshing Equations. Another important aspect is to employ the concept of imposed material force in optimisation. This term has been introduced by Uthman and Askes [28]. Furthermore, some examples will be illustrated to clarify the concept of imposed material force and its advantages over generated material force. The advantages of coupled solution over decoupled one will be illustrated with an example in term of imposed material force.

.

3.3 Formulation

In this section, the new arbitrary Lagrangian Eulerian method in hyperelastic setting will be introduced in rate form. This can be derived by taking the spatial and material time derivative of Equation (106):

$$\Delta_t \delta \ell = d_t \delta_x \ell + D_t \delta_x \ell + d_t \delta_X \ell + D_t \delta_X \ell \qquad \textbf{120}$$

The first two terms on the right hand side of Equation (120) represent the spatial and material time derivative of the spatial momentum Equation, in other words the linearization of the spatial momentum Equation with respect to time. The other two terms in the right hand side of Equation (120) represent the spatial and material time derivative of the material momentum Equation, thus linearisation of the material momentum Equation with respect to time.

3.3.1 Spatial momentum equations

We begin by reviewing Equation (109) given as:

$$\delta_x \ell = \int_\Omega \frac{\partial N}{\partial x} \cdot \sigma d\Omega$$

Making use of the above Equation the first term on the right hand side of Equation (120) which represents the spatial time derivative of the spatial momentum:

$$d_t \delta_x \ell = d_t \int_\Omega \frac{\partial N}{\partial x} \cdot \sigma d\Omega \qquad \textbf{121}$$

by which:

$$d_t \delta_x \ell = \int_\Omega \frac{\partial N}{\partial x} d_t \sigma d\Omega$$

Making use of the chain rule the above Equation can be written as:

$$d_t \delta_x \ell = \int_\Omega \frac{\partial N}{\partial x} \frac{d\sigma}{df} \frac{df}{dt} d\Omega$$

This can also be written as:

$$d_t \delta_x \ell = \int_\Omega \frac{\partial N}{\partial x} \frac{d\sigma}{df} \frac{df}{dt} F f d\Omega \qquad \textbf{122}$$

Thereby we made use of the relation between the direct and the inverse motion $f \cdot F = I$. Making use of the following relation [83]:

$$L = \frac{df}{dt} F = \nabla_X V \qquad \textbf{123}$$

where L represents the material velocity gradient, and substituting Equation (123) into (122) results in:

$$d_t \delta_x \ell = \int_\Omega \frac{\partial N}{\partial x} \frac{d\sigma}{df} L f d\Omega$$

$$d_t \delta_x \ell = \int_\Omega \frac{\partial N}{\partial x} \frac{d\sigma}{df} \nabla_X V f d\Omega$$

$$d_t \delta_x \ell = \int_\Omega \frac{\partial N}{\partial x} \frac{d\sigma}{df} \nabla_x V d\Omega \qquad \textbf{124}$$

The spatial gradient of the material velocity can be discretised as:

$$\nabla_x V = \frac{\partial N}{\partial x} V$$

Substitution in Equation (124) will produce the following:.

$$d_t \delta_x \ell = \int_\Omega \frac{\partial N}{\partial x} \frac{d\sigma}{df} \frac{\partial N}{\partial x} d\Omega V \qquad \textbf{125}$$

This term represents the offdiagonal term in the spatial momentum Equation, or in other words the coupling term. This is similar to the term derived in the total formulation (second term in Equation 115). This term represents the tangent that has been derived in [57 & 58] and was reviewed earlier (Equation 118). Now we turn to the second term in Equation (120) which represents the material time derivative of the spatial momentum Equation. Making use of Equation (109) this will give:

$$D_t \delta_x \ell = D_t \int_\Omega \frac{\partial N}{\partial x} \cdot \sigma d\Omega \qquad \textbf{126}$$

In order to avoid linearising the configuration, the above Equation is pulled back to the undeformed configuration Ω_0 as:

$$D_t \delta_x \ell = D_t \int_{\Omega_0} \frac{\partial N}{\partial X} \frac{\partial X}{\partial x} \cdot \sigma J d\Omega_0 \qquad \textbf{127}$$

Thereby the chain rule has been applied and the relation $d\Omega = J d\Omega_0$. Making use of the relation between the Cauchy stress tensor σ and the first Piola-Kirchhoff stress tensor P, that is $\sigma = J^{-1} F \cdot P$, will produce the following Equation:

$$D_t \delta_x \ell = \int_{\Omega_0} \frac{\partial N}{\partial X} \cdot D_t(P) d\Omega_0 \qquad \textbf{128}$$

Since the relation between the Kirchhoff stress tensor and the first Piola-Kirchhoff stress is given as $\tau = F \cdot P$, the material time derivative of the Kirchhoff stress tensor is given as:

$$Dt(\tau) = Dt(F) \cdot P + F \cdot Dt(P) \qquad \textbf{129}$$

Substitution of Equation (129) into (128) will result into:

$$D_t \delta_x \ell = \int_{\Omega_0} \frac{\partial N}{\partial X} F^{-1} \cdot (D_t(\tau) - D_t(F) P) d\Omega_0 \qquad \textbf{130}$$

Making use of the relation between the direct and the inverse motion $f \cdot F = I$ and the following relation [83]:

$$l = \frac{DF}{Dt} f = \nabla_x v \qquad \textbf{131}$$

Thereby l represents the spatial velocity gradient. Equation (130) can be written as:

$$D_t \delta_x \ell = \int_{\Omega_0} \frac{\partial N}{\partial X} F^{-1} \cdot (D_t(\tau) - lFP) d\Omega_0 \qquad \textbf{132}$$

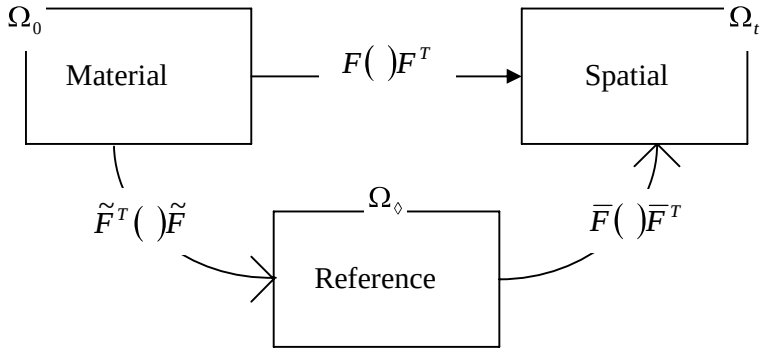

Figure 43- Stress transformation in the spatial representation between the reference, the material and the spatial configuration.

$$D_t \delta_x \ell = \int_{\Omega_0} \frac{\partial N}{\partial X} F^{-1} \cdot \left(Dt(\tau) - l\tau \right) d\Omega_0 \qquad \textbf{133}$$

The spatial deformation gradient can be decomposed into its referential deformation gradients as:

$$F = \overline{F} \cdot \widetilde{F} \ ,.$$

$$\text{and } F^t = \left(\overline{F} \cdot \widetilde{F} \right)^t = \widetilde{F}^t \cdot \overline{F}^t \qquad \textbf{134}$$

The following transformation can be obtained between the stress tensors in the material and spatial configuration (see Figure 43):

$$\overline{F}_{i\alpha} \cdot \widetilde{F}^t_{I\alpha} \left(\ \right) \widetilde{F}_{BJ} \cdot \overline{F}^t_{Bj} = \overline{F}_{i\alpha} \cdot \widetilde{F}_{\alpha I} \left(\ \right) \widetilde{F}^t_{JB} \cdot \overline{F}^t_{Bj} = F_{iI} \left(\ \right) F^t_{Jj} \qquad \textbf{135}$$

Thereby the last step was carried out with the help of the relations in (134). The rest of the formulation will follow the standard procedure of the Lagrangian formulation where some modifications regarding the direct and inverse motion will be included. The resulting Equations are similar to the Lagrangian one with no convection resulting from the material time derivative as would the case with the Eulerian formulation.

$$D_t \delta_x \ell = \int_{\Omega_0} \frac{\partial N}{\partial x} \cdot \left(Dt(\tau) - l\tau \right) d\Omega_0 \qquad \textbf{136}$$

Thereby Equation (136) resulted from Equation (133). Making use of the transformation in Equation (135) the relation between the Kirchhoff stress tensor τ and the second Piola Kirchhoff stress tensor S is given as:

$$\tau = F \cdot S \cdot F^T \qquad \textbf{137}$$

The following relation can be obtained:

$$F \cdot \frac{DS}{Dt} \cdot F^t = F \cdot \frac{D}{Dt} \left(F^{-1} \cdot \tau \cdot F^{-T} \right) \cdot F^T$$

$$F \cdot \frac{DS}{Dt} \cdot F^t = F \cdot \left(\frac{DF^{-1}}{Dt} \cdot \tau \cdot F^{-T} + F^{-1} \cdot \frac{D\tau}{Dt} \cdot F^{-T} + F^{-1} \cdot \tau \cdot \frac{DF^{-T}}{Dt} \right) \cdot F^T$$

$$F \cdot \frac{DS}{Dt} \cdot F^t = F \cdot \left(- f \cdot \frac{DF}{Dt} \cdot f \cdot \tau \cdot f^T + f \cdot \frac{D\tau}{Dt} \cdot f^T - f \cdot \tau \cdot f^T \cdot \frac{DF^T}{Dt} \cdot f^T \right) \cdot F^T$$

Making use of the relation (131) we obtain:

$$F \cdot \frac{DS}{Dt} \cdot F^t = \frac{D\tau}{Dt} - l \cdot \tau - \tau \cdot l^T \qquad \textbf{138}$$

Substitution of Equation (138) into Equation (137) will result in:

$$D_t \delta_x \ell = \int_{\Omega_0} \frac{\partial N}{\partial x} \cdot \left(F \cdot \frac{DS}{Dt} \cdot F^T + \tau \cdot l^T \right) d\Omega_0 \qquad \textbf{139}$$

Using the chain rule:

$$D_t \delta_x \ell = \int_{\Omega_0} \frac{\partial N}{\partial x} \cdot \left(F \cdot \frac{DS}{DC} : \frac{DC}{Dt} \cdot F^T + \tau \cdot l^T \right) d\Omega_0 \qquad \textbf{140}$$

The following transformation can be obtained between the strain tensors in the material and spatial configuration (see Figure 44); which is the inverse transformation of the one given in Equation (135):

$$\overline{F}_{i\alpha}^{-T} \cdot \widetilde{F}_{I\alpha}^{-1}(\ )_{IJ}\, \widetilde{F}_{BJ}^{-T} \cdot \overline{F}_{Bj}^{-1} = \overline{F}_{i\alpha}^{-T} \cdot \widetilde{F}_{\alpha I}^{-T}(\ )_{IJ}\, \widetilde{F}_{JB}^{-1} \cdot \overline{F}_{Bj}^{-1} = F^{-T}(\ )F^{-1} \qquad \textbf{141}$$

The material time derivative of the Green strain tensor C can be given as the pull back (using the above transformation) of the rate of the deformation tensor:

$$\frac{1}{2}\frac{DC}{Dt} = F^T \cdot D \cdot F \qquad \textbf{142}$$

Making use of the relation given (131), the above relation can be written as:

$$D = \frac{1}{2}\left(l + l^T\right)$$

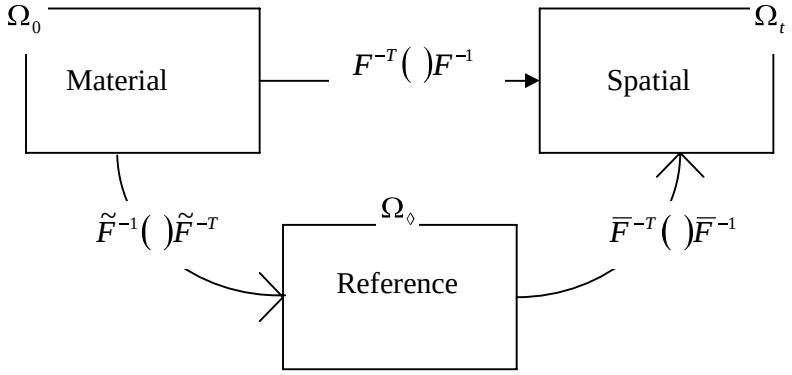

Figure 44- Strain transformation in the spatial representation between the reference, the material and the spatial configuration.

Using Equation (142) we can write Equation (140) as:

$$D_t\delta_x\ell = \int_{\Omega_0}\frac{\partial N}{\partial x}\cdot\left(C^\tau : D + \tau\cdot l^T\right)d\Omega_0$$

Thereby the spatial moduli C^τ have been obtained by pushing the material moduli C^S forward using the relation $C^\tau_{mnpq} = F_{im}F_{jn}F_{kp}F_{lq}C^S_{ijkl}$, making use of the relation between the Kirchhoff stress tensor and the Cauchy stress tensor $\tau = J\sigma$, the above Equation can be written as:

$$D_t\delta_x\ell = \int_{\Omega}\frac{\partial N}{\partial x}\cdot\left(C^\sigma : D + \sigma\cdot l^T\right)d\Omega \qquad \textbf{143}$$

As in the Lagrangian formulation the above Equation consists of the material and geometrical tangent stiffness contributions. The second term gives the geometrical contribution as:

$$\left(D_t \delta_x \ell\right)_{jk}^{geom} = \int_{\Omega} \frac{\partial N_I}{\partial x_j} \cdot \sigma_{jk} \cdot \frac{\partial N_J}{\partial x_k} d\Omega \delta_{rs} v_{sJ} \qquad \textbf{144}$$

where the geometrical tangent contribution can be obtained from the above Equation and Equation (111) as:

$$I \overline{\otimes} \sigma = \left[\left(\lambda_0 \ln J - \mu_0\right) I \overline{\otimes} I\right] + \mu_0 I \overline{\otimes} b \qquad \textbf{145}$$

The material contribution given by the first term on the right hand side of Equation (143) can be written as:

$$\left(D_t \delta_x \ell\right)_{ij}^{mat} = \int_{\Omega} \frac{\partial N_I}{\partial x_k} \cdot C_{kijl}^{\sigma} \cdot \frac{\partial N_J}{\partial x_l} d\Omega v_{jJ} \qquad \textbf{146}$$

Making use of the transformation between the stress tensors in Equation (135), the second Piola Kirchhoff stress tensor can be obtained from Equation (111):

$$S = JF^{-1} \cdot \sigma \cdot F^{-T} = \lambda_0 \ln J C^{-1} + \mu_0 \left(I - C^{-1}\right) \qquad \textbf{147}$$

Taking the derivative with respect to the right Green strain tensor:

$$C^S = 2\frac{\partial S}{\partial C} = \lambda_0 C^{-1} \otimes C^{-1} - \lambda_0 \ln J \left[C^{-1} \overline{\otimes} C^{-1} + C^{-1} \underline{\otimes} C^{-1}\right] + \mu_0 \left[C^{-1} \overline{\otimes} C^{-1} + C^{-1} \underline{\otimes} C^{-1}\right]$$

Making use of the relation $C_{ijkl}^{\sigma} = F_{im} F_{jn} F_{kp} F_{lq} C_{ijkl}^{S}$, we can obtain:

$$C^{\sigma} = \lambda_0 I \otimes I - \lambda_0 \ln J \left[I \overline{\otimes} I + I \underline{\otimes} I\right] + \mu_0 \left[I \overline{\otimes} I + I \underline{\otimes} I\right] \qquad \textbf{148}$$

The total tangent is given as the sum of the material and geometrical tangent stiffness fourth order tensors:

$$C = \lambda_0 I \otimes I - \lambda_0 \ln J I \underline{\otimes} I + \mu_0 I \underline{\otimes} I + \mu_0 I \overline{\otimes} b \qquad \textbf{149}$$

The results obtained for the spatial Equations from the rate formulation are identical to those obtained with the total formulation in [57&58] (Equation 116).

3.3.2 Material momentum equations

In this section, the same procedure that was followed to obtain the linearised spatial Equations will be carried out to obtain the linearised material Equations. First we review Equation (110) as:

$$\delta_X \ell = \int_{\Omega_0} \frac{\partial N}{\partial X} \cdot \sum d\Omega_0$$

The fourth term on the right hand side of Equation (120) which represents the material time derivative of the material momentum Equation can rewritten with the help of the above relation as:

$$D_t \delta_X \ell = D_t \int_{\Omega_0} \frac{\partial N}{\partial X} \cdot \sum d\Omega_0 \qquad \textbf{150}$$

This can be written as:

$$D_t \delta_X \ell = \int_{\Omega_0} \frac{\partial N}{\partial X} D_t \sum d\Omega_0$$

Making use of the chain rule the above Equation can be written as:

$$D_t \delta_X \ell = \int_{\Omega_0} \frac{\partial N}{\partial X} \frac{d \sum}{dF} \frac{dF}{Dt} d\Omega_0$$

This can also be written as:

$$D_t \delta_X \ell = \int_{\Omega_0} \frac{\partial N}{\partial X} \frac{d \sum}{dF} \frac{dF}{Dt} fF d\Omega_0$$

Thereby we made use of the relation between the direct and the inverse motion $f \cdot F = I$. Making use of the relation (131), the above Equation can be given as:

$$D_t \delta_X \ell = \int_{\Omega_0} \frac{\partial N}{\partial X} \frac{d \sum}{dF} lF d\Omega_0$$

$$D_t \delta_X \ell = \int_{\Omega_0} \frac{\partial N}{\partial X} \frac{d \sum}{dF} \nabla_x v F d\Omega_0$$

$$D_t \delta_X \ell = \int_{\Omega_0} \frac{\partial N}{\partial X} \frac{d \sum}{dF} \nabla_X v d\Omega_0 \qquad \textbf{151}$$

The material gradient of the spatial velocity can be discretised as:

$$\nabla_X v = \frac{\partial N}{\partial X} v$$

Substitution in Equation (151) will produce the following:

$$D_t \delta_X \ell = \int_{\Omega_0} \frac{\partial N}{\partial X} \frac{d \sum}{dF} \frac{\partial N}{\partial X} d\Omega_0 v \qquad \textbf{152}$$

This term represents the offdiagonal term in the material momentum Equation, or in other words the coupling term. This is similar to the term derived in the total formulation (Equation 117). This term representing the tangent has been derived [57 & 58] and will be given here again for completeness:

$$\frac{d \sum}{dF} \cdot F = \left[\lambda_0 \left[\ln J - 1\right] - \mu_0\right] I \otimes I + \mu_0 \left[I \otimes b - F^T \underline{\otimes} F^T - F^T \overline{\otimes} F^T\right] \qquad \textbf{153}$$

Making use of Equation (110) given as:

$$\delta_X \ell = \int_{\Omega_0} \frac{\partial N}{\partial X} \cdot \sum d\Omega_0$$

The third term in Equation (120) can be written with the help of the above Equation as:

$$d_t \delta_X \ell = d_t \int_{\Omega_0} \frac{\partial N}{\partial X} \cdot \sum d\Omega_0$$

This can also be written as:

$$d_t \delta_X \ell = d_t \int_{\Omega} \frac{\partial N}{\partial x} \frac{\partial x}{\partial X} \cdot \sum j d\Omega$$

Thereby the chain rule has been applied as well as the relation $d\Omega = J d\Omega_0$. Making use of the relation between the Eshelby stress tensor and the material nominal stress tensor $\sum = Jf \cdot \pi$ [57 & 58] will produce the following Equation:

$$d_t \delta_X \ell = \int_{\Omega} \frac{\partial N}{\partial x} \cdot d_t(\pi) d\Omega \qquad \textbf{154}$$

Since the relation between the material Kirchhoff stress tensor Γ and the material first Piola-Kirchhoff stress π is given as $\Gamma = f \cdot \pi$, the spatial time derivative of the material Kirchhoff stress tensor is given as:

$$dt(\Gamma) = dt(f) \cdot \pi + f \cdot dt(\pi) \qquad \textbf{155}$$

Substitution of Equation (155) into (154) will result into:

$$d_t \delta_X \ell = \int_{\Omega} \frac{\partial N}{\partial x} f^{-1} \cdot (dt(\Gamma) - dt(f)\pi) d\Omega \qquad \textbf{156}$$

Making use of the relation (123) and the relation between the direct and the inverse motion:

$$d_t \delta_X \ell = \int_{\Omega} \frac{\partial N}{\partial x} f^{-1} \cdot (dt(\Gamma) - Lf\pi) d\Omega$$

$$d_t \delta_X \ell = \int_{\Omega} \frac{\partial N}{\partial x} f^{-1} \cdot (dt(\Gamma) - L\Gamma) d\Omega$$

The material deformation gradient can be decomposed into its referential deformation gradients as:

$$f = \tilde{f} \cdot \bar{f} \text{ and } f^t = \left(\tilde{f} \cdot \bar{f} \right)^t = \bar{f}^t \cdot \tilde{f}^t \qquad \textbf{157}$$

The following transformation can be obtained between the stress tensors in the material and spatial configuration (see Figure 45):

$$\tilde{f}_{i\alpha} \cdot \bar{f}_{I\alpha}(\,) \bar{f}_{BJ} \cdot \tilde{f}_{Bj} = \tilde{f}_{i\alpha} \cdot \bar{f}_{\alpha I}(\,) \bar{f}^t_{JB} \cdot \tilde{f}^t_{Bj} = f(\,) f^t \qquad \textbf{158}$$

Thereby the last step was carried out with the help of the relations in (157). The formulation will follow the same path as in the spatial representation:

$$d_t \delta_X \ell = \int_\Omega \frac{\partial N}{\partial X} \cdot \left(dt(\Gamma) - L\Gamma \right) d\Omega \qquad \textbf{159}$$

Thereby Equation (159) resulted from Equation (156). Making use of the transformation in Equation (158) the relation between the material Kirchhoff stress tensor and the material second Piola Kirchhoff stress tensor is given as:

$$\Gamma = f \cdot s \cdot f^t \qquad \textbf{160}$$

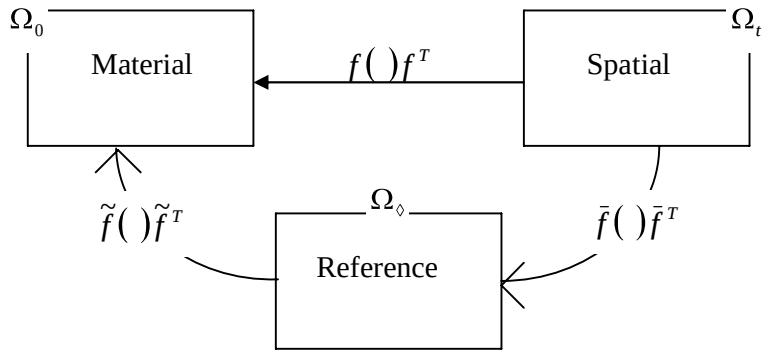

Figure 45- Stress transformation in the material representation between the reference, the material and the spatial configuration.

The following relation can be obtained:

$$f \cdot \frac{ds}{dt} \cdot f^T = f \cdot \frac{d}{dt}\left(f^{-1} \cdot \Gamma \cdot f^{-T} \right) \cdot f^T$$

$$f \cdot \frac{ds}{dt} \cdot f^t = f \cdot \left(\frac{df^{-1}}{dt} \cdot \Gamma \cdot f^{-T} + f^{-1} \cdot \frac{d\Gamma}{dt} \cdot f^{-T} + f^{-1} \cdot \Gamma \cdot \frac{df^{-T}}{dt} \right) \cdot f^T$$

$$f \cdot \frac{ds}{dt} \cdot f^t = f \cdot \left(-F \cdot \frac{df}{dt} \cdot F \cdot \Gamma \cdot F^T + F \cdot \frac{d\Gamma}{dt} \cdot F^T + F \cdot \Gamma \cdot F^T \cdot \frac{df^T}{dt} \cdot F^T \right) \cdot f^T$$

Making use of the relation (123) we obtain:

$$f \cdot \frac{ds}{dt} \cdot f^t = \frac{d\Gamma}{dt} - L \cdot \Gamma - \Gamma \cdot L^T \qquad \textbf{161}$$

Substitution of Equation (161) into Equation (159) will result in:

$$d_t \delta_X \ell = \int_\Omega \frac{\partial N}{\partial X} \cdot \left(f \cdot \frac{ds}{dt} \cdot f^T + \Gamma \cdot L^T \right) d\Omega \qquad \textbf{162}$$

Using the chain rule:

$$d_t \delta_X \ell = \int_{\Omega} \frac{\partial N}{\partial X} \cdot \left(f \cdot \frac{ds}{dc} : \frac{dc}{dt} \cdot f^T + \Gamma \cdot L^T \right) d\Omega \qquad \textbf{163}$$

The following transformation can be obtained between the strain tensors in the material and spatial configuration (see Figure 46):

$$\tilde{f}^{-T}_{i\alpha} \cdot \bar{f}^{-1}_{I\alpha}(\,)\bar{f}^{-T}_{BJ} \cdot \tilde{f}^{-1}_{Bj} = \tilde{f}^{-T}_{i\alpha} \cdot \bar{f}^{-T}_{\alpha I}(\,)\bar{f}^{-1}_{JB} \cdot \tilde{f}^{-1}_{Bj} = f^{-T}(\,)f^{-1}$$

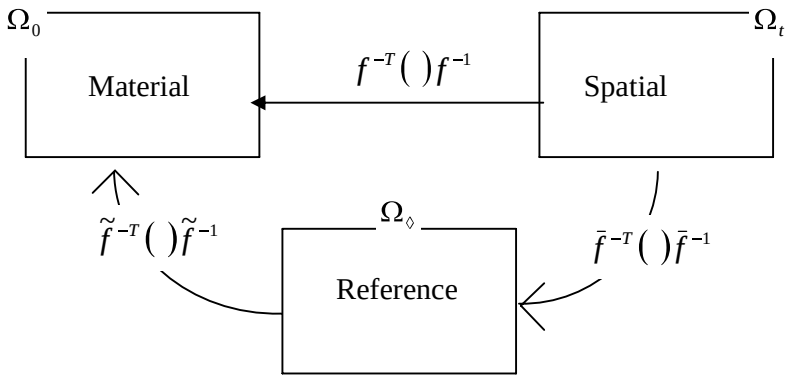

Figure 46- Strain transformation in the material representation between the reference, the material and the spatial configuration.

The spatial time derivative of the material Green strain tensor can be given as the pull back (using the above transformation) of the material rate of the deformation tensor:

$$\frac{1}{2}\frac{dc}{dt} = f^T \cdot d \cdot f \qquad \textbf{164}$$

Making use of the relation given (123), the above relation can be written as:

$$d = \frac{1}{2}\left(L + L^T\right)$$

Using Equation (164) we can write Equation (163) as:

$$d_t \delta_X \ell = \int_{\Omega} \frac{\partial N}{\partial X} \cdot \left(C^{\Gamma} : d + \Gamma \cdot L^T\right) d\Omega$$

Thereby the material moduli C^{Γ} have been obtained by pushing the spatial moduli C^s back using the relation $C^{\Gamma}_{mnpq} = f_{im} f_{jn} f_{kp} f_{lq} C^s_{ijkl}$, making use of the relation between the material Kirchhoff stress tensor and the Eshelby stress tensor $\Gamma = j\sum$, the above Equation can be written as:

$$d_t \delta_X \ell = \int_{\Omega_0} \frac{\partial N}{\partial X} \cdot \left(C^{\Sigma} : d + \sum \cdot L^T\right) d\Omega_0 \qquad \textbf{165}$$

As in the spatial formulation the above Equation consists of material and geometrical tangent stiffness contributions. The second term gives the geometrical contribution as:

$$\left(d_t \delta_X \ell\right)_I^{geom} = \int_{\Omega_0} \frac{\partial N_I}{\partial X_j} \cdot \sum_{jk} \cdot \frac{\partial N_J}{\partial X_k} d\Omega_0 V_J \qquad \textbf{166}$$

where geometrical tangent contribution can be obtained from the above Equation and Equation (112) as:

$$C^{geom} = I \overline{\otimes} \sum = \left[\frac{1}{2}\lambda_t \ln J\left[\ln J - 2\right] + \frac{1}{2}\mu_t\left[I : C + 2 - n^{\dim} - 2\ln J\right]\right] I \overline{\otimes} I - \mu_t C \overline{\otimes} I \qquad \textbf{167}$$

The material contribution given by the first term on the right hand side of Equation (165) can be written as:

$$\left(d_t \delta_X \ell\right)_I^{mat} = K_{ijIJ}^{mat} V_{jJ} = \int_{\Omega_0} \frac{\partial N_I}{\partial X_k} \cdot C_{kijl}^{\Sigma} \cdot \frac{\partial N_J}{\partial X_l} d\Omega_0 V_{jJ}$$

Making use of the transformation between the stress tensors in Equation (160), and the following relations:

$$C_{ijkl}^{\Sigma} = jf_{im} f_{jn} f_{kp} f_{lq} C_{mnpq}^{s} \quad , \qquad C^s = 2\frac{\partial s}{\partial c}$$

The material tangent can be obtained as:

$$\begin{aligned} C^{mat} = C^{\Sigma} = &\left[W_t - 2\lambda_t LnJ + 2\mu_t + \lambda_t\right] I \otimes I + \left[-W_t + \lambda_t LnJ - \mu_t\right] I \underline{\otimes} I + \\ &\left[-W_t + \lambda_t LnJ - \mu_t\right] I \overline{\otimes} I - \mu_t I \otimes C - \mu_t C \otimes I + \mu_t C \overline{\otimes} I + \mu_t C \underline{\otimes} I + \\ &\mu_t I \underline{\otimes} C + \mu_t I \overline{\otimes} C \end{aligned} \qquad \textbf{168}$$

The total tangent is given as the sum of the material and geometrical tangent stiffness fourth order tensors:

$$\begin{aligned} C^{tot} = C^{geom} + C^{mat} = &\left[\frac{1}{2}\lambda_t \ln J\left[\ln J - 4\right] + \lambda_t + \frac{1}{2}u_t\left[I : C + 4 - n^{\dim} - 2\ln J\right]\right] I \otimes I \\ &+ \left[\frac{1}{2}\lambda_t \ln J\left[-\ln J + 2\right] + \frac{1}{2}u_t\left[-I : C - 2 + n^{\dim} + 2\ln J\right]\right] I \underline{\otimes} I - \\ &+ u_t\left[C \overline{\otimes} I + C \underline{\otimes} I + I \underline{\otimes} C - I \otimes C - C \otimes I\right] \end{aligned} \qquad \textbf{169}$$

The results obtained for the material Equations from the rate formulation are identical to those obtained with the total formulation in [57&58]. The advantage in this new rate formulation is that no convection is required compared to the traditional A.L.E rate formulation. The results also highlight the striking duality between the spatial and material formulations.

3.3 Examples

The first example deals with a cubical structure with the dimension $10*10*10$, fixed at one end and subjected to a concentrated compression load at the other end $P=-1000$ as shown in Figure 47. The continuum is discretised with a finite element mesh of 512 solid elements. The modulus of elasticity is $E=1000$ and Poisson ratio $\nu=0$, which implies that the Lamé constants are $\lambda=0$ and $\mu=500$. A Lagrangian solution was carried out first with the Newton Raphson scheme for 50 increments. The solution is shown in Figure 47 where it is clear from the stress overview its localisation under the applied concentrated loads.

The same calculations were carried out in terms of imposed material force to obtain the optimised solution. The initial spatial and material configurations are given in Figure 48. The spatial configuration is subjected to a concentrated compression load of $P=-1000$ while the material configuration under imposed material force of $P=1000$. A staggered A.L.E Newton Raphson solution of 50 increments was carried out to give the optimised spatial and material configuration (see Figure 48). It is clear that the localisation obtained in the Lagrangian solution is no longer there. The remeshing towards the points where the loads were applied results in smoothing the stresses. The results can be improved even further by increasing the level of mesh refinements.

In order to illustrate the influence of mesh refinement the second example will be discretised with 2000 solid elements. The structure with the dimension $10*10*10$ is fixed at one end and subjected to a concentrated load at the other end. The initial spatial and material configurations are given in Figure 49. The spatial configuration is subjected to a concentrated compression load of $P=-400$ while the material configuration under imposed material force of $P=400$. Thus the concept of imposed material forces is used again. The modulus of elasticity is $E=1000$ and Poisson ratio is $\nu=0$. A staggered A.L.E Newton Raphson solution of 4 increments was carried out to give the optimised spatial and material configuration (see Figures 49). As it is clear from the results the method provides a local optimised solution. Thus mesh refinements does not have much influence except for the local area around the load.

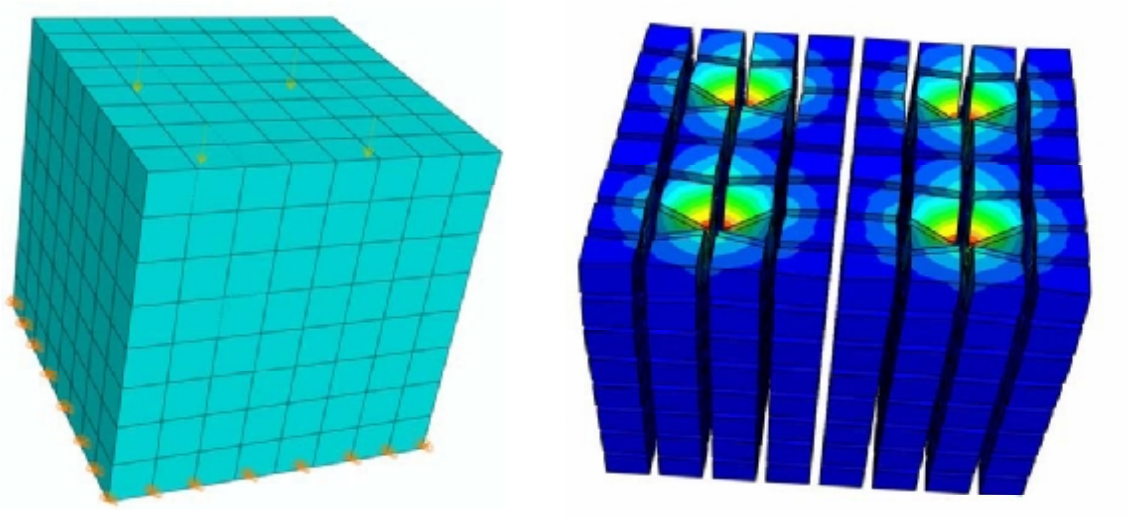

Initial configuration **Lagrangian solution**

Figure 47 512 element discretization

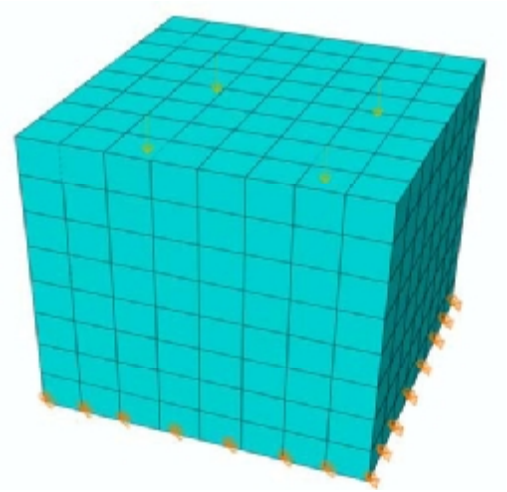

Initial spatial configuration

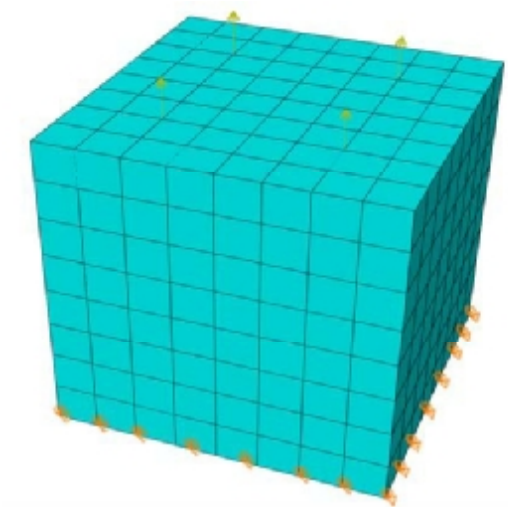

Initial material configuration

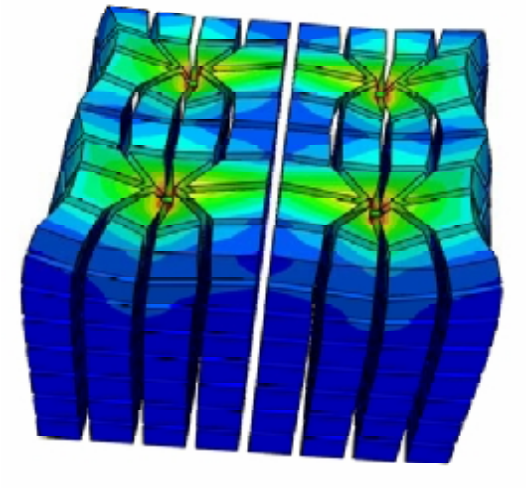

Optimised spatial configuration

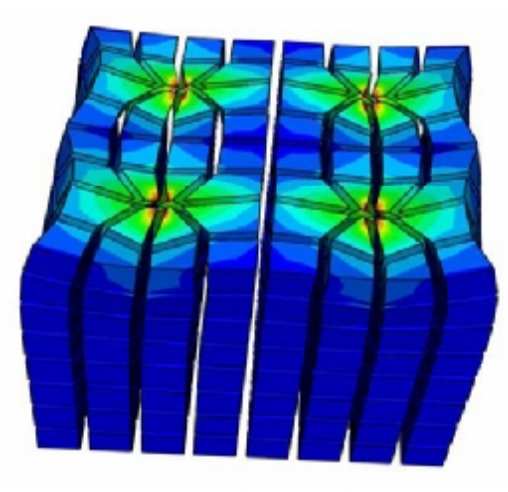

Optimised material configuration

Figure 48 512 element discretization

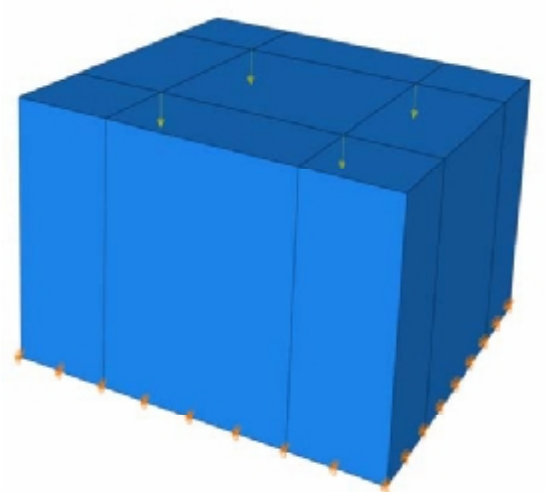

Initial spatial configuration

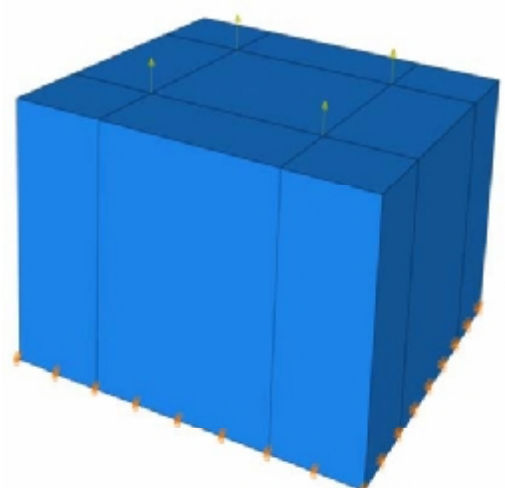

Initial material configuration

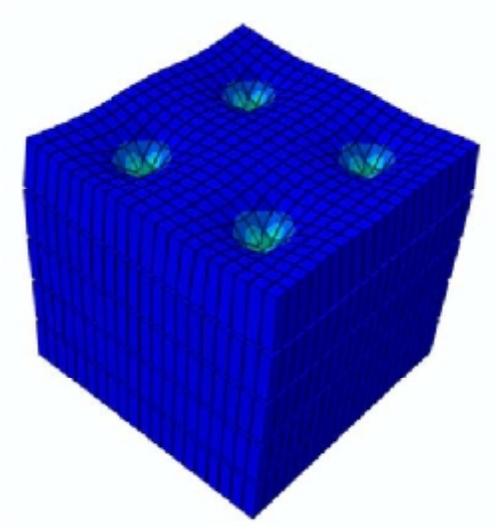

Optimised spatial configuration

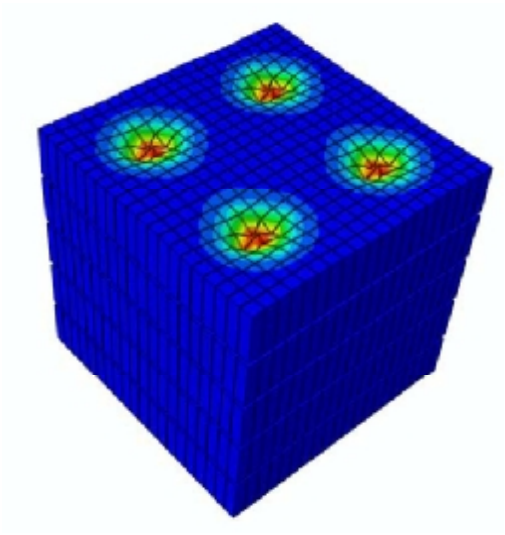

Optimised material configuration

Figure 49 2000 finite element mesh refinement

4 A.L.E HYPERELASTODYNAMIC FORMULATION OF CONTINUUM MECHANICS

4.1 Motivation

In this chapter we consider a new formulation and numerical implementation of a three dimensional hyperelastodynamic ALE model. Our objective is to motivate our development of the theory to optimise the shape or meshing in dynamic setting for a discretised continuum with finite elements. Since the main thrust is for numerical solution and implementation of shape and mesh optimisation in dynamic setting, an attempt is made to formulate the governing Equations in a form suitable for our subsequent numerical implementation with the finite element method. To this end, once the governing Equations are developed that highlight the essential mathematical aspects of the theory, the corresponding numerical algorithms are summarised in a Table that highlights the essential steps involved in the actual numerical implementation.

4.2 Introduction

In the previous chapter a rate ALE formulation was developed for statics in which the potential energy is minimised with respect to spatial as well as material coordinates. In this chapter the framework will be extended to a dynamic setting. Variational arbitrary Lagrangian Eulerian hyperelastodynamics will be introduced using the ALE Hamiltonian principle. A vanishing variation of the total Lagrangian function can be obtained in terms of its variation with respect to the spatial coordinates at fixed material and reference coordinates plus its variation with respect to the material coordinates at fixed spatial and referential coordinates. We will introduce the momentum and the continuity Equations from the variation in total Lagrangian function. The spatial motion problem will introduce the spatial momentum and continuity Equation while the material motion will introduce the material momentum and continuity Equation. The weak form of the momentum and continuity Equations is obtained through discretisation. Next, both Equations will be linearised and integrated in time.

We will use the implicit Newmark time-stepping algorithm for the momentum and the continuity Equations as a spatial and material variational integrator. The time stepping algorithm will include a Newton-Raphson equilibrium iteration loop. The results represent the optimised spatial and material configuration.

A scheme of the iteration procedure will be given. We illustrate some examples giving their optimised spatial and material configuration. Furthermore, we will treat the concept of imposed material force in the material configuration.

4.3 Basic formulations

In this section a review of some basic spatial and material basic relations will be given [53, 56]. We begin by introducing the spatial acceleration a as the material time derivative of the spatial velocity as well as the material acceleration A as the spatial time derivative of the material velocity. The spatial and material acceleration can be given respectively as:

$$a = D_t v(X,t), \; A = d_t V(x,t) \qquad \textbf{170}$$

Further we will make use of the following general relations between the material and the spatial time derivatives:

$$D_t\{\bullet\} = d_t\{\bullet\} + \nabla_x\{\bullet\}\cdot v = d_t\{\bullet\} + \nabla_x\{\bullet\}\cdot \bar{c} \qquad \textbf{171}$$

$$d_t\{\bullet\} = D_t\{\bullet\} + \nabla_X\{\bullet\}\cdot V = D_t\{\bullet\} + \nabla_X\{\bullet\}\cdot \bar{C} \qquad \textbf{172}$$

where $\bar{c}$ and $\bar{C}$ are the spatial and material convective velocities respectively. The first term on the right hand side of each Equation is the spatial and material time derivative while the second term is the convective term. An additional useful relation will be the material and spatial time derivative of an integral or the so called Reynolds transport theorem:

$$\frac{D}{D_t}\int_{\beta_t} r(x,t)dV_t = \int_{\beta_t}\left(\frac{Dr(x,t)}{Dt} + r\frac{\partial v_i}{\partial x_i}\right)dV_t \qquad \textbf{173}$$

$$\frac{d}{d_t}\int_{\beta_0} R(X,t)dV_0 = \int_{\beta_0}\left(\frac{dR(X,t)}{dt} + R\frac{\partial V_i}{\partial X_i}\right)dV_0 \qquad \textbf{174}$$

R and r are functions of the material and spatial coordinates, respectively.

4.4 Hamilton's principle

The Hamiltonian principle of least action is proven to be equivalent to the Newtonian Equations of motion. According to the Hamiltonian principle the total Lagrangian can be obtained through integrating the Lagrangian l_ξ over the time t:

$$\ell = \int_{t_0}^{t_1} l_\xi Dt \qquad \textbf{175}$$

The total variation in the Lagrangian can be given as its variation with respect to the spatial coordinates x at fixed material and referential coordinates X and ξ plus its variation with respect to the material coordinates X at fixed spatial and referential coordinates x and ξ:

$$\delta\ell = \delta_x \ell + \delta_X \ell = 0 \qquad \textbf{176}$$

In what follows we will illustrate the derivation of the spatial and material variational Equations according to the Hamiltonian principle.

4.4.1 Spatial variational equation

We begin by writing the Lagrangian in the spatial domain as:

$$\ell\left[x(X,t)\right] = \int_{t_0}^{t_1} l\left[x(X,t), v(X,t), t\right] Dt \qquad \textbf{177}$$

where the Lagrangian in the spatial domain is given as a function of the spatial coordinates, spatial velocity and the time. Let $\delta x(X,t)$ describe a small variation around the spatial motion $x(X,t)$. We assume a variation of a spatial motion is permitted within a certain time interval. In other words $\delta x(X,t_0)$=0 and $\delta x(X,t_1)$=0 hold. Using conventional differential calculus we can express Equation (175) in the spatial domain as:

$$\ell\left[x(X,t)+\delta x(X,t)\right] = \int_{t_0}^{t_1} l\left[x(X,t)+\delta x(X,t), v(X,t)+\delta v(X,t), t\right] Dt \qquad 178$$

The Taylor expansion of the spatial Lagrangian of terms linear in $\delta x(t)$ is given as:

$$l\left[x(X,t)+\delta x(X,t), v(X,t)+\delta v(X,t), t\right] = l\left[x(X,t), v(X,t), t\right] + \left(\frac{\partial l}{\partial x}\cdot\delta x + \frac{\partial l}{\partial v}\cdot\delta v\right) + O(\varepsilon^2) \qquad \textbf{179}$$

where $O(\varepsilon^2)$ represent the higher order terms which will be neglected.

We note, using $\partial_t f(t)g(t) = \dot{f}(t)\cdot g(t) + f(t)\cdot\dot{g}(t)$, that

$$\frac{\partial l}{\partial v}\cdot\delta v=\frac{D}{Dt}\cdot\left(\frac{\partial l}{\partial v}\cdot\delta x\right)-\left(\frac{D}{Dt}\cdot\frac{\partial l}{\partial v}\right)\cdot\delta x \qquad \textbf{180}$$

This yields

$$\ell\left[x(X,t)+\delta x(X,t)\right]=$$
$$\ell\left[x(X,t)\right]+\int_{t_0}^{t_1}\left[\frac{\partial l}{\partial x}-\frac{D}{Dt}\left(\frac{\partial l}{\partial v}\right)\right]\cdot\delta x\cdot Dt+\int_{t_0}^{t_1}\frac{D}{Dt}\left(\frac{\partial l}{\partial v}\delta x\right)\cdot Dt+O(\varepsilon^2) \qquad \textbf{181}$$

Neglecting the second order terms, we can write the variation of the total Lagrangian with respect to the spatial coordinates as:

$$\delta_x\ell=\delta\ell\left[x(X,t)+\delta x(X,t)\right]=\int_{t_0}^{t_1}\left[\frac{\partial l}{\partial x}-\frac{D}{Dt}\left(\frac{\partial l}{\partial v}\right)\right]\cdot\delta x\cdot Dt+\frac{\partial l}{\partial v}\delta x\Big|_{t_0}^{t_1} \qquad \textbf{182}$$

As stated above the variation of the spatial motion vanishes at t_0 and t_1. This will give:

$$\delta_x\ell=\int_{t_0}^{t_1}\left[\frac{\partial l}{\partial x}-\frac{D}{Dt}\left(\frac{\partial l}{\partial v}\right)\right]\cdot\delta x\cdot Dt \qquad \textbf{183}$$

Since this property holds for any admissible spatial variation δx and taking into account that the spatial variation will vanish at t_0 and t_1, this will result in:

$$\frac{D}{Dt}\left(\frac{\partial l}{\partial v}\right)-\frac{\partial l}{\partial x}=0 \qquad \textbf{184}$$

The Lagrangian is simply the difference between the kinetic and the potential energy:

$$l(x,v,t)=T(v,t)-U(x,t) \qquad \textbf{185}$$

Equation (184) can then be written as:

$$\delta_x\ell=\frac{D}{Dt}\left(\frac{\partial T(v,t)}{\partial v}\right)-\frac{\partial U(x,t)}{\partial x}=0 \qquad \textbf{186}$$

which is simply Newton's second law of motion; the momentum conservation principle states that the material time derivative of the linear spatial momentum equals the net force. The net force is given as:

$$\frac{\partial U(x,t)}{\partial x}=\int_{\beta_t}\nabla_x\cdot\pi\cdot dV_t+\int_{\beta_t}\rho_t b_t\cdot dV_t \qquad \textbf{187}$$

where the spatial linear momentum is:

$$\frac{\partial T(v,t)}{\partial v}=\int_{\beta_t}P_t\cdot dV_t \qquad \textbf{188}$$

Substituting Equations (188& 187) into Equation (186) results in:

$$\delta_x\ell=D_t\int_{\beta_t}P_t\cdot dV_t-\int_{\beta_t}\nabla_x\cdot\pi\cdot dV_t-\int_{\beta_t}\rho_t b_t\cdot dV_t=0 \qquad \textbf{189}$$

where b_t is the spatial body force, π is the spatial momentum flux (or the first Piola-Kirchhoff stress) and P_t is the spatial momentum density. We proceed by defining the spatial momentum density as:

$$P_t = \rho_t g \cdot v \qquad \textbf{190}$$

where ρ_t is the spatial density and g is the spatial covariant metric coefficient which defines the space-dependent base vectors. We substitute Equation (190) into (189) and apply the first Equation of Reynolds transport theorem (173), which results in the following spatial variational Equation:

$$\delta_x \ell = \int_{\beta_t} \left[\frac{D}{D_t}(\rho_t g \cdot v) + \rho_t v v_{,x} - \nabla_x \pi - \rho_t b_t \right] dV_t$$

$$= \int_{\beta_t} \left[\rho_t \frac{Dv}{D_t} + v\left(\frac{D\rho_t}{D_t} + \rho_t v_{,x} \right) - \nabla_x \pi - \rho_t b_t \right] dV_t \qquad \textbf{191}$$

4.4.2 Material variational equation

Analogously we begin by writing the Lagrangian in the material domain as:

$$\ell[X(x,t)] = \int_{t_0}^{t_1} l[X(x,t), V(x,t), t]\, dt \qquad \textbf{192}$$

where the Lagrangian in the material domain is given as a function of the material coordinates, material velocity and the time. Let $\delta X(x,t)$ describe a small variation around the material motion $X(x,t)$. We assume a variation of a material motion is permitted within a certain time interval. In other words $\delta X(x,t_0)$=0 and $\delta X(x,t_1)$=0 hold. Using conventional differential calculus we can express Equation (192) in the material domain as:

$$\ell[X(x,t) + \delta X(x,t)] = \int_{t_0}^{t_1} l[X(x,t) + \delta X(x,t), V(x,t) + \delta V(x,t), t]\, dt \qquad \textbf{193}$$

The Taylor expansion of the material Lagrangian of terms linear in $\delta X(t)$ is given as:

$$l[X(x,t) + \delta X(x,t), V(x,t) + \delta V(x,t), t] = l[X(x,t), V(x,t), t] + \left(\frac{\partial l}{\partial X} \cdot \delta X + \frac{\partial l}{\partial V} \cdot \delta V \right) + O(\varepsilon^2) \qquad \textbf{194}$$

We note using $\partial_t f(t)g(t) = \dot{f}(t) \cdot g(t) + f(t) \cdot \dot{g}(t)$

$$\frac{\partial l}{\partial V}\cdot\delta V=\frac{d}{dt}\cdot\left(\frac{\partial l}{\partial V}\cdot\delta X\right)-\left(\frac{d}{dt}\cdot\frac{\partial l}{\partial V}\right)\cdot\delta X \qquad \textbf{195}$$

This gives $\ell\left[X(x,t)+\delta X(x,t)\right]$

$$\ell\left[X(x,t)\right]+\int_{t_0}^{t_1}dt\cdot\left[\frac{\partial l}{\partial X}-\frac{d}{dt}\left(\frac{\partial l}{\partial V}\right)\right]\cdot\delta X+\int_{t_0}^{t_1}dt\cdot\frac{d}{dt}\left(\frac{\partial l}{\partial V}\delta X\right)+O(\varepsilon^2) \qquad \textbf{196}$$

Neglecting the second order terms, we can write the variation of the total Lagrangian with respect to the material coordinates as:

$$\delta_X\ell=\delta\ell\left[X(x,t),\delta X(x,t)\right]=\int_{t_0}^{t_1}dt\cdot\left[\frac{\partial l}{\partial X}-\frac{d}{dt}\left(\frac{\partial l}{\partial V}\right)\right]\cdot\delta X+\frac{\partial l}{\partial V}\delta X\Big|_{t_0}^{t_1} \qquad \textbf{197}$$

According to our assumption the variation of the material motion vanishes at t_0 and t_1. This will give:

$$\delta_X\ell=\int_{t_0}^{t_1}dt\cdot\left[\frac{\partial l}{\partial X}-\frac{d}{dt}\left(\frac{\partial l}{\partial V}\right)\right]\cdot\delta X \qquad \textbf{198}$$

Since this property holds for any admissible material variation δX and taking into account that the material variation will vanish at t_0 and t_1, this will result in:

$$\delta_X\ell=\frac{d}{dt}\left(\frac{\partial l}{\partial V}\right)-\frac{\partial l}{\partial X}=0 \qquad \textbf{199}$$

Again, the Lagrangian is simply the difference between the kinetic and the potential energy:

$$l(X,V,t)=T(V,t)-U(X,t) \qquad \textbf{200}$$

Substitution of Equation (200) into (199) results in:

$$\delta_X\ell=\frac{d}{dt}\left(\frac{\partial T(V,t)}{\partial V}\right)-\frac{\partial U(X,t)}{\partial X}=0 \qquad \textbf{201}$$

which represents the momentum conservation principle, the spatial time derivative of the linear material momentum equals the net force. The net force is given as:

$$\frac{\partial U(X,t)}{\partial X}=\int_{\beta_0}\nabla_X\Pi\cdot dV_0+\int_{\beta_0}\rho_0 B_0\cdot dV_0 \qquad \textbf{202}$$

while the material linear momentum is expressed as:

$$\frac{\partial T(V,t)}{\partial V}=\int_{\beta_0}P_0\cdot dV_0 \qquad \textbf{203}$$

Substituting Equations (202& 203) into Equation (201) results in:

$$\delta_X \ell = d_t \int_{\beta_0} P_0 \cdot dV_0 - \int_{\beta_0} \nabla_X \Pi \cdot dV_0 - \int_{\beta_0} \rho_0 \cdot \mathrm{B}_0 \cdot dV_0 = 0 \qquad \textbf{204}$$

where B_t is the material body force, Π is the material momentum flux (or like first Piola-Kirchhoff stress) and P_0 is the material momentum density. We proceed by defining the material momentum density as:

$$P_0 = \rho_0 G \cdot V \qquad \textbf{205}$$

where ρ_0 is the material density and G is the material covariant metric coefficient which defines the space-dependent base vectors. We substitute Equation (205) into (204) and apply the second Equation of Reynolds transport theorem (174). We obtain the following material variational Equation:

$$\delta_X \ell = \int_{\beta_0} \left(\frac{d}{d_t}(\rho_0 G V) + \rho_0 V V_{,X} - \nabla_X \Pi - \rho_0 B_0 \right) dV_0$$

$$= \int_{\beta_0} \left[\rho_0 G \frac{dV}{dt} + \rho_0 V \frac{dG}{dt} + VG \left(\frac{d\rho_0}{dt} + \rho_0 V_{,X} \right) - \nabla_X \Pi - \rho_0 B_0 \right] dV_0 \qquad \textbf{206}$$

In the next sections we will derive the spatial and material continuity Equations. The continuity Equations will be used to derive the spatial and material non-conservative form of the momentum Equations from their derived conservative momentum Equations.

4.5 Continuity Equations

In a Lagrangian mesh mass conservation is enforced through the following Equation:

$$\rho_t \cdot J = \rho_0 \qquad \textbf{207}$$

In the context of the newly developed ALE scheme this will no longer hold true. Mass conservation is instead imposed through the partial differential Equations treated in this section.

4.5.1 Spatial continuity equation

The mass m in a spatial domain is given by:

$$m = \int_{\beta_t} \rho_t dV_t \qquad \textbf{208}$$

Mass conservation requires that the mass of any spatial domain be constant. Therefore, the material time derivative of m vanishes, i.e.

$$\frac{Dm}{Dt} = \frac{D}{Dt} \int_{\beta_t} \rho_t dV_t = 0 \qquad \textbf{209}$$

Applying Reynolds theorem, Equation (173), to the above yields

$$\int_{\beta_t} \left(\frac{D\rho_t}{Dt} + \rho_t v_{,x} \right) dV_t = 0 \qquad \textbf{210}$$

Since the above holds for any subdomain β_t, it follows that

$$\frac{D\rho_t}{Dt} + \rho_t v_{,x} = 0 \qquad \textbf{211}$$

The above Equation represents the mass conservation Equation (continuity Equation) in the spatial domain. Applying the material time derivative Equation (171), results in:

$$\frac{d\rho_t}{dt} + \rho_{t,x} v + \rho_t v_{,x} = 0 \qquad \textbf{212}$$

The above Equation is a conservative form of the continuity Equation in the spatial domain. Letting the trial solution be ρ_t and the test function $\delta\rho_t$, the weak form of the spatial continuity Equation can be obtained by multiplying the strong form, Equation (212), by a test function and integrating over the spatial domain:

$$\int_{\beta_t}[\delta\rho_t \frac{d\rho_t}{dt} + \delta\rho_t \rho_{t,x} v + \delta\rho_t \rho_t v_{,x}]dV_t = 0 \quad \textbf{213}$$

The trial and test function are discretised via:

$$\rho_{tJ}(x,t) = \sum_{J=1}^{N} N_J(x)\rho_{tJ}(t)$$

$$\delta\rho_{tI}(x) = \sum_{I=1}^{N} N_I(x)\delta\rho_{tI} \quad \textbf{214}$$

where N is the number of interior nodes. Substituting Equation (214) into (213) results in:

$$\sum_{J=1}^{N}\sum_{I=1}^{N} \delta\rho_{tI} \int_{\beta_t}[N_I N_J \frac{d\rho_{tJ}}{dt} + N_I v_x N_{J,x}\rho_{tJ} + N_I v_{x,x} N_J \rho_{tJ}]dV_t = 0 \quad \textbf{215}$$

Since this holds for arbitrary $\delta\rho_{tI}$ at interior nodes, we obtain:

$$\frac{d\rho_{tJ}}{dt}\int_{\beta_t} N_I N_J dV_t + \rho_{tJ}\int_{\beta_t} N_I v_x N_{J,x} dV_t + \rho_{tJ}\int_{\beta_t} N_I v_{x,x} N_J dV_t = 0 \quad \textbf{216}$$

where $I = 1$ to N. We define the following matrices:

$$m^{\rho} = \int_{\beta_t} N_I N_J dV_t \quad \textbf{217}$$

$$l^{\rho} = \int_{\beta_t} N_I v_x N_{J,x} dV_t \quad \textbf{218}$$

$$k^{\rho} = \int_{\beta_t} N_I v_{x,x} N_J dV_t \quad \textbf{219}$$

Where; $m^{\rho}, l^{\rho}, k^{\rho}$ are the spatial capacity, transport, and divergence matrices. Substituting into Equation (216) gives the following spatial finite element matrix Equation:

$$m^{\rho}\frac{d\rho_t}{dt} + l^{\rho}\rho_t + k^{\rho}\rho_t = 0 \quad \textbf{220}$$

4.5.2 Material continuity equation

Analogously the mass M in a material domain is given by:

$$M = \int_{\beta_0} \rho_0 dV_0 \quad \textbf{221}$$

Mass conservation requires that the mass of any material domain be constant. Therefore, the spatial time derivative of M vanishes, i.e.

$$\frac{dM}{dt} = \frac{d}{dt}\int_{\beta_0} \rho_0 dV_0 = 0 \quad \textbf{222}$$

Applying Reynolds theorem, Equation (174), to the above yields:

$$\int_{\beta_0}\left(\frac{d\rho_0}{dt}+\rho_0 V_{,X}\right)dV_0=0 \qquad \textbf{223}$$

Since the above holds for any subdomain β_0, it follows that

$$\frac{d\rho_0}{dt}+\rho_0 V_{,X}=0 \qquad \textbf{224}$$

The above Equation represents the mass conservation Equation (continuity Equation) in the spatial domain. Applying the spatial time derivative Equation (171) results in:

$$\frac{D\rho_0}{Dt}+\rho_{0,X}V+\rho_0 V_{,X}=0 \qquad \textbf{225}$$

Letting the trial solution be ρ_0 and the test function $\delta\rho_0$, the weak form of the material continuity Equation can be obtained by multiplying the strong form Equation (225) by the test function and integrating over the material domain:

$$\int_{\beta_0}\left[\delta\rho_0\frac{D\rho_0}{Dt}+\delta\rho_0\rho_{0,X}V+\delta\rho_0\rho_0 V_{,X}\right]dV_0=0 \qquad \textbf{226}$$

The trial and test function are discretised by:

$$\rho_{0L}(X,t)=\sum_{L=1}^{N}N_L(X)\cdot\rho_{0L}(t)$$

$$\delta\rho_{0K}(X)=\sum_{K=1}^{N}N_K(X)\cdot\delta\rho_{0K} \qquad \textbf{227}$$

Substituting Equation (226) into (227) results in:

$$\sum_{L=1}^{N}\sum_{K=1}^{N}\delta\rho_{0K}\int_{\beta_0}\left[N_K N_L\frac{D\rho_{0L}}{Dt}+N_K V_X N_{L,X}\rho_{0L}+N_K V_{X,X}N_J\rho_{0L}\right]dV_0=0 \qquad \textbf{228}$$

Since this holds for arbitrary $\delta\rho_{0K}$ at interior nodes, we obtain:

$$\frac{D\rho_{0L}}{Dt}\int_{\beta_0}N_K N_L dV_0+\rho_{0L}\int_{\beta_0}N_K V_X N_{L,X}dV_0+\rho_{0L}\int_{\beta_0}N_K V_{X,X}N_L dV_0=0 \qquad \textbf{229}$$

where $K=1 \quad to \quad N$. We define the following matrices:

$$M^{\rho}=\int_{\beta_0}N_K N_L dV_0 \qquad \textbf{230}$$

$$L^{\rho}=\int_{\beta_0}N_K V_X N_{L,X}dV_0 \qquad \textbf{231}$$

$$K^{\rho}=\int_{\beta_0}N_K V_{X,X}N_L dV_0 \qquad \textbf{232}$$

Here $M^{\rho}, L^{\rho}, K^{\rho}$ are the material capacity, transport, and divergence matrices. Substituting into Equation (229) gives the following material finite element matrix Equation:

$$M^{\rho}\frac{D\rho_0}{Dt} + L^{\rho}\rho_0 + K^{\rho}\rho_0 = 0 \qquad \textbf{233}$$

4.6 Momentum Equations

We will now proceed with the spatial and material variational Equations to obtain the spatial and material momentum Equations. For simplicity, we will derive a non-conservative form of spatial and material momentum Equations:

4.6.1 Spatial Momentum equation

Upon a closer look at the second term in Equation (191), we can recognise Equation (211) which vanishes, giving:

$$\int_{\beta_t}\left[\rho_t \frac{Dv}{Dt} - \nabla_x \cdot \pi - \rho_t b_t\right] dV_t = 0 \qquad \textbf{234}$$

Since the above Equation holds for an arbitrary domain, the Equation can be reduced to:

$$\rho_t \frac{Dv}{Dt} - \nabla_x \cdot \pi - \rho_t b_t = 0 \qquad \textbf{235}$$

The material time derivative of the velocity can be written out by Equation (171) as:

$$\rho_t\left(\frac{\partial v}{\partial t} + v_{,x} \cdot v\right) - \nabla_x \cdot \pi - \rho_t b_t = 0 \qquad \textbf{236}$$

The above Equation represents the non-conservative form of the spatial momentum Equation. The weak form can be obtained through multiplying the above Equation by the test function δv and integrating over the spatial configuration:

$$\int_{\beta_t} \delta v \cdot \left[\rho_t\left(\frac{\partial v}{\partial t} + v_x v\right) - \nabla_x \cdot \pi - \rho_t b_t\right] dV_t = 0 \qquad \textbf{237}$$

Expanding the second term by the product rule results in:

$$\int_{\beta_t}\left[\delta v \rho_t\left(\frac{\partial v}{\partial t} + v_{,x} v\right) - \nabla_x(\delta v \pi) + \nabla_x(\delta v)\pi - \delta v \rho_t b_t\right] dV_t = 0 \qquad \textbf{238}$$

We apply Gauss's theorem and write out the second term as:

$$\int_{\beta_t} \nabla_x(\delta v \pi) dV_t = \int_{\Gamma_u} \delta v\left[n \cdot \pi\right] \cdot d\Gamma + \int_{\Gamma_t} \delta v n \pi \cdot d\Gamma \qquad \textbf{239}$$

where n is the outward normal to the spatial domain, Γ_u and Γ_t are the kinematic and traction boundaries respectively. Since the test function vanishes on the complement of the traction boundaries, Equation (239) becomes:

$$\int_{\beta_t} \nabla_x(\delta v \pi) dV_t = \int_{\Gamma_t} \delta v n \pi \cdot d\Gamma = \int_{\Gamma_t} \delta v \cdot t \cdot d\Gamma \qquad \textbf{240}$$

where t are the surface tractions. Substituting Equation (240) into (238) results in:

$$\int_{\beta_t}\left[\delta v\rho_t\left(\frac{\partial v}{\partial t}+v_{,x}v\right)+\nabla_x(\delta v)\pi-\delta v\rho_t b_t\right]dV_t-\int_{\Gamma_t}\delta vtd\Gamma=0 \qquad \textbf{241}$$

The discretisation of the trial and test functions are given by:

$$v_J(x,t)=\sum_{J=1}^{N}N_J(x)v_J(t)$$

$$\delta v_I(x)=\sum_{I=1}^{N}N_I(x)\delta v_I \qquad \textbf{242}$$

Substituting the above Equations (242) into Equation (241) results in:

$$\delta v_I\int_{\beta_t}\left[\rho_t N_I^x N_J^x\frac{\partial v}{\partial t}+\rho_t N_I^x v_x N_{J,x}^x v+N_{I,x}^x\pi-\rho_t N_I^x b_t\right]dV_t-\delta v_I\int_{\Gamma_t}N_I^x td\Gamma=0 \qquad \textbf{243}$$

Since this holds for arbitrary δv_I, we obtain:

$$\frac{\partial v}{\partial t}\int_{\beta_t}\rho_t N_I^x N_J^x dV_t+v\int_{\beta_t}\rho_t N_I^x v_x N_{J,x}^x dV_t+\int_{\beta_t}N_{I,x}^x\pi dV_t-\int_{\beta_t}\rho_t N_I^x b_t dV_t-\int_{\Gamma_t}N_I^x td\Gamma=0 \qquad \textbf{244}$$

We can write the above Equation as:

$$r_x=m^x\frac{\partial v}{\partial t}+l^x v+f^{\text{int}}-f^{ext}=0 \qquad \textbf{245}$$

The above Equation represents the finite element Equations in the spatial domain, where m^x and l^x are the spatial mass and convective matrices respectively, r_x is the spatial residual, while f^{int} and f^{ext} are the spatial internal and external force vectors respectively, such that:

$$m^x=\int_{\beta_t}\rho_t N_I^x N_J^x dV_t \qquad \textbf{246}$$

$$l^x=\int_{\beta_t}\rho_t N_I^x v_x N_{J,x}^x dV_t \qquad \textbf{247}$$

$$f^{\text{int}}=\int_{\beta_t}N_{I,x}^x\pi\cdot dV_t \qquad \textbf{248}$$

$$f^{ext}=\int_{\beta_t}\rho_t N_I^x b_t dV_t+\int_{\Gamma_t}N_I^x\cdot t\cdot d\Gamma \qquad \textbf{249}$$

4.6.2 Material Momentum equation

A closer look at the second term in Equation (206), and taking Equation (224) into account reveals that:

$$\int_{\beta_0}\left[\rho_0 G\frac{dV}{dt}+\rho_0 V\frac{dG}{dt}-\nabla_X\Pi-\rho_0 B_0\right]dV_0=0 \qquad \textbf{250}$$

Since the above Equation holds for an arbitrary domain, the Equation can be reduced to:

$$\rho_0 G\frac{dV}{dt}+\rho_0 V\frac{dG}{dt}-\nabla_X \Pi-\rho_0 B_0=0 \qquad \textbf{251}$$

The spatial time derivative of the velocity can be written out by Equation (172) as:

$$\rho_0 V\left(\frac{DG}{Dt}+G_{,X}\cdot V\right)+\rho_0 G\left(\frac{DV}{Dt}+V_{,X}\cdot V\right)-\nabla_X \Pi-\rho_0 B_0=0 \qquad \textbf{252}$$

The above Equation represents the non-conservative form of the material momentum Equation. The weak form can be obtained through multiplying the above Equation by the test function δV and integrating over the material configuration:

$$\int_{\beta_0}\delta V\left[\rho_0 V\left(\frac{DG}{Dt}+G_{,X}\cdot V\right)+\rho_0 G\left(\frac{DV}{Dt}+V_{,X}\cdot V\right)-\nabla_X \Pi-\rho_0 B_0\right]dV_0=0 \qquad \textbf{253}$$

Expanding the second term by the product rule results in:

$$\int_{\beta_0}\Big[\delta V\rho_0 V\left(\frac{DG}{Dt}+G_{,X}\cdot V\right)+\delta V\rho_0 G\left(\frac{DV}{Dt}+V_{,X}V\right)-\nabla_X(\delta V\Pi)+\nabla_X(\delta V)\Pi-$$

$$\delta V\rho_0 B_0\Big]dV_0=0$$

254

We apply Gauss's theorem and write out the third term as:

$$\int_{\beta_0}\nabla_X(\delta V\Pi)dV_0=\int_{\Gamma_u}\delta V\left[N\cdot\Pi\right]d\Gamma+\int_{\Gamma_t}\delta VN\Pi d\Gamma \qquad \textbf{255}$$

where N is the outward normal to the material domain. Since the test function vanishes on the complement of the traction boundaries, Equation (255) becomes:

$$\int_{\beta_0}\nabla_X(\delta V\Pi)dV_0=\int_{\Gamma_t}\delta VN\Pi d\Gamma=\int_{\Gamma_t}\delta VTd\Gamma \qquad \textbf{256}$$

where T are the surface tractions. In order to ensure continuity on the traction boundary of the spatial and material domain, the jumps in the spatial and material stresses should balance each other:

$$T+t=0\Rightarrow T=-t \qquad \textbf{257}$$

The meaning of the above Equation is that applying an external spatial force leads to applying a material force equal in magnitude but with opposite direction. Substituting Equation (257) into Equation (256) results in:

$$\nabla_X(\delta V\Pi)=-\int_{\Gamma_t}\delta V\cdot t\cdot d\Gamma \qquad \textbf{258}$$

Substituting the above Equation into Equation (254) results in:

$$\int_{\beta_0}\delta V\rho_0 V\left(\frac{DG}{Dt}+G_{,X}V\right)+\delta V\rho_0 G\left(\frac{DV}{Dt}+V_{,X}\cdot V\right)+\nabla_X(\delta V)\Pi-\delta V\rho_0 B_0\cdot dV_0+$$

$$\int_{\Gamma_t}\delta V\cdot t\cdot d\Gamma=0 \qquad \textbf{259}$$

We apply Gauss's theorem for the first term and this will result in:

$$\int_{\beta_0}\left[\delta V\rho_0 V\frac{DG}{Dt}-\delta V_{,X}\rho_0 VGV+\delta V\rho_0 G\left(\frac{DV}{Dt}+V_{,X}\cdot V\right)+\nabla_X(\delta V)\Pi-\right.$$
$$\left.\delta V\rho_0 B_0\right]\cdot dV_0+\int_{\Gamma_t}\delta V\cdot t\cdot d\Gamma+\int_{\Gamma}\delta V\rho_0 VNGV\cdot d\Gamma=0 \qquad \textbf{260}$$

where N is the outward normal to the material domain. Since the test function vanishes on the complement of the traction boundaries, Equation 260 becomes:

$$\int_{\beta_0}\left[\delta V\rho_0 V\frac{DG}{Dt}-\delta V_{,X}\rho_0 VGV+\delta V\rho_0 G\left(\frac{DV}{Dt}+V_{,X}\cdot V\right)+\nabla_X(\delta V)\Pi-\right.$$
$$\left.\delta V\rho_0 B_0\right]\cdot dV_0+\int_{\Gamma_t}\delta V\cdot t\cdot d\Gamma=0 \qquad \textbf{261}$$

Writing out the first term in more detail will result in:

$$\int_{\beta_0}\delta V\rho_0 V\frac{DF^T}{Dt}F+\delta V\rho_0 VF^T\frac{DF}{Dt}-\delta V_{,X}\rho_0 VGV+\delta V\rho_0 G\left(\frac{DV}{Dt}+V_{,X}\cdot V\right)+$$
$$\nabla_X(\delta V)\Pi-\delta V\rho_0 B_0\cdot dV_0+\int_{\Gamma_t}\delta V\cdot t\cdot d\Gamma=0 \qquad \textbf{262}$$

The trial and test functions are discretised by:

$$V_L(X,t)=\sum_{L=1}^{N}N_L(X)\cdot V_L(t)$$
$$\delta V_K(X)=\sum_{K=1}^{N}N_K(X)\cdot\delta V_K \qquad \textbf{263}$$
$$\frac{DF}{Dt}=\sum_{L=1}^{N}N_{L,X}(X)\cdot V_L(t)$$

Substituting the above Equations (263) into Equation (262) results in:

$$\delta V_K\int_{\beta_0}\rho_0 N_L^X VFN_{K,X}^X V+\rho_0 N_K^X VF^T N_{L,X}^X V-\rho_0 N_{L,X}VGN_K V+\rho_0 N_K^X GN_L^X\frac{DV}{Dt}+$$
$$\rho_0 N_K^X GV_X N_{L,X}^X V+N_{K,X}^X\Pi-\rho_0 N_K^X B_0\cdot dV_0+\delta V_K\int_{\Gamma_t}N_K^X\cdot t\cdot d\Gamma=0 \qquad \textbf{264}$$

Since this holds for an arbitrary δV_K, we obtain:

$$\frac{DV}{Dt}\int_{\beta_0}\rho_0 N_K^X GN_L^X dV_0+V\int_{\beta_0}\rho_0 N_K^X GV_X N_{L,X}^X+\int_{\beta_0}\rho_0 N_L^X VFN_{K,X}^X+\int_{\beta_0}\rho_0 N_K^X VF^T N_{L,X}^X$$
$$-\int_{\beta_0}\rho_0 N_{L,X}VGN_K+\int_{\beta_0}N_{K,X}^X\Pi\cdot dV_0-\int_{\beta_0}\rho_0 N_K^X B_0 dV_0+\int_{\Gamma_t}N_K^X\cdot t\cdot d\Gamma=0 \qquad \textbf{265}$$

We can write the above Equation as:

$$r_X=M^X\frac{DV}{Dt}+L^X V+F^{\text{int}}+F^{ext}=0 \qquad \textbf{266}$$

The above Equation represents the finite element Equation in the material domain, where M^X and L^X are the material mass and convective matrices respectively, r_X is the material residual, while F^{int} and F^{ext} are the material internal and external force vectors respectively, such that:

$$M^X = \int_{\beta_0} \rho_0 N_K^X G N_L^X dV_0 \qquad \textbf{267}$$

$$L^X = \int_{\beta_0} \rho_0 N_K^X G V_X N_{L,X}^X + \int_{\beta_0} \rho_0 N_L^X V F N_{K,X}^X + \int_{\beta_0} \rho_0 N_K^X V F^T N_{L,X}^X + \int_{\beta_0} \rho_0 N_{L,X} V G N_K dV_0 \qquad \textbf{268}$$

$$F^{\text{int}} = \int_{\beta_0} N_{K,X}^X \Pi \cdot dV_0 \qquad \textbf{269}$$

$$F^{ext} = \int_{\beta_0} \rho_0 N_K^X B_0 dV_0 + \int_{\Gamma_t} N_K^X \cdot t \cdot d\Gamma \qquad \textbf{270}$$

4.7 Linearisation and Time Integration

In the following sections we will carry out the temporal discretisation of the spatial and material continuity Equations (220, 233) as well as the spatial and material momentum Equations (245, 266). Since these Equations are nonlinear they have to be linearised and finally integrated in time within the Newmark algorithm.

4.7.1 Linearised continuity equations and time integration scheme

Carrying out temporal discretisation according to Newmark algorithm on the spatial and material continuity Equations (220, 233) and linearising them with respect to the spatial and material densities respectively, we will obtain the following linearised form of the spatial and material continuity Equations:

$$\left(\frac{m^{\rho}}{\gamma \Delta t} + l^{\rho} + k^{\rho} \right) \cdot \Delta \rho_t = -r_t \qquad \textbf{271}$$

$$\left(\frac{M^{\rho}}{\gamma \Delta t} + L^{\rho} + K^{\rho} \right) \cdot \Delta \rho_0 = -r_0 \qquad \textbf{272}$$

PREDICTION

$i \leftarrow 0$

$\rho_{t+\Delta t}^{(i)} = \rho_t \,.$

$\left(\frac{d\rho}{dt} \right)_{t+\Delta t}^{i} = \left(\frac{\gamma - 1}{\gamma} \right) \cdot \left(\frac{d\rho}{dt} \right)_t$

– NEXT – ITERATION –

$i \leftarrow i + 1$

$K_{eff} = \frac{m^{\rho}}{\gamma \Delta t} + l^{\rho} + k^{\rho}$

$-r^{(i)} = m^{\rho} \left(\frac{d\rho}{dt} \right)_{t+\Delta t}^{(i)} + l^{\rho} \rho_{t+\Delta t}^{(i)} + k^{\rho} \rho_{t+\Delta t}^{(i)}$

$\Delta \rho^{(i)} = K_{eff}^{-1} \cdot r^{(i)}$

CORRECTION

$\rho_{t+\Delta t}^{(i)} = \rho_{t+\Delta t}^{(i-1)} + \Delta \rho^{(i)}$

$\left(\frac{d\rho}{dt} \right)_{t+\Delta t}^{(i)} = \left(\frac{d\rho}{dt} \right)_{t+\Delta t}^{(i-1)} + \frac{\Delta \rho^{(i)}}{\gamma \Delta t}$

IF $\cdot \left\| r^{(i)} \right\| > \varepsilon \left\| r^{(0)} \right\| \cdot$ *repeat* $\cdot$ *for* $\cdot$ *next* $\cdot$ *iteration* .

else $\cdot$ *go* $\cdot$ *to* $\cdot$ *the* $\cdot$ *top*

Figure 50 Flow chart of implicit integration of the continuity equations.

where γ=0.5 is a Newmark parameter, $\Delta t = t^{n+1} - t^n$ is the time interval and r_t, r_0 are the spatial and material residuals given by Equations (220, 233). A flow chart for implicit integration of the linearised spatial and material continuity Equations is given in Figure 50, where the Newton- Raphson method has been used as well.

Here we gave only the spatial scheme for the continuity Equation; the same scheme is applicable for the material continuity Equation. We have omitted the t note for the spatial motion to prevent any confusion with the time. ε is a certain required tolerance and K_{eff} is the effective tangent. As we can see the solution of the spatial and material continuity Equations will provide an updating of the spatial and material densities.

4.7.2 Linearised momentum equations and time integration scheme

The temporal discretisation is carried out according to Newmark algorithm on the spatial momentum Equations (245). This is followed by linearisation with respect to the spatial coordinates x at fixed material coordinates X plus its linearisation with respect to the material coordinates X at fixed spatial coordinates x. This will produce the following linearised spatial momentum Equations:

$$\begin{aligned} r_x^{Ik+1} &= r_x^{Ik} + dr_x^I = 0 \\ dr_x^I &= \sum_{K=1}^{n} K_{xx}^{IK} \cdot dx_K + \sum_{L=1}^{n} K_{xX}^{IL} \cdot dX_L \end{aligned} \qquad \textbf{273}$$

where the summation gives the assembly over the global node numbers (n), dr_x^I denotes the iterative spatial residual at iteration (k+1) and K_{xx}^{IK}, K_{xX}^{IL} are the iteration matrices given as:

$$\begin{aligned} K_{xx} &= \frac{m^x}{\beta \Delta t^2} + l^x \frac{\gamma}{\beta \Delta t} + \frac{\partial f^{\text{int}}}{\partial x} - \frac{\partial f^{ext}}{\partial x} \\ K_{xX} &= \frac{m^x}{\beta \Delta t^2} \cdot F + l^x \frac{\gamma}{\beta \Delta t} \cdot F + \frac{\partial f^{\text{int}}}{\partial X} - \frac{\partial f^{ext}}{\partial X} \end{aligned} \qquad \textbf{274}$$

where β=0.25 is a Newmark parameter. In the same way we carry out time discretisation on the material momentum Equation (266), followed by linearisation with respect to the spatial coordinates x at fixed material coordinates X plus its linearisation with respect to the material coordinates X at fixed spatial coordinates x. This will produce the following linearised material momentum Equation:

$$r_X^{Jk+1} = r_X^{Jk} + dr_X^J = 0$$
$$dr_X^J = \sum_{K=1}^{n} K_{Xx}^{JK} \cdot dx_K + \sum_{L=1}^{n} K_{XX}^{JL} \cdot dX_L \qquad \textbf{275}$$

dr_x^J denotes the iterative material residual at iteration (k+1) and K_{Xx}^{JK}, K_{XX}^{JL} are the effective iteration matrices given as:

$$K_{Xx} = \frac{M^X}{\beta \Delta t^2} \cdot f + L^X \frac{\gamma}{\beta \Delta t} \cdot f + \frac{\partial F^{\text{int}}}{\partial x} - \frac{\partial F^{ext}}{\partial x}$$
$$K_{XX} = \frac{M^X}{\beta \Delta t^2} + L^X \frac{\gamma}{\beta \Delta t} + \frac{\partial F^{\text{int}}}{\partial X} - \frac{\partial F^{ext}}{\partial X} \qquad \textbf{276}$$

The Newton-Raphson method embedded in the implicit Newmark time integration scheme for the spatial and material momentum Equations enforced by the continuity Equations is given in Figure 51. For the internal terms in Equations (274) and (276) we refer the reader to reference [57, 58]. In what follows the so called follower load effect will not be taken into account. In this particular case the fourth terms on the right hand side of Equations (274) and (276) will vanish and $f_{material}^{ext} = -F_{spatial}^{ext}$ in the spatial and material finite element Equations (245, 266).

PREDICTION

$i \leftarrow 0$

$x_{t+\Delta t}^{(i)} = x_t$

$X_{t+\Delta t}^{(i)} = X_t$

$$a_{t+\Delta t}^{(i)} = -\frac{\Delta t}{\beta} v_t + \frac{\Delta t^2}{\beta}(1-\beta)\cdot a_t$$

$$A_{t+\Delta t}^{(i)} = -\frac{\Delta t}{\beta} V_t + \frac{\Delta t^2}{\beta}(1-\beta)\cdot A_t$$

$$v_{t+\Delta t}^{i} = v_t + \Delta t[(1-\gamma)a_t + \gamma \cdot a_{t+\Delta t}^{(i)}]$$

$$V_{t+\Delta t}^{i} = V_t + \Delta t[(1-\gamma)A_t + \gamma \cdot A_{t+\Delta t}^{(i)}]$$

$- NEXT \ - ITERATION \ -$

$i \leftarrow i+1$

Solve equations (274) and (276) for $K_{eff}^{(i)}$.

Solve equations (245) and (266) for $r_x^{(i)}$ and $r_X^{(i)}$.

Solve equations (273) and (275) monolithically for $dx^{(i)}$ and $dX^{(i)}$.

CORRECTION

$$x_{t+\Delta t}^{(i)} = x_{t+\Delta t}^{(i-1)} + dx^{(i)}$$

$$X_{t+\Delta t}^{(i)} = X_{t+\Delta t}^{(i-1)} + dX^{(i)}$$

$$v_{t+\Delta t}^{(i)} = v_{t+\Delta t}^{(i-1)} + \frac{\gamma}{\beta \Delta t}\cdot dx^{(i)}$$

$$V_{t+\Delta t}^{(i)} = V_{t+\Delta t}^{(i-1)} + \frac{\gamma}{\beta \Delta t}\cdot dX^{(i)}$$

$$a_{t+\Delta t}^{(i)} = a_{t+\Delta t}^{(i-1)} + \frac{1}{\beta \Delta t^2}\cdot dx^{(i)}$$

$$A_{t+\Delta t}^{(i)} = A_{t+\Delta t}^{(i-1)} + \frac{1}{\beta \Delta t^2}\cdot dX^{(i)}$$

Solve the spatial and material continuity equations and update ρ_t and ρ_0 (include spatial and material continuity scheme).

If $\left\|r^{(i)}\right\| > \varepsilon \left\|r^{(0)}\right\|$ repeat for next iteration.

Else $t \leftarrow t + \Delta t$ and go to the top.

Figure 51 Integration scheme of the spatial and material momentum equations

4.8 Examples

The first example is of a structure $(150*150*40)$ spatially fixed at the end corners (Figure 52), subjected to a uniformly distributed load at the top $(P=50)$. The loads were applied at a distance of (60) from each ends. The concept of generated material force has been implemented to optimise the mesh and consequently the wave propagation. The boundary of the material configuration is constrained such that it allows the nodes on the boundary to be relocated and move freely on the boundary plane while preventing it from moving in perpendicular direction to that plane (Figure 53). The structure was discretised with (900) fully integrated solid elements of $(2*2*2)$ integration points. The initial spatial and material mass densities are equal to (10). The structure has a modulus of elasticity of (1000). The time interval is taken as $(t=0.5)$.

The optimised spatial and material configurations through (10) increments (or time steps) are given in Figures 54A-54T. The solution gives the optimised mesh in terms of energy minimisation. The optimised spatial configuration shows the wave propagation towards the fixed ends while from the material configuration mesh motion can be seen towards the middle where the loads were applied and away from the boundary.

The second example presents a structure of $(150*150*40)$ spatially fixed at one corner end (Figure 55) and subjected to a uniform distributed load at the free end $(P=40)$. This has been applied over an area of $(50*50)$. As in the previous example the concept of generated material force has been implemented to optimise the mesh and consequently the wave propagation. The boundary of the material configuration is constrained in such that it allows the nodes on the boundary to be relocated and move freely on the boundary plane while preventing it from moving in perpendicular direction to that plane (Figure 56). The structure was discretised with (900) fully integrated solid elements of $(2*2*2)$ integration points. The initial spatial and material mass densities are equal to (10). The structure has a modulus of elasticity of (1000). The time interval is taken as $(t=0.5)$.

The Newton Raphson scheme solution has been carried out in (10) increments. The solution gives the optimised mesh in terms of energy minimization. The optimised spatial and material configurations are shown in (Figure 57 & 58). The optimised spatial configuration shows the wave propagation from the free edge towards the rigid end (Figure 57). The optimised material configuration shows the mesh motion towards the rigid end and away from the free end as shown in (Figure 58).

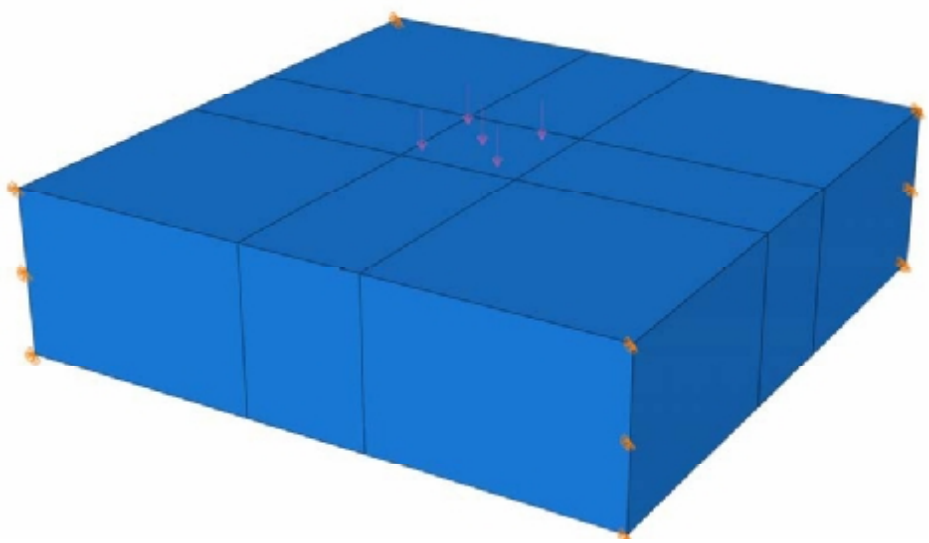

Figure 52 Initial spatial configuration

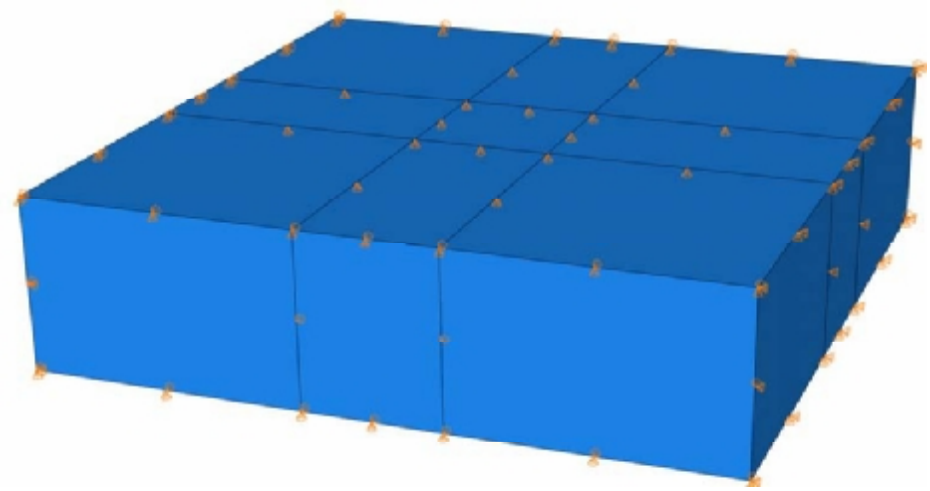

Figure 53 Initial material configuration

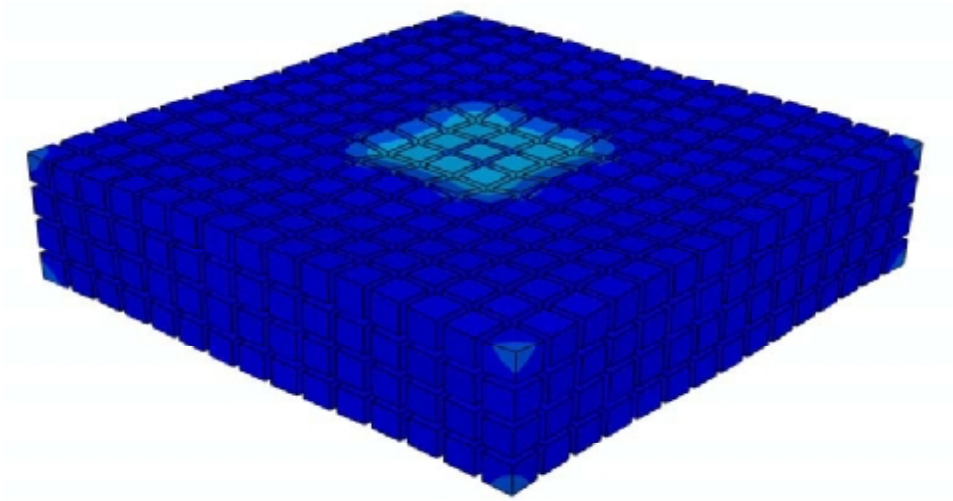

Figure 54A Top view, spatial configuration at the end of the second increment

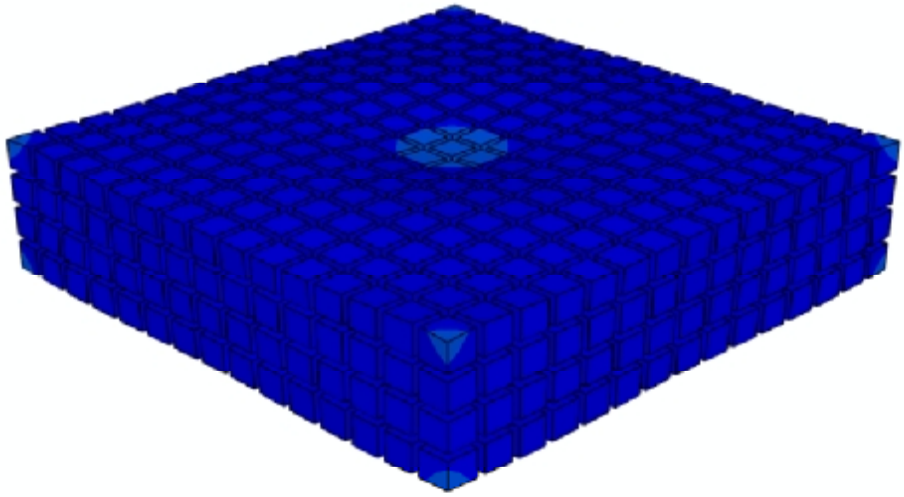

Figure 54B Bottom view, spatial configuration at the end of the second increment

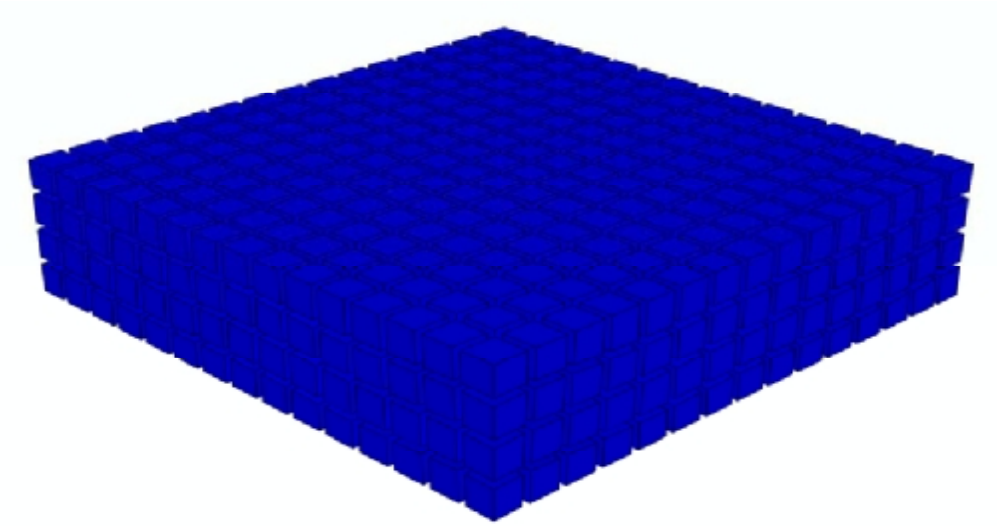

Figure 54C Top view, material configuration at the end of second increment

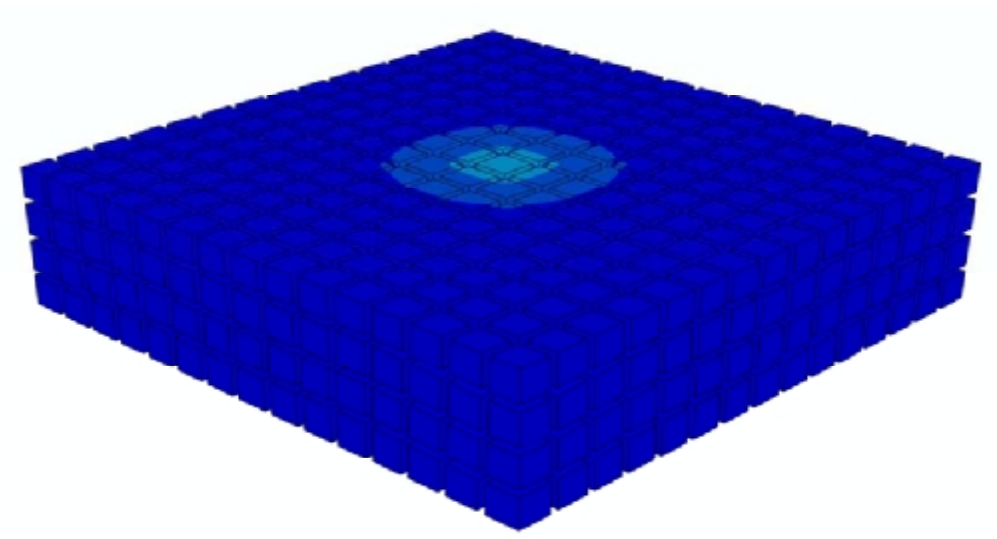

Figure 54D Bottom view, material configuration at the end of second increment

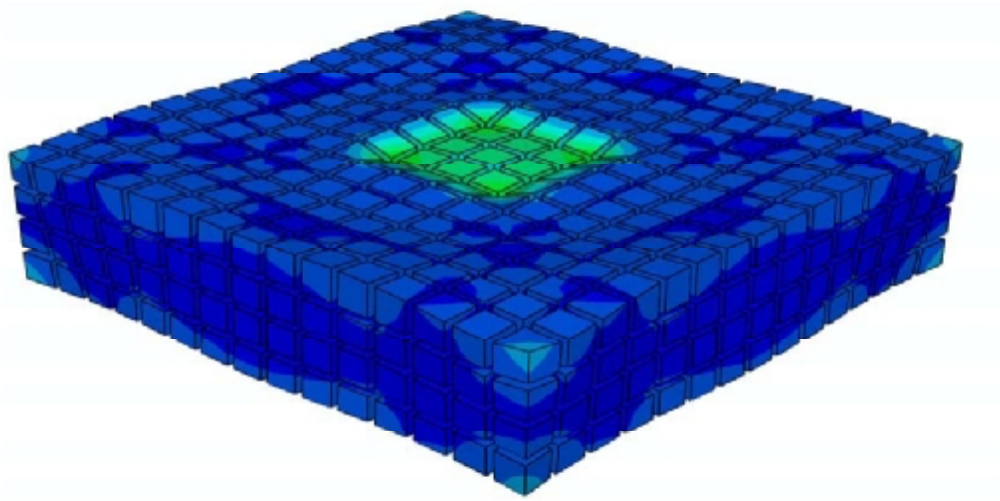

Figure 54E Top view, spatial configuration at the end of the fourth increment

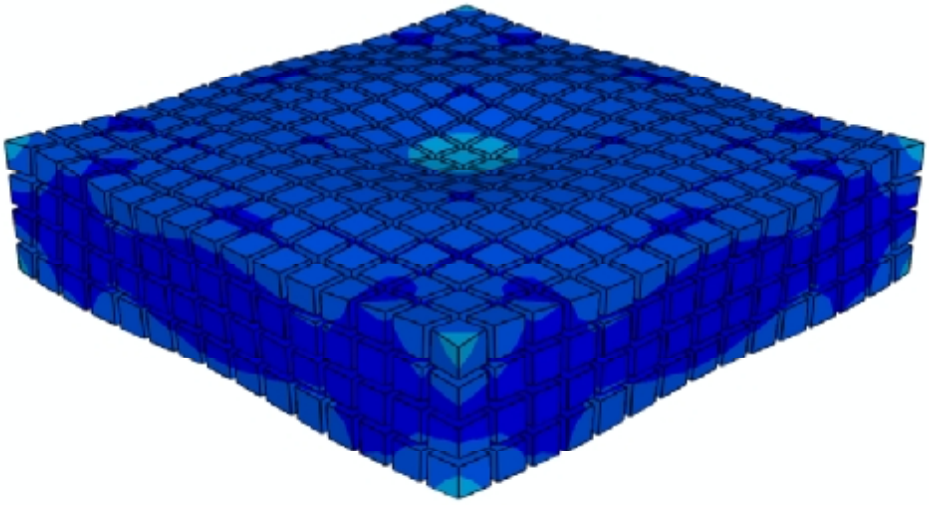

Figure 54F Bottom view, spatial configuration at the end of the fourth increment

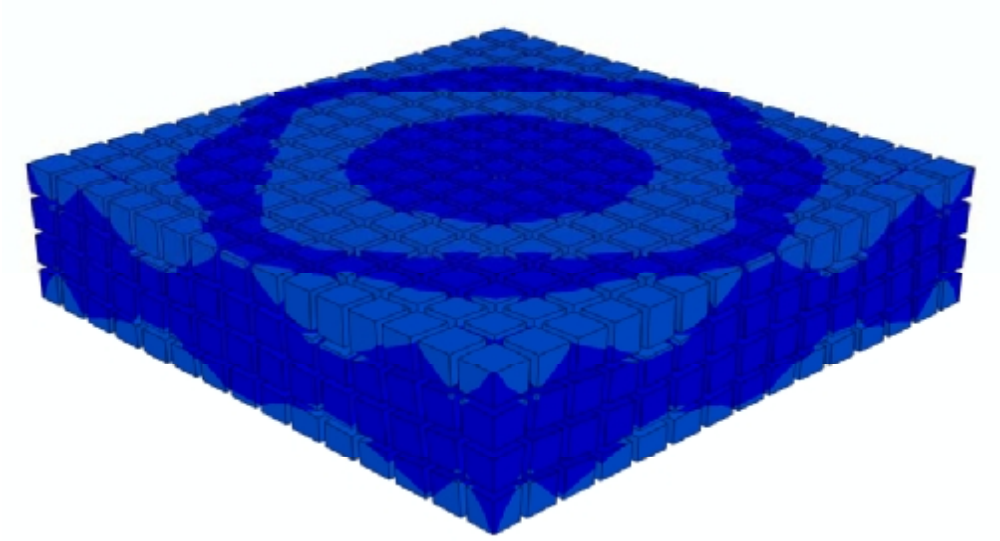

Figure 54G Top view, material configuration at the end of fourth increment

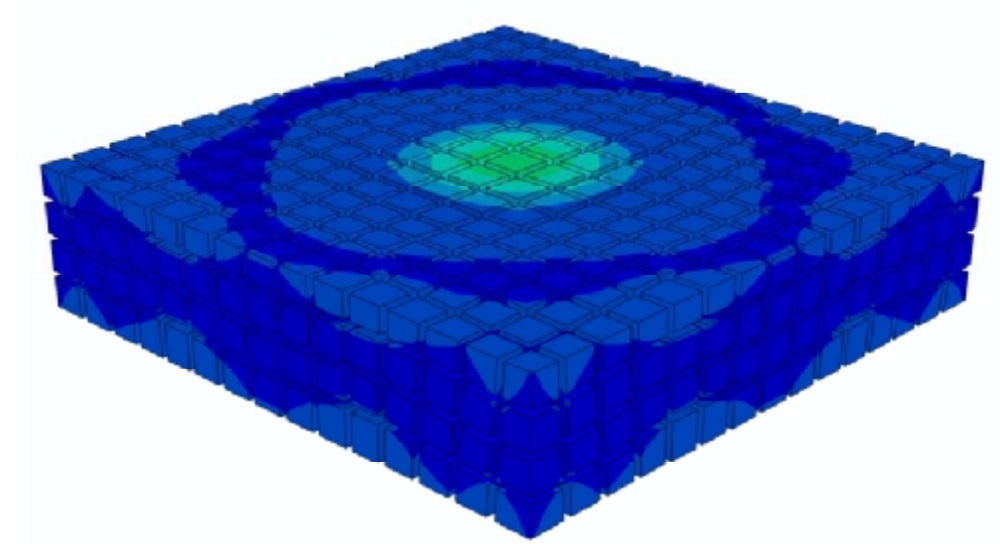

Figure 54H Bottom view, material configuration at the end of fourth increment

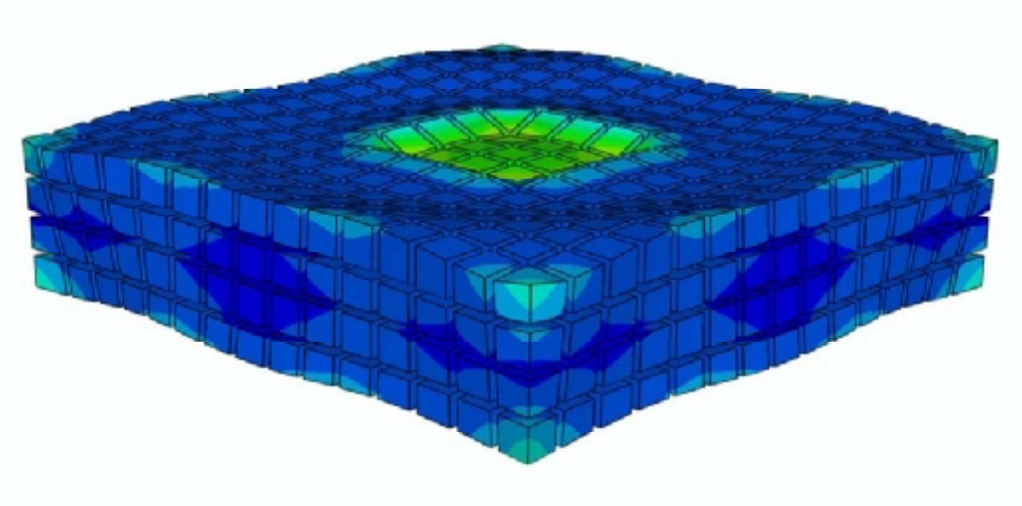

Figure 54I Top view, spatial configuration at the end of the sixth increment

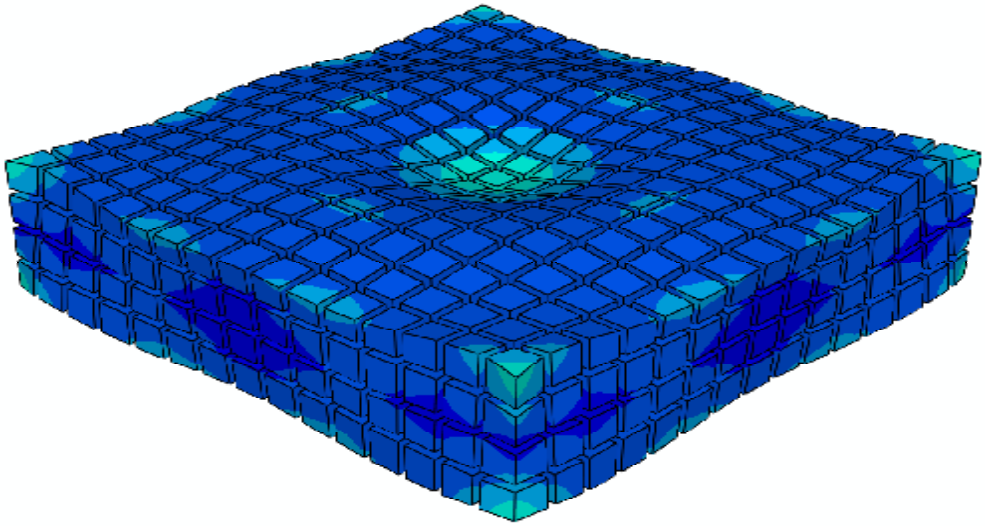

Figure 54J Bottom view, spatial configuration at the end of the sixth increment

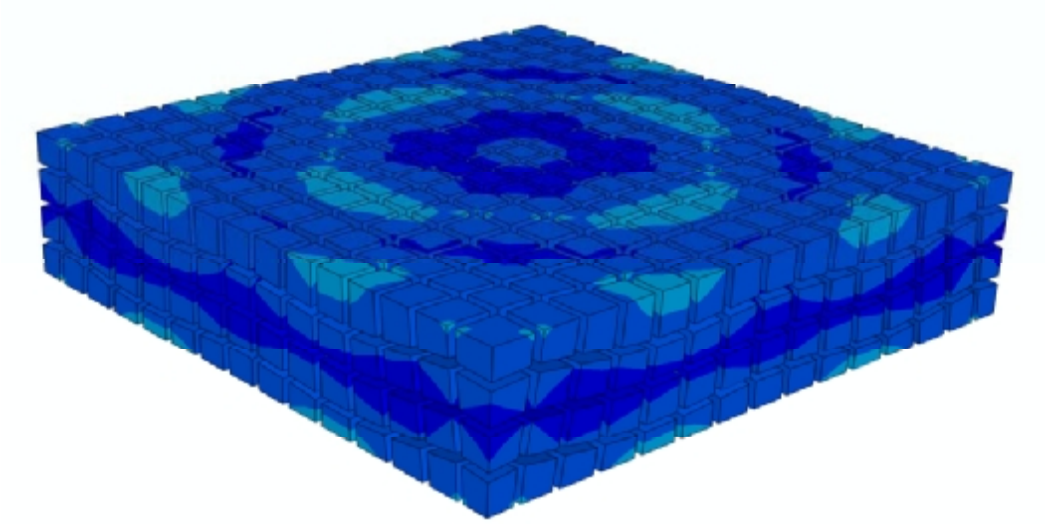

Figure 54K Top view, material configuration at the end of sixth increment

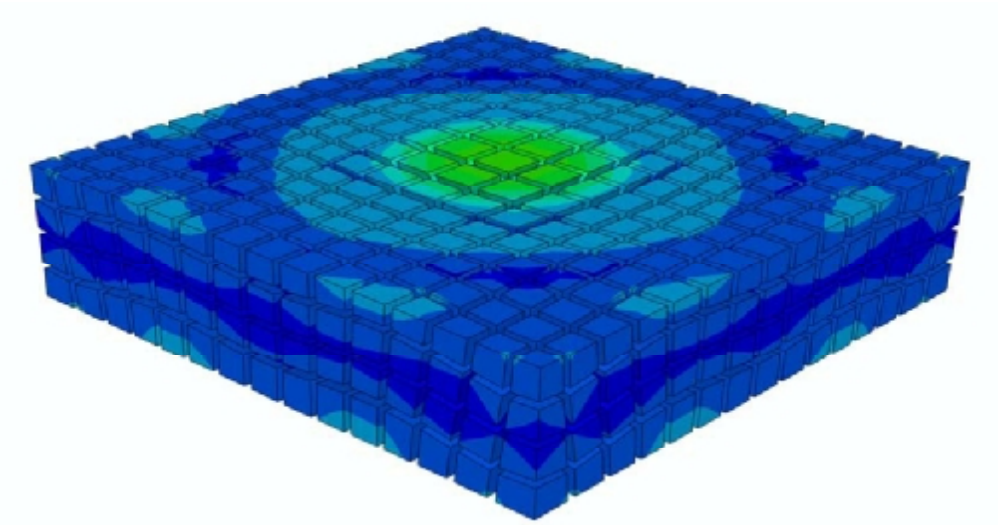

Figure 54L Bottom view, material configuration at the end of sixth increment

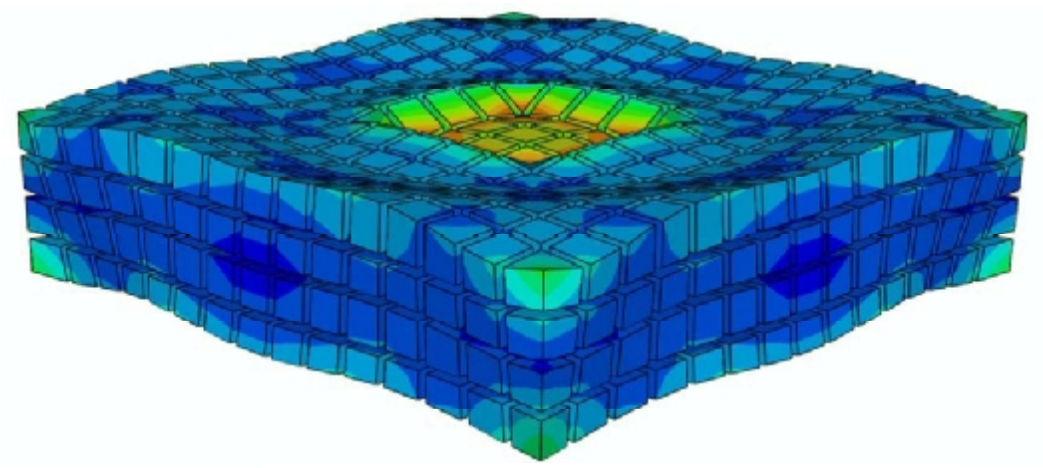

Figure 54M Top view, spatial configuration at the end of the eighth increment

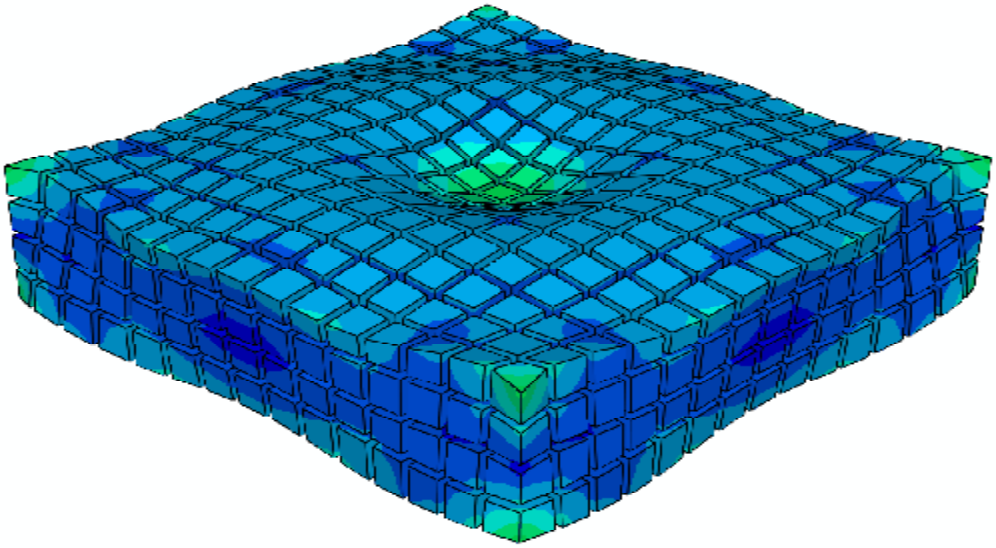

Figure 54N Bottom view, spatial configuration at the end of the eighth increment

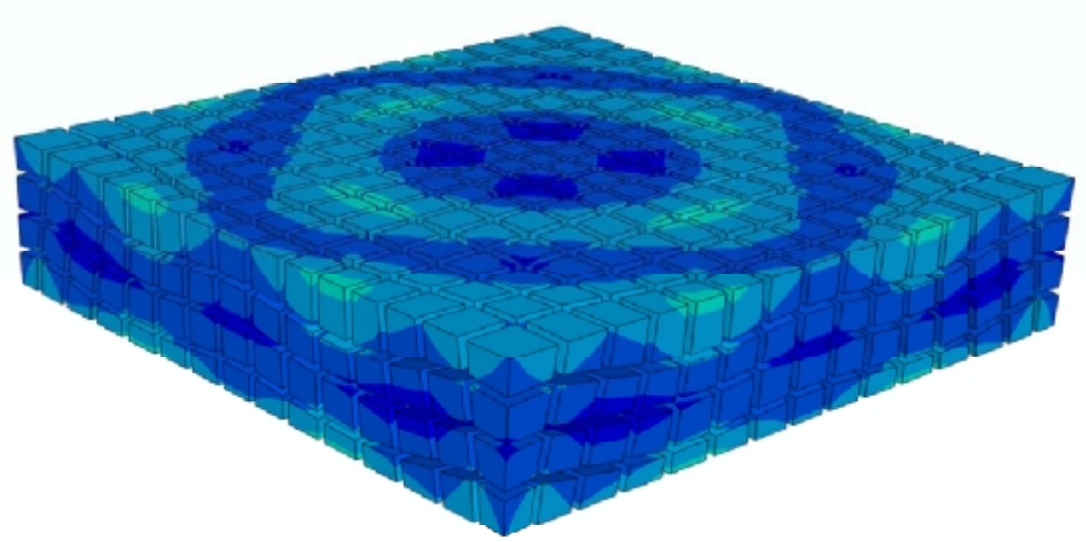

Figure 54O Top view, material configuration at the end of eighth increment

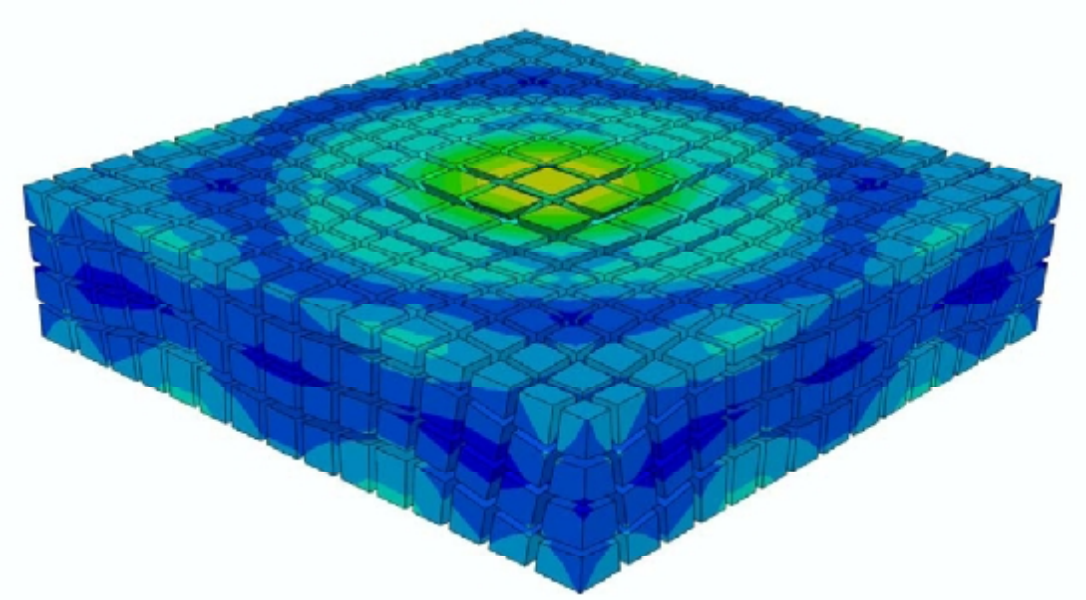

Figure 54P Bottom view, material configuration at the end of eighth increment

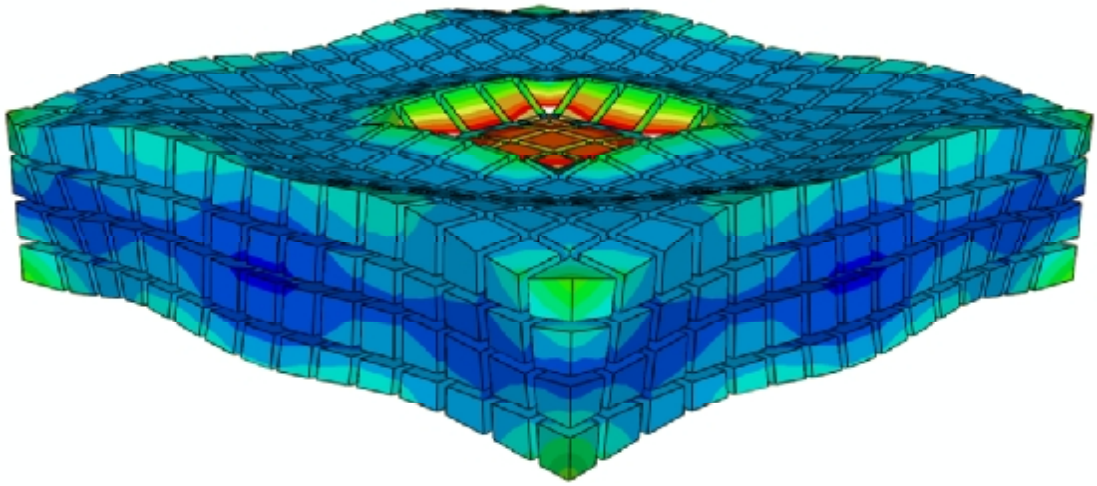

Figure 54Q Top view, spatial configuration at the end of the tenth increment

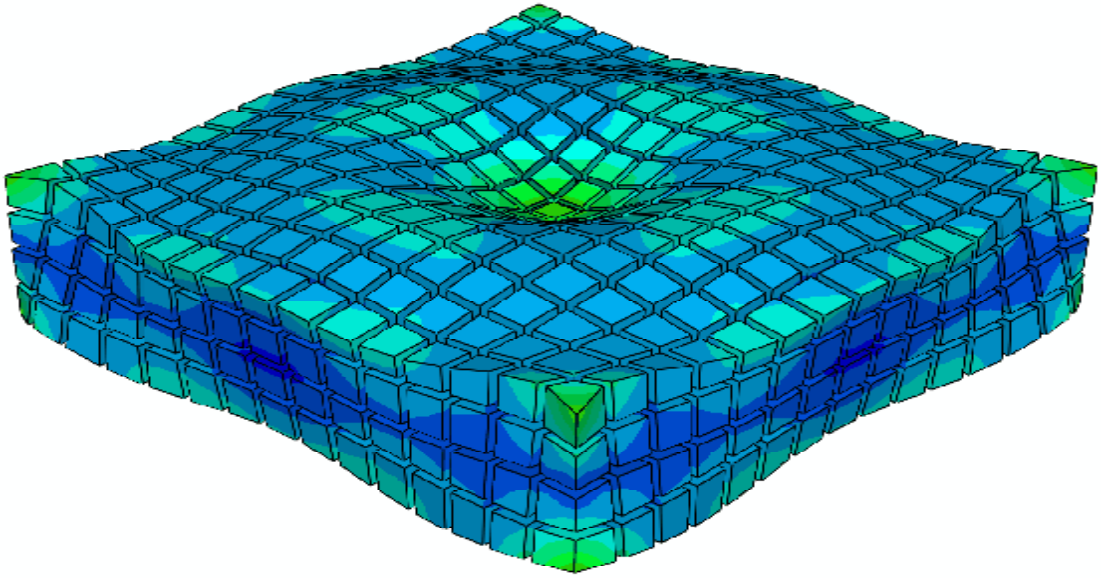

Figure 54R Bottom view, spatial configuration at the end of the tenth increment

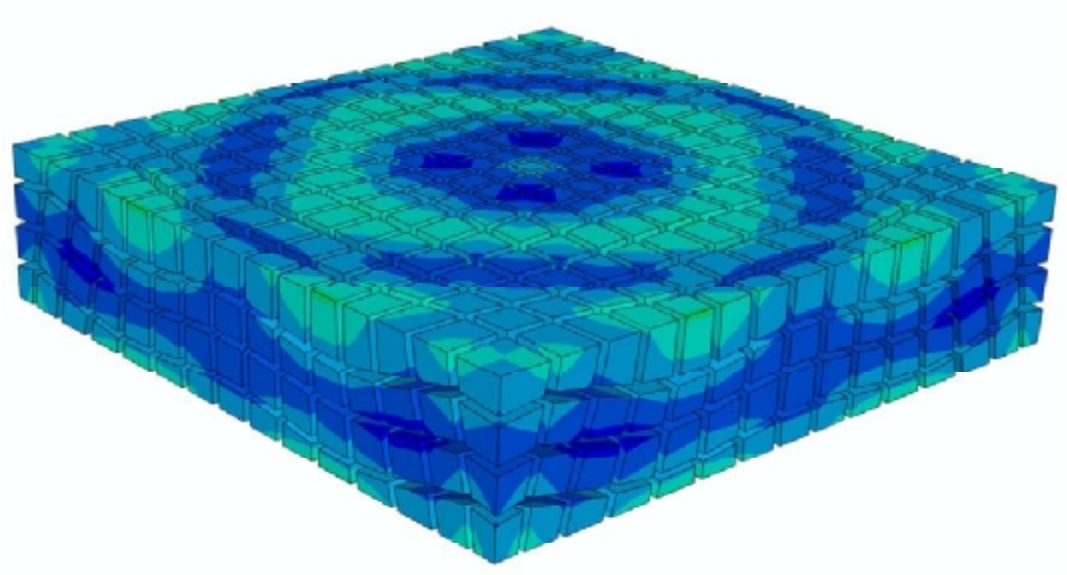

Figure 54S Top view, material configuration at the end of tenth increment

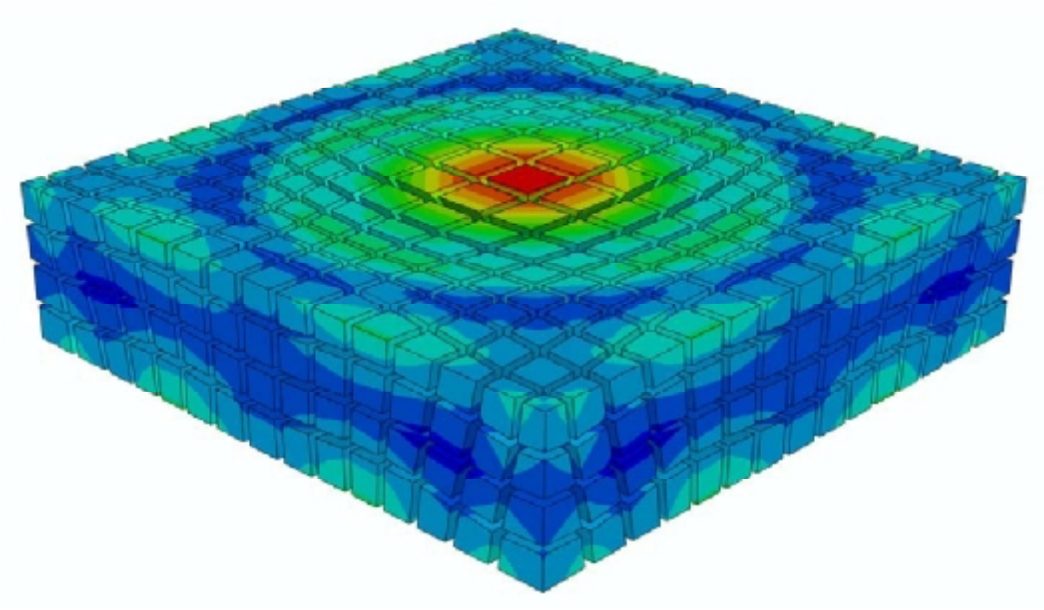

Figure 54T Bottom view, material configuration at the end of tenth increment

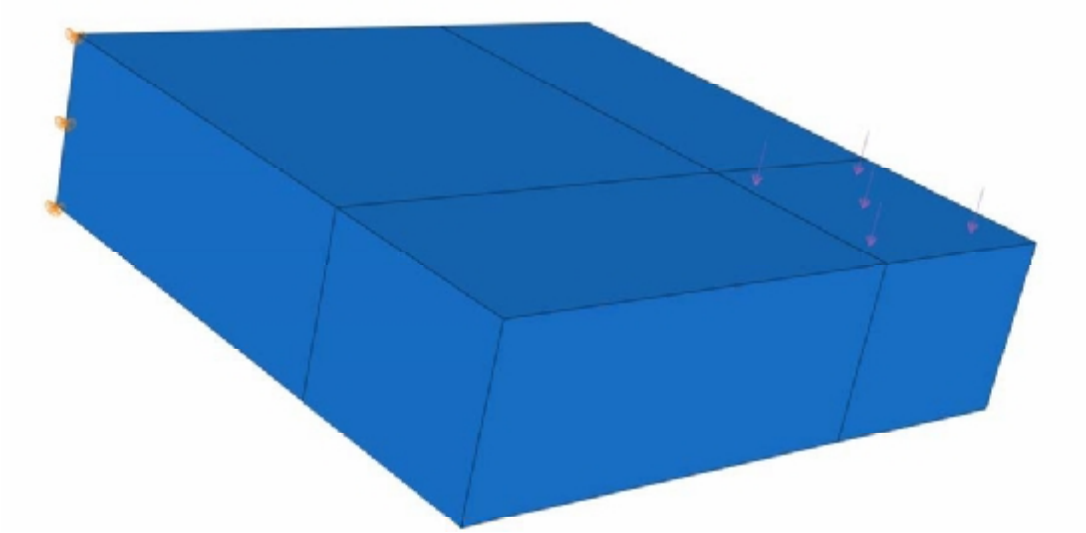

Figure 55 Initial spatial configuration

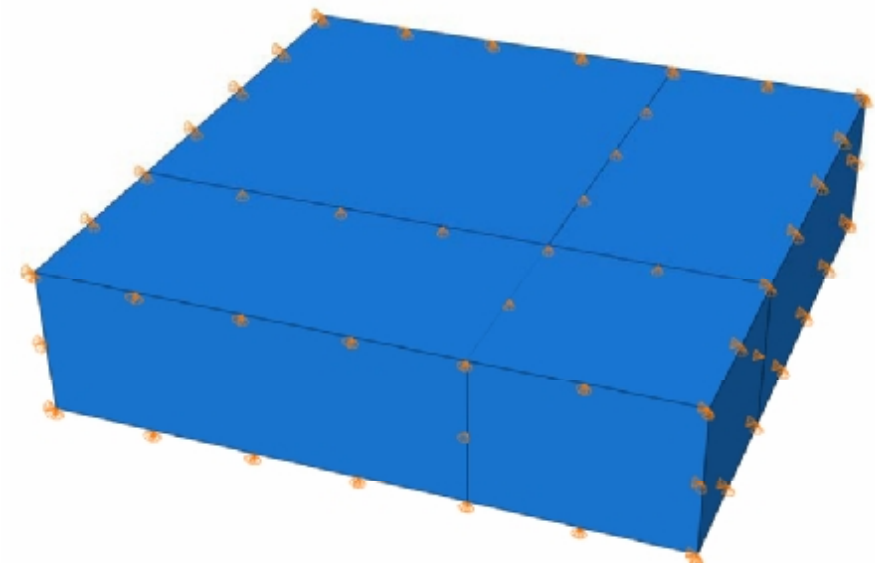

Figure 56 Initial material configuration

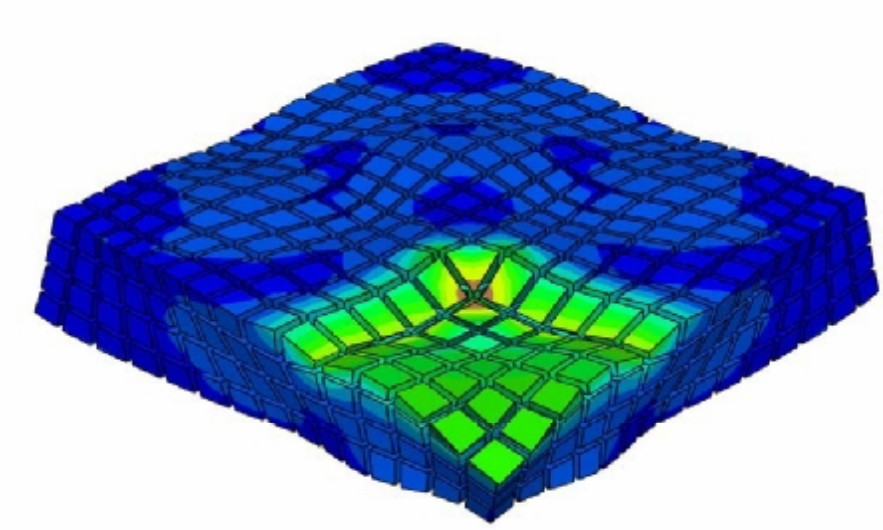

Figure 57 Optimised spatial configuration

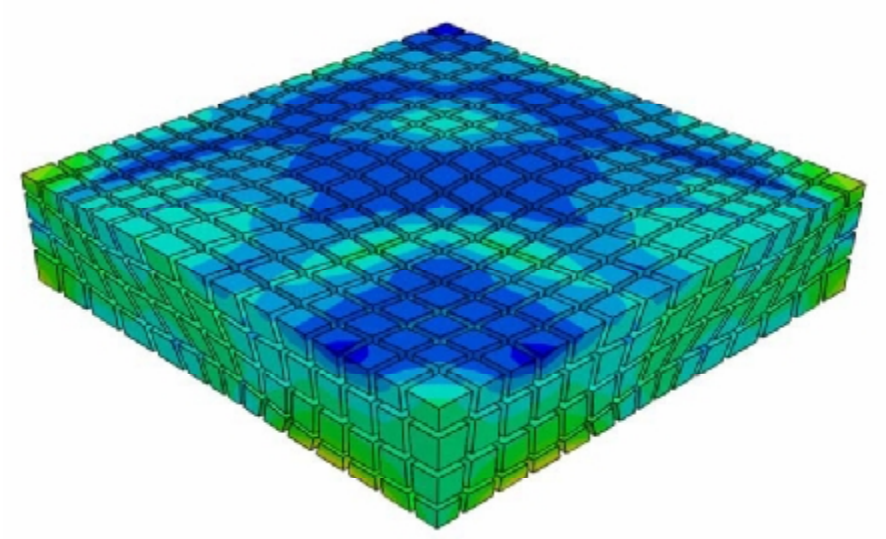

Figure 58 Optimised material configuration

5 A.L.E HYPERELASTOPLASTIC FORMULATION OF CONTINUUM MECHANICS

5.1 Motivation

The goal of the proposed ALE method is to develop a new formulation for solving the physical problem with a control of the distortion of the finite element mesh in a multiplicative finite strain plasticity setting. The new method provides solutions for three dimensional problems in which previous works were limited to two dimensional problems [45 & 46].

The aim is to provide the framework and implementation details of arbitrary Lagrangian Eulerian hyperelastoplasticity problem classes. This ALE formulation is based on the dual balance of momentum in terms of spatial forces (the well-known Newtonian forces) as well as material forces (also known as configurational forces). The balance of spatial momentum results in the usual Equation of motion, whereas the balance of the material momentum indicates deficiencies in the nodal positions, hence providing an objective criterion to optimise the shape or the finite element mesh. The main difference with traditional ALE approaches is that the combination of the Lagrangian and Eulerian description is no longer arbitrary, in other words the mesh motion is no longer user defined but completely embedded within the variational mechanical formulation.

The new ALE hyperelastoplasticity setting will be developed in a decoupled rate form. We will deal with two systems of partial differential Equations: The discretised spatial and the material momentum Equation. The spatial Equation will then be linearised by taking the material time derivative while the material Equation will be linearised by taking the spatial time derivative. The solution defines the optimal spatial and material configuration in the context of energy minimisation in hyperelastic setting.

The new ALE hyperelastoplasticity setting will be developed at finite strain. In this ALE hyperelastoplastic formulation additional Equations are required to update the stresses. The principle of maximum plastic dissipation as well as the consistency conditions in spatial and material setting will introduce the spatial plastic parameters and rate form of the stress-strain relations. The solution defines the optimal spatial and material configuration in the context of energy minimisation in hyperelastoplasticity setting.

5.2 Introduction

In this section the ALE method will be developed in a decoupled rate form. The ALE decoupled method consists of three steps: the first step where the mechanical Equation is solved (Lagrangian step), a second step where the remeshing occurs (Eulerian step) and a third step where the internal variables are convected. As in previous sections the developed method for combining the Lagrangian and Eulerian solution has the advantage that the motion is embedded into the formulation, hence the motion is no longer user defined. In the previous sections the frameworks developed for hyperelastic and hyperelastodynamic settings. In this section these will be extended to a hyperelastoplasticity framework. The solution gives the optimised shape or mesh in terms of energy minimisation.

As in chapter three (the hyperelastic framework), the spatial and material momentum Equations are linearised by taking the material and the spatial time derivative respectively. The ALE hyperelastic formulations were developed in updated form and parameterised in terms of velocity, thus no convection was required. In this chapter the hyperelastoplastic formulation will be developed in rate form and parameterised in terms of velocity. Another difference is to exclude the coupling terms and thus provide an ALE formulation in decoupled form. This will provide a relatively simple framework to extend the formulation to plasticity. The solution of these Equations provides the optimised configuration in hyperelastoplastic setting in terms of energy.

In the hyperelastoplastic framework the solution requires extra Equations to update the stresses in the spatial and material configurations. The linearised spatial and material momentum Equations provide the spatial and material motions. The spatial and material constitutive Equations will be developed in rate form to provide the scheme to update the stress in the spatial and material setting. The spatial and material constitutive Equation will be derived using the principle of maximum plastic dissipation and the consistency condition. A new spatial plasticity parameter will be derived. A few examples that present the solution will be given for the hyperelastoplasticity Equations.

5.3 Basic formulations

The basic Equation that defines the spatial and material motion has been illustrated in the previous sections. In this section additional Equations are presented to define the elastic and plastic ranges. The spatial and material deformation gradient can be decomposed into elastic and plastic parts [83]:

$$F = F_e \cdot F_p \quad \text{and} \quad f = f_p \cdot f_e \tag{277}$$

and their Jacobians are given respectively by [83]:

$$J = \det F \,,\; j = \det f$$
$$J^e = \det F^e \,,\; J^p = \det F^p \,,\; j^e = \det f^e \text{ and } j^p = \det f^p$$

The relation between the spatial and material velocity fields are given by [83]:

$$v = -F \cdot V \tag{278}$$

while the relation between the spatial and material time derivative can be given through convection as follows [59]:

$$\frac{D\{\bullet\}}{Dt} = \frac{d\{\bullet\}}{dt} + \nabla_x \{\bullet\} \cdot v = \frac{d\{\bullet\}}{dt} - \nabla_X \{\bullet\} \cdot V \tag{279}$$

The derivative of a scalar function with respect to the material motion deformation gradient is given by [53]:

$$\frac{d\{\bullet\}_t}{df} = \{\bullet\}_t F^t - F^t \cdot \frac{D\{\bullet\}_t}{DF} \cdot F^t \tag{280}$$

The spatial and material right Cauchy-Green strain tensors are given respectively as:

$$C = F^t F \text{ and } c = f^t f$$

The relation between the spatial and material free energy density is given as [83]:

$$W_0(c; X) = J W_t(C; x) \tag{281}$$

5.4 Spatial and Material momentum equations

The concept of the newly developed ALE technique is the variation of the total potential energy with respect to the spatial coordinates at fixed material coordinates plus its variation with respect to the material coordinates at fixed spatial coordinates. This variation should vanish resulting into two independent Equations. As has been illustrated in previous sections, the variation of the potential energy Equation with respect to the spatial coordinates will result into the spatial momentum Equation while the variation of the potential energy with respect to the material coordinates will give the material momentum Equation. Next the spatial momentum Equation will be linearised with respect to the spatial and material coordinates while the material momentum Equation will be linearised with respect to the material and spatial coordinates. The current section on hyperelasticity will provide an alternative formulation were the ALE hyperelastic Equations will be developed in decoupled rate form. Thus the spatial momentum Equation will be linearised by taking its material time derivative while the material momentum Equation will be linearised by taking its spatial time derivative. The solution of the spatial and material momentum Equation will provide the optimal location of nodes in the spatial and material configuration in terms of energy. This alternative formulation provides a simpler basis to extend the formulation to plasticity. Below is given the derivation for the spatial and material momentum Equations.

5.4.1 Spatial momentum equation

The first part of the formulation follows the same steps as in chapter three. We begin by reviewing that part and continue in producing the rate form of the spatial momentum Equation. The internal nodal forces in the spatial domain are given as [57 and 58]:

$$\delta_x l = \int_{\Omega} \frac{\partial N}{\partial x} \cdot \sigma d\Omega \qquad \textbf{282}$$

Using the chain rule and the relation $d\Omega = Jd\Omega_0$:

$$\delta_x l = \int_{\Omega_0} \frac{\partial N}{\partial X} \frac{\partial X}{\partial x} \cdot \sigma J d\Omega_0 \qquad \textbf{283}$$

Making use of the relation between the Cauchy stress tensor σ and the Nominal stress tensor P, that is $\sigma = J^{-1} F \cdot P$, and linearising by taking the material time derivative will produce the following Equation:

$$D_t \delta_x l = \int_{\Omega_0} \frac{\partial N}{\partial X} \cdot D_t(P) d\Omega_0 \qquad \textbf{284}$$

Since the nominal stress can be given in terms of the second Piola-Kirchhoff stress as $P = SF^T$, the material time derivative of the nominal stress results in:

$$D_t(P) = f \cdot \left(F \cdot D_t(S) \cdot F^T + F \cdot S \cdot F^T \cdot f^T \cdot D_t(F)^T\right) \qquad \textbf{285}$$

The Truesdell rate of Cauchy stress based on the material time derivative $D_t(\ )$ and the spatial velocity gradient l can be derived as:

$$\sigma^{\nabla \hat{T}} = jF \cdot \frac{DS}{Dt} \cdot F^t = F \cdot \frac{D}{Dt}\left(JF^{-1} \cdot \sigma \cdot F^{-T}\right) \cdot F^T \qquad \textbf{286}$$

$$= jF \cdot \left(J\frac{DF^{-1}}{Dt} \cdot \sigma \cdot F^{-T} + JF^{-1} \cdot \frac{D\sigma}{Dt} \cdot F^{-T} + JF^{-1} \cdot \sigma \cdot \frac{DF^{-T}}{Dt} + \frac{DJ}{Dt}F^{-1} \cdot \sigma \cdot F^{-T}\right) \cdot F^T$$

$$= jF \cdot \left(-Jf \cdot \frac{DF}{Dt} \cdot f \cdot \sigma \cdot f^T + Jf \cdot \frac{D\sigma}{Dt} \cdot f^T - Jf \cdot \sigma \cdot f^T \cdot \frac{DF^T}{Dt} \cdot f^T + \frac{DJ}{Dt} f \cdot \sigma \cdot f^T\right) \cdot F^T$$

$$\sigma^{\nabla \hat{T}} = jF \cdot \frac{DS}{Dt} \cdot F^T = \frac{D\sigma}{Dt} - l \cdot \sigma - \sigma \cdot l^T + (trace(l))\sigma \qquad \textbf{287}$$

where Equation (131) has been used in the last step. Making use of Equations (285 & 286), Equation (284) can be transformed into:

$$D_t \delta_x l = \int_{\Omega_0} \frac{\partial N}{\partial X} \cdot f\left(\sigma^{\nabla \hat{T}} + \sigma l\right) J d\Omega_0$$

$$D_t \delta_x l = \int_{\Omega} \frac{\partial N}{\partial x}\left(\sigma^{\nabla \hat{T}} + \sigma l\right) d\Omega \qquad \textbf{288}$$

The above Equation is associated with the Lagrangian formulation except the first term where the Truesdell rate of Cauchy stress is in terms of material time derivative. In order to simplify the solution this term has to be transformed into spatial time derivative, this will leave a Lagrangian Equation to be solved plus transport terms, which will be solved separately in a convective stage.

5.4.1 Material momentum equation

In similar way we can derive the material momentum Equations, the internal nodal force in the material domain is given as [57 and 58]:

$$F^{\text{int}} = \int_{\Omega_0} \frac{\partial N}{\partial X} \cdot \Sigma \cdot d\Omega_0 \qquad \textbf{289}$$

where Σ is the material momentum flux, Ω_0 is the material domain and $\frac{\partial N}{\partial X}$ is the derivative of the shape function with respect to the material coordinate. Making use of the chain rule and the relation $d\Omega_0 = jd\Omega$, we obtain:

$$F^{\text{int}} = \int_{\Omega} \frac{\partial N}{\partial x} \frac{\partial x}{\partial X} \cdot \Sigma \cdot j \cdot d\Omega \qquad \textbf{290}$$

Using the following relation between the fluxes in the material domain:

$$\Pi = j \frac{\partial x}{\partial X} \Sigma = jf^{-1} \Sigma \qquad \textbf{291}$$

Substituting Equation (291) into Equation (290) will result in:

$$F^{\text{int}} = \int_{\Omega} \frac{\partial N}{\partial x} \cdot \Pi \cdot d\Omega \qquad \textbf{292}$$

The linearization will be carried out by taking the spatial time derivative:

$$\frac{dF^{\text{int}}}{dt} = \int_{\Omega} \frac{\partial N}{\partial x} \cdot \frac{d\Pi}{dt} \cdot d\Omega \qquad \textbf{293}$$

Since the material deformation gradient can be decomposed into its referential deformation gradients as:

$$f = \overset{\approx}{f} \cdot \bar{f} \text{ and } f^t = \left(\overset{\approx}{f} \cdot \bar{f} \right)^t = \bar{f}^t \cdot \overset{\approx}{f}^t$$

The following transformation can be obtained between the material and the spatial domain:

$$\overset{\approx}{f}_{i\alpha} \cdot \bar{f}_{I\alpha}(\,)_{IJ}\, \bar{f}_{BJ} \cdot \overset{\approx}{f}_{Bj} = \overset{\approx}{f}_{i\alpha} \cdot f_{\alpha I}(\,)_{IJ}\, \bar{f}^t_{JB} \cdot \overset{\approx}{f}^t_{Bj} = f(\,) f^t$$

Using the following relation between the material momentum fluxes:

$$\Pi = \Xi \cdot f^t \qquad \textbf{294}$$

We can write the spatial time derivative of Equation (294) as follows:

$$\frac{d\Pi}{dt} = f^{-1} \cdot \left(f \cdot \frac{d\Xi}{dt} \cdot f^{t} + f \cdot \Xi \cdot f^{t} \cdot f^{-t} \cdot \frac{df^{t}}{dt} \right) \qquad \textbf{295}$$

Making use of the above transformation, we can write the relation between the material momentum fluxes as follows:

$$\Sigma = jf \cdot \Xi \cdot f^{t} \qquad \textbf{296}$$

The first term in the right hand side of Equation (295) can be written as:

$$\overset{\nabla}{\Sigma} = j^{-1} f \cdot \frac{d\Xi}{dt} \cdot f^{t} = j^{-1} f \cdot \frac{d\left(jf^{-1} \cdot \Sigma \cdot f^{-t} \right)}{dt} \cdot f^{t}$$

$$= \frac{d\Sigma}{dt} + f \cdot \frac{df^{-1}}{dt} \cdot \Sigma \cdot f^{-t} \cdot f^{t} + f \cdot f^{-1} \cdot \Sigma \cdot \frac{df^{-t}}{dt} \cdot f^{t} + j^{-1} \frac{dj}{dt} \cdot \Sigma$$

$$= \frac{d\Sigma}{dt} - f \cdot f^{-1} \cdot \frac{df}{dt} \cdot f^{-1} \cdot \Sigma \cdot f^{-t} \cdot f^{t} - f \cdot f^{-t} \cdot \Sigma \cdot f^{-t} \cdot \frac{df^{t}}{dt} \cdot f^{-t} \cdot f^{t} + j^{-1} \frac{dj}{df} \cdot \frac{df}{dt} \cdot \Sigma$$

where $\overset{\nabla}{\Sigma}$ is the Truesdell rate of the Eshelby stress tensor. Making use of Equation (123) for the material velocity gradient will result in:

$$\overset{\nabla}{\Sigma} = \frac{d\Sigma}{dt} - L \cdot \Sigma - \Sigma \cdot L^{t} + TRACE(L) \cdot \Sigma \qquad \textbf{297}$$

Making use of Equations (297), (296) and (123) and substituting them into (295) will result in:

$$\frac{d\Pi}{dt} = jf^{-1} \cdot \left(\overset{\nabla}{\Sigma} + \Sigma \cdot L^{t} \right) \qquad \textbf{298}$$

Substituting Equation (298) into (293) will result in:

$$\frac{dF^{\text{int}}}{dt} = \int_{\Omega_0} \frac{\partial N}{\partial X} \cdot \left(\overset{\nabla}{\Sigma} + \Sigma \cdot L^{t} \right) \cdot d\Omega_0 \qquad \textbf{299}$$

Equation (299) represents the linearised material momentum Equation; in the following section the Equation for the stress update procedure will be derived in the spatial as well as the material domain.

5.5 Strong form of spatial stress update

Since the Truesdell rate of Cauchy stress is given in terms of material time derivative, the solution in terms of the spatial time derivative needs to be convected. In this section the necessary formulation of the updated stresses will be developed in the spatial domain. The maximum plastic dissipation formulated in strain space implies that the actual right Cauchy-Green tensor C is the argument of the maximum principle. Thus for any strain tensor $\tilde{C}$ the maximum principle in term of material time derivative is given as:

$$C = \arg\left[\max_{C}\left\{-\frac{\partial W\left(\tilde{C}, C^P\right)}{\partial C^P} : \dot{C}^P\right\}\right]$$

Thereby C^P is the plastic strain tensor and is given as:

$$C^P = F^{PT} F^P$$

Furthermore, W is the spatial free energy density and $\dot{C}^P$ is the material time derivative of the plastic strain tensor. Reformulating the above argument in term of constrained minimisation problem leads to

$$C = \arg\left[\min_{C}\left\{\frac{\partial W\left(\tilde{C}, C^P\right)}{\partial C^P} : \dot{C}^P\right\}\right]$$

The unconstrained problem can be introduced by introducing the following Lagrangian functional:

$$L^P = \frac{\partial W\left(C, C^P\right)}{\partial C^P} : \dot{C}^P + \dot{\gamma}\phi\left(C, C^P, Q\right)$$

where $\phi\left(C, C^P, Q\right)$ defines the strain space of the formulation and is assumed to be isotropic, $\dot{\gamma}$ is the plastic parameter and Q is an internal state variable. The optimised solution is found via:

$$\frac{\partial L^P}{\partial C} = 0 \Rightarrow \qquad \frac{\partial W\left(C, C^P\right)}{\partial C^P \partial C} : \dot{C}^P = -\dot{\gamma}\frac{\partial \phi}{\partial C} \qquad \textbf{300}$$

The material time derivative of the second Piola-Kirchhoff stress tensor can be given as:

$$\frac{DS}{Dt} = \frac{\partial^2 W}{\partial C \partial C} : \dot{C} + \frac{\partial^2 W}{\partial C \partial C^P} : \dot{C}^P \qquad \textbf{301}$$

The first and second terms on the right hand side represent the elastic and plastic contributions respectively. Substituting Equation (300) into (301) gives:

$$\frac{DS}{Dt} = \rho 2 \frac{\partial^2 W}{\partial C \partial C} : \dot{C} - 2\dot{\gamma}\frac{\partial \phi}{\partial C} \qquad \textbf{302}$$

Next, we make use of the relation between the Cauchy stress tensor and the second Piola-Kirchhoff stress tensor to obtain:

$$\frac{D\left(JF^{-1}\sigma F^{-t}\right)}{Dt} = \rho 2\frac{\partial^2 W}{\partial C\partial C} : \dot{C} - 2\dot{\gamma}\frac{\partial \phi}{\partial C}$$

Pushing forward by making use of Equation (135) will produce the following:

$$\sigma^{\nabla \hat{T}} = J^{-1}F\frac{D\left(JF^{-1}\sigma F^{-t}\right)}{Dt}F^{t} = J^{-1}\rho 4\frac{\partial^2 W}{\partial g\partial g} : D - 2J^{-1}\dot{\gamma}\frac{\partial \phi}{\partial g}$$

where g is the spatial metric tensor, thereby we made use of Equations (287) and (142). This can be written as:

$$\frac{D\sigma}{Dt} - l\sigma - \sigma l^{t} + trace(l)\sigma = J^{-1}\rho 4\frac{\partial^2 W}{\partial g\partial g} : D - 2J^{-1}\dot{\gamma}\frac{\partial \phi}{\partial g}$$

Making use of Equation (279), we can write the first term in the above Equation in term of the spatial time derivative as:

$$\frac{d\sigma}{dt} + \sigma_{,x}v = l\sigma + \sigma l^{t} - trace(l)\sigma + J^{-1}\rho 4\frac{\partial^2 \Psi}{\partial g\partial g} : d - 2J^{-1}\dot{\gamma}\frac{\partial \Phi}{\partial g}$$

Making use of the product rule the above Equation can be given as:

$$\frac{d\sigma}{dt} + (\sigma v)_{,x} - \sigma v_{,x} = l\sigma + \sigma l^{t} - trace(l)\sigma + J^{-1}\rho 4\frac{\partial^2 \Psi}{\partial g\partial g} : d - 2J^{-1}\dot{\gamma}\frac{\partial \Phi}{\partial g} \qquad \textbf{303}$$

Since the Cauchy stress tensor is not the only state variable that needs to be updated, other state variables that are given in term of the material time derivative and needs to be convected is the left Cauchy-Green elastic deformation tensor b^{e}. Making use of Equation (300) the following can be derived:

$$\dot{C}^{P} = -\dot{\gamma}\left(\frac{\partial^2 W}{\partial C\partial C^{P}}\right)^{-1} : \frac{\partial \Phi}{\partial C}$$

Using the strain tensor transformation yields:

$$\left(F^{t}b_{e}^{-1}F\right)^{\bullet} = -\dot{\gamma}\left(\frac{\partial^2 W}{\partial C\partial C^{P}}\right)^{-1} : \frac{\partial \Phi}{\partial C}$$

Using the push forward operation we obtain the following Equation:

$$F^{-t}\left(F^{t}b_{e}^{-1}F\right)^{\bullet}F^{-1} = -\dot{\gamma}\left(\frac{\partial^2 W}{\partial g\partial b_{e}^{-1}}\right)^{-1} : \frac{\partial \Phi}{\partial g}$$

The left hand side of the above Equation can be written as:

$$F^{-t}\left(F^{t}b_e^{-1}F\right)^{\bullet}F^{-1} = f^{t}\left(F^{t}b_e^{-1}F\right)^{\bullet}f$$
$$= \dot{b}_e^{-1} + l^{t}b_e^{-1} + b_e^{-1}l = \overset{\nabla}{b}{}_e^{-1}$$

where $\overset{\nabla}{b}{}_e^{-1}$ is the Truesdell rate of the left Cauchy-Green elastic deformation tensor. Putting the resulting right hand side back into the Equation yields:

$$\dot{b}_e^{-1} + l^{t}b_e^{-1} + b_e^{-1}l = -\dot{\gamma}\left(\frac{\partial^2 W}{\partial g \partial b_e^{-1}}\right)^{-1} : \frac{\partial \Phi}{\partial g}$$

Making use of Equation (279), we can write the first term in the above Equation in term of the spatial time derivative as:

$$b_{e,t}^{-1} + b_{e,x}^{-1}v = -l^{t}b_e^{-1} - b_e^{-1}l - \dot{\gamma}\left(\frac{\partial^2 W}{\partial g \partial b_e^{-1}}\right)^{-1} : \frac{\partial \Phi}{\partial g}$$

Making use of the product rule the above Equation can be given as:

$$b_{e,t}^{-1} + \left(b_e^{-1}v\right)_{,x} - b_e^{-1}v_{,x} = -l^{t}b_e^{-1} - b_e^{-1}l - \dot{\gamma}\left(\frac{\partial^2 W}{\partial g \partial b_e^{-1}}\right)^{-1} : \frac{\partial \Phi}{\partial g} \qquad \textbf{304}$$

In the material configuration the convection step is not needed in the traditional ALE setting. The material configuration concerns the material particles where the loading history is stored. Thus the formulation developed so far will be sufficient to solve the spatial Equation and obtain the spatial stresses, displacements etc, perform the remeshing with the material Equations to obtain the new location of the material coordinates and finally convect the state variable according to the newly derived Equations (303 & 304). Thus a traditional ALE solution will be obtained where the mesh is improved to obtain a beter approximation of the exact elastoplastic material behaviour. In the next section the elastoplastic tangent modulus will be derived for the spatial as well as the material configurations.

5.6 Tangent modulus

5.6.1 Material elastic tangent modulus

The second Piola-Kirchhoff stress tensor in the material motion problem is given as:

$$\Xi = 2\frac{dW_t}{dc} = jc^{-1}W_0 + 2j\frac{DW_0}{DC}:\frac{DC}{Dc} \qquad \textbf{305}$$

Taking the spatial time derivative of Equation (305) will result in:

$$\overset{\bullet}{\Xi}(c) = \begin{bmatrix} \frac{1}{2}\, jc^{-1}\otimes c^{-1}W_0 - jc^{-1}\,\overline{\otimes}\, c^{-t}W_0 + jc^{-1}\otimes\left[\frac{DW_0}{DC}:\frac{DC}{Dc}\right] + \\ jc^{-1}\otimes\left[\frac{DW_0}{DC}:\frac{DC}{Dc}\right] + jc^{-1}\otimes\left[\frac{DW_0}{DC}:\frac{DC}{Dc}\right] + \\ 2j\left[\frac{DC}{Dc}\right]^T : \frac{D^2W_0}{DC^2}:\left[\frac{DC}{Dc}\right] + 2j\left[\frac{DW_0}{DC}:\frac{D^2C}{DcDc}\right] \end{bmatrix} : \dot{c} \qquad \textbf{306}$$

where we have written W_0 for the potential energy which is function of the material right Cauchy Green strain tensors $W(c)$. Using the transformation in Equations (296 and 297), Equation (306) can be written in term of the Truesdell rate of the Eshelby stress tensor.

5.6.1 Spatial elastoplastic tangent modulus

In this section, the spatial constitutive Equation will be derived in the elastoplastic domain. This is needed to be able to solve the derived spatial momentum Equation (288). The first term where the Truesdell rate of Cauchy stress tensor is given in term of the second Piola-Kirchhoff stress tensor (287) needs to be defined. In order to obtain the Truesdell rate of the Cauchy stress tensor, the material time derivative of the second Piola-Kirchhoff stress tensor must be defined. The following will provide the elastoplastic constitutive law using the principle of maximum plastic dissipation; the derived Equations follow the framework presented by J.C. Simo [73 & 74] except for the rate that will be in term of the material time derivative. A brief review with the necessary modifications is given below. We begin by determining the plastic parameter by enforcing the consistency conditions, a state of plastic loading for which $\dot{\gamma} > 0$ requires $D\phi(C, C^P, Q)/Dt = 0$. The chain rule then yields:

$$\frac{D\phi}{Dt} = \frac{\partial\phi}{\partial C}:\dot{C} + \frac{\partial\phi}{\partial C^P}:\dot{C}^P + \frac{\partial\phi}{\partial Q}:\dot{Q} = 0 \qquad \textbf{307}$$

The following linear hardening law will be used:

$$\dot{Q} = \dot{\gamma} H$$

Equation (307) can be written as:

$$\frac{D\phi}{Dt} = \frac{\partial \phi}{\partial C} : \dot{C} + \frac{\partial \phi}{\partial C^P} : \dot{C}^P + \frac{\partial \phi}{\partial Q} \cdot \dot{\gamma} H = 0$$

Making use of Equation (300) the above Equation can be written as:

$$\frac{\partial \phi}{\partial C} : \dot{C} - \dot{\gamma} \frac{\partial \phi}{\partial C^P} : \left(\frac{\partial W}{\partial C \partial C^P} \right)^{-1} : \frac{\partial \phi}{\partial C} + \frac{\partial \phi}{\partial Q} \cdot \dot{\gamma} H = 0$$

The plastic parameter can be given as:

$$\dot{\gamma} = \frac{\frac{\partial \phi}{\partial C} : \dot{C}}{\frac{\partial \phi}{\partial C^P} : \left(\frac{\partial W}{\partial C \partial C^P} \right)^{-1} : \frac{\partial \phi}{\partial C} - \frac{\partial \phi}{\partial Q} \cdot H} \qquad \textbf{308}$$

By inserting the plastic parameter (308) into Equation (302), the material rate of the second Piola--Kirchhoff stress tensor is found as:

$$\frac{DS}{Dt} = \rho 2 \frac{\partial^2 W}{\partial C \partial C} : \dot{C} - 2 \frac{\frac{\partial \phi}{\partial C} \otimes \frac{\partial \phi}{\partial C}}{\frac{\partial \phi}{\partial C^P} : \left(\frac{\partial W}{\partial C \partial C^P} \right)^{-1} : \frac{\partial \phi}{\partial C} - \frac{\partial \phi}{\partial Q} \cdot H} : \dot{C} \qquad \textbf{309}$$

As it is clear that the first term gives the elastic contribution while the second term presents the plastic contributions. Finally pushing forward by making use of Equation (286), we can obtain the Truesdell rate of the Cauchy stress tensor.

5.7 Examples

The first example is a solid structure that is fixed at one end and kept free at the other end. The structure has the dimensions $(20*10*10)$, elastic parameters are $(\mu = 38.46, \lambda = 57.69)$, linear hardening parameter $(h = 0.7)$ and the yield stress (0.4). The displacement load applied at the end is equal to 5.4 (Figure 59). The structure is discretised with two finite elements. This Lagrangian problem is solved within 60 Newton Raphson increments. The elastoplastic curve illustrating the solution is shown in Figure 60. The material starts yielding in the second increment reaching plastic stress of (0.4101) and plastic strain of (0.0033). The yield surface starts to expand as the load increases and the material hardens. The load versus the displacement that illustrates this hardening path is clearly shown in Figure 62. The linear hardening path is shown in Figure 60 that gives the plastic strain versus the plastic strain.

In order to optimise the shape of the structure, the developed ALE hyperelastoplastic formulation will be applied to the same problem. The same material parameters will be used. The spatial and material configurations are shown in Figure 61; note that in the material configuration boundary nodes are free to move in all directions; hence the concept of imposed material force is used. The spatial configurations have the same dimensions, boundary conditions and applied loads while the material configuration the same conditions were applied except for the load where a compression load of the same magnitude as the spatial force. As in the Lagrangian problem two equally sized elements have been used. The ALE hyperelastoplastic solution is obtained in three steps: A first step where the spatial problem is solved, a second step where the material problem is solved and a final step where the convection of the state variables is achieved according to the Equations developed in previous sections. The solution is carried out in 60 Newton Raphson increments. The resulting elastoplastic curve is shown in Figure 62. The total displacement of the nodes is the difference between their final spatial and material coordinates. It is clear that the optimised solution is more pronounced under large deformation. This is due to the relative distortion that increases under larger loads. This is expected to increase further by increasing the applied load.

Another way of improving the results is to apply the method of generated material force. The aim as we viewed in previous sections is to improve the solution by relocating the internal nodes; thus provide an optimised mesh to obtain beter result. The same spatial problem is solved as we highlighted with the imposed method, however the material problem is changed. The external boundaries are constrained while the internal nodes are allowed to move only in the direction of the load (Figure 63). As in the Lagrangian and the ALE imposed solutions, a spatial load is applied of the same magnitude in 60 Newton's Raphson increments. The load displacement curve is plotted in Figure 64. An improvement in the solution is more

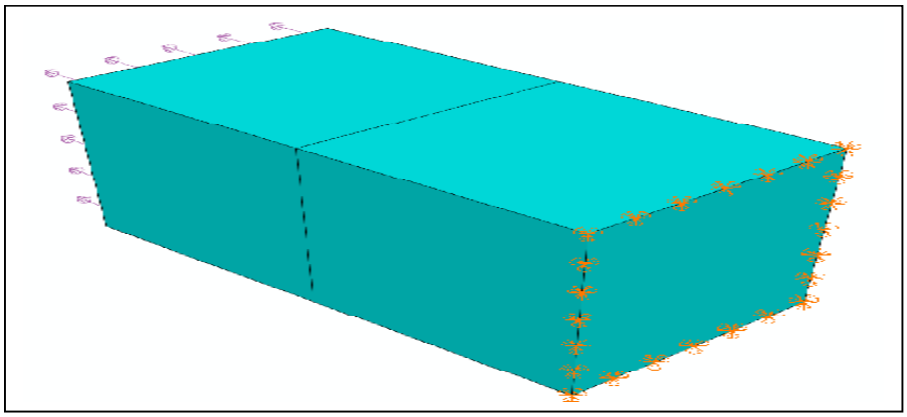

Figure 59 Lagrangian Problem

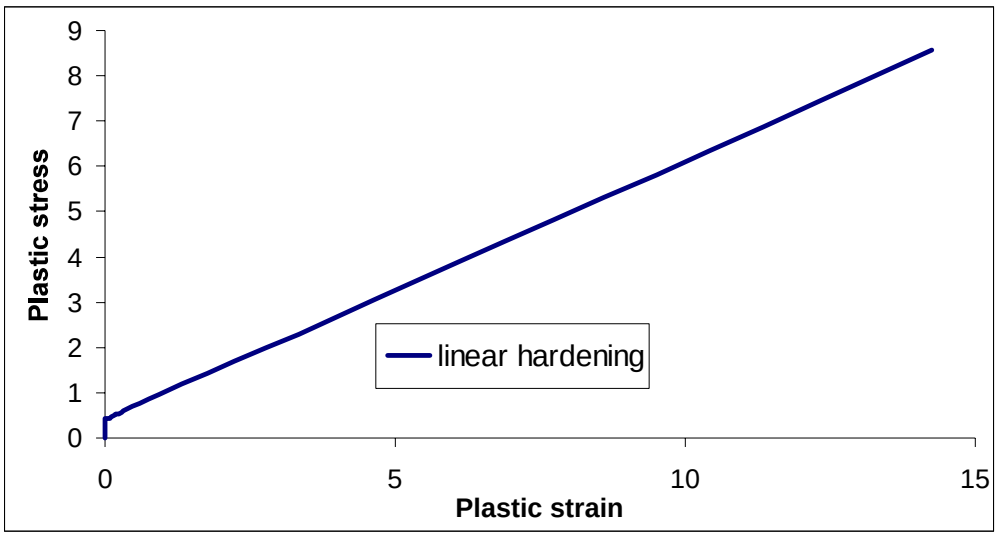

Figure 60 Linear hardening

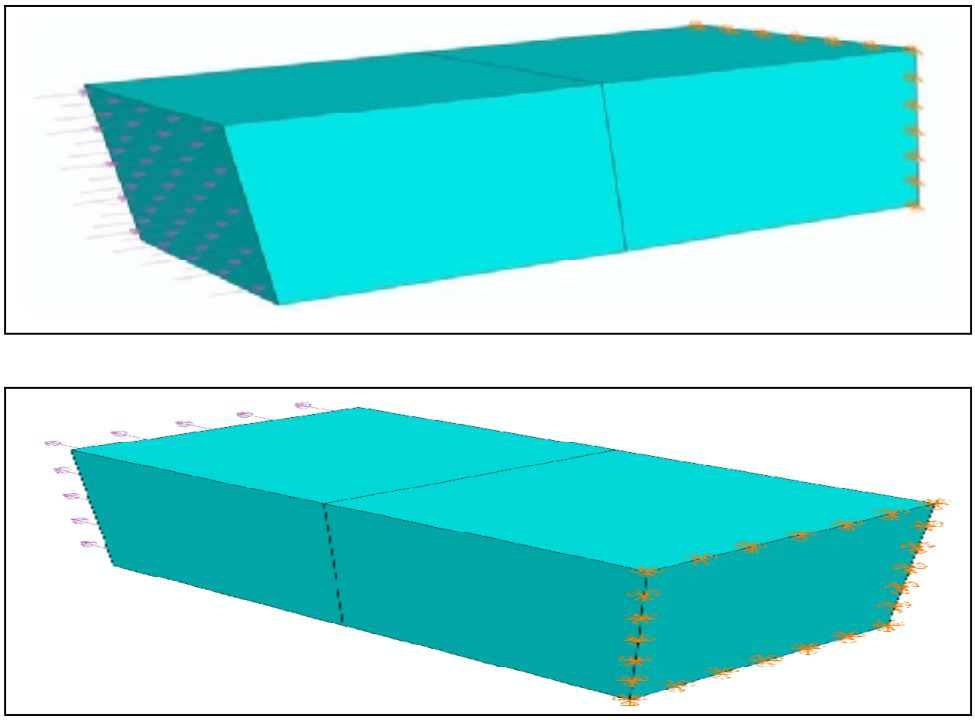

Figure 61 ALE material (top) and spatial (bottom) problem

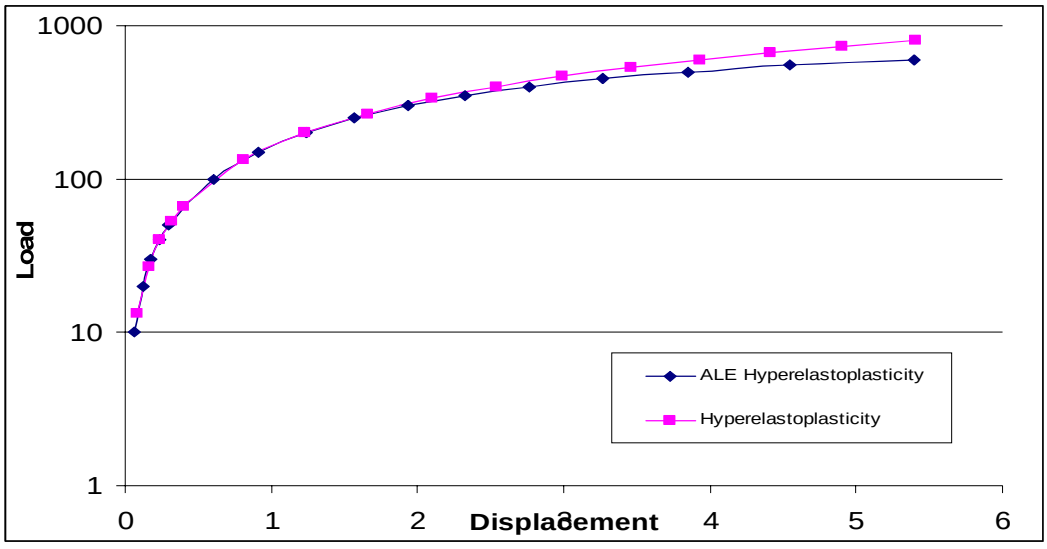

Figure 62 ALE versus Lagrangian hyperelastoplastic solution

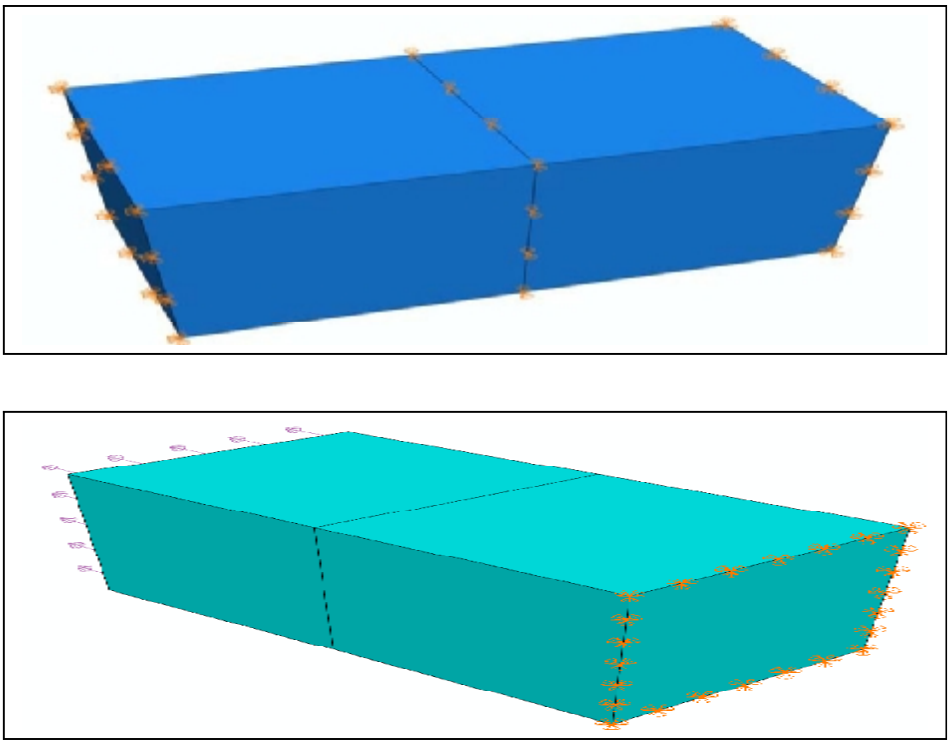

Figure 63 ALE material (top) and spatial (bottom) problem

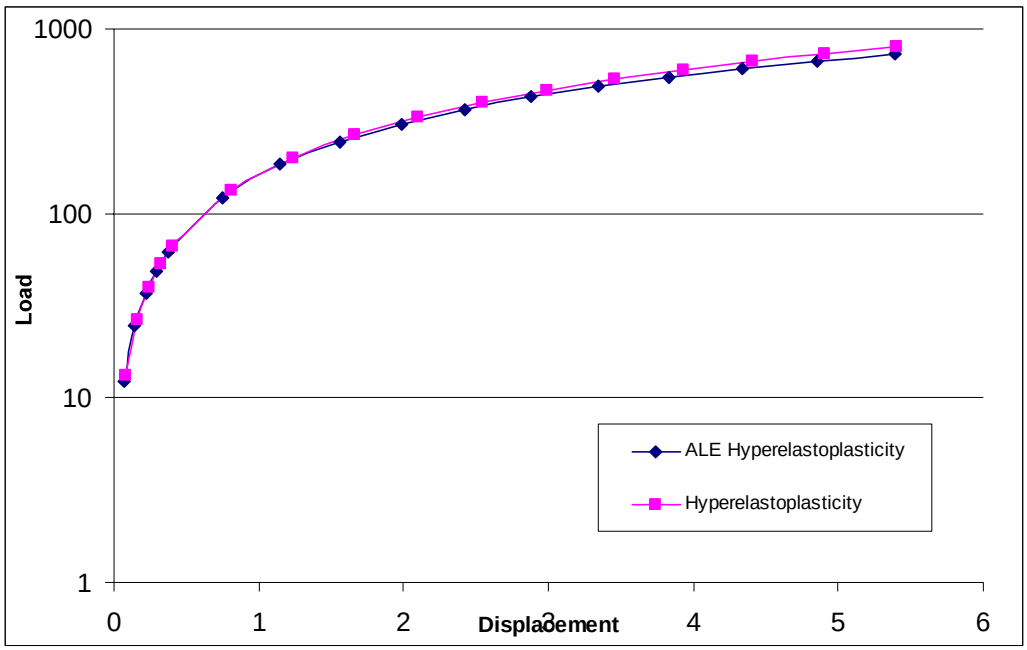

Figure 64 ALE versus Lagrangian hyperelastoplastic solution

pronounced under large deformation. The solution give less improvement than the method with generated material force as expected due to its limitation to relocate only the internal nodes. Thus the imposed force method searches for an optimised configuration where all the nodes except for the fixed ones are free to relocate while the generated force method optimises the mesh and is limited to the internal nodes.

Another example illustrating the use of imposed material force in improving the Lagrangian results is now demonstrated. The Lagrangian problem represents a structure of $40*50*50$ elements, the elastic parameters are $\mu = 384.6, \lambda = 576.9$, linear hardening parameter is $(h = 0.7)$ and the yield stress is 0.816. The uniform compression load applied over the end surface plane is equal to 800 (Figure 65). The structure is discretised with 100 $(4*5*5)$finite elements. The structure is constrained in three directions in the lower plane. In order to improve the result we use the imposed material method to solve the same problem. The spatial configuration will have the same boundary and load conditions as in the Lagrangian problem, while the material configuration will have the same conditions except for the load in opposite direction. The problems are solved within 400 increments. The solution after 50, 100, 150 and 200 increments are presented in Figures 67, 68, 69 and 70 respectively. The differences between the Lagrangian and the A.L.E solution can be verified, the elements in the Lagrangian solution get distorted as the solution progresses while the elements in the A.L.E solution maintain beter shape as part of the distortion will be taken by the material configuration.

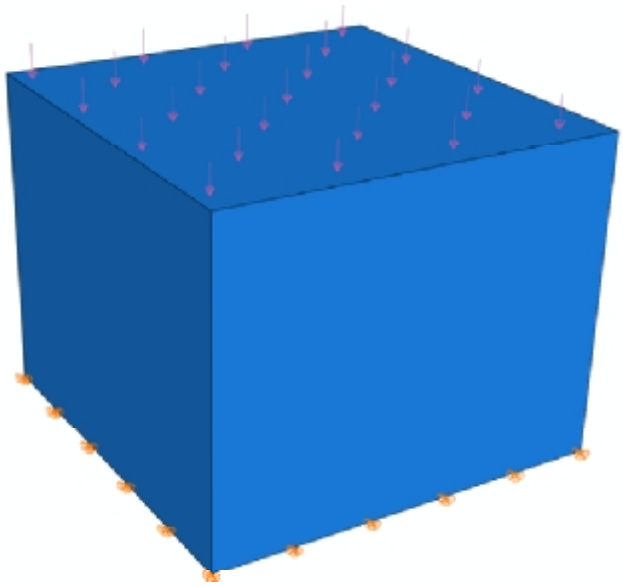

Figure 65 Lagrangian Problem

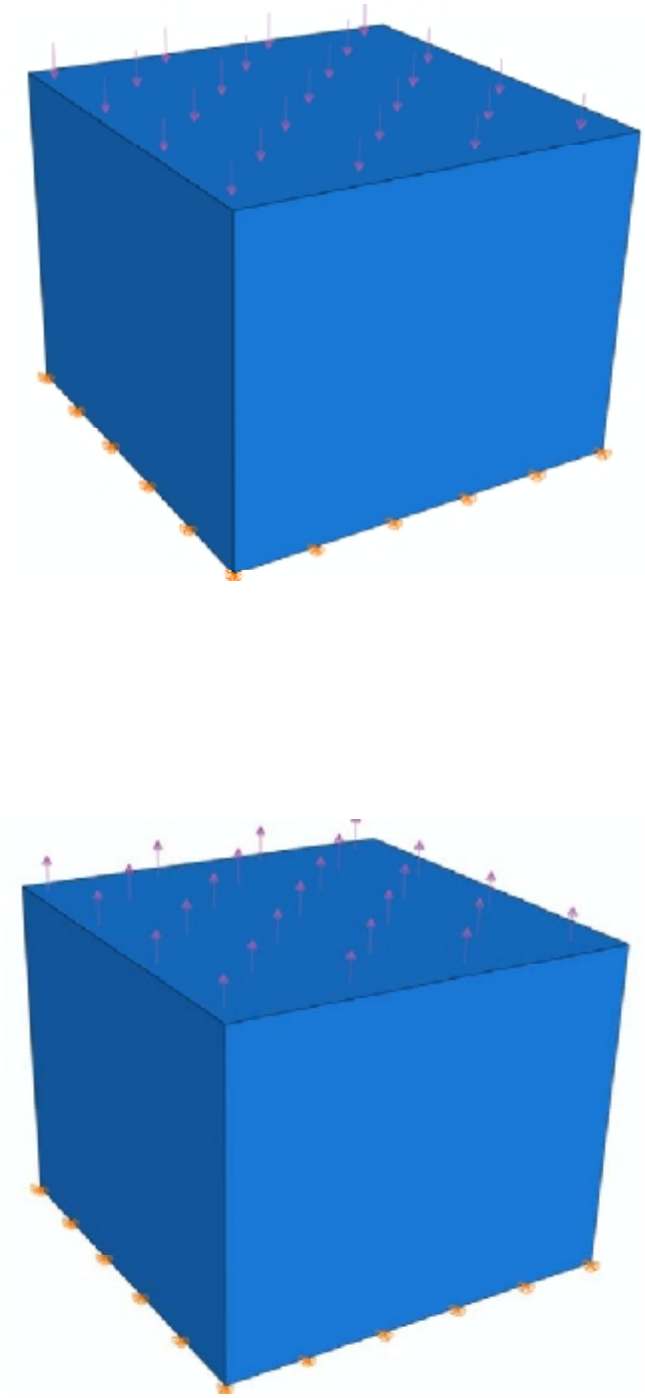

Figure 66 A.L.E Problem, Top the spatial and bottom the material configurations

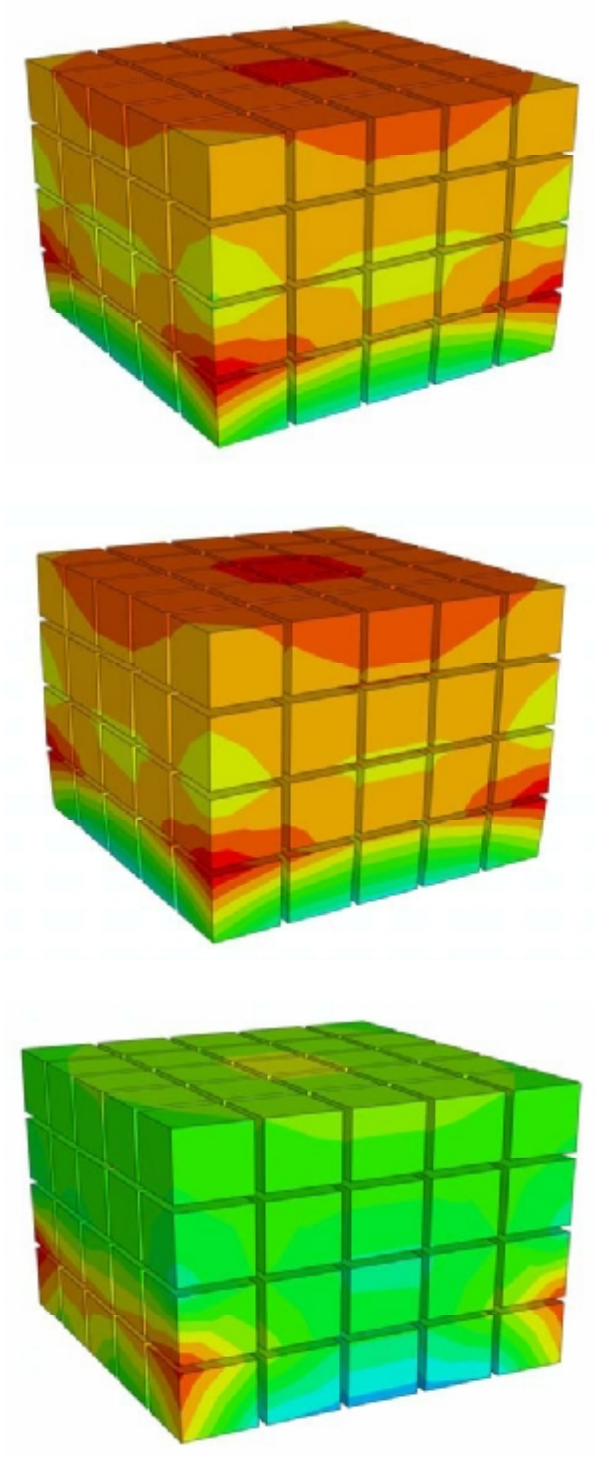

Figure 67 The results after 50 increments, Top the Lagrangian solution, middle the ALE spatial and bottom the ALE material configurations

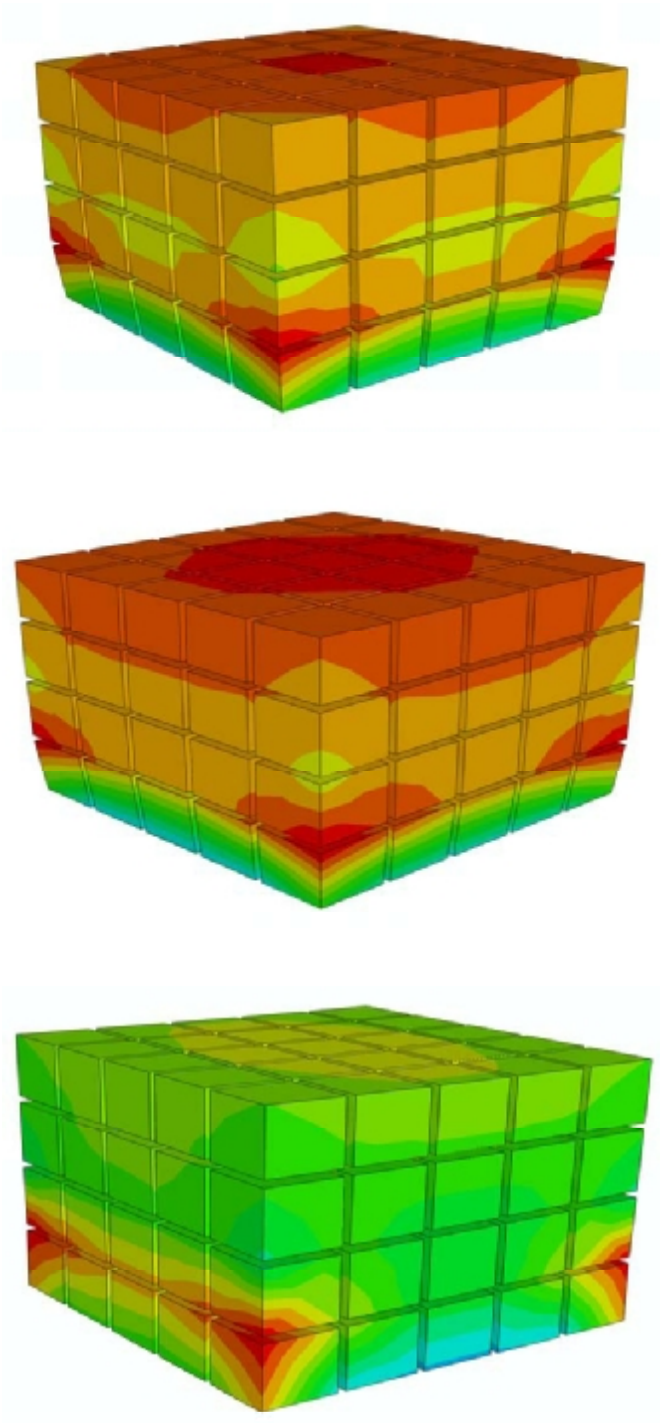

Figure 68 The results after 100 increments, Top the Lagrangian solution, middle the ALE spatial and bottom the ALE material configurations

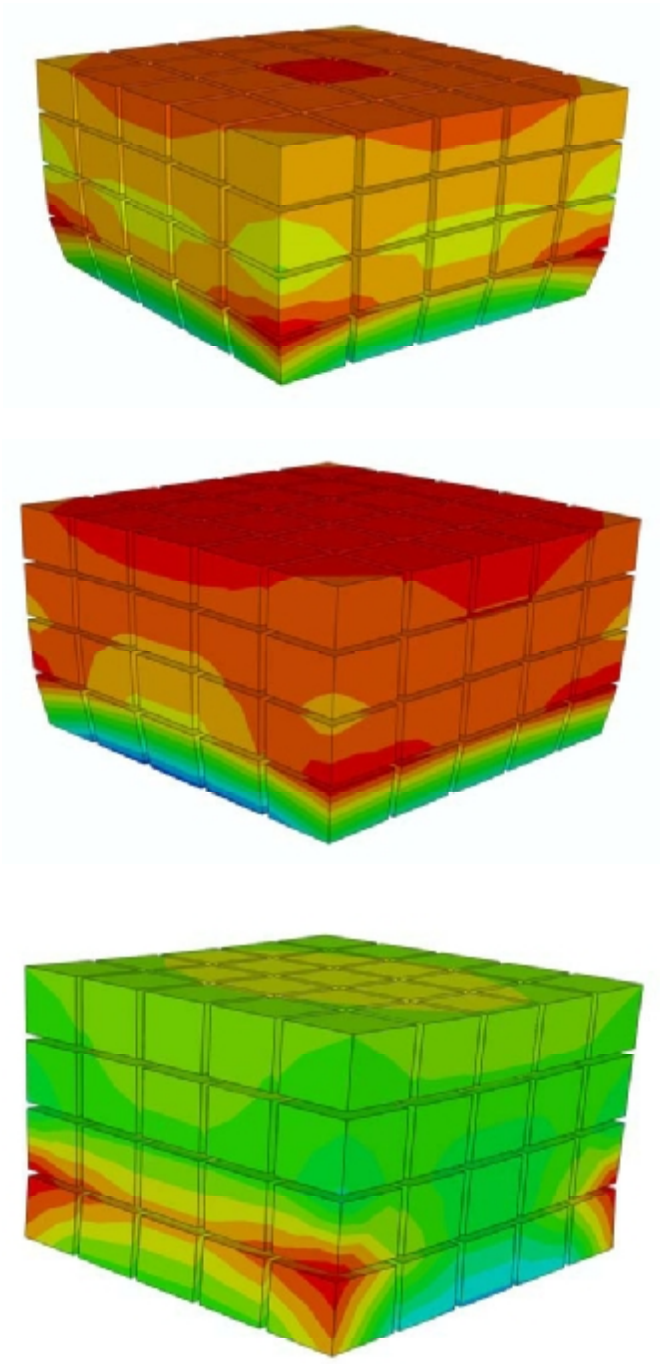

Figure 69 The results after 150 increments, Top the Lagrangian solution, middle the ALE spatial and bottom the ALE material configurations

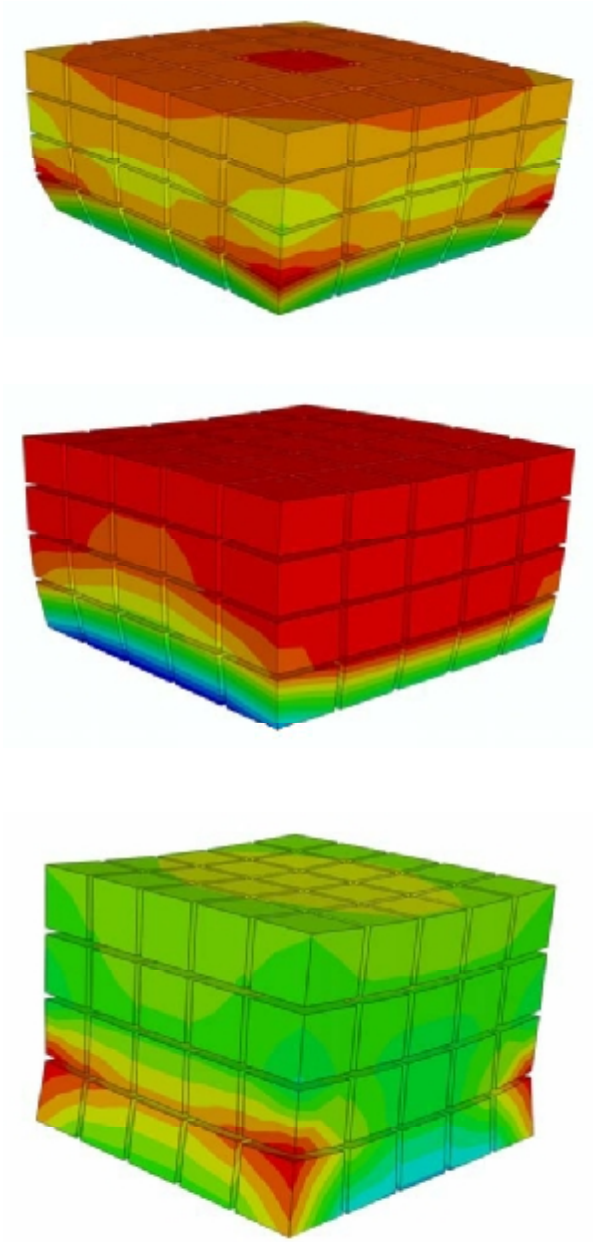

Figure 70 The results after 200 increments, Top the Lagrangian solution, middle the ALE spatial and bottom the ALE material configurations

As the material progressively deforms plastically in the Lagrangian configuration, the elements in the lower part near the fixed boundary become distorted. This is not the case for the A.L.E where the structural optimisation is used; the progressive plastic deformation is balanced in the material configuration. The elements are less distorted and the stress distribution is smoothened in the spatial configuration compared to the Lagrangian configuration as this can be seen at the end of the calculations (Figure 70). The final displacements of the nodes can be obtained as the difference between the spatial node positions and the material node positions. The imposed material force works as a damper and increases exponentially as the level of plastic deformation progresses. In other words, the larger the plastic deformation is, the larger the amount of remeshing in the material configuration. The resulting elastoplastic curve is shown in Figure 71. It is clear that the optimised solution is more pronounced under large deformation. This is due to the relative distortion that increases under larger loads. This is expected to increase further by increasing the applied load.

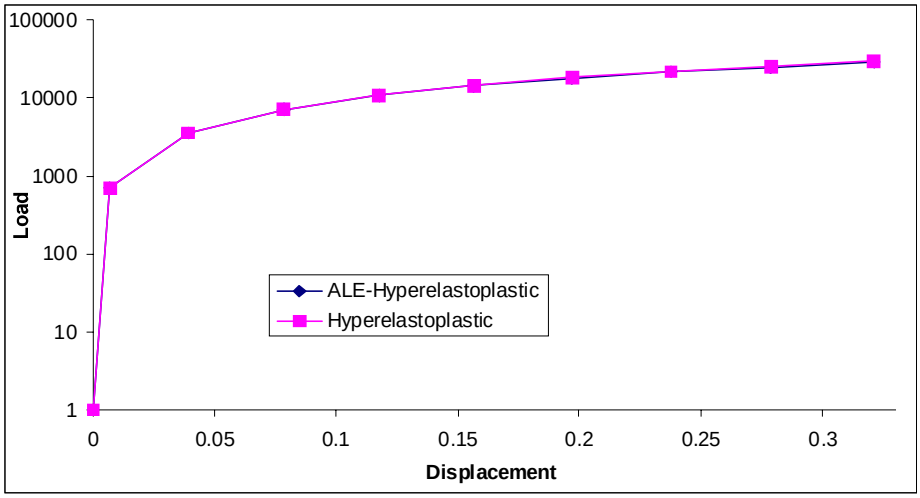

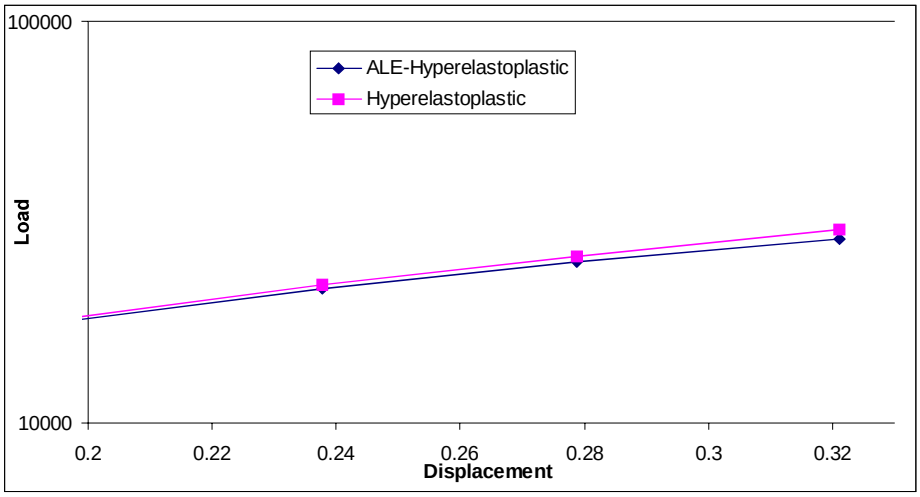

Figure 71 ALE versus Lagrangian hyperelastoplastic solution

6 CONCLUSIONS AND REMARKS

We have discussed structural optimisation based on the concept of material forces. The material force or more generally configurational force is the derivative of the strain energy with respect to the undeformed coordinate. The relocation of the nodes in such a way to allow for these forces to be vanished will result in minimising the total potential energy. As a result an optimum initial shape for the structure will be obtained. In this thesis, two types of material forces were introduced the *generated material force* and the so-called *imposed material force*. The two methods were applied in structural optimisation, static setting, dynamic setting and elastoplastic setting.

Although the generated material force was already known and used in different research fields, the one introduced in this thesis differs in the way the formulations were developed. These formulations were obtained from stored energy functional based on variational principals. Thus the material domain was totally derived from the same energy functional. In previous methods, this was not the case, and new arbitrary mathematical formulas had to be developed. The methods developed and implemented in this report are firmly rooted in continuum mechanics, in contrast to previous methods that employ generated material forces and that are, as a consequence, more arbitrary.

The imposed material force that has been introduced here has made the material force method a more effective tool to optimise structures.

The most important differences between these two methods are as follows:

1. The generated material force can be invoked to improve the quality of the mesh and as result the quality of the solution, while the imposed material force is invoked to optimise the solution. In other words the so called imposed material force is concerned with shape of optimisation while the generated material force is concerned with mesh optimisation.
2. The imposed material force ensures continuity on the traction boundary surface between the material configuration and spatial configuration while the generated material force leads to discontinuities on the traction boundary between the spatial and material domain.
3. The discontinuity on the traction boundary of the generated material force between the spatial and material domain results in improvement of internal node locations, while the nodes on the external boundaries are only allowed to move *tangentially* to the boundaries in the material domain. This has provided an optimum solution for the internal nodes and a local optimum solution for traction boundary nodes. The continuity in the traction boundary surface between the spatial and material domain ensures an optimum location not only for the internal nodes but also for the external traction nodes. The generated material force can be introduced by constraining the traction boundary nodes in the material domain from their motion perpendicularly to these boundary surfaces. The imposed material forces on the traction boundary surface are kept free in the material domain, and an applied

spatial force in the spatial domain is linked to an imposed material force in the material domain. This material force has exactly the same magnitude as the associated spatial force but with opposite direction. Thus the material force eliminated the spatial force on the traction boundary to ensure continuity between spatial material surfaces.

Although the two methods have their differences, there are many similarities: first, the formulation of the spatial domain is identical while in the material domain the formulation of the external forces differs as we mentioned above. These formulations have been derived from the same variational principle. Second, the implementation and computational cost of the two methods are quite similar. In both methods, the first iteration is purely Lagrangian. Third, both methods provide an optimum location for the internal nodes in term of minimising the energy.

In chapter two, we have used the generated and imposed material force in truss optimisation. We have distinguished between two types of generated and imposed material force, namely coupled and decoupled solutions. The coupled method provided a coupled solution of the spatial and material Equations, thus the spatial and material Equations will be solved in one time step. The decoupled solution solves the spatial and material Equations in two sub time steps, thus solving the spatial Equations in the first sub time step followed by solving the material Equation in the second sub time step. This makes the decoupled method more expensive and less accurate than the coupled method. This has been illustrated in detail using a simple truss structure with fixed ends and one free internal node. The imposed material force method was used. The results of the coupled solution were obtained in one increment and provide the same results as the reference solution. Another important conclusion is the reliability of the imposed material force method to obtain optimised solutions where the generated material force method can not be used. In case of using a decoupled solution using the imposed material force method, a much lower accuracy will be obtained for lower number of increments. The accuracy improves by increasing the number of increments. Although the same accuracy can be achieved with the decoupled solution, the number of increments needed to obtain the same solution as the coupled method is very large, keeping in mind that the solution is for one degree of freedom only. An optimum level of internal energy can be obtained through relocating the internal node; furthermore a quadratic rate of convergence has been observed.

A comparison between the imposed and generated material force method illustrates the importance of the imposed material force as a general case of the generated material force for optimising truss structures. In the generated material force method the nodes on which the traction forces are applied in the spatial domain, will have fixed motion in the material domain. As a result these nodes will not be optimised. In the imposed material force method the nodes where the traction forces are applied in the spatial domain, are free in the material domain. Thus in contrast to the generated material force method these nodes will be also optimized. As a result the introduction of the imposed material provides an effective tool to optimise trusses in cases where the

generated material force method failed. Another important aspect is the use of hyperelastic setting to develop the necessary tools; this makes the method general and applicable for large deformation. The imposed material force method provides an optimised undeformed (material configuration) and optimised deformed configuration (spatial configuration).

The material force was extended from two dimensions to three dimensions. The method was proven to be effective in three dimensional cases for generated material force as well as for imposed material force. The Newton Raphson scheme shows a quadratic rate of convergence. As is the case in shape optimisations problems; the method provides a global optimum for a lower number of degrees of freedoms while a local optimum could be obtained for a large number of degrees of freedoms.

The material force method was not limited to unconstrained structural optimisation but new formulations were developed to obtain optimised structures satisfying certain design criteria. The developed spatial and material Equations were constrained using the penalty method. A large enough value of the penalty parameter enforces the constraint accurately. The inequality constraint applied to the material force method was proven to be effective in optimising two dimensional truss structures within certain design space or within certain range. The optimised deformed and undeformed configurations were constrained within certain required space; this can be an engineering design requirement to optimise a bridge within certain height. The results for two dimensional truss structures shows that these developed formulation were effective in constraining the spatial and the material domain within the required space. Unlike the unconstrained structural optimisation the inequality constraint optimisation shows linear convergence. This means a relatively slower rate of convergence than the quadratic rate of convergence obtained with the unconstrained optimisation problem. Another type of inequality constraint that was developed and implemented is to have a certain amount of deflection for certain nodes. In this case the inequality constraint was applied only in the spatial domain, since the generated material force method was used. Thus these nodes in material domain were fixed. The results show that the design requirement for the spatial nodes to deflect within certain range has been met and an optimised truss structure is obtained. Again a linear convergence rate was observed while a quadratic rate of convergence is obtained in the unconstrained optimised structural problem. Although in both types of inequality constraint optimisation problems the generated material force method was used, the developed formulation is general. It can be used in conjunction with the imposed material force method.

In chapter three, an alternative ALE formulation was developed for the hyperelastic setting. The difference from the previous formulation is the parameterisation in terms of the spatial and material velocities instead of the spatial and material displacements. The solutions are exactly the same as the previous ones for statics, but the rate format allows a more straightforward extension to dynamics and dissipative material behaviour. A linearisation of the spatial momentum Equation with respect to the spatial coordinates plus the material coordinate can be replaced by taking the spatial rate plus the

material rate of the spatial momentum Equation. A linearisation of the material momentum Equation with respect to the material coordinates plus the spatial coordinate can be replaced by taking the material rate plus the spatial rate of the material momentum Equation. This resulted in coupled linearised spatial and material Equations. The diagonal terms resulted from the material rate of the spatial momentum Equation and the spatial rate of the material momentum Equation. The offdiagonal terms resulted from the spatial rate of the spatial momentum Equation and the material rate of the material momentum Equation.

A staggered ALE hyperelastic and a Lagrangian solution were compared; the results show improvement in mesh quality in the ALE solution. The imposed material force method was tested for highly nonlinear elastic deformation where a large number of increments were used. The results show the mesh motion tends to relocate towards the deformed areas; this was not the case in the Lagrangian solution. Thus we obtained an improvement in the mesh quality around the highly deformed areas, smoothening of the stresses and a general improvement of the results. The results in the Lagrangian solution show local deformation as expected. Although the imposed material force method has been used in the applications, the generated material force method also provides improvement in mesh quality and the results as it was illustrated in earlier works. Thus, the ALE hyperelastic solution has the advantage over the Lagrangian solution in that part of the mesh distortion will be transformed from the spatial domain into the material domain. However, the imposed and generated material force methods are similar in that part of the internal mesh distortion in the spatial domain will be carried out by the material domain as the internal nodes are free to move internally in both methods. This gives the imposed material force method the advantage of reducing the distortion more effectively as the spatial boundary nodes are free to move in the material domain. The total amount of the displacement can be found as the spatial displacement minus the material displacement.

In Chapter four, an ALE hyperelastodynamic setting was developed by making use of the physical and inverse motion based on the Hamiltonian principle. In the Hamiltonian principle the total Lagrangian was obtained through integrating the Lagrangian density over the time. The total variation in the Lagrangian was given as its variation with respect to the spatial coordinates at fixed material coordinates plus its variation with respect to the material coordinates at fixed spatial coordinates. The resulting spatial variational Equation produced the non-conservative spatial momentum Equation, while the material variational Equation produced the non-conservative material Equation. The spatial non-conservative momentum Equation resulted in conservative spatial momentum Equation plus the spatial continuity Equation. The material non-conservative momentum Equation resulted in conservative material momentum Equation plus the material continuity Equation. These Equations were nonlinear, thus they were linearised and integrated in time within the Newmark algorithm.

In the spatial domain, temporal discretisation was carried out according to Newmark algorithm on the spatial momentum Equations, followed by

linearisation with respect to the spatial coordinates at fixed material coordinates plus its linearisation with respect to the material coordinates at fixed spatial coordinates. A temporal discretisation was also carried out according to Newmark algorithm on the spatial continuity Equations and linearising them with respect to the spatial density. In the material domain, temporal discretisation was carried out according to Newmark algorithm on the material momentum Equations, followed by linearisation with respect to the material coordinates at fixed spatial coordinates plus its linearisation with respect to the spatial coordinates at fixed material coordinates. A temporal discretisation was carried out according to Newmark algorithm on the material continuity Equations and linearising them with respect to the material density. The Newton-Raphson method embedded in the implicit Newmark time integration scheme for the spatial and material momentum Equations was solved first followed by solving the spatial and material continuity Equations.

The scheme does not provide fully coupled solutions of non-conservative momentum Equation, instead a relative coupled solution was provided as explained above. A fully coupled solution can be obtained by linearising the non-conservative spatial and material momentum Equation with respect to the spatial coordinate and density plus linearisation with respect to the material coordinate and density. Although the fully coupled solution will provide more accurate results; the partially decoupled solution is relatively simpler to formulate. The formulation ensures continuity where the material force is imposed.

Examples with propagating waves were studied to verify the effectivity of the approach. The examples provide a highly non-linear setting where the generated material force method is used. The wave propagates from the impact force towards the fixed boundary. The mesh concentration is clear around the propagated wave as expected.

Finally, in Chapter five the formulation was also extended to an ALE hyperelastoplastic setting where the physical and inverse motion are used based on the principle of maximum energy dissipation. The formulation is developed for large deformation based on the multiplicative decomposition of the deformation gradient into elastic and plastic parts. The new formulation combines the concept of traditional ALE methods and the new ALE method, i.e. the concept of traditional ALE methods in solving the spatial setting first followed by solving the material setting and final sub step to convect the state variables, and the concept of the new ALE method in using the physical and inverse motion. The developed formulation has the advantage over the traditional ALE methods in that the mesh motion is not arbitrary but rooted in the mechanical formulation. The Equation that describes the mesh motion is derived from the same energy functional that describes the material motion. This simplifies the complexity of deriving Equations that describes the mesh motion and provided more accuracy because they are no longer arbitrary. The spatial domain describes the material behaviour in elastoplastic setting while the material domain provides the mesh motion in elastic setting. In order to establish the physical and inverse motion, the material time derivative of the spatial momentum Equation and the spatial time derivative of the material

momentum Equation is derived. Since the material rate of stress and strain tensors were obtained in the spatial setting, these state variables were convected to obtain them in term of the spatial rate.

The applications show the effectiveness of the developed formulation for large deformations. The generated material force method improved the mesh quality; as a result this improved the elastoplastic material behaviour. In case of using the imposed material force method the elastoplastic material behaviour improved even further. In general both methods provide improved solutions compared to the lagrangian solution. The imposed material force method smoothens the stresses and results in less mesh distortion compared to the lagrangian solution as part of the distortion in the spatial domain were carried by the material domain. The material domain acts as a damper where its contribution increases as the deformation increases.

As a final word, the introduction of imposed material force method represents a powerful tool for optimisation that has been introduced for the first time. The method presents a generalised form of the generated material force method and produces results in some cases where the generated material force method failed to do.

7 RECOMMENDATIONS FOR FURTHER RESEARCH

The introduction of the imposed material force method represents an important step in continuum and structural optimisation problems. Due to the time limitation for research, further work is required to improve the developed formulation, the coding, the application and other areas.

In structural optimisation the Inequality constraint problem can be formulated with other methods than the penalty method that has been implemented. Other methods such as the argumented lagrangian method have the advantage over the penalty method especially for nonlinear settings.

In ALE hyperelastodynamic formulation developed here is not fully coupled as the conservative form of the spatial and material momentum Equations are solved first followed by solving the spatial and material continuity Equations. In order to obtain more accurate solution the spatial and material non conservative momentum Equations should be linearised in terms of the spatial and material coordinates and densities. This will provide a fully coupled solution and more accurate results.

In coding the formulation some simplified features were neglected that are important to be taken into account. As the formulation is based on hyperelastic setting the symmetry should be taken into account, this will save a lot of memory space, computational cost and can provide much more mesh refinement. Another coding aspect is the inversion method where the direct method has been used. Other numerical inversion methods that take care of zero pivot or singularity problems should be used. An improvement in convergence can be obtained by taking into account negative eigenvalue problems and adding some cutbacks to the coding especially for the plasticity behaviour part where smaller size time step increments are required than in the elastic behaviour part. In general a reduction in increment size would be very useful for all settings to improve the convergence rate for large deformation problems.

In applications the focus was on continuous configuration. More attention should be paid to discontinuity in shapes where singularity is present. The ALE methods are more useful in that case. Other field that needs further research is where softening is present; degradation of material property will cause excessive mesh distortion. In that case the ALE method will be more useful and it would have a major improvement of the results compared to the lagrangian solution. Finally the method is general and can be applicable for other areas where the material behaviour is based on hyperelastic setting.

8 REFERENCES

[1] P. Fleron, “The minimum weight of trusses”. Bygningsstatiske Meddelser 1964, 35, 81-96.
[2] P. Pedersen, “On the minimum mass layout of trusses”. AGARD Symposium on Structural Optimisation (NATO, held in Instanbul, 1969, 36, pp. 11-1-17.
[3] P. Pedersen, “Optimal joint position for space trusses” J. Struct. Div. ASCE 1973, 99(ST12), 2459-2476.
[4] W. Prager, “Introduction to structural optimisation”, Udine: Springer-Verlag. 1974.
[5] A. Makris, G. Provatidis. “Weight minimisation of displacement-constrained truss structures using a strain energy criterion” Comput. Methods Appl. Mech. Engrg. 2002 ,191 ,2159-2177.
[6] N.L. Pedersen, A.K. Nielsen. “Optimisation of practical trusses with constraints on eigenfrequencies, displacements, stresses, and buckling” Struct Multidisc Optim 2003 25, 436-445.
[7] W. Dorn, R. Gomery. “Automatic design of optimal structures” J. Mec.1964, 3, 25-52.
[8] W. Dobbs, LP. Felton. “Optimisation of truss geometry” Proc ASCE 1969 95(ST10): 2105-2119.
[9] G. Sved, Z. Ginos. “Structural optimisation under multiple loading” Int J Mech Sci 1968 10:803-805.
[10] UT Ringertz “On topology optimisation of trusses” Eng Optim 1985 9:209-218.
[11] U. Kirsch, “On singular topologies in optimum structural design” Struct Multidisc Optim 1990, 2, 133-142.
[12] G. I. N. Rozvany, T. Birker. “On singular topologies in exact layout optimisation” Struct Multidisc Optim 1994, 8, 228-235.
[13] M. Zhou. “Difficulties in truss topology optimisation with stress and local buckling constraints” Struct Multidisc Optim 1996, 11, 134-136.
[14] G. I. N. Rozvany. “Difficulties in truss topology optimisation with stress, local buckling and system stability constraints” Struct Multidisc Optim 1996, 11, 213-217.
[15] G. I. N. Rozvany. “On design-dependent constraints and singular topologies” Struct Multidisc Optim 2001, 21, 164-172.
[16] S. V. Selyugin. “Optimisation criteria and algorithms for bar structures made of work hardening elastoplastic materials” Struct Multidisc Optim 1992, 4, 218-223.
[17] T. Buhl, C.B.W. Pedersen, O. Sigmund. “Stiffness design of geometrically non-linear structures using topology optimisation “Struct Multidisc Optim 2000, 19(2), 93-104.
[18] S. V. Selyugin. “Some general results for optimal structures” Struct Multidisc Optim 2004, 26, 357-366.
[19] K. Dems. ,Z. Mroz. “Multiparameter structural shape optimisation by the finite element method” Int J Numer Methods Eng 1978, 13, 247-263.
[20] S.V. Selyugin “On optimal physically non-linear trusses” Structural Optimisation 1995, 10, 159-166.

[21] Gil L1uis. ,Antoni Andreu. “Shape and cross-section optimisation of a truss structure “ computers and structures 2001, 79, 681-689.
[22] D. Wang, W.H. Zhang, J.S. Jiang. “Truss shape optimisation with multiple displacement constraints” Comput. Methods Appl. Mech. Engrg. 2002, 191, 3597-3612.
[23] Y.C. Toklu. “Nonlinear analysis of trusses through energy minimization” computer and structures. 2004, 82, 1581-1589.
[24] Manfred Braun. “Structural Optimisation by Material Forces” Advances in Mechanics and Mathematics. 2005, 11, 211-218.
[25] H. Askes , S. Bargmann , E. Kuhl and P. Steinmann. “Structural optimisation by simultaneous equilibration of spatial and material forces” commun. Numer. Meth. Engng. 2005, 21, 433-442.
[26] M Braun. “Configurational forces induced by finite-element discretization” Proc. Estonian Acad. Sci. Phys. Math. 1997, 46(1/2), 24-31.
[27] R. Mueller, G. A. Maugin. “On material forces and finite element discretizations” Computational Mechanics. 2002, 29, 52-60.
[28] Z. Uthman and H. Askes, “A hyperelastodynamic ALE formulation based on spatial and material forces” ‘3rd European Conference on computational Mechanics. 2006 eds. C.A. Mota soares et al., Dordrecht (CD Rom proceedings).
[29] Swantje Bargmann, “Strukturoptimierung von Fachwerken basierend auf diskreten raumlichen und materiellen kraften” 2004, master thesis.
[30] M. Ohsaki, “Optimum design of flexible structure under constraints on strain energy and asymptotic stability” Comput. Methods Appl. Mech. Engrg. 2003, 192, 4487-4496.
[31] A. Kaveh and V. Kalatjari, “Size/geometry optimization of trusses by the force method and generic algorithm” Math. Mech. 2004, 84(5), 347-357.
[32] O. Hasancebi and F. Erbatur, “Layout optimization of trusses using simulated annealing” 2002, 33, 681-696.
[33] P. Martinez, P. Marti and O.M. Querin “Growth method for size, topology, and geometry optimisation of truss structures” Struct. Multidisc. Optim, Online first number 10.1007/s00158-005-0594-1.
[34] J. D. Eshelby, “The force on an Elastic Singularity” Mathematical and Physical Science. 1951, 244, 87-112.
[35] J. D. Eshelby, “The elastic energy momentum tensor” Journal of elasticity 1975, 5, 321-335.
[36] T. Belytschko and J. M. Kennedy, “Computer models for Subassembly Simulation” Nucl. Eng. Design. 1978, 49, 17-38.
[37] J. Donea, P. Fasoli-Stella, S.Giuliani, “Lagrangian and Eulerian finite element techniques for transient fluid-structure interaction problems” 1977, Paper B1/2 , Trans. 4th internat. Conf. on Structural Mechanics in Reactor Technology. San Francisco. CA.
[38] T.J.R. Hughes, W.K. Liu and T.K. Zimmermann, “Lagrangian-Eulerian finite element formulation from incompressible viscous flows” 1979, US-Japan Seminar on Interdisciplinary Finite Element Analysis. Cornell University, Ithaca, NY.

[39] J. Donea, S. Giuliani and J.P. Halleux, “An arbitrary Lagrangian Eulerian finite element method for transient dynamic fluid-structure interactions” Computer Method in Applied Mechanics and Engineering. 1982, 33, 689-723.
[40] T.J.R. Hughes, W.K. Liu, T.K. Zimmermann, “Lagrangian-Eulerian finite element formulation for incompressible viscous flows” Computer Method in Applied Mechanics and Engineering. 1981, 29, 329-349.
[41] T. Belytschko and T.J.R. Hughes “Computational Methods for transient analysis” Elservier North Holland. 1983.
[42] W.K. Liu, T. Belytschko and H. Chang, “An arbitrary Lagrangian Eulerian finite element method for path dependent materials” Computer Method in Applied Mechanics and Engineering. 1986, 58, 227-245.
[43] T. Yamada and F. Kikuchi “An arbitrary Lagrangian Eulerian finite element method for incompressible hyperelasticity” Computer Method in Applied Mechanics and Engineering. 1993, 102, 149-177.
[44] A. Huerta and F. Casadei, “New ALE applications in non-linear fast-transient solid dynamics” Engineering Computations. 1994, 11, 317-345.
[45] A. Rodriguez-Ferran, A. Perez-Foguet and A. Huerta. “Arbitrary Lagrangian-Eulerian (ALE) formulation for hyperelastoplasticity” International Journal for Numerical Methods in Engineering. 2002, 53, 1831-1851.
[46] F. Armero, E. Love. “An arbitrary Lagrangian Eulerian finite element method for finite strain plasticity” International Journal for Numerical Methods in Engineering. 2003, 57, 471-508.
[47] H. Askes, “Advanced spatial discretisation strategies for localised failure” mesh adaptivity and meshless methods, Dissertations, Delft University of Technology (2000).
[48] Z. Uthman, “Adaptive Strategies for Finite Element Analysis based on error assessment”, MSc thesis, Delft University of Technology 2002.
[49] R. Mueller, D. Gross, G. A. Maugin. “Use of material forces in adaptive finite element methods” computational mechanics. 2004. 33, 421-434.
[50] Maugin, G.A., “Material Inhomogeneities in Elasticity”. 1993. Chapman & Hall, London.
[51] Maugin, G.A., “Material forces: concepts and applications” Appl. Mech. Rev. 1995. 48, 213-245.
[52] P. Steinmann, “Application of material forces to hyperelastoplastic fracture mechanics”. I. Continuum mechanical setting, International Journal of Solids and Structures. 2000. 37, 7371-7391.
[53] P. Steinmann, “On spatial and material settings of hyperelastodynamics” Acta Mech. 2002, 156, 193-218.
[54] P. Steinmann, “On spatial and material settings of thermo-hyperelastodynamics” J. Elasticity. 2002, 66, 109-157.
[55] P. Steinmann, “On spatial and material settings of hyperelastostatic crystal defects” J. Mech. Phys. Solids. 2002, 50, 1743-1766.
[56] E. Kuhl, P. Steinmann, “On spatial and material settings of thermo-hyperelastodynamics for open systems” Acta Mech. 2003, 160, 179-217.
[57] E. Kuhl, H. Askes, P. Steinmann, “An ALE formulation based on spatial

and material settings of continuum mechanics" Part 1: Generic hyperelastic formulation, Comput. Methods Appl. Mech. Engrg. 2004. 193, 4207-4222.
[58] H. Askes, E. Kuhl, P. Steinmann, "An ALE formulation based on spatial and material settings of continuum mechanics" Part 2: Classification and applications. Comp. Meth. Appl. Mech. Eng. 2004. 193, 4223-4245.
[59] E. Kuhl and P. Steinmann, "A hyperelastodynamics ALE formulation based on referential, spatial and material settings of continuum mechanics", Acta Mechanics. 2005. 174, 201-222.
[60] L.E. Elsgolc, "Calculus of variations". Pergamon Press. (1961).
[61] K. Washizu, "On variational principles applied to dynamical problems of elastic bodies", Massachusetts Institute of Technology. 1957. ASRL TR 25-23.
[62] K. Washizu, "Variational Methods in Elasticity and Plasticity", Pergamon Press, 1968. Oxford.
[63] D. C. Drucker, "Variational Principles in the Mathematical Theory of Plasticity", Proc. Symp. Appl. Math. 1958. Vol. 8, p.7.
[64] S. J. Lee and R. T. Shield, "Variational Principles in Finite Elastostatics", Z. angew. Math. Phys. 1980. 31, 437-453.
[65] C. Johnson, "Existency Theorem for plasticity problems", Journal de Mathematiques pures et Appliques. 1976a, 55, 431-444.
[66] C. Johnson, "On Finite Element Methods for Plasticity Problems", Numerische Mathematik. 1976b, 26, 79-84.
[67] M. R. Hestenes, "Modern Mathematics for the Engineer", McGraw-Hill. 1956, p. 75.
[68] W. R. Hamilton, Phil. Trans. R. Soc. Lond. 1834, 124, 247.
[69] L. Ya. Ainola, "Castigliano's variational problem of dynamics in nonlinear elasticity theory" Izd. AN EstSSR, seriya fiz. –matem. 1.tekhn. nauk, 1961, vol. 10, No. 1.
[70] Y. Y. Yu, "Generalized Hamilton's principle and variational equation of motion in nonlinear elasticity theory with application to plate theory" J. Acoust. Soc. Am. 1964. Vol. 36, No. 1.
[71] P. Hartman, and G. Stampacchia, "On nonlinear elliptic differential functional equations," Acta Mathematica. 1966, 115, 271-310.
[72] S. Dafermos, "Traffic equilibria and variational inequalities," Transportation Science. 1980, 14, 42-54.
[73] J. C. Simo, "A Framework for Finite Strain Elastoplasticity Based on Maximum Plastic Dissipation and the Multiplicative Decomposition", Part I. Continuum Formulation. Computer methods in Applied Mechanics and Engineering, 1988a, 66, 199-219.
[74] J. C. Simo, "A Framework for Finite Strain Elastoplasticity Based on Maximum Plastic Dissipation and the Multiplicative Decomposition", Part II. Continuum Formulation. Computer methods in Applied Mechanics and Engineering, 1988b, 68, 1-31.
[75] J. C. Simo and T.J.R. Hughes, "Computational Inelasticity", 1998, Springer-Verlag, New York.
[76] P. Wolfe, "Recent Development in Nonlinear Programming", 1962.

[77] M. R. Hestenes, “Multiplier and Gradient Methods”, Journal of Optimisation Theory and Application, 1969, Vol. 4, No. 5.
[78] A. Miele, E. E. Cragg, R. R. Iyer, and A. V. Levy, “Use of the Augmented Penalty Function in Mathematical Programming Problems”, Part I, Journal of Optimisation Theory and Applications”, 1971, Vol. 8, No. 2.
[79] A. Miele, P. E. Moseley, A. V. Levy, and G. M. Coggins, “On the Method of Multipliers for Mathematical Programming Problems”, Journal of Optimisation Theory and Applications, 1972, Vol. 10, No. 1.
[80] R. Courant, Bull. Amer. Math. Soc., 1943, 49, 1-23.
[81] Gertjan Kloosterman. “Contact Method in Finite Element Simulations” 2002. PhD thesis, University Twente, Ponsen & Looijen.
[82] A. I. Lurie. “Analytical Mechanics”. Springer-Verlag 2002.
[83] A. Menzel and P. Steinmann. “A note on material forces in finite inelasticity”. Archive Applied Mechanics, Springer Berlin, Volume 74, Numbers 11-12, November, 2005.

TABLE OF SYMBOLS

x	The spatial coordinate,
X	The material coordinate,
ξ	The referential coordinates,
v	The spatial velocity,
V	The material velocity,
ρ_t	The spatial density,
ρ_0	The material density,
σ	The Cauchy stress tensor,
$\sum$	The Eshelby stress tensor,
Ξ	The material second Piola Kirchhoff stress tensor
l	The spatial velocity gradient,
L	The material velocity gradient,
Ω	The spatial configuration,
Ω_0	The material configuration,
g	The spatial metric tensors,
C	The material metric tensors,
Π	The material first Piola-Kirchhoff stress tensor,
π	The spatial first Piola-Kirchhoff stress tensor,
b_0	The material volume forces densities per unit volume,
B_t	The spatial volume forces densities per unit volume,
C	The right spatial Cauchy-Green strain tensor,
b	The left spatial Cauchy-Green strain tensor,
c	The right material motion Cauchy-Green strain tensor,
B	The left material motion Cauchy-Green strain tensor,
U_0	The material total potential energy,
U_t	The spatial total potential energy,
W_0	The material internal potential energy,
W_t	The spatial internal potential energy
V_0	The material external potential energy
V_t	The spatial external potential energy
DIV	The divergence with respect to the material coordinates,
div	The divergence with respect to the spatial coordinates,
D_F	The derivative with respect to the spatial deformation gradient,
d_f	The derivative with respect to the material deformation gradient,
K_0	The material kinetic energies,
K_t	The spatial kinetic energies,
p_0	The material momentum densities,
P_t	The spatial momentum densities,
Π_D^t	The material dynamical momentum fluxes,
π_d^t	The spatial dynamical momentum fluxes,

L The spatial Lagrangian density,

L_0 The material Lagrangian density,

F The spatial deformation gradient,

f The material deformation gradient,

τ The Kirchhoff stress tensor,

S The spatial second Piola Kirchhoff stress tensor,

Γ The material Kirchhoff stress tensor,

m The mass in a material domain,

M The mass in a spatial domain,

$D_t(\ )$ The material time derivative,

$t_t(\ )$ The spatial time derivative,

$\overset{\nabla}{\Sigma}$ The Truesdell rate of the Eshelby stress tensor,

$\sigma^{\nabla \hat{T}}$ The Truesdell rate of Cauchy stress,

$\overset{\nabla -1}{b_e}$ The Truesdell rate of the left Cauchy-Green elastic deformation tensor,

C^P The plastic strain tensor,

$\dot{C}^P$ The material time derivative of the plastic stain tensor,

b^e The left Cauchy-Green elastic deformation tensor,

J The spatial Jacobian,

j The material Jacobian,

$\varphi(X)$ The non-linear spatial deformation map in terms of the placement X,

$\phi(x)$ The non-linear material deformation map in term of the placement x,

$\delta_x \ell$ The variation of the total energy with respect to the spatial coordinated at fixed material position,

$\delta_X \ell$ The variation of the total energy with respect to the material coordinates at fixed spatial positions,

δ The variation,

Δ The linearization,

A An area,

E The modulus of elasticity,

$\frac{\partial N}{\partial X}$ The derivative of the shape function with respect to the material coordinates,

$\frac{\partial N}{\partial x}$ The derivative of the shape function with respect to the spatial coordinates,

F_e The spatial elastic deformation gradient,

F_p The spatial plastic deformation gradient,

f_e The material elastic deformation gradient,

f_p The material plastic deformation gradient,

J^e The spatial elastic Jacobian,

J^p The spatial plastic Jacobian,

j^e The material elastic Jacobian,

j^p	The material plastic Jacobian,
M^ρ	The material capacitance matrices,
L^ρ	The material transport matrices,
K^ρ	The material divergence matrices,
m^ρ	The spatial capacitance matrices,
l^ρ	The spatial transport matrices,
k^ρ	The spatial divergence matrices,
a	The spatial acceleration,
A	The material acceleration,
β	The spatial penalty parameters,
α	The material penalty parameters,
g_I	The spatial constraint,
G_I	The material constraint,
$\langle\ \rangle$	The Macaulay bracket,
n	The spatial normal,
N	The material normal,
T	The material surface tractions,
t	The spatial surface tractions,
r_X	The material residual,
F^{int}	The material internal force vectors,
F^{ext}	The material external force vectors,
r_x	The spatial residual,
f^{int}	The spatial internal force vectors,
f^{ext}	The spatial external force vectors.